Techno-Economic Analysis of CO_2 Capture Technologies for Small-Scale Dispatchable Gas Turbines

Mathew Dennis Wilkes

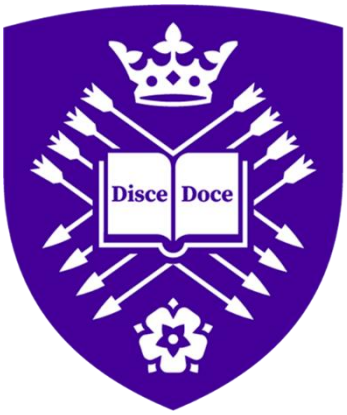

A thesis submitted in fulfilment of the requirements for the degree of Doctor of Engineering (EngD).

The University of Sheffield

Department of Mechanical Engineering

September 2023

Declaration of Authorship

I hereby declare that this thesis is entirely of my own work and original in content, and that all sources have been accurately reported and acknowledged, and that this document has not, in its entirety or in part, been submitted at any other institution to obtain an academic qualification.

Acknowledgements

I am extremely grateful to Professor Solomon Brown (primary supervisor), the Brown Research Group, and Professor Rachel Rothman (secondary supervisor) for providing their support, guidance, and expertise, without which this Engineering Doctorate (EngD) would not be possible.

I would like to extend my sincere thanks to the Engineering and Physical Science Research Council's (EPSRC) Centre for Doctoral Training (CDT) in Carbon Capture and Storage and Cleaner Fossil Energy (CCSCFE), reference: EP/L016362/1. The CDT in CCSCFE has provided me with the opportunity to undertake this EngD. Also, I would like to thank Drax Group Plc for industrially sponsoring and for providing support throughout the project.

I would like to give a special thanks to my parents, Anthony and Shelley Wilkes, for their unwavering support. Also, I would like to express my deepest gratitude to my partner, Georgie Leach, for motivating and supporting me throughout my research and thesis writing. Her encouragement and patience were crucial in keeping me focussed and on task.

Finally, I dedicate this thesis to the memory of my grandmother, **Mo Linehan** (1948-2020). Although she did not fully understand my research, her excitement towards my studies and belief in my ability has made this journey possible. You are gone but you will never be forgotten.

Lay Summary

The climate crisis has made it abundantly clear that we need to stop emitting CO_2 into the atmosphere and start removing it. A fundamental part of the UK governments Net-Zero plan is Carbon Capture Utilisation and Storage (CCUS). The solution is not as simple as banning fossil fuels and other point sources of CO_2. If we look at the energy sector as an example, impressive headway has already been made and between 1990 to 2020: CO_2 emissions have dropped by 63%. This is a direct result of using more renewable energy technologies; however, the issue with renewable sources such as wind or solar power, is their inherent intermittency. In order to maintain a constant supply of energy to all our homes and businesses, we need responsive and dispatchable power, i.e., power sources that can turn on quickly and on short notice to balance the supply and demand of energy.

Currently, the UK relies on gas turbines for dispatchable power generation. Gas turbines combust natural gas, a finite fossil resource, and in order to reach Net Zero goals they need to include Carbon Capture and Storage (CCS). The benchmark technology to capture CO_2 from power stations is chemical absorption using amine based solvents. It has been used since the 1930's and the only two power stations in the world with CO_2 capture use amines. There are a large range of other potential capture technologies, at various stages of deployment. One of the closest technologies to commercialisation is physical adsorption, it benefits from having no reactions occur hence the CO_2 can easily be separated from the capture material. Once you capture the CO_2, you need to prepare it to be transported to the storage site.

This study looks at evaluating CO_2 capture for open-cycle gas turbines (OCGTs), specifically looking at absorption using Monoethanolamine (MEA) and adsorption using Zeolite 13X. Both capture plants also have CO_2 conditioning included. The goal is to compare these technologies technically and economically, i.e., to see which technology is more cost effective. Within this study, process and economic models are developed and used to analyse the performance of each of the low-carbon dispatchable power plants. The benchmark technology can handle the flexible operation with only small drops in performance. An OCGT+CCS plant using MEA will cost 13.84 M£ to build, and 1.47 M£ to operate annually. Similarly, the adsorption technology can also handle the flexible operation with only small drops in performance. An OCGT+CCS plant using a zeolite adsorbent will cost 12.80 M£ to build, and 3.58 M£ to operate annually. Both technologies performed similarly during the simulated operating scenario. An MEA capture plant costs slightly more to build and less to operate compared to a Zeolite 13X capture plant; however, both technologies cost more than other forms of low-carbon power generation, in terms of electricity price and cost of CO_2 capture avoidance. This is due to the small plant size and short operating times. Other plants can operate continuously throughout the year, but the generator investigated in this study only operates a fraction of the time. Therefore, it cannot generate enough revenue to offset the high operating costs of running the CO_2 capture plant.

This project has highlighted some important challenges in reaching Net-Zero by 2050. If we want to ensure security of electricity supply, we need quick-response dispatchable generators. However, the current method will become too costly if we attach CCS. Therefore, alternative power generation or CO_2 capture technologies need to be investigated.

Abstract

The consistent rise in anthropogenic CO_2 emissions has led to the climate crisis. In order to minimise the average global temperature increase to <1.5°C, rapid decarbonisation of power and industrial CO_2 sources urgently needs to happen. Multiple independent consortiums have agreed that **Carbon Capture and Storage (CCS)** is crucial in achieving Net-Zero by 2050, and one of the focus points is providing low-carbon dispatchable power. Dispatchable power refers to sources that can quickly start-up and respond to fluctuations in energy supply and demand; thus providing grid stability and resilience. They also counteract the intermittency issues of renewable power sources, allowing for the uptake of more wind and solar energy on the grid. The quick-response nature and flexibility of open-cycle gas turbines (OCGTs), makes them ideal dispatchable generators. Within the UK, they are used by the Short Term Operating Reserve (STOR) as balancing capacity, to provide the National Grid with additional power during system imbalances or due to unforeseen generation unavailability.

In order to achieve Net-Zero, small-scale dispatchable OCGTs need CCS. Within the literature, sources routinely overlook these small-scale generators, majority of which fall within the Medium Combustion Plant Directive (MCPD). Currently, these plants are not required to be carbon capture ready, but future energy system restraints will require CO_2 abatement on these types of generators. Therefore, this study looks at evaluating CO_2 capture for modern gas turbines, specifically looking at OCGTs under <50 MWe. This techno-economic analysis focusses on two CO2 capture technologies

- **Chemical Absorption** using 30 wt.% Monoethanolamine (MEA).
  This is considered the benchmark CO2 capture technology for power generation sources, and it is currently the only technology deployed globally on a large scale power plant.
- **Vacuum-Pressure Swing Adsorption (VPSA)** using Zeolite 13X.
  This technology and sorbent material is close to commercialisation. A large quantity of research already exists in the literature, with several pilot-scale studies.

Within this study, process and economic models are developed and used to analyse the performance of each of the **OCGT+CCS** plants. Both capture plants work from identical CO_2 sources, and to ensure an accurate comparison both CO_2 streams are conditioned ready for pipeline transportation.

Both MEA and VPSA can handle highly transient flue gas production with only minor fluctuations in capture rate, purity, and energy demand. A 10 MWe **OCGT+MEA** plant will cost 13.84 M£ in capital investment and 1.47 M£ in annual operating costs. The **OCGT+VPSA** plant is comparable to MEA, costing 12.80 M£ in capital but with higher (3.58 M£) operating costs. The levelised cost of electricity (LCOE) for OCGT+MEA and OCGT+VPSA is 291-394 £/MWh and 420-588 £/MWh, respectively. The LCOE for OCGT+CCS is higher than other forms of low-carbon power generation, due to the low capacity factor and small plant size (economies of scale). These generators are usually decentralised and dispersed emitters, hence the high cost for conditioning the CO_2 ready for pipeline transportation. Similarities can be drawn to industrial sources of CO_2, which lie outside the range of the newly planned Track 1 Cluster networks. The results show these small decentralised emitters may benefit from Carbon Capture, Utilisation, and Storage (CCUS), i.e., directly converting the capture CO_2 stream into a saleable by-product to offset the high operating costs and low annual revenue.

This study has highlighted an important bottleneck in reaching Net-Zero by 2050. Dispatchable power is crucial for ensuring security of electricity supply; however, the current dispatchable technologies will become too costly if we attach CCS. Therefore, future work needs to investigate different capture and utilisation technologies in order to drive the levelised cost of electricity for **OCGT+CCUS** down. Moreover, OCGT+CCS needs to be compared against alternative dispatchable power sources such as hydrogen combustion and energy storage, to discover the most effective option for ensuring security of electricity supply.

List of publications

Throughout this EngD project, several peer-reviewed publications have been submitted and accepted in reputable international journals. The work has also been showcased to other academics at numerous conferences and networking events. The following articles investigated flexible CO_2 capture for small-scale gas turbines using the benchmark amine-absorption process, from which the information is shown in Chapter 3 Section 3.3.1 and Chapter 4 Section 4.1:

- Wilkes, M. D., & Brown, S. (2020). Evaluating the Transient Operation of PCC for Fast Response Gas Turbines in a Future Low-Carbon Energy System. Computer Aided Chemical Engineering, 48, 157-162. doi: https://doi.org/10.1016/B978-0-12-823377-1.50027-6
- Wilkes, M. D., Mukherjee, S., & Brown, S. (2021). Transient CO2 capture for open-cycle gas turbines in future energy systems. Energy, 216, 119258. doi: https://doi.org/10.1016/j.energy.2020.119258

The following articles investigated flexible CO_2 capture for small-scale gas turbines using vacuum-pressure swing adsorption, from which the information is shown in Chapter 3 Section 3.3.2 and Chapter 4 Section 4.2:

- Wilkes, M. D., & Brown, S. (2022). Evaluating the flexible operation of vacuum-pressure swing adsorption for CO2 capture from modern gas turbines. Computer Aided Chemical Engineering, 51, 427-432. doi: https://doi.org/10.1016/B978-0-323-95879-0.50072-2
- Wilkes, M. D., & Brown, S. (2022). Flexible CO2 capture for open-cycle gas turbines via vacuum-pressure swing adsorption: A model-based assessment. *Energy, 250*, 123805. doi: https://doi.org/10.1016/j.energy.2022.123805

The following articles investigated CO_2 compression and conditioning for a range of CO_2 sources and for the case evaluated above, from which the following the information is shown in Chapter 3 Section 3.3.3 and Chapter 5:

- Wilkes, M. D., Mukherjee, S., & Brown, S. (2021). Linking CO2 capture and pipeline transportation: sensitivity analysis and dynamic study of the compression train. International Journal of Greenhouse Gas Control, 111, 103449. doi: https://doi.org/10.1016/j.ijggc.2021.103449
- Wilkes, M. D., Mukherjee, S., & Brown, S. (2021). Compression system power requirements for various CO2 sources and transportation options. Computer Aided Chemical Engineering, 50, 1439-1444. doi: https://doi.org/10.1016/B978-0-323-88506-5.50222-9

Within the following article I used the information gained in the literature review in Chapter 2, to comprehensively review the state-of-the-art of CO_2 capture technologies applicable for lime production. This was a multidisciplinary review, with Dr Marco Simoni lead author:

- Simoni, M., Wilkes, M. D., Brown, S., Provis, J. L., Kinoshita, H., & Hanein, T. (2022) Decarbonising the lime industry: state-of-the-art. Renewable & Sustainable Energy Reviews, 168, 112765. doi: https://doi.org/10.1016/j.rser.2022.112765

The following articles investigated the economic feasibility of small-scale CO_2 capture, using the process models developed in the earlier papers to provide the necessary equipment and utilities information. The information can be found in Chapter 3 Section 0, Chapter 6, and Chapter 7 Section 7.2. The articles have been accepted towards the conference proceeding for the 16th Greenhouse Gas Control Technologies (GHGT) conference 23rd – 27th October 2022, and have been submitted for peer-review in Energy, respectively:

- Wilkes, M. D., & Brown, S. (2022). Cost of CO_2 capture for small-scale dispatchable power generation. Proceedings of the 16th Greenhouse Gas Control Technologies Conference (GHGT-16) 23-24 Oct 2022, Available at http://dx.doi.org/10.2139/ssrn.4271571
- Wilkes, M. D., Ejeh, J., Roberts, D., & Brown, S. (2022). Cost of small-scale CO_2 capture: technology comparison and case study evaluation.

List of Presentations

Throughout this EngD project, the research has been disseminated at various conferences, networking events, web events, and industrially focussed panels.

- Event: **UKCCSRC Early Career Researcher Winter School**
  Title: Techno-economic analysis of exhaust gas cleaning technologies for quick response fossil power generators (poster)
  Date: 12th – 14th February 2019
  Location: Sheffield, UK

- Event: **UKCCSRC Spring Web Series**
  Title: Insight into the transient operation of a post-combustion CO_2 capture system (poster)
  Date: 5th May 2020
  Location: UKCCSRC - https://ukccsrc.ac.uk/web-series/ukccsrc-spring-web-series/

- Event: **30th European Symposium and Computer Aided Process Engineering (ESCAPE)**
  Title: Evaluating the transient operation of PCC for fast response gas turbines in a future low-carbon energy system (poster)
  Date: 31st August – 2nd September 2020
  Location: Milan, Italy

- Event: **31st European Symposium and Computer Aided Process Engineering (ESCAPE)**
  Title: Compression system power requirements for various CO_2 sources and transportation options (presentation)
  Date: 6th -9th June 2021
  Location: Istanbul, Turkey

- Event: **32nd European Symposium and Computer Aided Process Engineering (ESCAPE)**
  Title: Evaluating the flexible operation of vacuum-pressure swing adsorption for CO_2 capture from modern gas turbines (key-note presentation)
  Date: 12th -15th June 2022
  Location: Toulouse, France

- Event: **The role of CCS in Transforming Foundation Industries**
  Title: Decarbonising energy for industry (presentation and panellist)
  Date: June 28th 2022
  Location: UKCCSRC - https://ukccsrc.ac.uk/web-events/

Table of Contents

Table of Figures

Table of Acronyms

AD	Adsorption	**AMP**	2-Amino-2-methyl-1-propanol
BAT	Best Available Technology	**BD**	Blowdown
BECCS	Bioenergy CCS	**BEIS**	Department of Business, Energy & Industrial Strategy
BMRS	Balancing Mechanism Reporting Service	**CaL**	Calcium looping
CAPEX	Capital Expenditure	**CC**	Carbon Capture
CCA	Cost of CO_2 Avoided	**CCA**	Cost of CO_2 Captured
CCC	Committee on Climate Change	**CCGT**	Combined-Cycle Gas Turbine
CCGT	Combined-Cycle Gas Turbine	**CCR**	Carbon Capture Readiness
CCR	Carbon Capture Readiness	**CCS**	Carbon Capture and Storage
CCS	Carbon Capture and Storage	**CCUS**	Carbon Capture, Utilisation, and Storage
CCUS	Carbon Capture, Utilisation, and Storage	**CDU**	Carbon Dioxide Utilisation
CDU	Carbon Dioxide Utilisation	**CEPCI**	Chemical Engineering Plant Cost Index
CF	Capacity factor	**CFG**	Cleaned flue gas
CHP	Combined Heat and Power	**CIF**	Carbon capture and storage Infrastructure Fund
CLC	Chemical looping combustion	**COE**	Cost of Electricity
CP	Carbon price	**CRF**	Capital recovery factor
CS	CO_2 sink	**CSIRO**	Commonwealth Scientific and Industrial Research Organisation
DAC	Direct Air Capture	**DEC**	Direct equipment costs
DLN	Dry Low-NOx burners	**DMPEG**	Dimethyl ethers of polyethylene glycol
DPA	Dispatchable Power Agreement	**EV**	Evacuation
FCC	Facility capital cost	**FCF**	Fixed Charge Factor
FGS	Flue gas source	**FOAK**	First of a kind
FOM	Fixed operating and maintenance	**FR**	Frequency Response
FTM	Facilitated transport membrane	**GHG**	Greenhouse gases
GPU	Gas Permeation Unit	**GTW**	Gas Turbine World
HRSG	Heat recovery steam generator	**HSE**	Health and Safety Executive
IAS	Ideal adsorption solution	**IEA**	International Energy Agency
IEAGHG	International Energy Agency Greenhouse Gas	**IED**	Industrial Emissions Directive
IGCC	Integrated Gasification Combined Cycle	**IL**	Ionic Liquid
ISBL	Inside battery-limits investment	**KO**	Knock-out drum
KPI	Key performance indicator	**LCCC**	Levelised capture and compression costs
LCOE	Levelised cost of electricity	**LDF**	Linear driving force
LULUCF	Land use, land use change, and forestry	**MCFC**	Molten carbonate fuel cell
MCPD	Medium Combustion Plant Directive	**MDEA**	Methyldiethanolamine
Me	Metal	**MEA**	Monoethanolamine
$MeCO_3$	Metal Carbonate	**MEL**	Minimum environmental load
MEM	Membrane	**MeO**	Metal oxide
MeOH	Methanol	**MMM**	Mixed matrix membrane
MOF	Metal organic framework	**MSG**	minimum stable generation
NFTM	Non-facilitated transport membrane	**NG**	Natural Gas
NGCC	Natural gas combined cycle	**NOAK**	Nth of a kind
NPV	Net Present Value	**NTU**	Number of transfer units
OCGT	Open-Cycle Gas Turbine	**OEM**	Original equipment manufacturer

OPEX	Operating Expenditure
PACT	Pilot-scaled Advanced Capture Testing
PCC	Post-Combustion Capture
PCPP	Pulverised coal power plant
PDAE	Partial differential algebraic equation
PEC	Purchased equipment cost
PI	Proportional integral
PID	proportional integral derivative
PM	Particulate matter
PR	Pressurisation
PSA	Pressure swing adsorption
PTSA	Pressure-temperature swing adsorption
PU	Purge
PUI	Process unit investment
PZ	Piperazine
RoCoF	Rate of change of frequency
RVPSA	Rapid vacuum-pressure swing adsorption
SAFT	Statistical associating fluid theory
SCGT	Simple Cycle Gas Turbine
SMR	Steam Methane Reforming
SOFC	Solid oxide fuel cell
STOR	Short-Term Operating Reserve
TCC	Total capital cost
TCM	Technology Centre Mongstad
TEG	Triethylene glycol
TRL	Technology Readiness Level
TSA	Temperature swing adsorption
UHC	Unburnt hydrocarbons
VFD	Variable frequency drive
VOM	Variable operating and maintenance
VPSA	Vacuum-pressure swing adsorption
VSA	Vacuum swing adsorption
VTSA	Vacuum-temperature swing adsorption
WC	Working capacity
WITC	Wyoming Integrated Test Center	

Nomenclature

a	Cost factor		a_0	Speed of sound in the inlet flow	m/s
a_T	Total packing surface area	m^2/m^3	a_w	Wetted packing surface area	m^2/m^3
A_w	Bed wall cross-sectional area	m^2	b	Cost factor	
b_i	Equilibrium adsorption constant	$m^3/kmol$	b_o	Pre-exponential constant	K
C_i	Fluid component concentration	$kmol/m^3$	C_g	Gas phase specific heat capacity	kJ/kg/K
C_p	Solid phase specific heat capacity	kJ/kg/K	$C_{p,w}$	Bed wall specific heat capacity	kJ/kg/K
C_v	Flow coefficient	kg/s/kPa	D	Diffusion coefficient	m^2/s
d_b	Bed diameter	m	d_i	Equilibrium adsorption constant	$m^3/kmol$
d_i	Impeller diameter	m	D_L	Axial dispersion coefficient	m^2/s
d_0	Pre-exponential constant	K	d_p	Packing nominal size	m
d_{pp}	Pellet particle diameter	m	E_i	Individual equipment cost	
F	Mass flowrate	kg/s	F_G	Gas capacity factor	
G	Gas molar flowrate	kmol/s	g	Acceleration due to gravity	m/s^2
H	Energy flow	kJ/s	$\Delta H_{b,i}$	Heat of adsorption for site 1	J/mol
$\Delta H_{d,i}$	Heat of adsorption for site 2	J/mol	h_l	liquid holdup	
Δh_p	Polytropic work/enthalpy change	j/kg	Δh_t	Actual change in enthalpy	J/kg
$h_{t,in}$	Inlet flow enthalpy		$h_{t,out}$	Outlet flow enthalpy	
h_W	Heat transfer coefficient between the gas and the column wall	$W/m^2/K$	$h_{w,a}$	Heat transfer coefficient between the column wall and external environment	$W/m^2/K$
K	Wall factor		k	Mass transfer coefficient	$kg.mol/m^2/s/atm$
k_n	Isentropic exponent		L	Liquid molar flowrate	kmol/s
l_w	Wall thickness	m	M	Molar holdup	
M_i	Impeller tip speed Mach number		$M_{CO_2}^{in}$	Input CO_2 mass flowrate	kg/s
$M_{CO_2}^{out}$	Output CO_2 mass flowrate	kg/s	$M_{CO_2}^{Product}$	Product CO_2 mass flowrate	kg/s
$M_{Total}^{Product}$	Total product mass flowrate	kg/s	n	Cost factor	
n_c	Isentropic compressor efficiency		n_v	Isentropic vacuum efficiency	
P	Pressure		Pr	Productivity	$mol/m^3/s$
$\bar{q}_i$	averaged absorption quantity of species i	kmol/kg	$q_{eq,i}$	equilibrium absorption quantity of species i	kmol/kg
Q_R	Energy supplied to the reboiler	mJ/h	$q_{sb,i}$	maximum equilibrium adsorption amount of species i on site 1	kmol/kg
$q_{sd,i}$	maximum equilibrium adsorption amount of species i on site 2	kmol/kg	r	Discount rate	
R	Universal gas constant	$m^3.atm/kg/mol/K$	R_d	Reboiler duty	GJ/tco_2
S	Sizing factor		Δs	Entropy change between the outlet and inlet compressor flows	J/K/kg

T	Temperature	K	T_g	Gas phase temperature	K
t	Time period		T_w	Bed well temperature	K
U	Energy holdup	kJ/s	μ_g	Dynamic viscosity	Pa.s
u_i	Impeller tip speed	m2/s	V_{in}	Volumetric flowrate	m^3/s
$\mathbf{v_D}$	Design speed	Hz	v_s	Superficial fluid velocity	m/s
$\mathbf{\Delta v_-}$	Turndown speed	Hz	$\mathbf{\Delta v_+}$	Overspeed	Hz
w	Work coefficient		x	Valve stem position	
γ	Ratio of specific heat capacities		z	Height/bed length	m
$\mathbf{z_{calc}}$	Calculated controller output	Hz	$\mathbf{z_{min}}$	Minimum controller output	Hz
$\mathbf{z_{max}}$	Maximum controller output	Hz	$\mathbf{z_{out}}$	Controller output	Hz

Greek letters

ε	Void fraction		ε_f	Energy flux	kJ/s
$\mathcal{N}$	Molar flux		η_p	Polytropic efficiency	
ρ	Density	kg/m^3	ρ_g	Density of the gas phase	kg/m^3
ρ_p	Solid phase density	kg/m^3	ρ_w	Bed wall mass density	kg/m^3
μ	Viscosity	kg/m/s	λ_e	Effective axial thermal conductivity	$W/m^2/K$
λ_w	Wall material thermal conductivity	W/m/K	ψ_L	Resistance coefficient	
ψ_p	Polytropic head coefficient				

Sub-/super- script

G	Gas phase	i	Components
in	Inlet	J	Stages
L	Liquid phase	n_e	Scaling factor
n	Time period	out	Outlet
p	Particle		

Chapter 1 : Introduction

Climate change and the rise in global temperature is a consequence of cumulative CO_2 emissions, as well as other greenhouse gases (GHG): methane, nitrous oxide, water vapour, ozone, and some fluorine gases [1]. Models estimate the atmospheric concentration of CO_2 needs to be limited to 450 ppm to prevent the global temperature rising more than 2°C. To remain within 450-650 ppm range, zero and low-carbon power sources must be implemented globally, and fossil fuel sources must have carbon capture, utilisation, and storage (CCUS) technologies attached [2]. The latest IEA roadmap for the global energy sector [3] explains the Net-Zero 2050 emissions target aims to minimise the average global temperature increase to 1.5°C.

Within the UK, the Climate Change Act (2008) aimed to reduce GHG emissions by 80% (in 2050) compared with 1990 levels; carbon budgets were on track to deliver this reduction [4]. However, the Sixth Carbon Budget published in 2020 supersedes the 2008 Climate Change Act goal and aims for Net Zero by 2050 at the latest [5]. In 2019, the UK territorial emissions were 41% lower than 1990 levels. The recommended legal limit for UK net GHG emissions requires a 78% decrease between 1990 and 2035. Figure 1 highlights the increased rate of action required to meet these new targets. The Net Zero pathways rely on the use of CCUS or carbon capture and storage (CCS) to meet the necessary reductions in carbon emissions from power generation and industry.

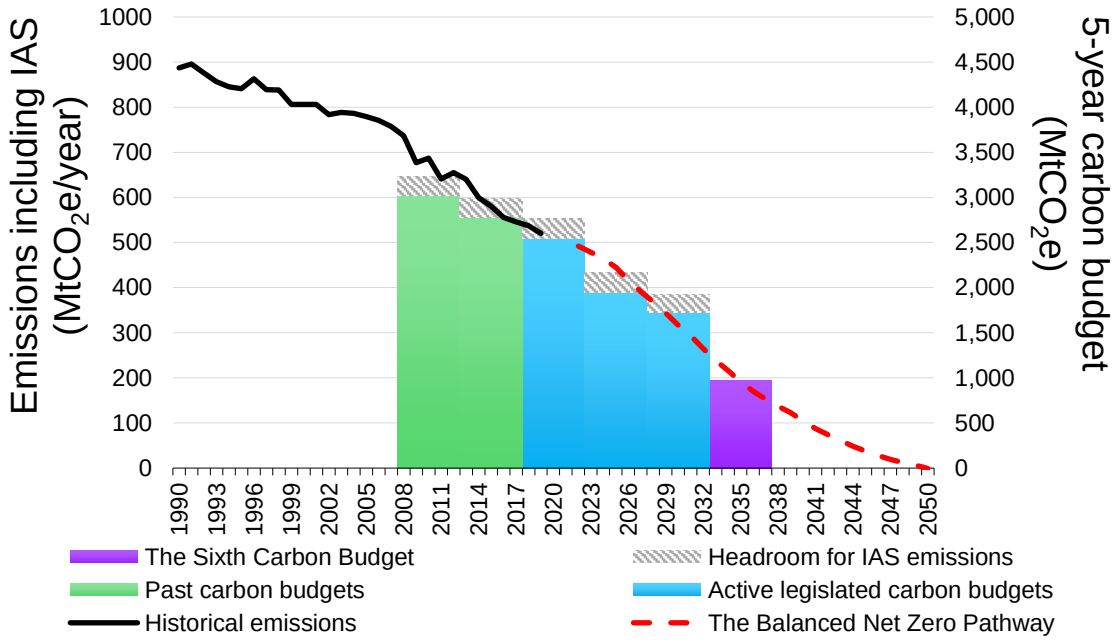

Figure 1: Greenhouse gas emissions and carbon budgets for the UK; included in the figure is the recommended 6th carbon budget and net-zero 2050 target. Data sourced from [5].
Note: IAS = international aviation and shipping.

The Global CCS Institute highlights the four principal areas CCS can aid in reaching Net Zero, in a cost-effective manner [6]:

- Deep decarbonisation of industrial sources such as: cement, iron, steel, and chemical sources.
- Production of hydrogen to aid in decarbonising hard-to-abate sectors.
- **Low-carbon dispatchable power** to aid in grid-stabilising services (inertia, frequency response, and voltage control) that cannot be provided by renewable power generation.
- Negative emissions with Bioenergy CCS (BECCS) and direct air capture (DAC)

The Global CCS Institute also highlighted the world's readiness for CCS [7]. No nation has established the necessary policy frameworks in order to drive commercialisation of CCS at an acceptable rate to meet climate targets set in the Paris agreement. The UK is ranked 4th in the world in the institute's readiness index assessment and is considered to be a leader in promoting and deploying CCS with long-term commitments to moving towards a low-carbon future. The UK previously ranked higher in the index; however, the removal of public funding and the cancellation of the White Rose and Peterhead CCS projects inevitably reduced the UK's overall score. In 2020, the UK government published a Ten Point Plant for Green Industrial Revolution [8], in which point 8 is investing in CCUS technologies. Included in the plan was a commitment to deliver two CCUS clusters by the mid-2020's, and four clusters by 2030. To reach these targets, the UK government has allocated £1bn in the Carbon Capture and Storage Infrastructure Fund (CIF) [9].

Although CO_2 emissions come from a range of sources, the energy sector accounts for 50% of the total GHG emissions globally [3] and 24% in the UK [10, 11]. Figure 2 shows the annual CO_2 (equivalent) emissions from each sector from 1990 to 2019 in the UK; the 2020 figures are provisional. Energy supply was consistently the major CO_2 contributor, which is consistent with global trends, until 2015-2016 where transport became the highest emitting sector. This is due to impressive improvement in power generation, moving away from fossil fuels towards more sustainable renewable sources, reducing the CO_2 emissions by 63% from 1990 to 2020. However, further reduction is required to reach Net Zero targets.

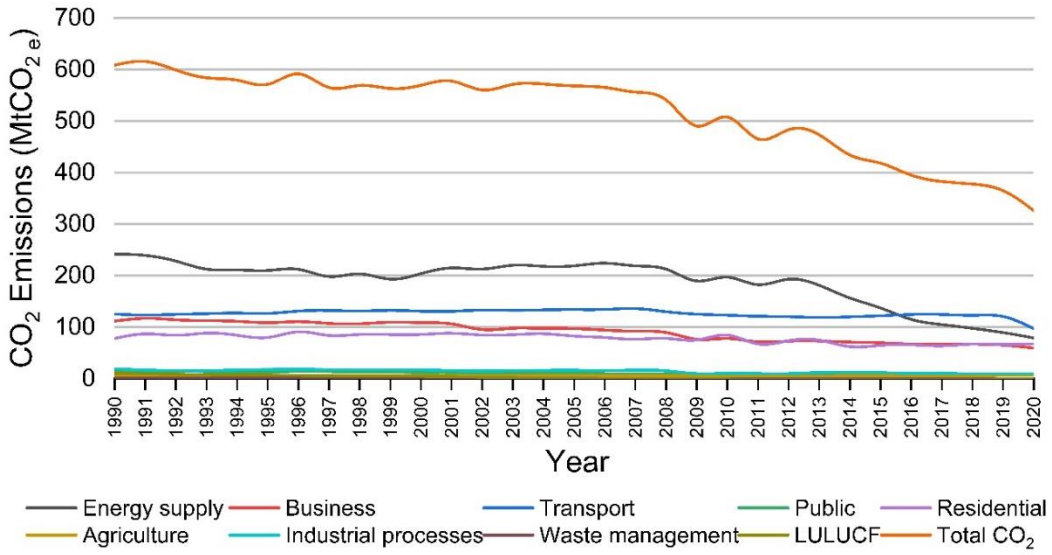

Figure 2: Historical (1990-2019) and provisional (2020) annual CO_2 emissions from each sector in the UK between 1990-2020. Data sourced from [11]. LULUCF stands for "Land use, land use change, and forestry". The total emissions only include CO_2 and not the other GHG's.

1.1. The Role of Gas in Future Energy Systems

The decarbonisation of the energy sector is crucial to achieving Net Zero; in particular, the provision of low-carbon dispatchable (flexible) power. Flexible power plants equipped with CCS provide system inertia, frequency, and voltage control, and ensure the grid is resilient and reliable [12]. The UK Committee on Climate Change (CCC) outlined a scenario for the electricity generation mix from 2016-2030 (see Figure 3). In 2016, almost half of electricity generated was supplied by gas which produced 13% of the UK's overall GHG emissions. Unabated coal is planned to be phased out by 2025 and the share for gas will likely drop due to an increase in renewable generation. However, the increase in intermittent renewables and inflexible nuclear makes balancing supply and demand of electricity

difficult. The National Grid has various balancing services such as the Short-Term Operating Reserve (STOR) where 'peaking plants' come on to counteract the imbalance during known fluctuations (e.g., daily peaks and seasonal changes) or when generators become unexpectedly unavailable. For system security and flexibility, the quick-response nature of gas systems is ideal; for example, open-cycle gas turbines (OCGTs) can reach full load in 15-30 minutes [13, 14]. Alternative technologies used by STOR include energy storage, diesel generators, interconnectors, and demand side response technologies [15].

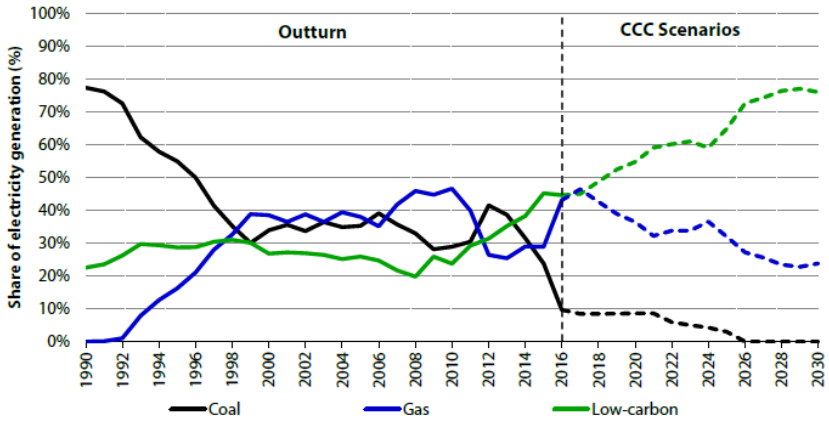

Figure 3: Historical (1990-2016) electricity generation mix and the predicted (2016-2030) share according to the Committee on Climate Change [4]

Energy UK [16] states the number of OCGT's will continue to grow due to the role small-scale decentralised energy could play in decarbonising the electricity sector. Figure 4 from Heuberger & Mac Dowell [17], also highlights the number of OCGT's is expected to increase with a significant generation share coming from renewables (wind, solar, pumped hydro, and biomass). The study showed that near-100% renewable power is feasible in many cases, however, a high penetration of intermittent renewables leads to realistic (balancing supply and demand) constraints on electricity grids with significant operational challenges. Dispatchable and quick-response capacity is essential to maintain quality and security of supply. To keep the UK on the lowest-cost path to reaching Net-Zero targets, as well as deliver secure and responsive electricity, quick-ramping fossil power will require CO_2 abatement technologies [4].

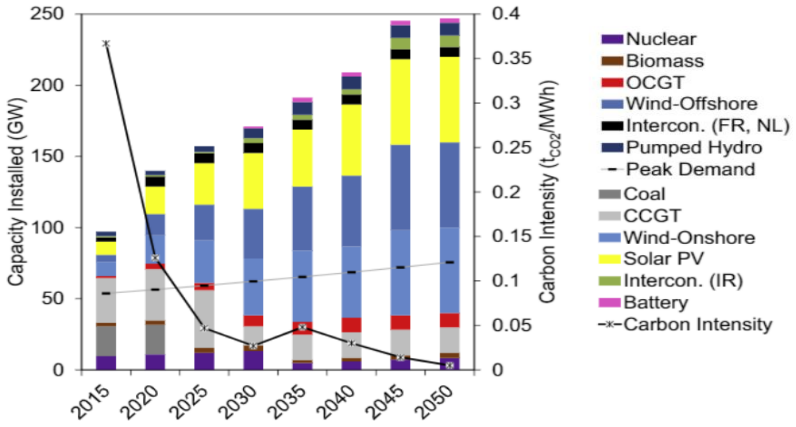

Figure 4: Installed capacity supply breakdown corresponding to UK's Clean Growth Strategy, included is the relative carbon intensity of the system, sourced from Heuberger & Mac Dowell [17]

Currently, small-scale power generators that fall under the medium combustion plant directive (<50 MWth input) emit up to 100 $ktCO_2$ per year and are not yet required to be CCS ready [18]; however, an expansion of the Carbon Capture Readiness (CCR) requirements could see these generators also encompassed in the Industrial Emissions directive (IED) [19]. Dispatchable and quick-response capacity is essential to maintain quality and security of supply. To keep the UK on the lowest-cost path to reaching Net-Zero targets, as well as deliver secure and responsive electricity, quick-ramping fossil power will require CO_2 abatement technologies [4].Dispatchable power generation

Power generation supply matches the demand required on the system, this fluctuates daily, weekly, seasonally, and annually. Dispatchable power refers to sources that can turn on or off to balance supply and demand. They provide grid stability, resilience, and reliability. For more information on dispatchable power generation linked with CCUS, see the Dispatchable power agreement (DPA) update from BEIS [20].

Staffell and Pfenninger [21] used National Grid's historical data to show the seasonal and diurnal profiles of energy demand in Britain (see Figure 5). Included in the figure is the predicted model outputs from the study Each year (2005, 2010, and 2015) follows similar patterns in terms of where the peak demands are located. These peaks are between 08:00-10:00 as people are commuting to work, and between 16:00-20:00 as people return home from work. The intensity of these peaks (total demand) varies depending on the season; winter requires the most power due to an increased heat supply to homes and businesses, whereas summer requires the least amount of power due to higher ambient temperatures. However, despite the consistency of demand profiles, it is difficult to predict exactly when power is going to be required.

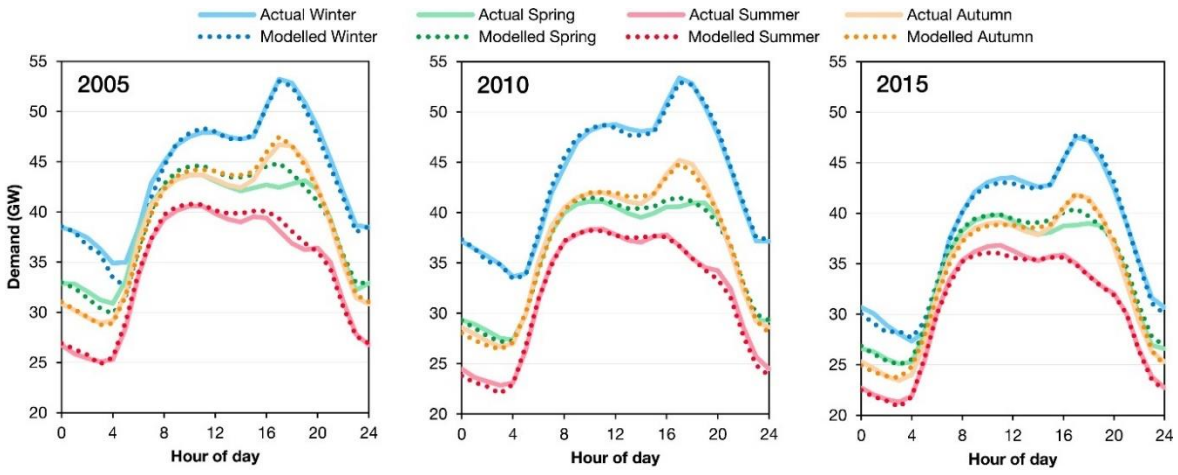

Figure 5: Demand profiles in Britain for 2005, 2010, and 2015, sourced from Staffell and Pfenninger [21]

Gonzalez-Salazar et al. [22] compared the operational flexibility of gas and coal fired power plants, in terms of their start-up, shutdown, and ramping capabilities, as well as the associated emissions for each operational procedure (Figure 6). Simple cycle gas turbines (SCGT), also known as OCGT, have a higher emissions rate per MWh due to their smaller size and transient operation. However, they are much better as quick-response generators. A typical OCGT (between 50-200 MW) has a ramping rate of 8-25% full load/min, and heavy-duty gas turbines operating in simple/open cycle mode ramp between 8-15% full load/min. The hot start-up time of 0.16 hours and a minimum load of 15% full load, i.e., the turndown capacity of the generator, make OCGTs an attractive technology for flexible generation [23].

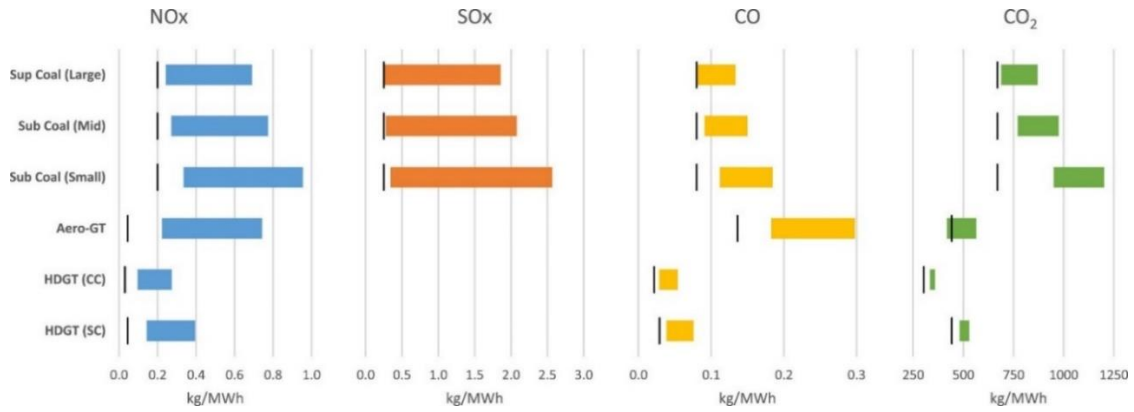

Figure 6: Emissions for gas- and coal-fired power stations, sourced from Gonzalez-Salazar et al. [22]. GT refers to gas turbine, HDGT is heavy duty gas turbine, CC is combined cycle, and SC is simple cycle.

For flexible power generation, gas turbines are desirable because of their lower greenhouse gas emissions (compared with other fossil fuel sources), operational flexibility, reliability, fast response, and their short lead times. For an OCGT, atmospheric air is compressed then drawn into the combustion chamber, where it is mixed with the fuel and ignited. The combustion gases expand and drive a gas turbine generating the work output [24]. OCGT's can be considered the most economic choice for peaking plants currently available on the market when compared to interconnectors, aggregated generating units, pumped storage, compressed air energy storage, flywheels, battery storage, and internal combustion engines [25].

1.1.1.Frequency response

Conventional fossil-based dispatchable power generation can also provide the grid with frequency response (FR). During typical operation, the frequency of the grid is 50 Hz; the operation limits are shown in Figure 7. When the demand is greater than the energy supplied, the frequency decreases. Conversely, when the demand is less than the energy generated, the frequency increases. When the frequency deviates above or below the operation limits, a failure event is triggered which causes power outages. The rate of change of frequency (RoCoF) after an imbalance is related to the amount of inertia in the system. Inertia is proportional to the rotational kinetic energy of the synchronous generator, i.e., the energy stored in large rotating generators and motors [26]. Renewable power increases the RoCoF but can be counteracted by de-loading and droop techniques [27]. However, FR is currently met mainly by gas turbines, e.g., combined cycle gas turbines (CCGT's), but as they have a delayed start and slow ramp times, the future FR capacity could be met by batteries and interconnectors [28]. Interestingly, OCGT's have much quicker start up and ramp times [22], and given the expected growth in future energy systems, OCGT's could play a significant role in FR and grid stability.

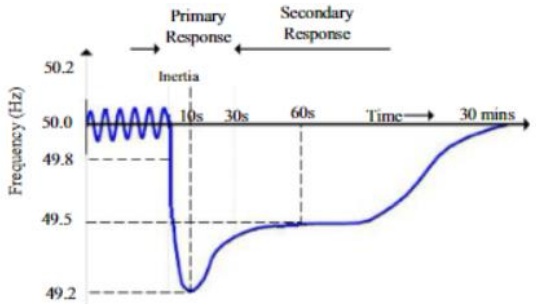

Figure 7: Frequency operating limits and response times, sourced from Dreidy et al. [27]

1.1.2.Gas turbine emissions

Industrial gas turbines used for electricity generation typically combust natural gas (NG) which is suitable for premixed combustion due to its high chemical stability, i.e., preventing flashback and premature self-ignition [29]. The combustion chamber's main function is to provide the turbine with high temperature fluid flow. However, this process produces a range of emissions, mainly CO_2 and NO_x. Other emissions from gas turbines include particulate matter (PM), volatile organic compounds (unburnt hydrocarbons), CO, and SO_x. The concentration of each species is highlighted in Table 1.

The complete combustion of a hydrocarbon produces carbon dioxide and water. Carbon dioxide is a GHG and is the baseline unit for calculating other GHGs global warming potentials. Although it is not the most detrimental in terms of radiative efficiency and lifespan, 60% of the global warming affects are attributed to CO_2 [30]. The global reaction scheme proposed by Jones & Lindstedt [31] is a four-step mechanism, shown in Equations 1-4.

$$C_nH_{2n+2} + \frac{n}{2}O_2 \rightarrow nCO + (n+1)H_2 \quad (1)$$

$$C_nH_{2n+2} + nH_2O \rightarrow nCO + (2n+1)H_2 \quad (2)$$

$$H_2 + \frac{1}{2}O_2 \leftrightarrow H_2O \quad (3)$$

$$CO + H_2O \leftrightarrow CO_2 + H_2 \quad (4)$$

Initially CO is formed, and the oxidation to CO_2 is slow. However, CO rapidly reacts with hydroxyl radicals [32] and the overall chemical equation is given by:

$$\boldsymbol{C_nH_{2n+2} + 2nO_2 \rightarrow nCO_2 + (n+1)H_2} \quad (5)$$

The control of air pollutants such as nitrogen and sulphur oxides are not only beneficial from environmental and health perspectives, but it also prevents degradation to downstream CO_2 capture equipment. Sulphur levels in NG pipelines regulated, therefore, SO_X emissions are extremely small, similar with PM emissions which are less than 25 ppmv (see Table 1). The main pollutants investigated by gas turbine manufacturers are NO_X and CO. Many simple/open cycle gas turbines have NO_X abatements units attached onto them. However, modern gas turbines are finely tuned machines that are efficient at limiting NO_X and CO through burner design and operation [33, 34]. For new gas turbines, dry low NO_X burners (DLN) are the best available technology (BAT). This primary control mechanism is also economically feasible for integrating into existing gas plants. Although the best post-combustion NO_X control mechanism (selective-catalytic reduction) is considered a BAT and is technically feasible for OCGTs, the high investment and operating costs make it economically unfavourable. New OCGTs that combust NG and are fitted with DLN emit <50 mg/Nm^3 of NO_X and between 5-40 mg/Nm^3 of CO [35], which are below regulation standards [36].

Emissions fluctuate depending on the design and operation of the gas turbine. OCGT's have to operate at intermediate loads, in order to follow daily and seasonal demand cycles. Operating characteristics have an effect on the level of pollutants emitted. Operating characteristics typically controlled are temperature, pressure, humidity, residence time, fuel type, and air-to-fuel ratio. During the initial start-up or low load operation, the temperature levels are insufficient for complete combustion of the fuel. This leads to lower combustion efficiencies and increased levels of combustion impurities as shown in Figure 8. However, the fluctuation in CO_2 concentration is minimal. Low-emission combustors are

capable of dramatically reducing the emissions levels, although they have challenges with instability. Dynamic stability in the combustion chamber prevents flame extinction and thermoacoustic combustion oscillation (pressure increase inside the combustion chamber). Therefore, any primary (preventative) abatement technology must not impede the combustion process [29, 37]. The minimum environmental load (MEL) is the minimum power output of the gas turbine that complies with emissions guidelines; it is a limiting factor determining the flexibility of gas turbines. MEL set-points are dependent on the type and original equipment manufacturer (OEM) of the turbine [38].

Table 1: Gas turbine exhaust composition data, sourced from Pavri & Moore [34]

Major Species	**Concentration (vol.%)**	**Minor Species**	**Concentration (PPMV)**
Nitrogen (N_2)	66-72	Nitric Oxide (NO)	20-220
Oxygen (O_2)	12-18	Nitrogen Dioxide (NO_2)	2-20
Carbon Dioxide (CO_2)	1-5	Carbon Monoxide (CO)	5-330
Water Vapour (H_2O)	1-5	Sulphur Dioxide (SO_2)	Trace-100
		Sulphur Trioxide (SO_3)	Trace-4
		Unburnt Hydrocarbons (UHC)	5-300
		Particulate Matter (PM)	Trace-25

Note: trace-100 means the emissions range is between trace amount up to 100 PPMV

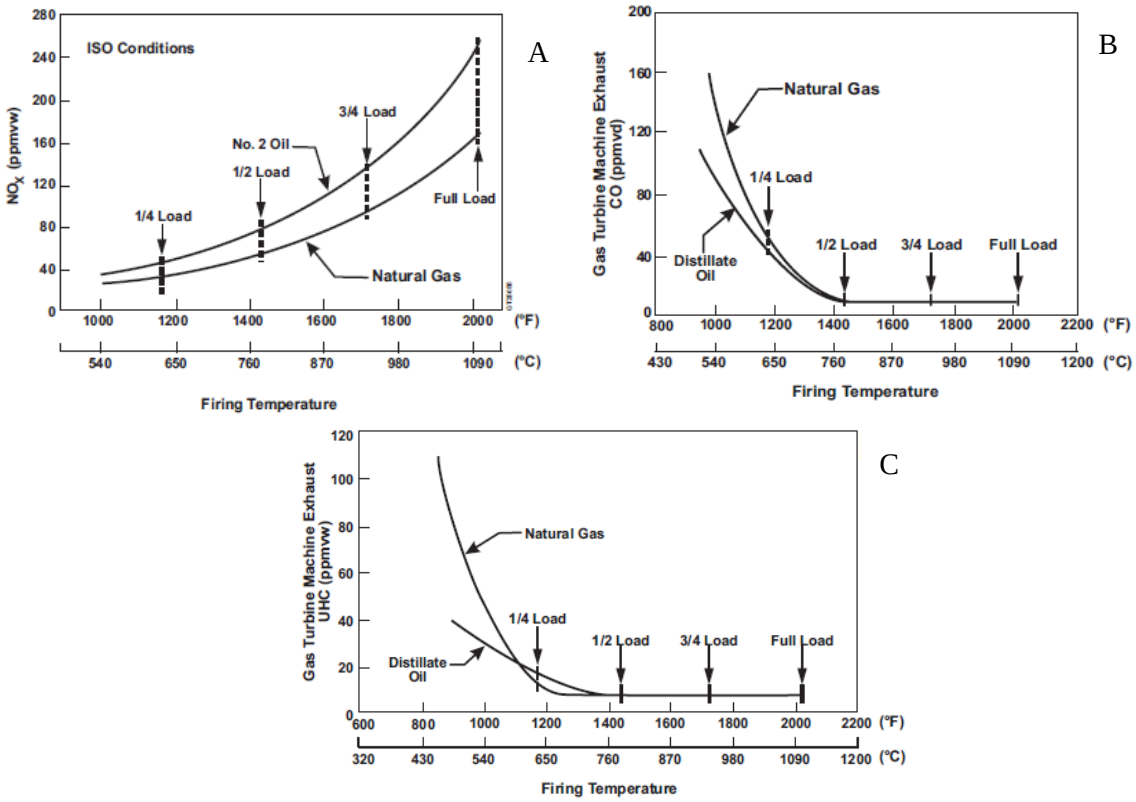

Figure 8: Effect of partial loading and temperature fluctuations on emissions concentrations. A) NO_X, B) CO, C) UHC, sourced from Pavri & Moore [34]

1.1.3.Modern gas turbines

Gas turbines consist of four main thermodynamic process: compression, combustion, expansion, and heat rejection. The ideal gas turbine cycle, also known as the Joules cycle or Brayton cycle (Joule-Brayton cycle), includes isentropic compression, constant pressure heat addition, isentropic expansion, and constant pressure heat rejection [39], as illustrated in Figure 9.

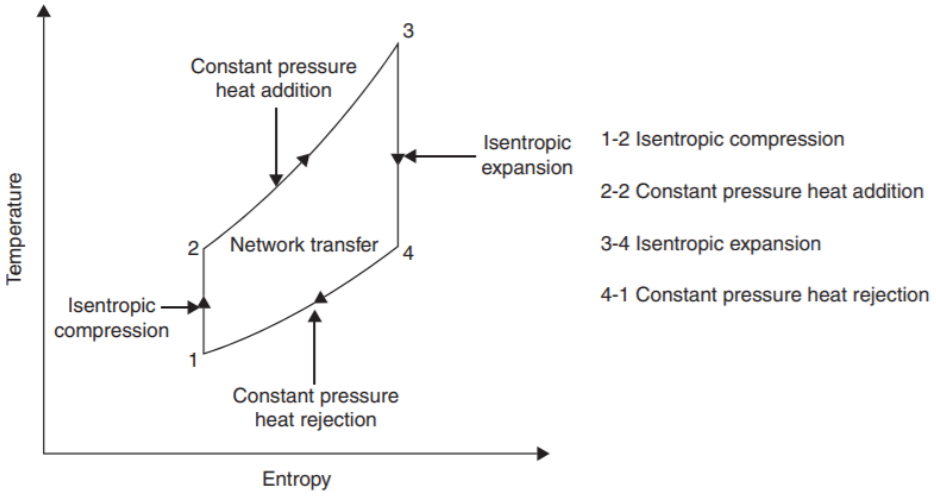

Figure 9: Ideal gas turbine cycle thermodynamic process, sourced from [39]

The efficiency of the gas turbine is the ratio of net work done and the heat supplied. Modern gas turbines (excluding aero-derivative) have a typical efficiency between 30-40% and produce less than 15 ppmv or 50 mg/m^3 of NO_X when coupled with low-NO_X burners. Operating features for a range of small gas turbines on the market are shown in Table 2. An illustration of a gas turbine (Siemens SGT-400) is shown in Figure 10. As all of the gas turbines are >560 kW, they fall under Medium Combustion Plant Directive MCPD [18]. The Overarching National Policy Statement for Energy (EN-1) [18] does not require combustion plants to be carbon capture ready if they are below 300 MW, i.e., plants that fall under the MCPD. Although, these generators are not currently obligated to include CCUS, future energy system restraints may require CO_2 abatement even on these types of generators especially going towards Net Zero 2050.

Interestingly, Table 2 shows the power output is directly proportional to the exhaust flowrate. Therefore, when incorporating exhaust ramping, any change in power output directly effects the exhaust flow, i.e., if the power decreases to 70% load, the exhaust flow also decreases to 70% of the maximum flowrate.

Table 2: Modern gas turbines on the market

Model	**MHPS H-25 Series**	**GE TM2500**	**SIEMENS SGT-600**	**Caterpillar TITAN™ 130**	**SIEMENS SGT-400**
Power Output (MWe)	41.0	33.7	24.5	16.5	10.4
Exhaust Temperature (°C)	114.0	-	81.3	55.8	33.8
Exhaust Flow (kg/s)	569.0	-	543.0	485.0	508.0
NO_x	15.0	25.0	≤9	-	≤25.0
Efficiency (%)	36.2	35.0	33.6	35.5	34.8
Source	[40]	[41]	[42]	[43]	[42]

Figure 10: Siemens SGT-400 gas turbine (left) and compact open-cycle package design [42]

Figure 11 from [39] illustrates the efficiency trends in simple and combined cycle gas turbines. Improving the efficiency is vital in reducing the CO_2 emissions; a 1% improvement in efficiency for a 1000 MW CCGT results in saving 50,000 tCO_2/year. However, a reduction in emissions is not enough to meet climate change targets. Further CO_2 removal, through the use of CCUS technologies, is required to ensure as much CO_2 is captured as possible. Jansohn [39] provided an update on modern gas turbines, explaining the effect CCS will have on the operation of future gas turbines. The addition of CCS will affect the operational flexibility, grid stabilisation characteristics, and low following capabilities; although this depends on the type of CCS used. Chapter 2 reviews the current literature around CCS/CCUS and highlights the most applicable technologies for OCGT's.

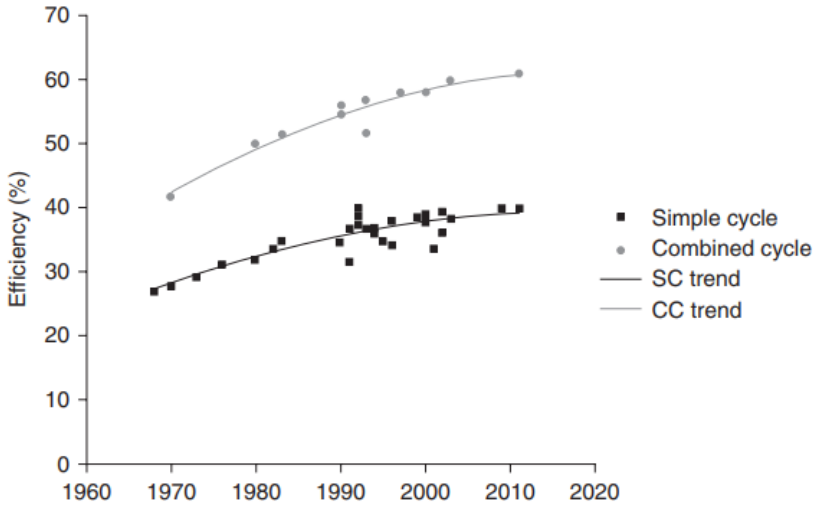

Figure 11: Gas turbine efficiency trend sourced from [39]

1.2. Aims & Objectives

This project is a model-based techno-economic analysis of exhaust gas cleaning technologies; primarily focussed on emissions from OCGTs, used for balancing services, e.g. STOR. For modern gas turbines, low emission burners limit the NO_X and CO levels to below regulatory standard, and sulphur levels in NG pipelines are kept as low as possible for safety and degradation reasons Therefore, this projects specifically looks at CO_2 capture technologies. The aim of this project is to techno-economically assess CO_2 for OCGT power stations, highlighting the applicable technologies that can work in conjunction with the transient nature of these generators.

As the power generators will have transient operation, a critical aspect of the project is analysing the effects of load variation on the capture technologies, i.e., changes in flue gas flowrate and composition. Figure 12 illustrates the aspects of CCUS investigated in this study. This project does not investigate utilisation technologies; thus, the term CCS will be used throughout the remainder of this document. The power generation plant (OCGT) will not be directly modelled, but information on the typical flue gas production will be calculated and used as input parameters in dynamic process models for CO_2 capture and compression. Realistic OCGT operation will be analysed using data from the Balancing Mechanism Reporting Service (BMRS) and OEM's. CO_2 compression is included to create a black box over the system to enable a fair comparison between the capture technologies, as well as enable a comparison to other low-carbon power generation technologies. Each capture system will have the same input flue gas flowrate and produce a CO_2 stream with the same end-point characteristics, ready for transportation to the storage facility. The project is broken down into two main components:

- **Technical evaluation** – the literature will be surveyed to discover the most applicable capture and compression technologies, focusing on existing and close to commercialisation systems, and adapting these systems to behave transiently. Process models for the capture and compression technologies will be developed and validated against data from the literature, then scaled to handle the flowrate from the OCGT.
- **Economic analysis** – once the capture and compression technologies have been chosen, the scaled process models will predict the geometries and process requirements. Enabling a cost estimation for the OCGT plants including CO_2 capture and compression. A comparison between the capture technologies will highlight the best available technology for OCGT's in future energy systems. A comparison will also be made against other low-carbon power sources to indicate the viability of implementing CCS for these dispatchable generators.

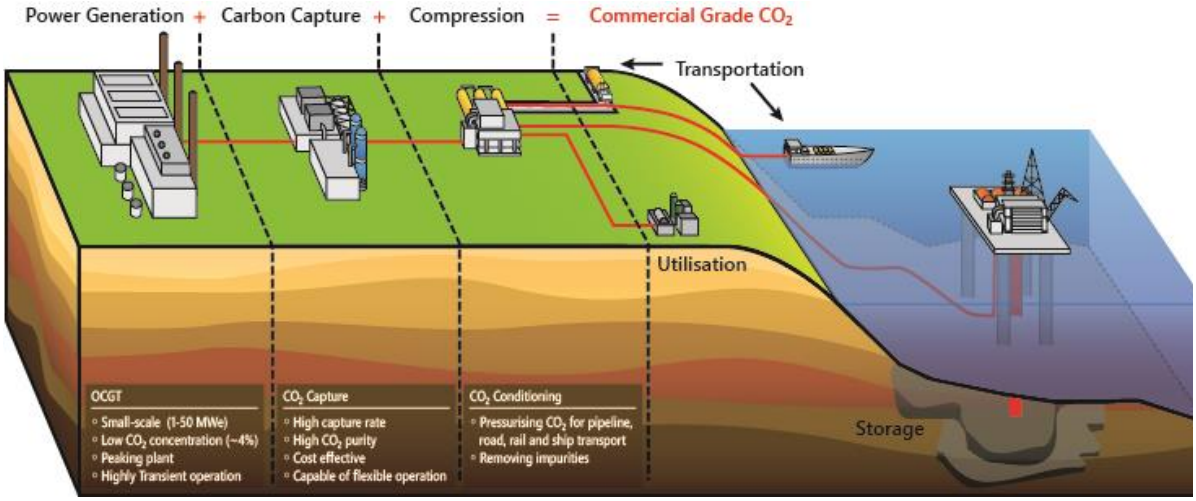

Figure 12: Illustration highlighting the aspects of CCUS investigated in this project (power generation, CO_2 capture, and CO_2 conditioning. Not included in this study is CO_2 transportation, utilisation, or storage.

Currently, no OCGT power generation plants have CO_2 abatement technologies incorporated, therefore, the accuracy of the end results is difficult to corroborate. The fidelity of the process and economic models will provide an insight into the exactitude of the results, they should not be used for engineering design purposes. The objective is to combine the technical and economic evaluations, in order to ascertain the most cost-effective capture technology for OCGT power plants. As these generators are small-scale and typically in decentralised locations, this work will also provide valuable information to small industrial CO_2 emitters.

This thesis is compiled of 8 main chapters, a reference section (Chapter 9), and three appendixes shown in Chapter 10. A brief description of each chapter is shown below.

Chapter 2: Literature Review

- This chapter critically reviews the current literature surrounding post-combustion CO_2 capture, highlighting the most applicable capture and conditioning technologies specifically for quick-response gas turbines. Included in the review, is an update on the international demonstration facilities current in operation and the technical/economic challenges of CCS.

Chapter 3: Modelling and Methodology

- This chapter details and describes the development of the dynamic process models for the chosen CO_2 capture and conditioning technologies. This chapter also explains the economic costing methodology and the assumptions used to calculate the cost of each technology.

Chapter 4: CO2 Capture Results

- This results chapter focusses on the CO_2 capture technologies. For each technology, the dynamic model is first validated against experimental data from the literature. The model is then scaled, and the case study results highlight the key operating parameters and performance indicators for the scaled capture system.

Chapter 5: CO2 Conditioning Results

- The conditioning train model is developed separately to the capture models, in order to compare two different process configurations. The dynamic models are first validated against results from the literature. The results show the comparison between conventional multi-stage compression and sub-critical liquefaction conditioning routes. Included in this chapter is a sensitivity analysis and dynamic study, to highlight the technical challenges of conditioning the small CO_2 stream ready for pipeline transportation.

Chapter 6: Economic Results

- This chapter is dedicated to the economic evaluation of the three main components of low-carbon dispatchable gas turbines: the OCGT plant, CO_2 capture plant, and CO_2 conditioning plant. This chapter highlights the capital cost breakdown, levelised cost of electricity, and cost of CO_2 avoidance for both capture technologies.

Chapter 7: Techno-economic comparison

- Within this chapter, the results from Chapters 4, 5, and 6, are combined and further analysed to techno-economically compare the two different OCGT+CCS options. The results are compared against other low-carbon power sources.

Chapter 8: Conclusion

- This chapter concludes the thesis and gives an overview of all the work that has been completed on this Engineering Doctorate. This chapter also explains the project limitations and highlights future research that should be conducted surrounding this topic.

1.3. Conclusion

Even though the total CO_2 emissions from within the UK is steadily declining, irrefutable damage to the climate has already been done. Maintaining on the current trajectory is not enough to reach the new targets in the Sixth Carbon Budget which aims to reach Net Zero by 2050 at the latest. CCS can aid in delivering low-cost Net Zero through low-carbon dispatchable power generation (grid-stabilisation services), maintaining security of supply, and system inertia. Recently, CCS is gaining more attention globally, with governments allocating large funding schemes to promote and accelerate the uptake of CCS. Emissions of CO_2 come from a range of sources; despite the impressive improvements in the UK energy system, further work is required to achieve the ambitious climate targets.

Energy systems require a varied mix of sources for system flexibility and security. More renewable power sources are required to combat climate change, but to combat their intermittency and connectivity issues, quick-response dispatched power is required. Gas turbines are ideal for this situation, as they have quick start-up times (in open-cycle configuration) and fast ramping capabilities. Currently, OCGTs are considered the best option for 'peaking plants', which come on the system during periods of high demand or during an imbalance between supply and demand. This issue with OCGTs is the combustion of fossil fuels (mainly NG) and the emissions produced. Modern gas turbines are equipped with low-NO_X burners and produce NO_X and CO below the regulatory standards. NG pipeline operators also maintain low levels of sulphur. Therefore, CO_2 is the main emission requiring further investigation.

This project is a techno-economic analysis of transient CO_2 capture technologies for quick-response OCGTs. Analysis of real-world gas turbine operating data will highlight the worst-case scenario for flexible operation, i.e., the most difficult situation future capture plants will have to be capable of handling. This data, alongside information from industrial suppliers, will be transformed into flue gas flowrate profiles. The OCGT itself can be modelled, but investigating real-world data shows the actual technical challenges that will be faced by future capture systems. Therefore, the flue gas flowrate profiles will be used as input parameters into dynamic process models for the chosen CO_2 capture technologies. The objective is to analyse the effect that transient flue gas production has on the capture system, quantifying the change in key performance indicators.

As CO_2 capture is an additional cost to the power generator with no substantial gain in by-product sales, the economics of CCS are extremely important. To not significantly impeded the cash flows for the power generation company, the capture systems need to be cost-effective and as cheap as possible. Therefore, economic models for the OCGT, capture plant, and compression system will be developed to highlight the cost of including CCS for OCGTs.

With the climate crisis and the focus on renewable technologies, it is easy to forget the smaller seemingly insignificant contributors. Large fossil-based power sources have been identified for CCS, but these are not the only emitters in energy systems. This project aims are identifying the technical and economic challenges small dispatchable generators will face in future energy systems. To achieve Net Zero, every source of CO_2 needs to be minimised!

Chapter 2 : Literature Review

This chapter presents a literature review focussing on CCS, specifically the current state-of-the-art CO_2 capture technologies and conditioning systems. The economics of CO_2 capture are extremely important in determining the feasibility of deploying these small-scale generators in future energy systems; therefore, this literature review also includes economic studies for CCS. Alongside the economic barriers, technical challenges for CCS technologies are also discussed within this chapter.

2.1. Carbon Capture and Storage (CCS)

There are three main categories for CO_2 capture on power generation sources: post-combustion, pre-combustion and oxy-combustion. Figure 13 highlights the technology readiness level (TRL) of various CCS technologies: post-combustion capture using amines is TRL9 (commercial), so too is pre-combustion capture for natural gas processing using the Selexol process, and oxy-combustion is currently at TRL7 (demonstration) [44, 45]. An up-to-date list of commercially available CCS technologies for power and industry can be found in the recent technical report by the Global CCS Institute [46].

This project focuses on post-combustion capture (PCC) as it can be easily retrofitted onto existing plants and does not affect the operation of the gas turbine. As of 2021, only two power generation sources have large-scale CO_2 capture attached: Boundary Dam in Canada (using Shell's Cansolv solvent) and Petra Nova in the United States (using Mitsubishi's KS-1 solvent) [47]. For this study it is important the capture systems are capable of:

- Capturing >90% CO_2 at a high purity (>95%) [48].
- Scalable to handle flow from a small-scale gas turbine (1-50 MWe).
- Operate flexibly, i.e., with a high degree of transient flue gas input.
- Cost-effective, as these generator work in the capacity market and have a low load factor.

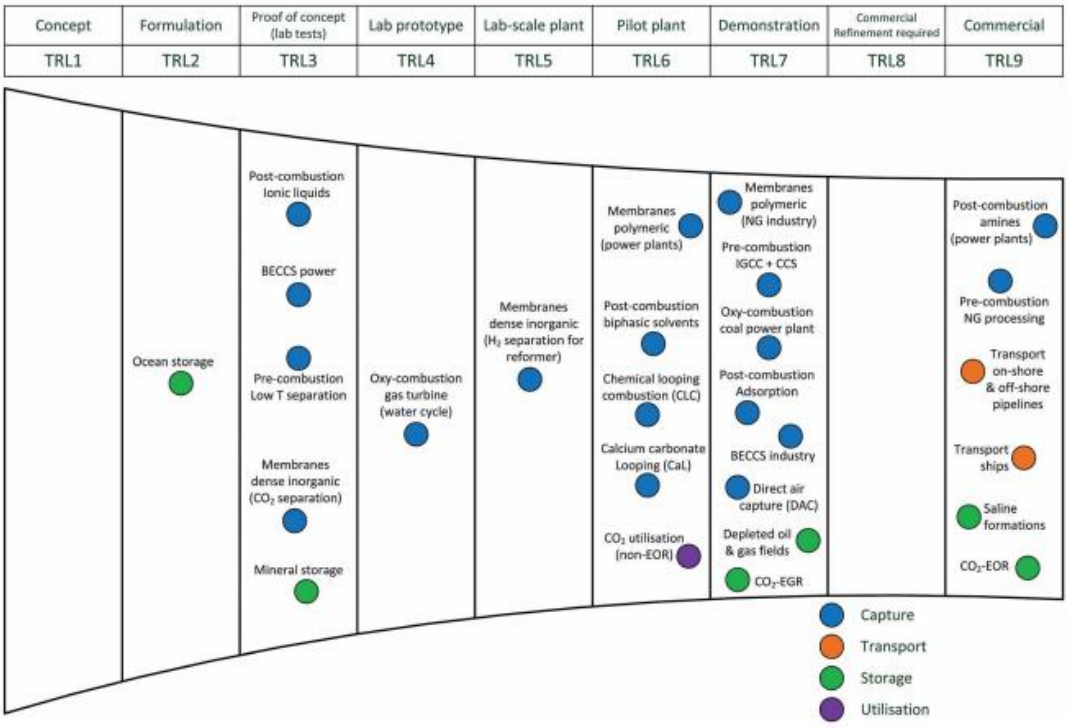

Figure 13: Technology readiness levels for carbon capture, utilisation, and storage technologies [44]

2.2. Post-combustion CO_2 capture Technologies

Several sources have reviewed CO_2 capture technologies specifically for PCC [49, 44, 50, 51, 52]. Figure 14 highlights the various technologies currently investigated in the literature and commercially. Within this section, the CO_2 capture technologies reviewed are chemical/physical absorption, adsorption, membrane separation, chemical looping, and fuel cell integration. Technologies such as microalgae bio-fixation [53] and cryogenic distillation [54] have scalability issues; therefore, they are not considered feasible for this particular application.

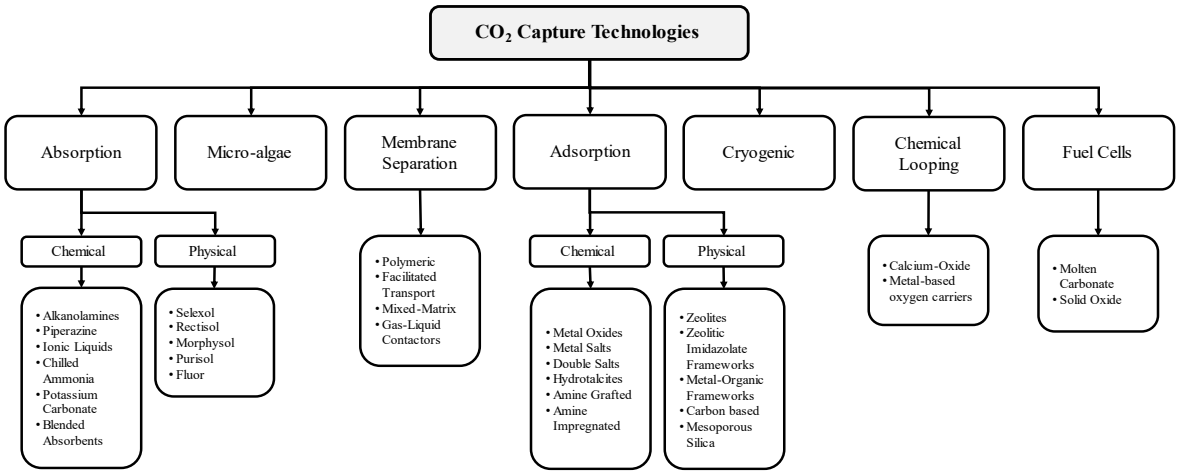

Figure 14: Post-combustion CO_2 capture technologies

2.2.1. Absorption

The sorption of a fluid absorbate into a solid/liquid absorbent is the process of absorption and is classified into two categories: chemical and physical. Both chemical and physical absorption have been used to commercially capture CO_2 (TRL9) [44]. This section reviews both absorption techniques, and their applicability for OCGT-PCC.

2.2.1.1. Chemical Absorption

Liquid-phase chemisorption (Figure 15) is a commercially available CO_2 capture technology. The benchmark solvent for this technology, and PCC in general, is 20-30 wt. % aqueous Monoethanolamine (MEA) in a packed bed. In absorption systems the gas and liquid flow in counter current configuration, and mixing is enabled by packing material (randomly or structured) or by horizontal trays. 'Lean' solvent (containing little/no CO_2) enters the column and 'rich' solvent (containing the absorbed CO_2) leaves at the bottom [55]. The reboiler duty for MEA absorption is between 3.6-4.0 GJ/tCO_2. Other solvent-based processes include alkanolamine absorption, aqueous ammonia absorption, chilled ammonia process, dual-alkali absorption, and sodium carbonate (Na_2CO_3) absorption [44].

As amine-absorption is considered the benchmark PCC technology and is [44], this is the chemical absorption method further discussed in this chapter. The most commonly accepted reaction mechanism for primary and secondary alkanolamine reactions with CO_2, includes the formation of zwitterions which instantaneously neutralise to form a carbamate [56]:

$$CO_2 + RNH_2 \leftrightarrow RNH_2^+COO^- \quad 6$$

$$RNH_2^+COO^- + RNH_2 \leftrightarrow RNHCOO^- + RNH_3^+ \quad 7$$

Tertiary amines such as Methyldiethanolamine (MDEA) are advantageous because they do not form carbamates and have a lower heat of regeneration than MEA. MDEA ($C_5H_{13}NO_2$) reacts to form bicarbonate ions [56]:

$$CO_2 + R_1R_2NR_3 + H_2O \leftrightarrow \ R_1R_2NR_3H^+ + HCO_3^- \quad (8)$$

MDEA is highly selective of H_2S over CO_2 at low pressures; thus, for CO_2 capture, the sorption pressure is approximately 50 bar. However, tertiary and hindered amines react too slowly to be used on their own. The sorption pressure for MDEA can be reduced to 25 bar with the addition of Piperazine (PZ), a chemical solvent that reacts with CO_2 similarly to the primary amine above. PZ ($C_4H_{10}N_2$) is a heterocyclic diamine and can further react with bicarbonate ions, leading to an increased mass transfer rate. The reaction of PZ with bicarbonate ions is:

$$C_4H_{10}N_2 + HCO_3^- \leftrightarrow (C_4H_9N_2)COO^- + H_2O \quad (9)$$

$$(C_4H_9N_2)COO^- + HCO_3^- \leftrightarrow (C_4H_8N_2) - (COO^-)_2 + H_2O \quad (10)$$

Piperazine limits the thermal degradation of MDEA, reducing the frequency of regeneration. For PCC, a blend of 50 wt. % H_2O, 45 wt. % MDEA, and 5 wt. % PZ, provides increased stability and 50% more CO_2 loading capacity compared to MEA [57]. Freeman et al. [58] and Rochelle et al. [59] investigated the use of PZ, and showed the main challenges come from the formation of precipitates and nitrosamines. MDEA and PZ blends have the greatest rate of CO_2 absorption, highlighted in Table 3. Another amine blend is PZ and 2-Amino-2-methyl-1-propanol (AMP), which has shown 20% lower reboiler duties. AMP is a sterically hindered amine, and forms weak carbamate salts, leading to a lower regeneration cost. These blends are limited to 40 wt. % with 5 wt. % PZ, to limit precipitation and deliver fast mass transfer rates [44]. Blends have become increasingly popular due to the possibility of combining the high absorption rates of primary and secondary amines, the high capacity of tertiary amines, and the lower enthalpy of regeneration of sterically hindered amines. The choice of solvent determines the kinetics and thermodynamics of the process [55].

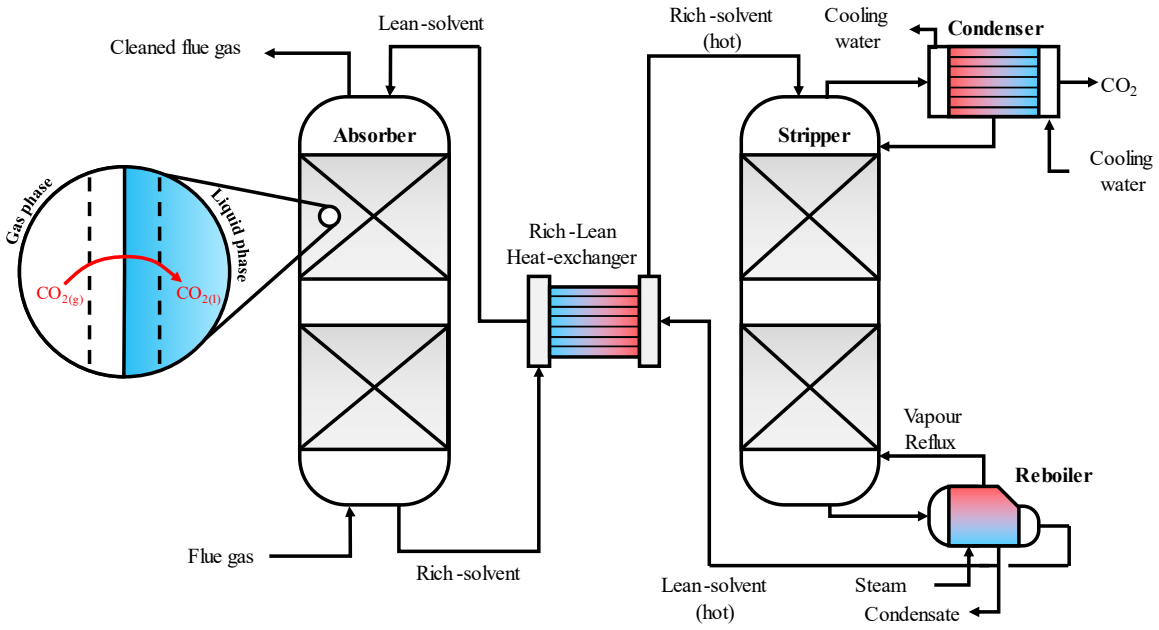

Figure 15: Absorption illustration and process design, adapted from [55]

Industrial absorption comprises of an absorber and stripping column. The packing material is typically structured and designed to give the maximum specific surface area and low pressure drop. The stripping column separates the solvent and absorbate using a temperature swing, with a condenser at the top to reflux the liquid and reboiler at the bottom to heat the incoming solution. This regeneration produces the highest energy penalty and takes place at 120°C and 0.2 MPa. This low pressure is an issue for transportation and storage [60]. An amine system on a modern power plant will decrease the thermal efficiency by approximately 30%, this includes capture, compression, transport, and storage [55].

Another solvent of interest in the literature are Ionic liquids (ILs). They consist of anions, cations and functional groups which deliver high CO_2 selectivity, solubility and designability. Liu et al. [61] compared MDEA and ILs, the study found the ILs decreased the energy demand by 42.8 and 66.04%, for single and multi-stage processes respectively. However, ILs are mostly synthesized at laboratory scale with a complex and costly synthesis process. They are not yet commercially viable; however, there are promising enhancement solvents that can be used to improve amines and membranes [62].

Table 3: Comparison of different amines [63]

Solvent	**mol**	k_{abs} **x** 10^7 **(mol/m²/Pa)**	**Capacity (mol/kg)**	$-H_{abs}$ **(kJ/mol)**	T_{max} **(°C)**	P_{max} **bar**	$P_{h_2 0}/P_{CO_2}$
AMP	5	2.4	0.96	73	140	6.1	0.49
MEA	7	4.3	0.47	70	121	2.2	0.81
MEA	11	3.6	0.66	70	125	2.7	0.67
PZ	8	8.5	0.79	64	163	14.3	0.33
PZ/AMP	5/2.3	7.5	0.7	71	134	4.5	0.54
PZ/AMP	2/4	8.6	0.78	72	128	3.4	0.63
PZ/MEA	2/7	7.2	0.62	80	104	0.7	1.38
MDEA/PZ	5/5	8.3	0.99	70	120	1.8	0.92
MDEA/PZ	7/2	6.9	0.8	68	120	1.4	1.15

Operating a capture plant with a high degree of transient operation can affect the performance of the process, and several studies, shown in Table 4, have presented experimental results for dynamic PCC operation. Tait et al. [64] performed pilot-scaled testing of Flexible-PCC operation at the UKCCSRC Pilot-scaled Advanced Capture Testing (PACT) facility. The test campaign looked at amine-absorption using approximately 30 wt.% MEA, demonstrating six dynamic operating scenarios based on a >500MW supercritical coal fired power station. In the shutdown procedure, the flue gas decreases to a minimum stable generation (MSG) point, below which the quantity of impurities is too high due to incomplete combustion. During the hot start-up procedure, the steam flowrate to the reboiler is introduced immediately to promote capturing CO_2 as quick as possible. The cold start-up scenario starts from the MSG point set at 30% baseload, then waits for the low-pressure steam turbine to reach full load before sending steam to the reboiler. There is an 18.6% reduction in daily emissions when performing a hot start-up compared to a cold start-up. Therefore, starting the capture plant once the GT is hot is a potential method to improve PCC performance. Interestingly, Tait et al. [64] discusses a frequency response scenario where steam for the reboiler is re-directed to the low-pressure steam turbine, to increase the coal plant power output. This increase is marginal compared to the power output of the plant. Also, when operating in open cycle configuration there is no steam turbine, therefore, for small-scale gas turbines (<50MW) steam re-routing is not a viable option.

Tait et al. [65] performed a set of dynamic experiments on gas-PCC, using 30 wt. % MEA at the Sulzer Chemtech pilot-scale facility in Winterthur, Switzerland. The authors presented five different dynamic operating scenarios, including a frequency response scenario where the steam flowrate to the reboiler

increases by 200%, representative of a situation where power output needs to be rapidly decreased to maintain grid frequency within allowable limits. The study highlighted no significant barriers to flexible use of gas-PCC. Moreover, the authors suggest altering the power output every 30 minutes to match settlement period in GB.

Montañés et al. [66] presented experimental results for the transient performance of control mechanisms for Flexible-PCC operation, for treatment of flue gas from a combined cycle combined heat and power plant at Technology Centre Mongstad (TCM). The dynamic experiments changed the flue gas, solvent, and steam flowrates to investigate capture plant ramping. These are the main three parameters manipulated in Tait et al. [64]. The capture plant ramping scenario is similar to the benchmark flexible operating scenario in Mac Dowell and Shah [67]. The results in Montañés et al. [66] showed that following a perturbation, the system took approximately 1 hour to reach steady-state. In a recent study Bui et al. [68] demonstrated three flexible operating scenarios at the TCM CO_2 capture facility, accompanied with dynamic modelling. The study found the stabilisation time (to allow complete solvent circulation and homogenous solvent compositions) is a minimum of three hours, although the report does state this time would be as quick as possible in a commercial system. Also, the demonstration scale plant took as long as 114 minutes to transition to new operating conditions following a change in one or more of the main process parameters. This is known as the transition time, and is difficult to incorporate into process models, and Bui et al. [68] concludes further improvements in the dynamic response of PCC models is required.

Table 4: Pilot plants evaluating flexible operation and performance of PCC using MEA as the solvent

Pilot facility	**Flue gas source**	**CO_2 feed (%)**	**Flue gas flowrate**	**Source**
Brindisi, Italy	Coal	11-12 vol.% dry	10,000 Nm^3/h [a]	[69]
CSIRO, Australia	Brown-Coal	10-11 vol.% wet	50 kg/h	[70]
Sulzer Chemtech, Switzerland	Natural Gas	4.27 vol.%	120.5 Nm^3/h [a]	[65]
Technology Centre Mongstad, Norway	Natural Gas	4.12 vol.% wet	60,000 Sm^3/h [b]	[66]
PACT, England	Coal	12 vol.%	200 Nm^3/h [a]	[64]

[a] N stands for nominal, which is at 0°C and 1 atm, [b] S stands for standard, which is 15°C and 1 atm

2.2.1.1. Physical Absorption

Physisorption using commercial solvents such as Selexol®, Rectisol®, Fluor® and Purisol® are more suited to high pressure and high CO_2 concentrations (35-40%). Typically used for acid-gas removal in natural-gas sweetening, CO_2 separation in Integrated Gasification Combined Cycles (IGCC), and the purification of syngas, hydrogen, and ammonia [71].

Physical solvents are highly selective of both H_2S and CO_2, with a large enough selectivity difference to recover each in separate stages [57]. The Rectisol® process uses Methanol (MeOH), a polar protic solvent, to separate H_2S and CO_2 from a syngas stream. It has a lower selectivity than Selexol®, however, it can operate at very low temperatures and can remove other contaminants such as NH_3, HCN and Carbonyls [72]. The Selexol® process uses dimethyl ethers of polyethylene glycol (DMPEG), Figure 16 is the process schematic for a dual-stage Selexol process for H_2S and CO_2 separation from syngas capable of achieving high CO_2 recovery (>90%) and high purity (>95%) [73, 74].

Table 5 highlights the relative solubilities of components in the Selexol and Rectisol solvents. Due to the high H_2O affinity, the moisture into the absorber must be kept low [75], this is an issue for wet flue gases. It is used as the base case for pre-combustion CO_2 capture in IEAGHG report [60], in which the cost and performance of different CO_2 capture technologies is assessed. As physical absorption systems are tailored towards pre-combustion capture, they are not considered applicable for this study.

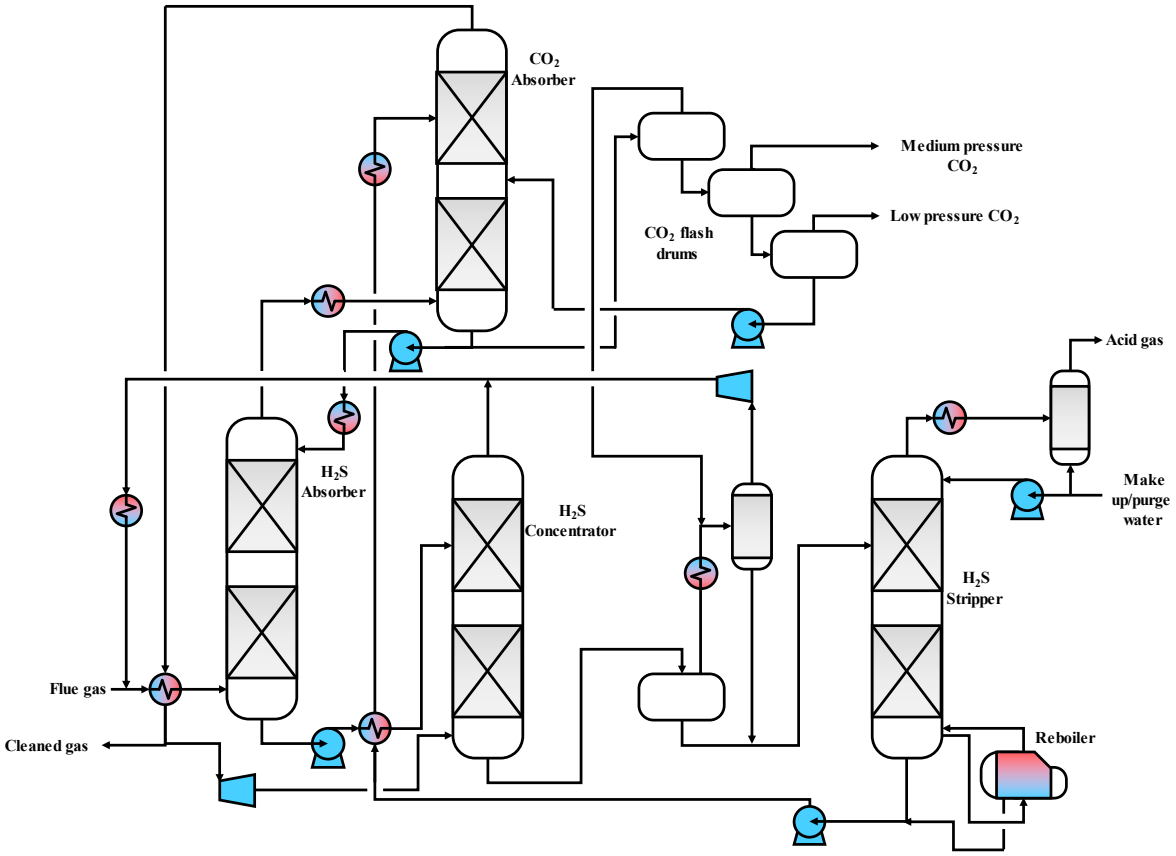

Figure 16: Dual- stage Selexol process for H_2S and CO_2 seperation, edited from [74]

Table 5: Relative solubilities of components in the Selexol and Rectisol solvents [75]

Component	Relative Solubility	
	Selexol®	Rectisol®
Carbon Dioxide (CO_2)	1.00	1.00
Water (H_2O)	730	300
Hydrogen (H_2)	0.013	0.0078
Methane (CH_4)	0.066	0.038
Ethane (C_2H_6)	0.42	0.17
Propane (C_3H_8)	1.01	0.51
Butane (C_4H_{10})	2.37	1.75
Pentane (C_5H_{12})	5.46	5.0
Hexane (C_6H_{14})	11.0	13.5
Heptane (C_7H_{16})	23.7	29.2

2.2.2. Adsorption

Adsorption is the adhesion of atoms, ions, and molecules of a fluid on to the surface of a solid material. It can be physically adsorbed (physi-sorption) involving weak van der Waals forces, or chemically adsorbed (chemi-sorption) with stronger covalent bonds. Chemical adsorbents such as hydrotalcites, metals oxides and amine loaded materials, have a similar regeneration issue experienced by amine absorbents. Several physical adsorbents have been extensively researched: zeolites, metal organic

frameworks (MOFs), silicas, and carbonaceous material [76, 77, 78, 44, 79]. Physical adsorption is advantageous because no new bond is formed. Enabling the possibility of pressure, temperature or vacuum swing regeneration at a much lower cost compared to amine-absorption. The adsorption methods are discussed below:

- **Pressure swing adsorption (PSA)** – adsorption occurs at higher than atmospheric pressure and desorption occurs at a lower pressure [78].
- **Temperature swing adsorption (TSA)** – adsorption occurs at elevated temperatures with the bed heated directly via a hot gas feed or indirectly via heating jackets or electric coils [80].
- **Vacuum swing adsorption (VSA)** – adsorption occurs at atmospheric pressure and desorption occurs under vacuum pressure [81].

Ben-Mansour et al. [78] provides an extensive review of physical adsorption and discusses various regeneration processes. The study highlights fixed bed pressures swing adsorption (PSA) as an economic option because of its comparatively simple application, low energy demand, and low investment cost. PSA is best suited for systems with high CO_2 partial pressure, ideal for pre-combustion capture in IGCC's. For post-combustion capture vacuum swing adsorption (VSA) is attractive as the feed stream is at atmospheric (or slightly elevated) pressure. However, PSA/VSA systems suffer scalability issues and multiple beds are required to deliver the specifications for downstream compression equipment [44]. With the relatively low thermal regeneration temperatures, and the availability of waste heat from the flue gas, Zanco et al. [82] suggests the more effective option would be temperature swing adsorption (TSA). In the literature high purities and recovery rates can be obtained by combining processes, i.e., pressure-temperature swing adsorption (PTSA), vacuum-pressure swing adsorption (VPSA) or vacuum-temperature swing adsorption (VTSA) [83, 84, 85, 86].

Material selection is crucial to economically capture CO_2 and recent advances have focused on discovering adsorbents that have a high CO_2 affinity, CO_2 capacity, material stability, good scalability, and low energy demand (for desorption). The characterisation of various commercially available physical adsorbents is shown in Table 6. Activated carbon is a carbonaceous adsorbent, which can be produced at low cost with good thermal stability, large porous surface area, high hydrophobicity, and can be used at atmospheric pressure and temperatures [87]. They have a good affinity to CO_2, but as shown in Table 6 it is lower than other adsorbent materials. Zeolites are the most commercially mature absorbent material, with Zeolite 13X repeatedly used in hydrogen production through PSA [88]. Synthetic Zeolites (such as Zeolite 5A and 13X) have highly crystalline structures, with high surface area to volume ratios. Although Zeolites have a moderate CO_2 loading, they suffer from a low selectivity of CO_2 over N_2, especially in the presence of moisture [89]. MOFs also have a crystalline structure and can be synthesised to have extremely large surface area and pore volumes, with a higher CO_2 capacity than both activated carbons and zeolites [44]. However, currently they are not manufactured at large scale and have a poor economic efficiency. MOFs also have problems with instability due to impurities in the flue gas and are more suited to low temperatures due to thermal degradation [78].

Traditional carbon capture adsorbents rely on a pre-treatment stage to remove SO_X and NO_X as they compete for adsorption sites. SO_X has a higher acidity, and NO_X has a higher polarity and adsorption strength, resulting in preferential adsorption. They also have the potential to permanently adsorb onto adsorption sites, reducing the effectiveness of capturing CO_2 [90]. Bui et al. [44] highlighted the recent advances have provided a low-cost alternative to liquid scrubbing systems for mid-size operations. However, for large scale processes the handling of solids becomes more complex and difficult.

Only a small number of studies have presented pilot-scale data for CO_2/N_2 adsorption systems, see Table 7. Wang et al. [85] achieved >90% capture and >95% purity with a two-unit VPSA system. The energy consumption is a sum of the power demand from blowers and pumps in the pilot facility. The on-site Watt metres measured a power demand of 2.44−2.65 MJ/kgCO_2. Lower than the 3.6-4.0 MJ/kgCO_2 for amine-absorption using the benchmark 30 wt.% MEA [44]. Several studies have

highlighted the potential for fluidised beds [91, 92, 93] and moving beds [94, 95, 96], however, as the majority of adsorption studies in the literature focus on fixed columns, this is the equipment further investigated in this study. Also, from Table 7, Zeolite 13X is the most studied post-combustion CO_2 capture adsorbent, due to its high CO_2/N_2 selectivity and high adsorption capacity at low CO_2 partial pressure [96].

Table 6: Comparison of different adsorbent materials

Adsorbent Material		T (°C)	P (kPa)	CO_2 (mol %)	Adsorption (mmol/g)	Surface Area (m^2/g)	Selectivity (CO_2/N_2)	Ref.
Activated Carbon	NORIT R2030CO2	30	120	17	2.4	942	7	[97]
	CFC	25	101.3	13	3.1	490.6	-	[98]
	Cu/Zn-20%AC	30	100	15	2.26	599.41	-	[99]
	Cu-20% AC	30	100	15	1.99	645.21	-	[99]
Zeolites	Zeolite 13X	50	100	15	3	585.5	-	[100]
	Zeolite 13X	25	120	25	4.5	-	-	[84]
	Zeolite 13X-APG	30	100	15.9	4.3	-	-	[84]
	Zeolite A5	30	100	16	3	499	-	[101]
MOF	Mg2-MOF-74	40	100	15	7.5	1800	63	[102]
	Na-rhoZMOF	25	100	20	6.2	-	440	[103]
	Mg-rhoZMOF	25	100	20	8	-	680	[103]
	MIL-101 (Cr)	30	101.3	15	1.05	3360	5.5	[104]

Jiang et al. [105] compared VPSA, TSA and TVSA configurations at lab-scale and found VPSA to be more effective due to a lower energy consumption and higher CO_2 productivity. VPSA systems have been investigated from lab- to pilot-scale [106, 107, 108, 85, 105] and usually comprise of two stages. The first stage captures >90% of the CO_2, and the second stage is used to increase the purity to >95% [109]. Luberti et al. [110] provides the design and simulation of a rapid VPSA process for PCC on a 10 MWth biomass combined heat and power (CHP) plant, the adsorption set-up is illustrated in Figure 17. To handle the high flowrates and overcome scalability issues of adsorption processes, the 1st stage the flue gas stream is split into two parallel two-bed VPSA units, to capture >90% CO_2. The 2nd stage, another two-bed VPSA unit, is used for purification to obtain >95% CO_2. The study uses a Skarstrom style four step adsorption configuration, shown in Figure 18. The steps are 1) pressurisation with the feed, 2) adsorption of CO_2 onto the sorbent material, 3) counter-current blowdown to remove non-adsorbed component, and 4) counter-current product purge. Other studies use more complicated step configurations with multiple columns interacting simultaneous, evident in the pilot studies shown in Table 7 and computation studies shown in Table 49 in Appendix A, although they do not offer any major advantages (in terms of capture rate and purity) over the more simplified designs.

Rui et al. [111] analysed CO_2 capture from flue gas using VPSA under unstable feed concentrations. The model-based study incorporated proportional integral derivative (PID) control strategies (closed-loop and open-loop feedback control) to adjust adsorption step duration for product quality control

during variable feed concentration. To the author's knowledge, adsorption technologies for Flexible-CCS have not previously been investigated.

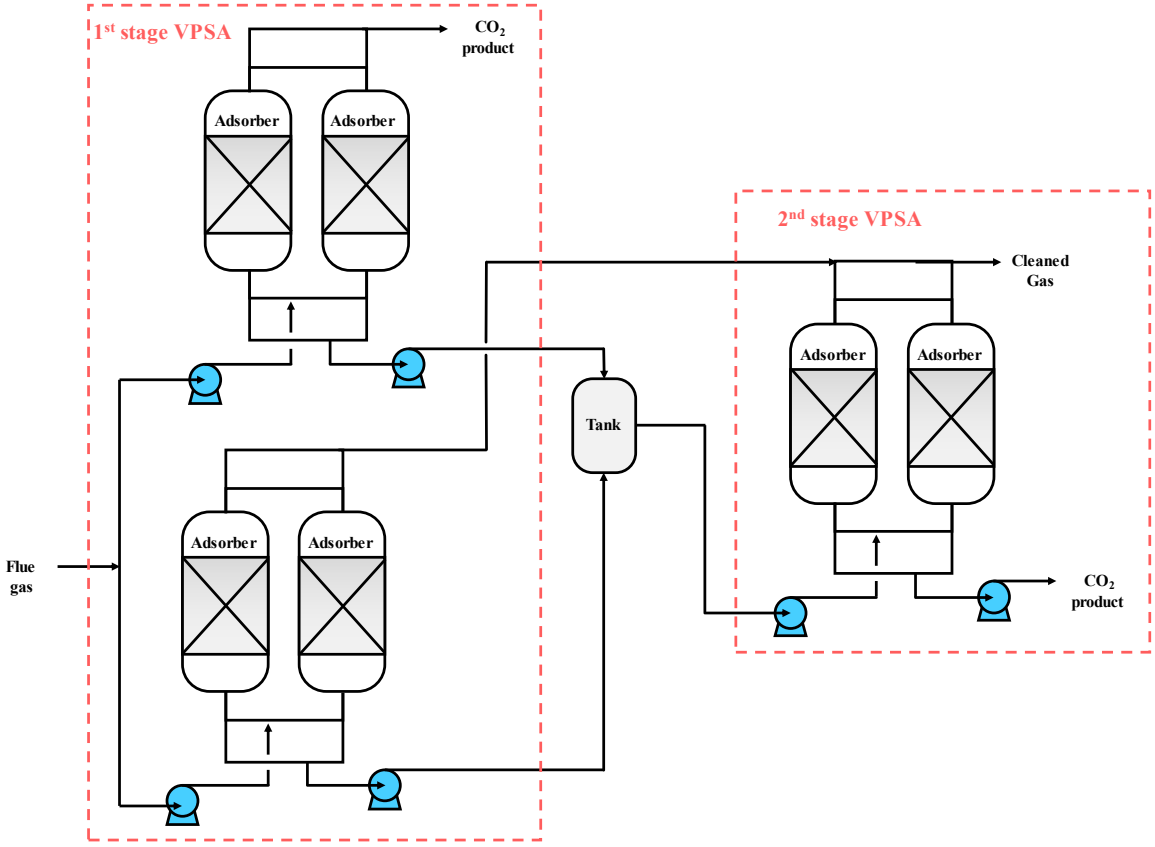

Figure 17: Two-bed two-stage RVPSA modified from Luberti et al. [110]

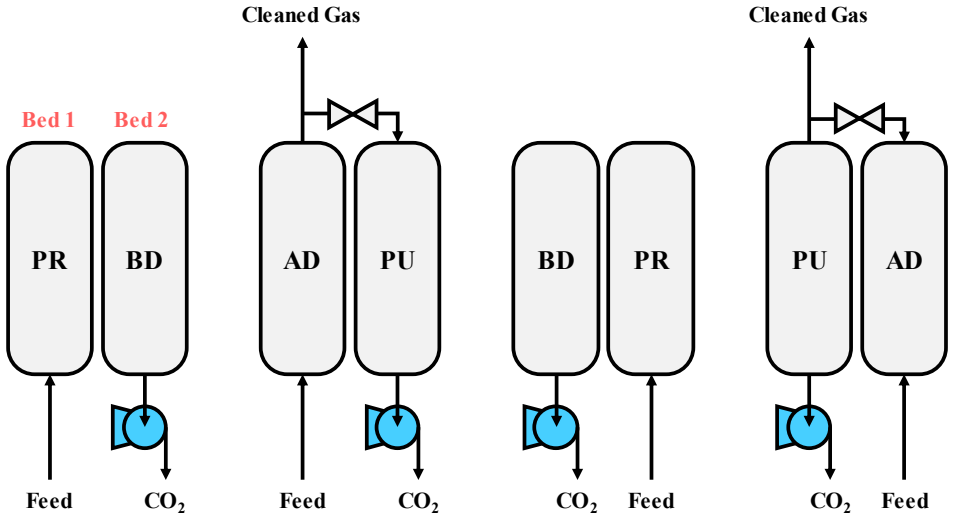

Figure 18: Two-column four-step adsorption configuration from Luberti et al. [110].

PR = pressurisation, AD = adsorption, BD = blowdown, and PU = purge.

Table 7: Pilot-scale studies of CO_2 adsorption from flue gas

Source	System	Configuration	CO_2 Feed (%)	Feed Flowrate	Recovery (%)	Purity (%)	Energy Consumption
[112]	PTSA	First stage is a PTSA unit, second stage is a PSA unit, using a Ca-X type zeolite. Feed comes from a dehumidifier unit attached to Yokosuka Thermal Power Station (coal and oil fired)	11.5	1000 N m^3/h	90	99	560 kWh/t-CO_2
[113]	TSA	Single bed TSA system with simulated flue gas. Lab scale comparison of Zeolite 13 X and 5A	10	20 N m^3/min	13X=65	13X=94	8.8 MJ/kgCO_2
					5A=83	5A=98	6.4 MJ/kgCO_2
[114]	VSA	Three bed VSA system using Zeolite 13X, evaluating the performance of 6 and 9 step cycles	8-22	66-115 L/min	6 step = 60-80	6 step = 82-83	6 step = 4-8 kW/tCO_2
					9 step = 60-70	9 step = 90-95	9 step = 6-10 kW/tCO_2
[107]	VPSA	Three bed seven step VPSA unit removes CO_2 from an existing coal-fired power station using Zeolite 13X APG	15	32.1-45.9 N m^3/h	79	85	2.37 MJ/kg
[85]	VPSA	The first unit is a 3 bed 8 step VPSA system using Zeolite 13X APG, the second unit is a 2 bed 6 step VPSA unit with activated carbon beads.	15-17	35.5−37.0 N m^3/h	90.20	95.60	2.44 MJ/kgCO_2
[115]	VSA	Single bed four step VSA with simulated flue gas feed for the basic system. Two bed four step VSA for the light product pressurisation (LPP) system. Both using Zeolite 13X	15	1000 SLPM	Basic: 95.9±1	Basic: 86.4±5.6	Basic: 472.2±36.7 kWh /tonne CO_2
					LPP: 94.8±1	LPP: 89.7±5.6	LPP: 475±36.7 kWh /tonne CO_2
[116]	VPSA	Dual-Reflux VPSA in four fixed beds using two different activated carbon adsorbents within a single bed. Using a flue gas from a 460MW CFB boiler.	11.1	100 N m^3/h	8 step = 42.7	8 step = 78.4	8 step = 764 kWh/MgCO_2
					9 step = 30.2	9 step = 89	9 step = 978 kWh/MgCO_2

2.2.3. Membrane Separation

Membranes are used for the physical separation of two or more components into a retentate and a permeate stream, by the use of a semipermeable barrier, illustrated in Figure 19. Membranes have been used for natural gas sweetening to reduce the CO_2 concentration >2% [117]. However, it is economically unfavourable with a low feed concentration or high-purity product requirement. There are also different characteristics between CO_2/CH_4 and CO_2/N_2 separation, such as the high feed pressure which delivers the driving force. In solution-diffusion theory the mass transport of a species across a membrane is proportional to the driving force (pressure/concentration gradient) and membrane thickness. Many studies have reviewed membrane technologies, highlighting that the two most important properties are selectivity and permeance [118, 119, 120, 121]. A comparison of different membranes is shown in Table 8, they can be classified into [119]:

- **Non-facilitated transport membrane (NFTM)** – the permeate dissolves then diffuses through the membranes, the process is called 'solution-diffusion'. Diffusion is governed by Fick's first law of diffusion. Due to the materials (typically polymeric membranes) swelling and plasticisation their limited to low temperature application.
- **Facilitated transport membrane (FTM)** – also follow solution-diffusion, but also have an active transport mechanism. Increasing the permeability and selectivity of the material. CO_2 reversibly reacts with a carrier (amines or ionic liquids), which then diffuses through the membrane.
- **Mixed matrix membrane (MMM)** – polymeric membranes are filled with inorganic particles (zeolites, carbon nanotubes, and MOFs) to improve gas separation and thermal stability. These types of membranes are gaining more attention and are the future of membranes separation process [121].

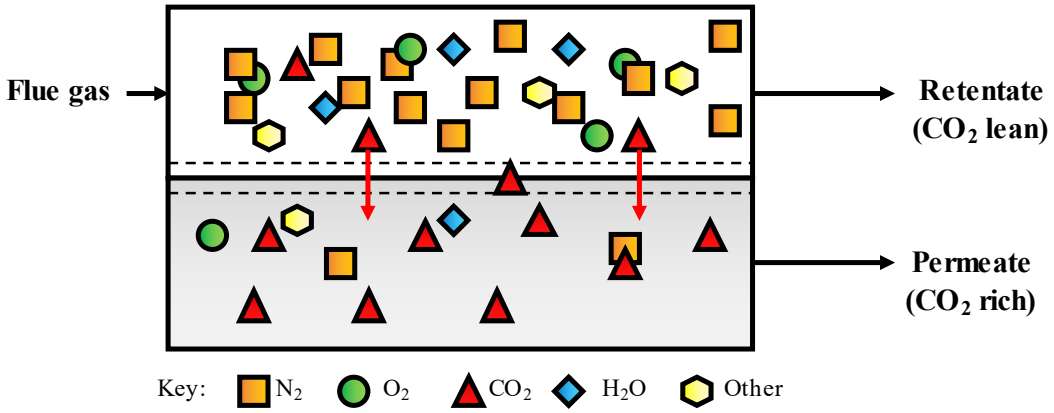

Figure 19: Illustration of CO_2 membrane separation from flue gas, adapted from Khalilpour et al. [119]

Single-stage membrane technologies cannot achieve a high enough purity and separation, due to the low CO_2 concentration in flue gas. For economic design, two and three-stage membranes systems are used industrially. When high quality permeate and retentate streams are required, the configurations in Figure 20 are the most efficient [119]. Yang et al. [122] investigated the use of membranes for post-combustion CO_2 capture, with the goal of >90% CO_2 separation, and >95% purity. The study showed for two stage membrane technologies to be competitive with amine absorption, the CO_2/N_2 selectivity needs to be moderately high (52) and the CO_2 permeance should be high (410 GPU or 135.5 mol/m^2/s/Pa). To deliver the driving force for gas separation, the flue gas can be compressed and the permeate side is under atmospheric conditions.

Table 8: Transport properties of various gas permeation membranes

Membrane		Feed gas composition	Operating condition	CO_2/N_2 selectivity	CO_2 permeance (Barrer)	Reference
NFTM	PEO	-	25°C, 0.79MPa	140	12	[123]
	PolyActive™ with 40 wt.% PEG-DBE	28% CO_2, 972% N_2	30°C, 1MPa	52	150	[124]
	PolyActive™ with 40 wt.% PEG	28% CO_2, 972% N_2	30°C, 1MPa	49	208	[124]
	PolyActive™ with 40 wt.% PEG-BR	28% CO_2, 972% N_2	30°C, 1MPa	50	400	[124]
	PolyActive™ with 40 wt.% PEG-DBE	28% CO_2, 972% N_2	30°C, 1MPa	40	700	[124]
	Pebax®	100% CO_2	30°C, 0.06MPa	45	73	[125]
	Pebax®-PEG	100% CO_2	30°C, 0.06MPa	47	151	[125]
FTM	PEI/PVA	6.5% CO_2, 93.5% N_2	25°C, 0.1MPa	160	850	[126]
	PVAm/PVA	10% CO_2, 90% N_2	25°C, 0.2Mpa	160	307.33	[127]
	PVAm–EDA/PS	20% CO_2, 80% N_2	22°C, 0.2MPa	106	607	[128]
	DAPA/PVA-PAA	9.9% CO_2, 90.1% N_2	125°C, 0.3MPa	700	0.951	[129]
	([emim][B(CN)4]) /PVDF	50% CO_2, 50% N_2	35°C, 0.2MPa	41.1	1778	[130]
MMM	Pebax®-PEG-DME	100% CO_2	30°C, 0.06MPa	43	606	[131]
	Pebax®-Fumed Silica	50% CO_2, 50% N_2	25°C, 1.2MPa	82.10	86.2	[132]
	PVAm-ZIF-8	15% CO_2, 85% N_2	1.1MPa	83	297	[133]
	Pebax®-PEG-PEI-GO	10% CO_2, 90% N_2	30°C, 0.2MPa	120	1330	[134]
	Pebax®-UiO-66	50% CO_2, 50% N_2	25°C, 0.3MPa	61	140	[135]

Another strategy is that the flue gas is kept under atmospheric conditions and the permeate is under vacuum conditions. The vacuum strategy has been shown to have a lower energy consumption and 35% less CO_2 capture cost [136, 137, 138, 139]. Turi et al. [140] compared a two-stage membrane system using the vacuum strategy against the benchmark MEA. The study found the membrane system is cost competitive. However, to offer a significant advantage over MEA, membrane technologies must have a better material permeance (>3500 GPU) and lower cost (>50 US$/m^2).

Yuan et al. [141] computationally investigated membrane-based capture from a natural gas power plant that has flexible electricity generation. The optimisation study showed the model is sensitive to market conditions (electricity demand, electricity price, and carbon price) and the optimal design is a balance between capital and operating costs. Asadi and Kazempoor [142] techno-economically evaluated membrane-based capture for Flexible-PCC. The membrane cost was set at 50 $/m^2, and the economic model showed a counter-current membrane design with feed compression and a sweep gas has the lowest costs (22.76 $/t$CO_2$). Interestingly, the design with the highest cost was a cross-flow vacuum system (118.90 $/t$CO_2$), had the lowest specific energy demand (0.492 MWh/tCO_2) of all the designs (0.765-1.221 MWh/tCO_2).

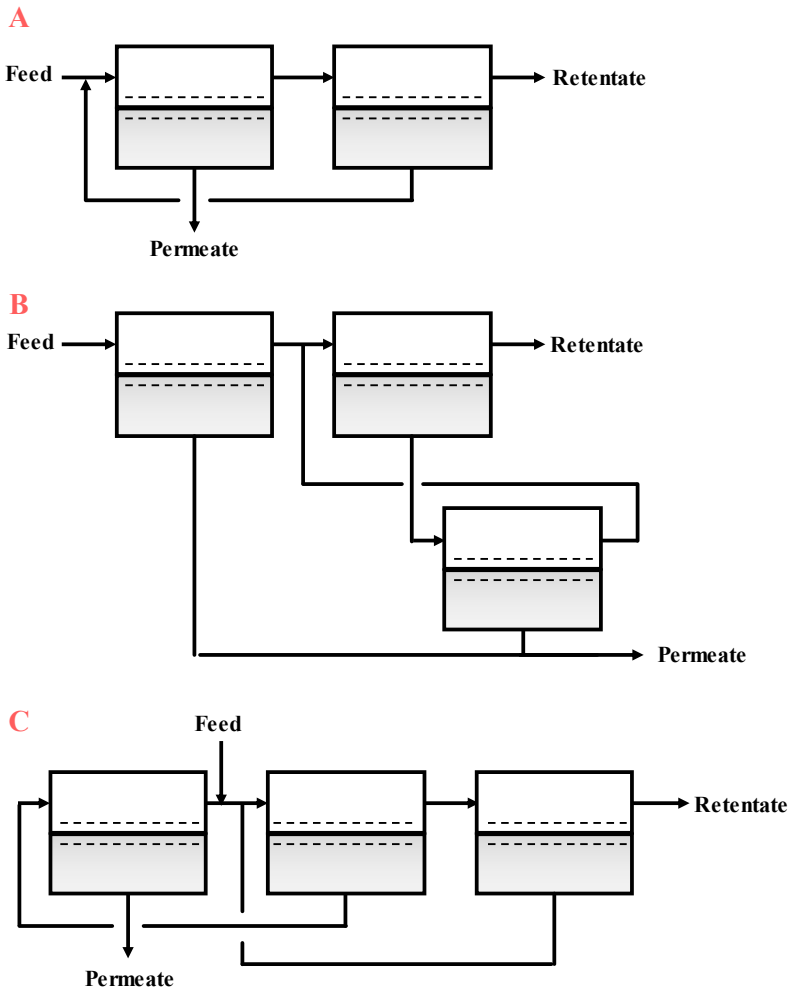

Figure 20: A) Two-stage stripper in series permeator, B) Single permeation stage in series with two-stage permeation cascade, and C) Two stage stripping with one-stage enriching [119].

Membrane based CO_2 separation has been investigated for hydrogen production (TRL5), power generation (TRL6), and natural gas reforming (TRL7) [44]. Table 9 shows the current pilot-scale studies for membrane-based CO_2 capture from power generation sources. MTR's Polaris™ membrane has been tested at the Wyoming Integrated Test Center (WITC) [143], and there are plans in Phase III to scale the design to handle approximately 10MWe of flue gas from the coal-fired Dry Fork power station [144]. Membranes for PCC are continuously improving; however, due to issues surrounding the weaker driving force in low CO_2 concentration flue gases and low capture rates, it is not further investigated for CO_2 capture on OCGT's.

Table 9: Pilot-scale CO_2 capture on power generation sources using membrane technologies

Location	Membrane	Membrane performance		Capture rate (%)	CO_2 purity	Ref.
		CO_2/N_2 selectivity	Permeance (GPU)			
EDP Sines power plant, Portugal	NTNU PVAm	80-300	74-230	-	75 vol.%	[145]
NCCC, USA	MTR Polaris™	50	1000	83-91	56-74 vol.%	[146]
EnBW power plant, Germany	PolyActive™	43	1062	42.7	50-75 mol.%	[147]
Tianjin University, China	Amine-based facilitated transport PVAm	96	1013	60.7-81.5	80.7-87.2 mol.%	[148]

2.2.4. Chemical Looping

An emerging technology that is gaining a lot of attention is chemical looping combustion (CLC), of which there are two types shown in Figure 21. Type I uses a reducer (fuel reactor) and a combustor (air reactor). In the reducer, metal oxide (MeO) particles convert fuel into CO_2 and H_2O, whilst reducing MeO to the base metal (Me). The reduced Me is then oxidised using air to generate heat and subsequently generate electricity [149]. The general reaction mechanisms for the reducer (Equation 11) and combustor/oxidiser (Equation 12) are shown below [150].

Reducer: $$4MeO + CH_4 \rightarrow 2\,H_2O + CO_2 \quad (11)$$

Combustor: $$4Me + 2O_2 \rightarrow 4MeO \quad (12)$$

Type II CLC systems use a carbonator and a calciner. In the carbonator reactor, the MeO sorbent (typically calcium) reacts with CO_2 to form a metal carbonate ($MeCO_3$). The $MeCO_3$ is then calcined to regenerate the sorbent and produce a pure CO_2 stream. Type II systems are advantageous as they simplify downstream CO_2 processing (compression, transportation, and storage) [149].

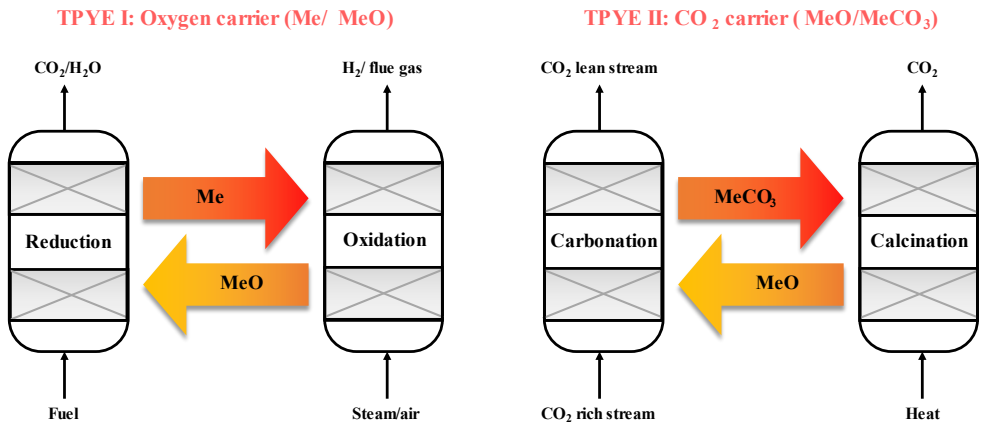

Figure 21: Chemical looping reaction system. Type I is an oxygen carrier such as Me/MeO. Type II is a CO2 carrier such as MeO/MeCO3 . Where Me stands for metal, MeO is metal oxide, and MeCO3 is metal carbonate [149]

This issue with CLC systems is the high capital costs, resulting in higher costs of electricity compared to other power generation technologies that include PCC [151]. To overcome the economic problems, the waste heat from the air reactor can be utilised to produce power. Diglio et al. [152] showed a small-scale CLC system with an air fed gas turbine can produce 0.5 MW of power (51% global energy efficiency) at 54 €/MWh, and the cost of CO_2 avoidance is 31 €/tCO_2. Khan et al. [150] showed a CLC system (using an internally circulating reactor) combined with a natural gas combined cycle (NGCC) plant, the cost of CO_2 avoidance is \$117.3/tCO_2 for capturing 95% of the total CO_2 emissions. The performance can be improved by adding a natural gas combustor after the CLC unit, lowering the cost of avoidance (51% capture rate) to \$60.2/tCO_2. In the study, NGCC with conventional (MEA) PCC (90% capture) has a cost of avoidance of \$93.8/tCO_2. Highlighting the potential CLC has for producing low-cost electricity (~65-105 \$/MWh [150]) and capturing >95% CO_2 [153]. However, few studies have investigated CLC for flexible response. Pozo et al. [154] mentions the potential of flexible operation but focuses on humid air turbine cycles and gas switching combustion, which is not applicable for PCC.

2.2.4.1. Calcium Looping

Calcium looping (CaL) was first proposed in Shimizu et al. [155] for CO_2 removal from combustion processes. It can be classified as a type II chemical looping process, using calcium carbonate as the CO_2 carrier, illustrated in Figure 22. The equilibrium reaction between calcium oxide (CaO) and CO_2 forms calcium carbonate ($CaCO_3$) [156]:

$$CaO + CO_2 \rightarrow CaCO_3 \qquad 13$$

Erans et al. [157] reviewed CaL for power generation and industrial CO_2 sources. A major advantage of this technology is the widely available and inexpensive natural sorbent material (limestone); however, this material suffers from sorbent degradation, as the reactivity decreases after continuous cycling [158]. Natural sorbents can be enhanced to limit their reactivity decay, although there are issues surrounding the scalability of sorbent modification processes [157].

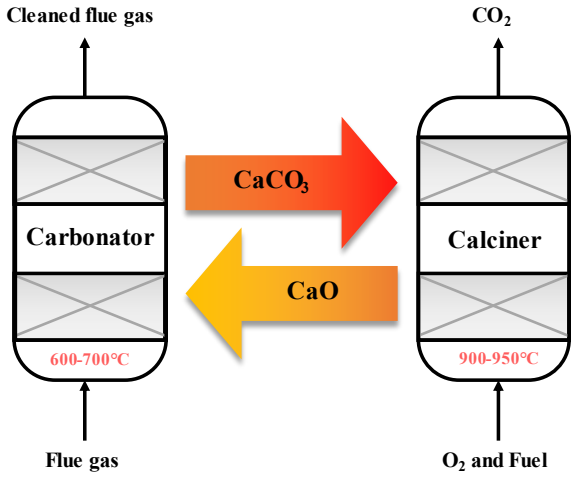

Figure 22: Calcium lopping (CaL) CO_2 capture from flue gas, edited from Mantripragada and Rubin [151]

CaL has been investigated under flexible operating scenarios. Cormos and Simon [159] assessed CaL under ramp, step, and sinusoidal input flowrates, to highlight the transient response (load following) in real power plants. Although the CO_2 capture efficiency is comparatively low (29-39%), the dynamic

simulation showed the minimum capture rate was at the maximum flue gas flowrate. Therefore, transient operation benefits CaL systems. Astolfi et al. [160] investigated CaL integrated pulverised coal power plants (PCPP), looking at a flexible sorbent storage system and analysing the system at different fuel inputs. The baseline results showed the specific energy demand is 2.34 $MJ_{LHV}/kgCO_2$, when the net power output and flue gas flowrate drop to 80%, 60% and 40% load, the specific energy demand of the capture system decreases to 2.21, 2.14 and 2.11 $MJ_{LHV}/kgCO_2$. Overall, the cost of electricity for the PCPP, PCPP+CaL, PCPP+FlexiCaL is 120.04, 119.23, and 114.66 €/MWh. The additional energy generation makes CaL an attractive CO_2 capture technology, and the results show it can operate flexibly.

2.2.5. Fuel cells

Fuel cells convert the chemical energy of a fuel directly into electrical energy, they are electrochemical energy conversion processes [161]. Offering higher power generation efficiencies compared to conventional hydrocarbon sources [162]. Two specific types of fuel cells have been investigated in the literature: molten carbonate fuel cells (MCFC) and solid-oxide fuel cells (SOFC). In MCFC's, illustrated in Figure 23, O_2 and CO_2 in the exhaust gas stream transport to the anode by carbonate ions (CO_3^{2-}). In the anode, internal reforming (or in a thermally integrated reactor) generates H_2, and O_2 is released by the carbonate ion, they react to form H_2O [163]. The MCFC anode (Equation 14), cathode (Equation 15), and overall reaction (Equation 16) are shown below [164].

Anode: $$CO_2 + \frac{1}{2}O_2 + 2e^- \rightarrow CO_3^{2-} \quad (14)$$

Cathode: $$H_2 + CO_3^{2-} \rightarrow H_2O + CO_2 + 2e^- \quad (15)$$

Overall: $$H_2 + \frac{1}{2}O_2 + CO_2 \rightarrow H_2O + CO_2 \quad (16)$$

By using a gas turbine to provide the exhaust gas stream, you can capture CO_2 as well as generate electricity. The high operating temperature allows a heat recovery steam generator (HRSG) to improve the overall energy efficiency. Therefore, generating a smaller overall energy penalty than conventional MEA based post-combustion capture attached to a Natural Gas Combined Cycle NGCC [163].

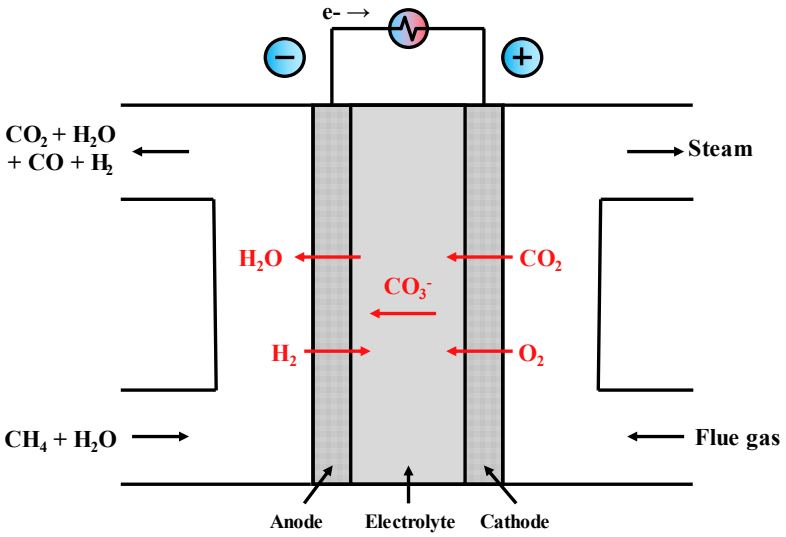

Figure 23: Molten carbonate fuel cell principles, edited from Campanari [163]

Duan et al. [162] showed an Integrated Gasification Combined Cycle (IGCC) integrated with MCFC, shown in Figure 24, has a superior thermal performance compared to IGCC's with pre-combustion or oxy-fuel combustion CO_2 capture. The efficiency of the MCFC case is even 2.97% higher than the baseline IGCC with no CO_2 capture, due to the electricity generated from the fuel cell. However, the proposed integration is economically uncompetitive, with a total cost of electricity 103.85 $/MWh compared to 59.27 $/MWh with no capture. The cost of CO_2 avoidance is 63.73 $/t$CO_2$. The cost for MCFC specific equipment was 3375 $/kW. Spinelli et al. [165] used between 1250-2000 $/kW in their economic comparison of integrated and non-integrated MCFC+NGCC systems. NGCC with MCFC (49 $/t$CO_2$) is 35% more cost effective compared to a base case NGCC+MEA (75$/t$CO_2$). Although the integration boasts both improved thermal and economic performance compared the MEA based capture, the long start-up times due to high operating temperatures, means the system is not suitable for flexible operation, a key challenge expected of future power specific capture technologies. Also, the integrated scheme is unsuitable for retrofitting onto existing NG plants. However, Cooper et al. [166] presented results for a feasibility study on retrofitting a coal-fired plant with MCFC. The exhaust from the coal burner unit (post SOx and NOx treatment) is sent to the cathode of the MCFC unit, fuel for the anode is from a steam-methane reformer. The results from the Aspen Plus simulation showed >90% capture and 1.41 GJ/tCO_2 energy requirement, significantly lower than amine-based capture.

A recent study from Ferguson and Tarrant [167] compared NGCC with MCFC CO_2 capture against the benchmark amine process. For the MCFC case the capital costs are 65% higher but it generates 42% more power for the same natural gas feed. The resulting cost of electricity for both technologies is comparable, £69.9/MWh for the MCFC case and £70.7/MWh for the amine case.

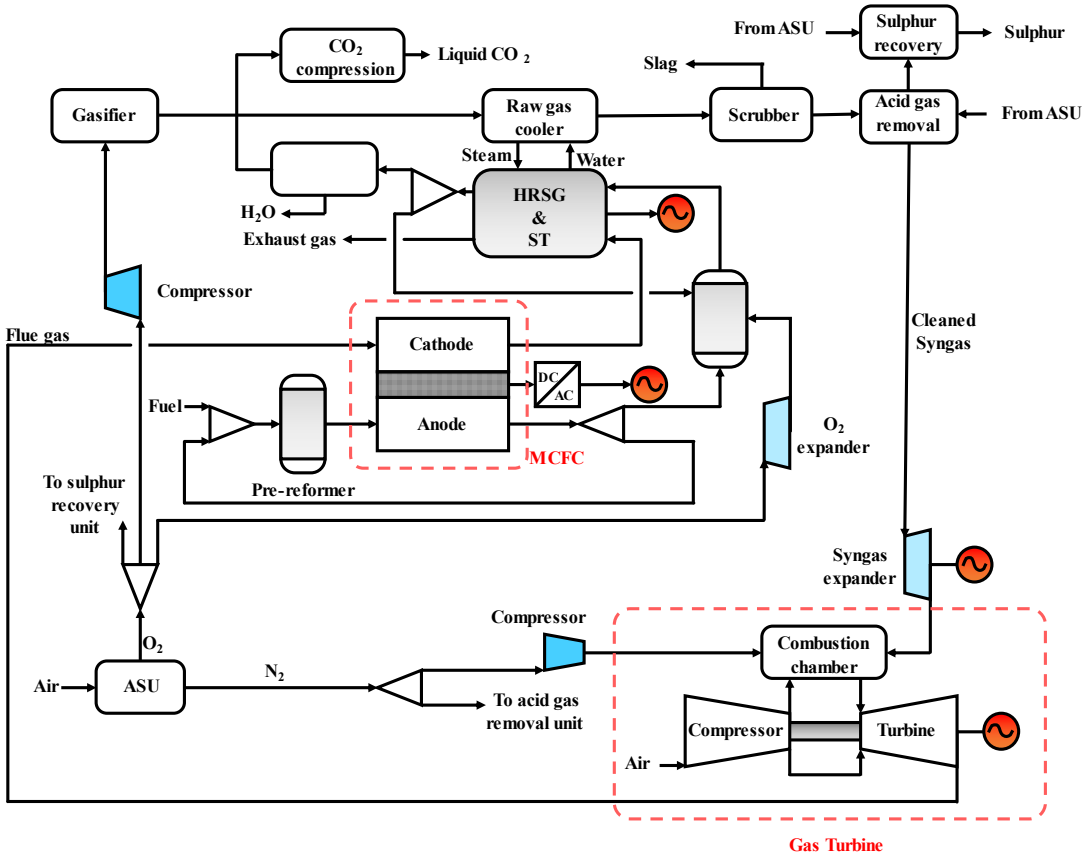

Figure 24: IGCC with integrated MCFC process flowsheet [162]

2.3. Demonstration facilities

The Global CCS Institute's CO_2RE project shows the global CCS facilities that are completed, currently operated, and in the planning stages [168]. Table 10 highlights the demonstration scale projects that have been completed or currently in operation. Many of the demonstration facilities globally use solvent-based systems to capture CO_2 from flue gas. From Figure 13, PCC with amine-absorption is already at TRL9 (commercial), the next closest PCC technology is adsorption at TRL7 (demonstration), with membrane separation, CLC and CaL all at TRL6 (pilot-scale). Although, the recent progress at the WITC for Membrane separation using MTR's Polaris™ [143] pushes the TRL to level 7 [45]. Air Product's Port Arthur steam methane reforming (SMR) CCS project [169], moves PSA/VSA to TRL9 [45]. Based on the literature survey and TRL updates, the two technologies further investigated in this project are MEA absorption (as this is the benchmark PCC process) and CO_2 adsorption (as this is the closest PCC technology to commercialisation).

Table 10: CO_2 capture demonstration scale facilities for power generation applications (PCC)

Facility	Process	Capture technology	Capacity (tCO_2/day)	Ref.
KEPCO's Nanko Power Station, Japan	MHI's KM CDR Process™	Absorption using various solvents	2	[170, 171]
Technology Centre Mongstad, Norway	Amine capture plant	MEA Absorption	200	[172, 68]
Shanghai Shidongkou CO_2 Capture Pilot Plant, China	Solvent capture plant	Absorption using KoSol (developed by KEPCO)	330	[173]
Brindisi CO_2 capture pilot facility, Italy	Amine capture plant	MEA Absorption	60	[69]
Le Havre Power Plant, France	Alstom Advanced Amine process (APP)	Absorption using UCARSOL™ FGC-3000	25	[174]
Esbjerg Power Station, Denmark	CASTOR/CESAR projects	Absorption using MEA, CASTOR1, and CASTOR2	24	[175]
Drax Power Station, England	MHI's Advanced KM CDR Process™	Absorption using KS-1™ and KS-21™ solvents	0.3	[176]
UKCCSRC PACT Facility, England	Amine capture plant	MEA Absorption	1	[64, 177]
SSE's Ferrybridge Power Station, England	CCPilot100+	Absorption using MEA and RS-2™ solvent	100	[178]
Mikawa Power Plant, Japan	Toshiba's Solvent System	Absorption using a new tertiary amine	10	[179]
Hadong Power Plant, Korea	KIERDRY® Process	Dry sorbent capture using KEP-CO2P1 and KEPCO2P2 sorbents	200	[180, 181]
Haifeng Power Plant, China	Carbon Capture Test Platform	Amine absorption using MEA and membrane separation using MTR Polaris™ membrane	20-50	[182]
WITC	MTR's membrane separation technology	Membrane separation using MTR's Polaris™ membrane	140	[143]
La Pereda pilot plant, Spain	CaOling Project	1.7 MWth Calcium looping plant	-	[183]

2.4. CO_2 Compression and Conditioning

The capture technologies will all work from identical exhaust gases. The CO_2 then needs compressing and conditioning in order to be ready for transportation and storage/utilisation. This also ensures the end CO_2 characteristics (pressure and temperature) are the same, enabling a more accurate comparison and evaluation.

CO_2 is gaseous at standard ambient temperature and pressure, with a density of 1.98 kg/m^3. Looking at the P-T diagram for CO_2 (Figure 25) the liquid region (blue shaded area) is below the critical point temperature of 31°C, and above the triple point (-56.6°C and 5.18 bar). Sublimation/deposition occurs at -78.5°C and under atmospheric pressure [184].

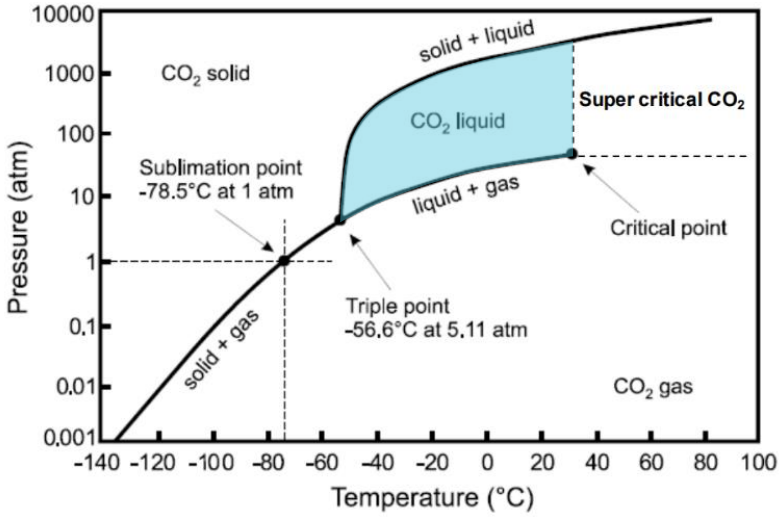

Figure 25: P-T diagram for Carbon Dioxide [186]

For post-combustion capture technologies, with a relatively high CO_2 purity (>99% v/v), the impact of impurities on the thermodynamic properties is often neglected. However, it has been recognised that CO_2 capture streams from sources such as coal and bio-mass fired power plants, contain a higher quantity of impurities compared to natural gas fired power plants [185]. Non-condensable gases, such as nitrogen, argon, oxygen, hydrogen, and carbon monoxide, influence the relationship between temperature and pressure. Table 11 shows the effects these impurities have on equilibrium pressure at -50°C, therefore, to minimise the work requirement of compression system they must be kept as low as possible. Water content must be minimised to prevent the formation of carbonic acid, which is corrosive and limits material selection, water is typically removed using dehydrators and knock-out drums in-between the compressor stages [186, 187].

Table 11: Effect of impurities on CO2 absolute vapour pressure [186]

Component	Condensation temperature (°C)	Mixture	Absolute vapour pressure at -50°C (bara)
CO_2	-48.9	100% CO_2	6.7
N_2	-174.6	CO_2 with 0.05%N_2	7
Ar	-162.4	CO_2 with 0.05%Ar	6.8
O_2	-159.5	CO_2 with 0.05%O_2	6.9
H_2	-244	CO_2 with 0.05%H_2	10.3
CO	-168.2	CO_2 with 0.05%CO	7

It is worth noting, any substantial release of CO_2 in an enclosed area is potentially hazardous, and if inhaled may cause dizziness, headaches, respiratory problems, asphyxia, and unconsciousness. It is stored in its liquid state under pressure, therefore care must be taken when storing CO_2 on a site, to prevent the container rupturing if heated or overfilled. As mentioned previously, the water content must be kept to a minimal to prevent the formation of carbonic acid which can corrode steel, leading to weaknesses in the container [184]. For wet CO_2 conditions stainless steel should be used for rotating equipment (compressors), if the CO_2 contains <5ppm H_2O then low-alloy carbon steels can be used.

2.4.1. Compressor Design

IEAGHG [60] examines the options available for CO_2 compression and looks at optimising each technology for integration with CO_2 capture. It highlighted the use of axial compressors, which can handle a higher flowrate and have a higher efficiency than centrifugal compressors. However, the report is supported by industrial vendors such as Rolls Royce, MAN Diesel, GE and Ramgen, and the vendor feedback showed axial compressors have a much higher capital expenditure (CAPEX) and are not yet applicable to CO_2 compression. Reciprocating compressors used to be the conventional method for CO_2 compression, they are positive displacement machines where a specified volume of gas is drawn in then compressed and released. However, due to the smaller capacities and non-dynamic behaviour there has been a shift in preference in the CCS industry, with centrifugal designs becoming more favourable. These compressors are dynamic machines capable of continuous operation, which can be categorised into single shaft in-line between bearing and multi-shaft integral gear types. A comparison of centrifugal compressor designs is shown in Table 12.

Table 12: Comparison of different compressor designs [188, 189, 190]

Option	**In-line centrifugal**	**Integrally geared centrifugal**
Pressure ratio	1.7-2:1	1.7-2:1
Max discharge pressure (bar)	690	350
Inlet capacity range (m3/h)	170-850,000	500-500,000
Maximum Power (MW)	38	60
Adiabatic efficiency (%)	70-87	80
Flexibility	Less	Less
Space requirements	Less	Less
Relocation	Less difficult	Less difficult
Fuel Consumption	High	High
Operating Cost	Less	Less
Advantages	• Highest reliability • Requires fewer intercoolers than integrally geared	• High reliability • Lower power consumption compared to in-line designs
Disadvantages	• Sensitive to entrained liquid • High noise levels • Limited pressure ratio	• Complex maintenance and repair • Higher gear losses • Large footprint
Investment cost range	Rolls Royce Cost Range: 600-900 €/kW [a]	MAN Diesel & Turbo Cost Range: 300-600 €/kW [a]

[a] sourced from IEAGHG [60],

2.4.2. Compression System

Centrifugal compressors have a low-pressure ratio (between 1.7-2:1) and a multistage system is required, with intercooling between each stage to make the process as close to isothermal as possible (Figure 26). When CO_2 is in the gas phase a compressor is needed to increase the pressure, whilst in the liquid phase a pump can be used [191]. Supercritical liquefaction then pumping the CO_2 is economically beneficial due to the lower capital and operating costs of liquid pumps (Figure 27). However, due to the low boiling point of CO_2 at elevated pressures, cooling systems must be in place to keep the system under isothermal conditions and below the saturation temperature. For intermediate storage the overall pressure increase is not as large as that required for pipeline transportation, therefore, a subcritical liquefaction system is required [185].

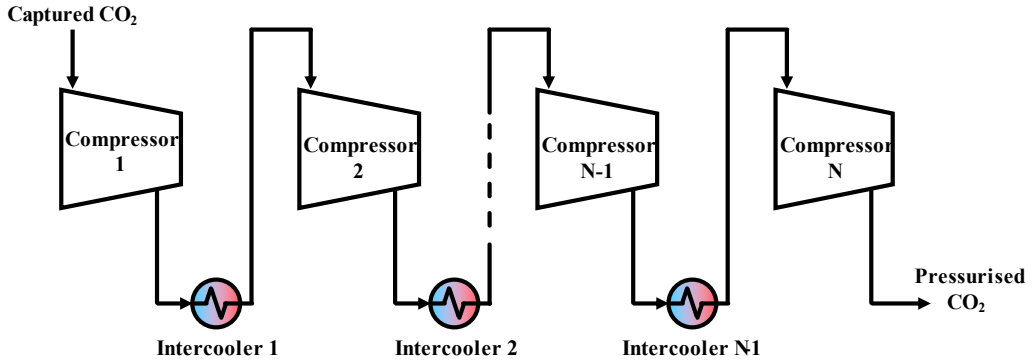

Figure 26: Multistage centrifugal compression system

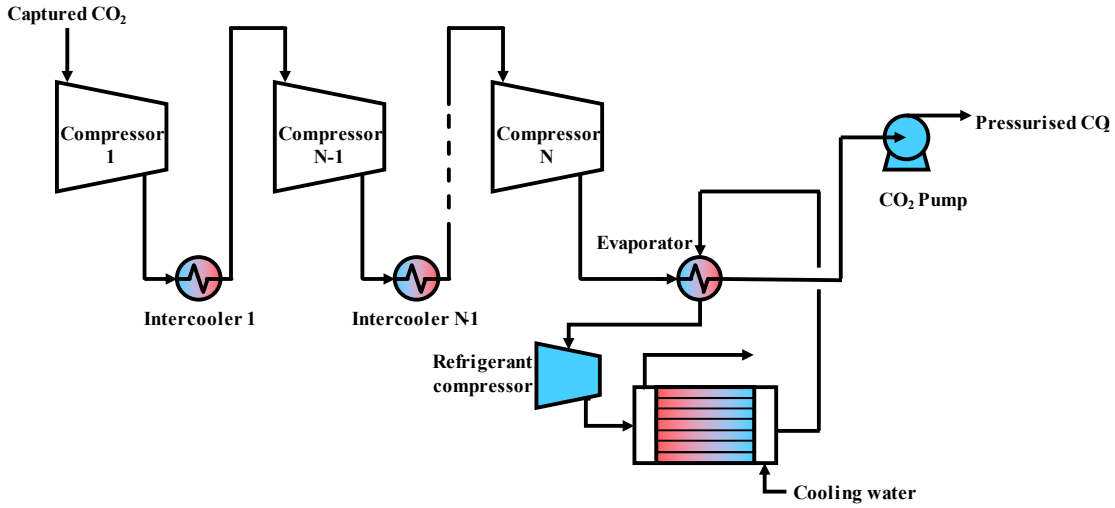

Figure 27: Multistage centrifugal compression, with subcritical liquefaction and pumping system

An early study by Aspelund and Jordal [192] investigates the interface between CO_2 capture and transportation, stating the energy requirement for CO_2 conditioning is between 90 and 120 kWh/tonne CO_2. Several studies have looked at optimising and comparing conditioning strategies, mainly focused on the aforementioned multistage compression and liquefaction process, illustrated in Figure 28. Witkowski & Majkut [193] compared 13 different compression strategies for high purity CO_2 compression, captured from a pulverised coal-fired power plant using post-combustion (amine-based) CO_2 capture. The baseline strategy used a 14 stage in-line centrifugal compression with intercooling to keep the system under isothermal conditions. The number of stages required depends on the

compression ratio, desired output pressure, discharge temperature, and the efficiency of intercoolers. The report compared strategies with multistage in-line centrifugal compressors, multistage integrally geared centrifugal compressors, advanced supersonic shockwave compressors, and compression accompanied with liquefaction and liquid pumping. Power savings up to 21% can be achieved through integrally geared compressors, and over 45% using a refrigerated subcritical liquefaction process. IEAGHG [60] also reported a reduced energy consumption when incorporating early liquefaction then liquid pumps, although it was only a 0.2 MW decrease. This saving is potentially offset by an increased cooling water demand.

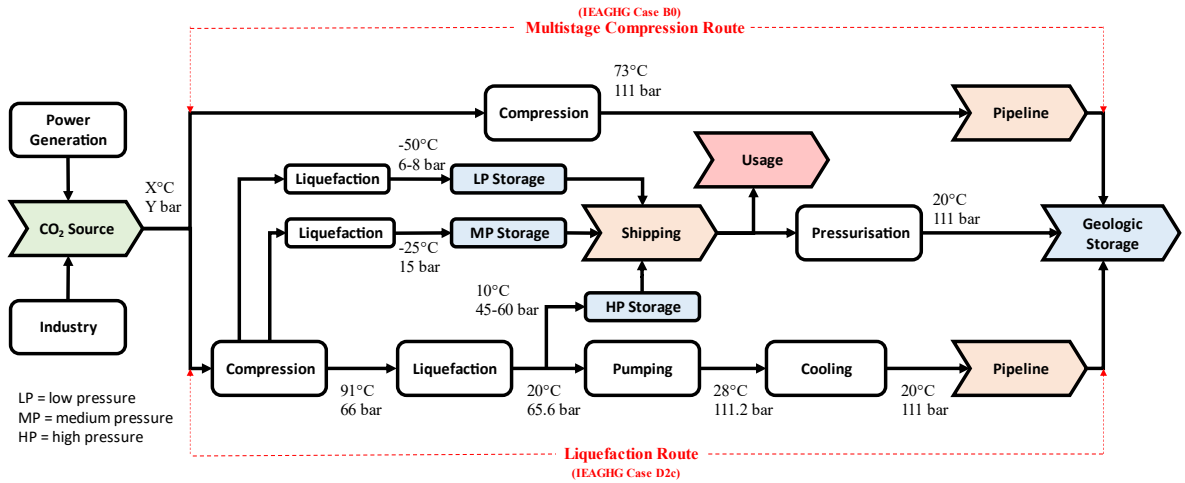

Figure 28: CO_2 conditioning options for shipping and pipeline transportation

2.4.2.1. Liquefaction

A drive in the literature for ship-based transport has resulted in several reports focussing on optimising the liquefaction process [194, 195, 196, 197, 198]. Alabdulkarem et al. [194] developed process models in Aspen HYSYS to investigate CO_2 liquefaction cycles using various refrigerants (NH_3, CO_2, C_3H_8 and R134a). Liquefaction at 50 bar using NH_3 resulted in 5.1% lower power consumption compared to the conventional multistage process. Jackson and Brodal [197] showed an open-CO_2 refrigeration cycle will have a lower energy consumption compared to NH_3, when the cooling temperature is below 20 °C, similar to the conclusions in Hegerland et al. [199]. Interestingly, in the literature there is conflicting evidence as to whether a closed remigration cycle is more effective over an open refrigeration cycle [200].

Lee et al. [195] compared different sea water temperatures for intercooling in a CO_2 liquefaction process. To liquefy CO_2 (6.5 bar and -50.6 °C) the total power consumption ranges from 90-140 kWh/ton CO_2 for seawater ranging from 5-30 °C. The lower the sea water temperature, the lower the overall power consumption is. The power demand is comparable to the results in Aspelund and Jordal [192], which also showed liquefaction be to 10% more energy efficient than conventional multistage compression.

Deng et al. [196] investigated the impact of delivery pressure and impurities on the liquefaction process. Delivering CO_2 at 40 bar post-liquefaction consumes 13% less power than at 7 bar, as less cooling is required in the NH_3 refrigeration cycle. For pure CO_2 the cooling duty drops from 43.3 MW at 7 bar, to 22.2 MW at 70 bar. Although the cooling requirement is lowest at 70 bar, the overall energy consumption is offset by the increase in compression power. An economic analysis of the different delivery pressures showed the highest cost occurs at 7 bar delivery, which is consistently used in the literature for ship-based CO_2 transport.

2.4.2.2. Intercooling

Three factors effect compressor power consumption: pressure ratio, efficiency, and inlet temperature [201]. Therefore, the CO_2 stream needs to be cooled using heat-exchangers prior to each compression stage. Romeo at al. [201] performs an energetic and economic analysis of CO_2 compression, optimising the intercooling step through heat integration with a low-pressure steam turbine. The proposed integration reduces the incremental cost of electricity by 23% (3.54 to 2.71 €/MWh). Giannaris et al. [202] discusses utilising compression waste heat for condensate pre-heating (used for solvent regeneration). However, the quantity of waste heat is small compared to the waste heat available from the flue gas, the economic option is to maximise the size of the flue gas cooler. The available waste compression heat could be increased by reducing the heat-exchanger size or removing certain intercoolers entirely. This technique was investigated by Pfaff et al. [203] and used for condensate pre-heating, which improved the net efficiency of the overall process (by 0.59 % points). Only increasing the intercooler outlet temperature has a negative effect on the net efficiency, as the increased compressor power demand counteracts the energy savings from condensate pre-heating.

2.4.2.3. Dehydration

When the CO_2 stream is cooled, the combination of high pressure and low temperature reduces the partial pressure of H_2O by condensation, knock-out (KO) drums are then used for vapour-liquid separation. Some water will condense in the cooling stages, and this should run out in the knock-out vessel. If further moisture removal is required, liquid adsorption or solid adsorption can be used. For liquid-phase absorption, triethylene glycol (TEG) is a proven sorbent for Natural Gas dehydration. It is similar in design to an amine-absorption CO_2 capture system, as it uses a tray or packed absorption columns [204, 205]. TEG is disadvantageous due to inability to maintain the low water specification (<30ppm), potential emissions of TEG into the atmosphere, TEG contaminating the CO_2 stream, low operating temperature (>40°C), and lower reliability compared to solid adsorption using a desiccant [206]. In dehydration using a solid adsorbent, the wet gas flows through an adsorption bed, then once the sorbent is saturated the bed is thermally regenerated using some of the dried gas product, a minimum of two beds is required for continuous operation. A schematic is shown in Figure 29 and the sorbent material can be an activated alumina, molecular sieve, or silica gel. The most efficient is molecular sieves, which can reduce the water content in the gas stream to less than 1ppm. The size of the dehydration unit depends on the flowrate of gas processed and the level of moisture control [60].

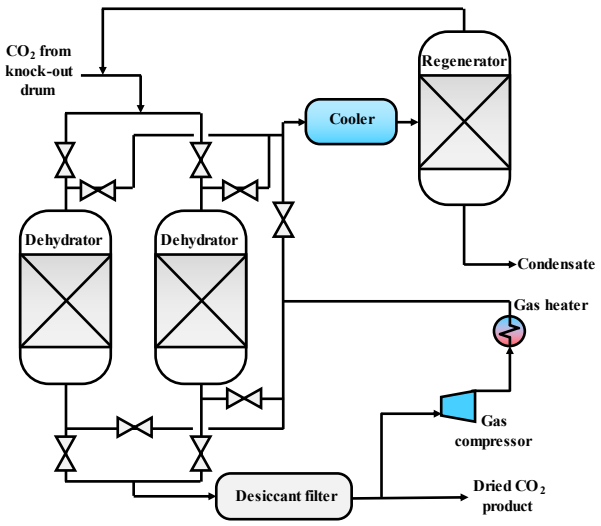

Figure 29: Dehydration using a molecular sieves [205]

2.4.3. Transport and Storage Specifications

CO_2 is typically transported and stored in its liquid state (blue region on Figure 25), either at ambient temperature in cylinders/non-insulated storage tanks between 45-64 bar, or at refrigerated temperatures (-35°C to -15°C) in insulated storage tanks between 12-25 bar. Other non-CCS industries generally store CO_2 at 20 barg and -30°C, or in high pressure cylinders at 58.6 bar and 21°C [207]. For example, in the food/beverage industry, CO_2 is typically transported at 17 bar, -30°C in 2-30 tonne tankers for land-based transport, the composition specifications are shown in Table 13. HSE [184] states there is nothing to suggest these storage methods would not be suitable for the CCS industry, assuming the level of impurities can be kept to a minimum.

Table 13: Carbon dioxide specification for beverages [208]

Component	Concentration
CO_2	99.9% v/v
H_2O	20 ppm v/v
NH_3	2.5 ppm v/v
O_2	30 ppm v/v
NO_X (NO/NO_2)	2.5 ppm v/v (each)
Non-volatile residue (particulates)	10 ppm w/w
Non-volatile organic residue (oil)	5 ppm w/w
Volatile hydrocarbons	50 ppm v/v
Acetaldehyde	0.2 ppm v/v
Aromatic Hydrocarbons	0.02 ppm v/v
Carbon Monoxide	10 ppm v/v
Methanol	0.5 ppm v/v
Carbonyl Sulphide	0.1 ppm v/v
Hydrogen Sulphide	0.1 ppm v/v
Sulphur Dioxide	1 ppm v/v

For large scale CCS projects, the quantity of CO_2 captured is extremely large and the economic choice for transportation is through pipelines. Table 14 highlights pipeline specifications used for various projects globally. Kinder Morgan, the largest CO_2 pipeline operator in the world, has developed standards for pipeline transportation. Jensen et al. [209] reports the Kinder Morgan CO_2 pipeline specifications, explaining the pressure and temperature should be >10.3 MPa and <120°F respectively. Ensuring the CO_2 stream is kept above the critical pressure point and below the critical temperature point, preventing supercritical fluid flow. The Canyon Reef Project was the first large scale CO_2 pipeline in the USA, moving 4.4 Mt CO_2/year from Shell Oil Company gas processing plant in Val Verde, Texas. The Weyburn pipeline transports 1.8 Mt CO_2/year to the Weyburn EOR project in Saskatchewan, Canada. DYNAMIS is a European project that looked at large-scale hydrogen production with CCS, building on from work from the ENCAP project for the CO_2 transportation specifications. The CarbonNet project looked at the feasibility of developing a commercial CCS hub in Latrobe Valley, Australia.

Transportation through pipeline is desirable for large CO_2 flows, however, for smaller-scale (<5Mtpa) operations shipping transportation is less capital intensive. Shipping is also favourable for longer distances (>500km) and short project durations (<20 years) [210]. MEP [211] presented a feasibility study for full-scale CCS in Norway, it looks at shipping in storage vessels at 6-8 bar at -50°C (low), 15

bar at -25°C (medium) and 45-60 bar at +10°C (high). The report concluded all evaluated solutions are technically feasible, the low-pressure scenario is proven for liquid petroleum gas (LPG) shipping, medium pressurisation is proven for food grade CO_2, and although the high-pressure scenario is not a mature technology is does have the lowest energy demand.

Table 14: CO_2 pipeline specifications

Component	Kinder Morgan [a]	Canyon Reef [b]	Weyburn [c]	Dynamis [d]	CarbonNet [e]
CO_2	95 mol.%	>95%	96%	>95.5%	>95.5 vol.%
H_2O	600 ppmw	No free H_2O	<20ppmw	<500 ppmv	<100 ppmv
CO	-	-	0.1%	<2000 ppmv	900-5000 ppmv
N_2	4 mol.%	4%	<300ppmw	<4 vol.%	-
O_2	10 ppmw	<10 ppmw	<50ppmw	100-1000 ppmv for EOR <4 vol.% for Aquifer	-
H_2S	10-200 ppmw	<1500 ppmw	0.9%	200ppmv	<100 ppmv
SO_X	-	-	-	100 ppmv	200-2000 ppmv
Total Sulphur	35 ppmw	<1450 ppmw	-	-	-
NO_X		-	-	100 ppmv	250-2500 ppmv
Hydrocarbons	5 mol.%	<5%	100 ppmw	<2vol.% for EOR <4 vol.% for Aquifer	<0.5%

[a] [209], [b] [212], [c] [213], [d] [214] and [e] [215]

2.4.3.1. Effect of Stream Impurities

There is a wide range of potential sources of CO_2, with each technology producing CO_2 streams at different pressures, temperatures, and compositions. Power generation sources have been the focus in industry and academia over the last three decades [44], and now there is a growing interest in other sources such as the production of hydrogen, fertilisers, cement, iron, and steel [6]. For more information on the current developments within the CCS community see [44, 216]. Table 15 highlights the characteristics of various capture CO_2 streams from power and industrial sources that will be used in the CO_2 conditioning study.

Table 15: Captured CO_2 source characteristics.

Source	Temperature (°C)	Pressure (bar)	Composition (%)			Source
			CO_2	H_2O	N_2	
Post-MEA	38	1.6	95.88	4.11	0.01	[60]
Post-NH3	20	6.0	99.00	0.40	0.00	[217]
Pre-MDEA	30	1.1	96.02	3.92	0.02	[218]
Pre-Selexol	-5	1.2	99.77	0.17	0.00	[60]
	1	4.8	97.30	0.07	0.03	
SMR-PSA	21	1.0	99.40	0.00	0.00	[219]
Steel-Membrane	40	1.0	98.97	0.00	1.00	[220]

MCFC	30	1.0	99.95	0.05	0.00	[162]
SOFC/Chemical Looping	30	1.1	100.00	0.00	0.00	[221]

Notes: monoethanolamine (MEA), Ammonia (NH3), Methyl-diethanolamine (MDEA), molten-carbonate fuel cells (MCFC), pressure swing adsorption (PSA), solid oxide fuel cells (SOFC), and steam methane reforming (SMR).

Brunsvold et al. [222] presented results from the IMPACTS project, which investigated the affect impurities have on CO_2 transportation and storage, The findings showed an optimal moisture content between 250-350 ppm for pipeline transportation, above which the CCS chain costs increase significantly. Moisture in CO_2 pipeline causes corrosion due to reaction with impurities, stress corrosion cracking, and hydrate formation. Nitrogen, although chemically inert, effects the physical properties of the CO_2 stream, including increasing the bubble point and reducing the compressibility. The IMPACT project found increasing the N_2 concentration from 5,000 ppm to 50,000 ppm increased the cost by 5%, therefore, a limit of 5,000 ppm is advisable.

Peletiri et al. [223] used process simulation (Aspen HYSYS and gPROMS) to investigate the effects of a wide range of impurities on CO_2 pipeline transportation. N_2 has the most impact, with 10 mol% increasing the pressure and heat losses by 25 and 87.2% respectively. Interestingly, H_2S has the smallest impact, leading to Peletiri et al. [223] concluding specifications for CO_2 pipelines could be altered to allow for higher H_2S and lower N_2 concentrations.

Skaugen et al. [224] performs a techno-economic analysis of transporting 500 kg/s CO_2 in pipelines over a 500km distance. The analysis showed a 20-40% increase in cost for transporting CO_2 with a high level of residual impurities (N_2, O_2, and CH_4) from air (oxy-fuel combustion) and natural gas (gas sweetening), compared to a base case feed with 93 mol.% CO_2 and 7 mol.% H_2O.

Kahlke et al. [225] presents results from the CLUSTER project, the report investigated the dynamic behaviour of a CCS cluster, looking at the effect various CO_2 streams have on transport, injection, and storage network. The main factor affecting the thermophysical properties of the CO_2 stream is the CO_2 concentration, not the level of individual impurities. The dynamic simulations highlighted an important issue with mass flowrate changes; if the design point of the pipeline is set at the maximum flow from all streams in the network, most of the time the pipeline will be underutilised, more so when energy networks have a high penetration of renewable power. To increase capacity utilisation, Kahlke et al. [225] suggests reducing the design capacity and including intermediate storage, i.e., partial storage of CO_2 during peak loads and transporting CO_2 during low loads.

2.4.3.2. Effect of pipeline phase

Another issue for pipeline operation and cost is the formation of two-phase flow, which lowers the bulk density of the fluid, increasing the work required of compressors and transport equipment [209]. Harkin et al. [215] compared different pipeline operating phases and found operating in the dense phase (16.5 MPa inlet pressure, 20 MPa design pressure) rather than gas phase (5 MPa inlet pressure, 7 MPa design pressure) saved 10% on the net present cost.

Roussanaly et al. [226] presented results from the COCATE project, the paper looked at transporting CO_2 from a range of emitters in Le Havre, France, to a CO_2 hub in Rotterdam, Netherlands. The economic comparison showed onshore pipeline transportation (17.1 €/tCO_2) is favourable over a shipping network (18.9 €/tCO_2), however, this is a case specific conclusion. The report also compared dense phase vs gaseous phase pipeline operation. The dense phase operates at 110 bar, whereas the gaseous phase is at 9 bar, both supply CO_2 to the hub which transforms the stream to 150 bar dense phase ready for injection storage in the North Sea. Dense phase transportation proved to be a more economic option, 30% lower NPV of costs than gaseous transportation. Roussanaly et al. [226] state this is case specific, and for networks smaller than 40km gaseous transportation could still be a viable option.

2.4.3.3. Effect of transient CO_2 production

CO_2 compression is sometimes included in wider studies looking at CO_2 capture from fossil fuel-based power stations [227, 228, 229, 230, 231, 232] . Spitz et al. [228] investigated dynamic CO_2 compression as part of a wider study looking at flexible gas-PCC operation. Process models for the MEA based capture plant and the CO_2 compression train were developed in gPROMS gCCS, whereas the Gas Turbine was modelled in Thermoflow GT Master. One of the flexible operating strategies incorporated additional regeneration of stored solvent. A technical limitation of this strategy is the decreased desorber pressure (to maintain the lean loading level), accompanied with an increased volumetric flow into the compression train, resulted in higher power requirements. This issue is remedied with a pre-compression stage, to counteract the decreased desorber pressure, however, this increases the cost of the compression system. [232] also investigated gas-PCC and included an economic analysis at various loads (40%-100%). Interestingly, the compression trains contribution to the energy penalty increases at lower loads, counteracting the reduced energy demand in the capture plant (reduced solvent usage).

Nienoord et al. [233] focuses on the interface between capture and compression, modelling both components in Dymola (a software based on Modelica®). Flowrate changes coming from the capture plants causes the anti-surge valves in the compression plant to open, restoring the flow to above the surge point. Dense phase compression narrows the flow rate range (below the choke point and above the surge point). Nienoord et al. [233] suggests using parallel compression trains to overcome the turndown issue, this is also highlighted in [60].

Jensen et al. [209] investigates the other side of the problem, relating to the transportation and storage issues with variable CO_2 flowrate. Changes in mass flow will affect the temperature and pressure within the pipeline, causing operational challenges and maintenance problems. A similar issue arises with geologic CO_2 storage, intermittent flowrates cause variation in pressure, leading to the Joule-Thomson effect and potential freezing of valves and joints.

2.5. CCS technical challenges

Although CO_2 capture technologies have been utilised since the 1930's [234], there are still many technical challenges preventing its wide-spread deployment. The benchmark amine absorption has a high energy demand to regenerate the solvent (~120°C), and despite extensive research into other capture methods it still remains one of the most cost-effective separation technologies [235]. Some of the challenges facing capture and transporting CO_2 for flexible OCGT's are:

- Minimising the parasitic energy demand, i.e., so the overall net-power losses are not as significant [236].
- Capturing CO_2 from dilute sources, as the lower the CO_2 concentration the more expensive it is per tCO_2 [237].
- Capable of flexible operation, i.e., handling fluctuations in flue gas characteristics (flowrate, composition, temperature, and pressure) [238].
- Developing an adequate infrastructure to transport large quantities of CO_2 [239].
- Cost-effective design of transportation networks given the high level of impurities and non-condensable [239].

The aim of most capture systems in the literature is 90% recovery rate at 95% CO_2 purity [48]. However, this is a limiting guideline as many capture technologies, including the benchmark amine absorption, can capture >95% of CO_2 in the flue gas. Gibbins and Lucquiaud [235] highlight the importance of not artificially constraining capture level thresholds, as this then becomes the de facto maximum capture rate, i.e., there should be incentives to capture as much CO_2 as possible and not just meet regulatory guidelines.

There are also specific challenges associated with different CO_2 capture technologies. For example, absorption systems require a high water demand [240]. OCGT power plants are useful as they do not have a steam system and have very low water requirements, however, this means they are often located away from easily accessible water sources. Within the UK, as of May 2022 there were 28 operational single cycle gas turbines, ranging from 2.5 to 600 MWe capacity [241]. The dispersed location of these sites is shown in Figure 30. Therefore, sourcing energy, feedstock, and water for the capture systems will be challenging [242]. Alternate sources of thermal energy or cooling may need to be considered, for example, auxiliary cooling (for lubricants and machinery oils) using air cooled fin-fan coolers is considered the best available technology where water cooling in unviable [243].

Figure 30: Site location of single cycle gas turbines within the UK, data sourced from BEIS [241].

In terms of adsorption systems, the majority of commercially available sorbent materials are susceptible to high moisture content; therefore, it is imperative there is a dehydration unit prior to CO_2 capture to maximise performance and material longevity. Dehydration units are expensive, and it is often the main barrier to commercialisation for adsorption systems [244]. Alongside impurities, most capture technologies require the inlet flue gas temperature for the capture process to be around 30-50°C, which requires the use of a direct contact cooler (DCC) [245]. Therefore, there needs to be a pre-treatment section to conditioning the flue gas stream ready for CO_2 capture, these units are dependent on the capture technology and will be included in the economic assessment

The cost of developing and deploying CCS in the UK is also a challenge, and hence the UK Government established the 'CCUS Cost Challenge Taskforce' in 2018. An extensive quantity of research has been direct towards the costs for the electricity sector, which cannot be used to accurately assess the costs for other applications (decarbonising heating, transport, and industry) [246]. As this project focuses on power generation CCS applications, it is imperative to know the current baseline costs for power-PCC. The Caledonia Clean Energy Project (CCEP) produced a phase 2 feasibility report [247], in which it showed the CCGT+PCC power price is between £80-90/MWh. This is the guideline price used by the CCUS Cost Challenge Taskforce.

There are also challenges with CO_2 utilisation and storage, as this is beyond the scope of the project it is not included in this literature review.

2.6. Capture Economics

For the economic assessment of CO_2 abatement technologies, the individual technologies for carbon capture can be compared against one another to identify the most cost optimal technology/process design. There are many factors affecting the emissions control costs [212]:

- Technology used (both the capture technology and generation source)
- System boundary
- Timeframe
- Level of maturity
- Costing measures and metrics
- Costing Assumptions

Rubin [248] reported the various cost measures and metrics used for CO_2 capture and storage systems. Cost of CO_2 avoided ($/tCO$_2$) is the most commonly used metric. It compares the cost of electricity (COE) of a plant with CCS, with a reference plant without CCS. However, CO_2 avoidance is only complete once the CO_2 is sequestrated or utilised elsewhere. Therefore, the avoidance costs must include compression, transport, and storage/utilisation [249, 250, 251, 248].

$$Cost\ of\ CO_2\ avoided\ (£/tCO2) = \frac{(COE)_{CCS} - (COE)_{ref}}{\left(\frac{tCO_2}{MWh}\right)_{ref} - \left(\frac{tCO_2}{MWh}\right)_{CCS}} \quad 17$$

Cost of CO_2 captured ($/tCO$_2$) metric only considers the capture process, not the transport and storage. It compares the reference COE, and the COE of the plant with carbon capture (CC). It is useful for comparing individual capture process [252, 251].

$$Cost\ of\ CO_2\ captured\ (£/tCO2) = \frac{(COE)_{CC} - (COE)_{ref}}{\left(\frac{tCO_2}{MWh}\right)_{CC}} \quad 18$$

Cost of CO_2 abated ($/tCO$_2$) is used when moving from different scenarios, i.e., changing generation mix or using alternative fuels. It compares the net present value (NPV) of a reference and a low-carbon source. This metric does not assume the same amount of useful product is produced, or that CCS is even involved [253, 254].

$$Cost\ of\ CO_2\ abated(£/tCO2) = \frac{(NPV)_{low-C} - (NPV)_{ref}}{tCO_{2_{ref}} - tCO_{2_{low-C}}} \quad 19$$

In all the metric the COE needs to be calculated first, using Equation 20 [248].

$$COE = \frac{\big((TCC)(FCF) + (FOM)\big)}{(CF)(8766)(MW)} + VOM + (HR)(FC) \quad 20$$

Where COE is the cost of electricity (£/MWh), TCC is the total capital cost (£), FCF is the fixed charge factor (percentage/year), FOM is the fixed operating and maintenance cost (£/year), CF is the capacity factor (percentage), 8766 total hours in a year (hours), MW is the net plant capacity (MW), VOM is the variable operating and maintenance costs (£/year), HR is the heat rate (MJ/MWh), and FC the fuel cost (£/MJ). Rubin [248] explains, unless otherwise stated the COE represents the levelised cost of electricity (LCOE), which is the amount of revenue (from energy sales) required to equal/fully recover the CAPEX and operating expenditure (OPEX) of the plant, whilst earning a specified rate of return over the plant life (embedded in the FCF). The LCOE is the discounted lifetime cost of constructing and operating a

power generation asset, defined as the ratio of the total CAPEX and OPEX costs to the electricity generated and sold. The net present value (NPV) of total costs (CAPEX and OPEX), the NPV of electricity generated then sold, and the LCOE equations are [255]:

$$\text{NPV ot total costs} = \sum_n \left(\frac{\text{TCC}_\text{n}}{(1+r)^n} + \frac{\text{FOM}_\text{n}}{(1+r)^n} + \frac{VOM_n}{(1+r)^n} \right) \quad 21$$

$$NPV\ of\ electricity\ generation = \sum_n \frac{(\text{net electricity generated})_\text{n}}{(1+r)^n} \quad 22$$

$$LCOE = \frac{NPV\ of\ total\ costs}{NPV\ of\ total\ costs} = \frac{\sum_n \left(\frac{\text{TCC}_\text{n}}{(1+r)^n} + \frac{\text{FOM}_\text{n}}{(1+r)^n} + \frac{VOM_n}{(1+r)^n} \right)}{\sum_n \frac{(\text{net electricty generated})_\text{n}}{(1+r)^n}} \quad 23$$

Where r is the discount rate [%], and n is the time period. From BEIS [255], the discount rate is dependent on the generation type and its novelty. For first of a kind (FOAK) gas CCS projects the discount rate is 8.9%, whereas for Nth of a kind (NOAK) gas CCS projects the discount rate is 7.8%.

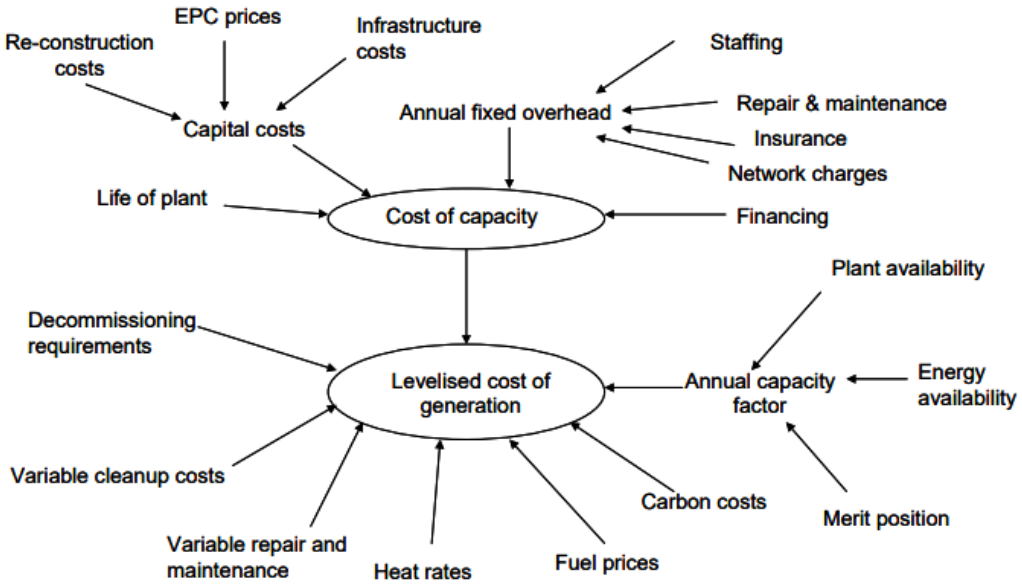

Figure 31: Drivers for levelised costs from Mott MacDonald [256]

Mott MacDonald published a report that summarised the costing methodology for power generation technologies in the UK, commissioned by the Department of Energy and Climate Change (now BEIS) in 2009/2010 [256]. Within the report the LCOE is the favoured metric for comparisons. The main components of levelised cost are the capital costs (required to start operation), on-going fixed costs (to keep the plant generating), and variable costs of operation. The drivers for levelised cost are highlighted in Figure 31. The report also showed the LCOE of different power generation sources (2023 project start), and OCGT's without CCS cost between 131.4-134.6 £/MWh depending on the discount rate used (7.5% or 10%). CO_2 capture for OCGT's was not investigated due to the small size of plant.

2.6.1. Techno-economic analysis of CO_2 capture

Alhajaj et al. [231] combined process and economic models of an amine absorption carbon capture plant. The report focussed on identifying optimal design and control variables from an economic perspective. It highlighted the current limitations in literature revolving around the separation of cost and capture models, and the inconsistent sizing factors. This model was combined with the capture model from Alhajaj et al. [230], to calculate the capital expenditure and operating expenses. The model used the capital recovery factor (CRF) from Rao & Rubin [249] set at 0.15, which corresponds to a plant with a 30-year lifetime and 14.8% interest rate. The levelised capture and compression costs (LCCC) depend on the degree of capture and range approximately between 60-70 $/t$CO_2$. Within the literature the cost of MEA CO_2 capture is between 40-100 $/t$CO_2$, depending on the size of study and the economic assumptions [257].

Zanco et al. [258] techno-economically compared absorption, adsorption, and membrane separation for PCC from a generic flue gas source containing 12 vol.% CO_2. The economic choice (analysed through a Pareto front) depended on the plant size, for larger plants solvent-based capture with piperazine is the most cost effective. Whereas, for smaller plant sizes membranes and adsorption technologies are economically favourable. At a plant size of 5000 tons per day and 90% capture, the absorption, adsorption, and membrane technologies cost 23.4 78 €/CO_2, 78 €/CO_2, and 70 €/CO_2, without CO_2 compression. Highlighting the importance of plant size in the economics of CCS projects.

Economies of scale also plays an important role for costing OCGT's. Pauschert [259] showed the impact of plant size on various power generation technologies; the gas turbine cost for OCGT's (also called SCGT's or combustion turbines) with a power output of 5, 25, and 150 MW, is 560, 440, and 240 $/kW, respectively (2008 figures for the U.S.). Updated figures for OCGT prices ($/kW) compared to the plant size can be found in latest version of Gas Turbine World's GTW Handbook. Parsons Brinckerhoff [260] showed the TCC for OCGT's (100 MWe) ranges between 532.5-719 £/kW, and Pöyry [25] showed it ranges between 461.1-519.6 €/kW. These cost estimates will form the guidelines for the economic calculations within this project.

BEIS [261] analysed several carbon capture technologies on different power sources (natural gas, coal, and biomass). PCC technologies on CCGTS, using a GE 9HA.01 turbine with a net efficiency >62%, produce the lowest LCOE for capturing >90% CO_2. Figure 32 shows the breakdown of the technologies costs and uses and unabated CCGT plant as the baseline. The unabated plant is more expensive in the long-run due to an expected increase in carbon price, from 21.6 GBP/tonne CO_2 in 2017 to 223.3 GBP/tonne CO_2 in 2050. The metric used was an increased LCOE (£/MWh), which enabled a comparison between different generation sources. The economic analysis showed the post-combustion amine system (using a proprietary solvent) costs 69.9 £/MWh, followed closely by another CCGT plant using integrated MCFC costing 70.1 £/MWh. Interestingly, looking at a carbon footprint metric, the best technology is MCFC producing 27.1 kgCO_2/MWh, followed by the amine system at 39.3 kgCO_2/MWh. Therefore, the metric used determines the outcome of the economic comparison. Also, the carbon price plays an important role in metrics such as the cost of CO_2 avoided, which for the two technologies mentioned generates negative figures, due to the savings associated with lower emissions. The amine-CCGT system (Case 1) has a negative CCA result due to the inclusion of a variable carbon price (21.6-223.3 £/tCO_2), which means over the lifetime of the plant the cost for the capture system is less than an unabated plant. As the LCOE metric was used in BEIS [261] this will be the metric used in this project's economic analysis. Secondary metrics of interest are cost of CO_2 captured, and cost of CO_2 avoided, to give supporting information on the economics behind the actual capture technologies.

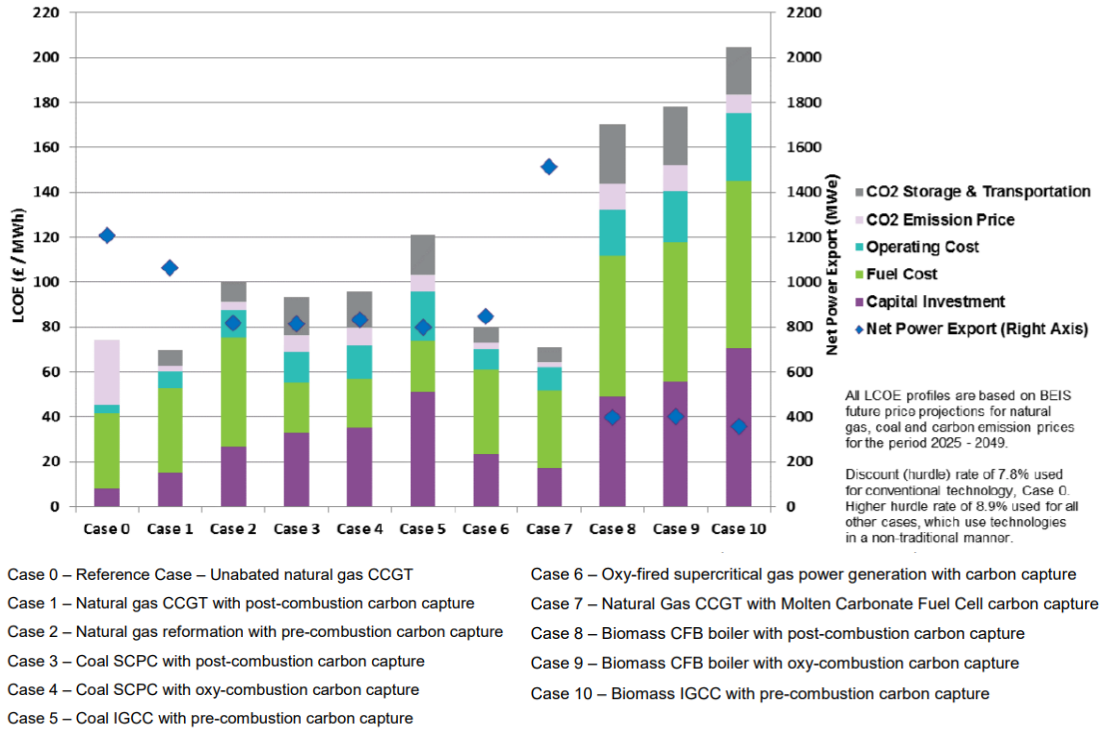

Figure 32: Levelised cost of electricity for different power generation and capture technologies from BEIS [261]

Table 16: Comparison of different power generators incorporating CO_2 capture sourced from [261]

Case [a]	Net Power Output (MWe)	CO_2 Captured (kg/h)	Capture Rate (%)	Carbon Footprint (kg CO_2/MWh)	Cost of Avoidance (£/tCO_2) [b]	LCOE (£/MWh) [b]
Case 0	1208	0	0	329.4	-	74.2
Case 1	1065	361,105	90.8	34.3	-14.5	69.9
Case 2	818	353,319	90.4	45.8	91.1	100
Case 3	814	692,310	90.0	94.6	81.3	93.3
Case 4	833	685,896	89.2	100.2	95.1	96.0
Case 5	800	673,147	90.3	90.4	195.1	120.8
Case 6	848	283,546	90.0	37.1	20.0	80.1
Case 7	1509	477,597	92.1	27.1	-11.7	70.7
Case 8	396	523,849	90.0	146.5	524.1	170.1
Case 9	402	523,093	89.9	146.2	566.1	177.9
Case 10	356	356,162	90.8	101.9	571.7	204.3

[a] based on Figure 32 and [261], [b] includes carbon priced from 2017-2050 ranging between 21.6-223.3 £/tonne CO_2, see Table 5-7 in [261] for more information.

Another crucial aspect to consider is the frequency of use, i.e., the capacity or load factor of the plant, this can be seen in Figure 31. The LCOE for OCGT's depends on the capacity and usage. LeighFisher [262] compared various power generation technologies with different capacity factors and including CCS. Within the study two capacity factor are used for OCGT's, critical peak is 500 hours per annum

(5.7%) and for peak is 2000 hours per annum (22.8%). Figure 33 shows the LCOE for OCGT power generation at different power outputs and CF's, the raw data is source from LeighFisher for plants commissioned in 2013 [262]. As you decrease in plant size the cost dramatically increases, especially with a low-capacity factors. This is a potential issue for OCGT-PCC. The study also showed cost breakdown (construction, FOM and VOM cost estimates) for OCGT-PCC shown in Table 17. The size of the OCGT plant and information on the PCC plant is not provided; therefore, it is difficult to compare the OCGT-PCC LCOE range (173-198 £/MWh) to the technologies investigated in BEIS [261].

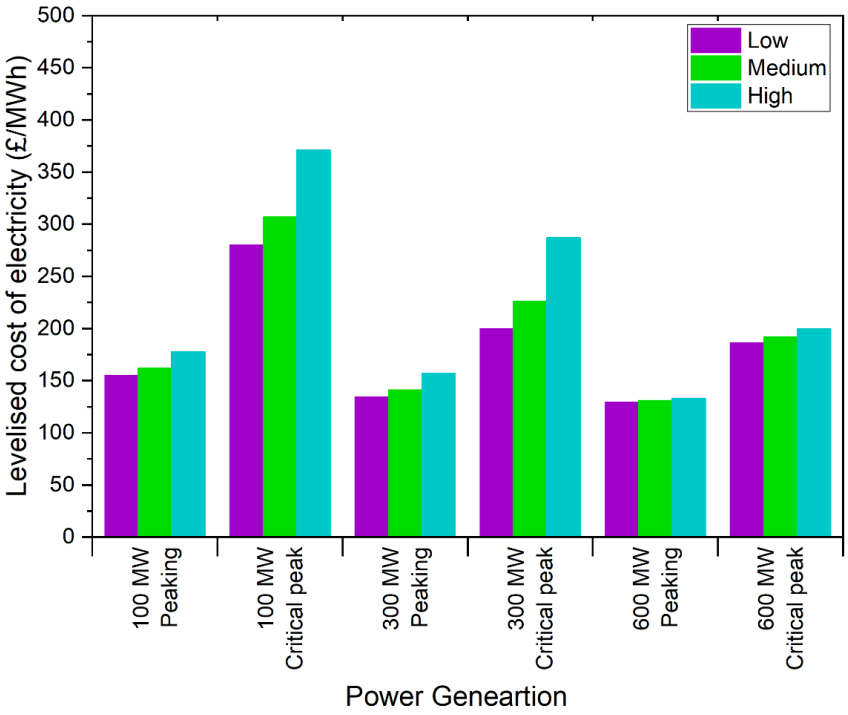

Figure 33: Levelised cost of electricity for OCGT generation at different power outputs and capacity factors . Peaking assumes 2000 hours per annum (CF=22.8%) and critical peak assumes 500 hours per annum (CF=5.7%). Data sourced from LeighFisher [262]

Table 17: OCGT - PCC cost breakdown from LeighFisher [262]

Technology		Construction Cost (£/kW)	FOM (£/MW/year)	VOM (£/MWh)	LCOE (£/MWh)
OCGT - PCC	Low	1907	26584	2.48	173
	Medium	2347	31752	2.97	183
	High	2969	36894	3.38	198

Parsons Brinckerhoff reported a cost model update for non-renewable power generation technologies [263]. In which, the study used a 5-10% CF for OCGT's; however, the report does not present LCOE data. BEIS [255] showed the electricity generation costs for projects commissioned in 2025, 2030, 2035 and 2040. Table 18 shows the LCOE of OCGT's at different power outputs, the study used 500 hours (5.7% CF) and 2000 hours (22.8% CF) for the annual operating time. For 100 MWe plants commissioned in 2025, the LCOE ranges between 161-383 £/MWh. For 600 MWe plants commissioned in 2025, the LCOE ranges between 136-209 £/MWh. As the commissioning date influence the costs, this assumption needs to be specified in the economic model. Also, as the total annual operating hours also affects the LCOE, this will also be investigated in this project.

Table 18: Levelised cost of electricity of electricity for OCGT's from BEIS [255]

Power output (MW)	Annual operating time (hours)	Estimate level	2025 (£/MWh)	2030 (£/MWh)	2035 (£/MWh)	2040 (£/MWh)
100	500	High	383	406	429	446
		Medium	315	337	361	377
		Low	286	307	330	347
100	2000	High	186	209	232	248
		Medium	169	191	214	231
		Low	161	183	207	223
299	500	High	295	318	341	358
		Medium	236	258	282	298
		Low	206	228	251	268
299	2000	High	164	186	210	226
		Medium	149	171	194	211
		Low	141	164	187	203
300	500	High	298	321	345	361
		Medium	234	257	280	297
		Low	207	229	252	269
300	2000	High	164	187	210	227
		Medium	148	170	194	210
		Low	141	163	187	203
400	500	High	237	260	284	301
		Medium	216	239	263	280
		Low	201	224	248	265
400	2000	High	150	172	196	213
		Medium	144	167	191	208
		Low	141	163	187	204
600	500	High	209	231	254	271
		Medium	199	222	245	261
		Low	192	214	237	254
600	2000	High	140	162	185	202
		Medium	137	159	183	199
		Low	136	158	181	197

EIA [264] showed the LCOE (2021) for dispatchable power generation technologies in the U.S.: CCGT (34.51 $/MWh), OCGT (107.83 $/MWh), geothermal (36.02 $/MWh), and battery storage (121.84 $/MWh). Highlighting the high cost per MWh for OCGT's. Similarly in the UK, the Sixth Carbon Budget [265] showed the cost difference for renewable, firm and dispatchable power generation up to 2050, shown in Table 19. Dispatchable sources range between 100-205 £/MWh in 2035 and 110-220 £/MWh. This will be used as a guideline for cost calculations. Although it does not state the capacity factor used in calculating the LCOE.

Table 19: Cost of different power generation sources [265]

Generation type	2020 (£/MWh)	2035 (£/MWh)	2050 (£/MWh)
Unabated gas plant (excluding carbon price)	50	60	60
Intermittent renewables (wind and solar)	65	40-45	25-40
Firm power generation (Nuclear)	-	85-105	85-105
Dispatchable low-carbon power (gas-CCS, BECCS, and hydrogen)	-	100-205	110-220

It is essential any PCC technology is lower in cost than Carbon Dioxide Removal (CDR) technologies, such as BECCS, DAC, and nature-based solutions [266]. The estimated cost of capture for DAC ranges between 273-1227 $/t$CO_2$ depending on the economic assumptions (utilities cost, plant life, and

CAPEX) [267]. This is why the levelised cost of capture metric is important as it enables comparisons to other capture sectors, not just power related [47].

DAC can be used to offset carbon emissions from gas turbines [268], therefore, any PCC plant attached onto an OCGT power generator must be more affordable than DAC. DAC can also be used to ensure any residual and indirect emissions are captured; thus, creating carbon neutral/negative processes. Cheng et al. [269] used DAC to show the potential for a carbon-negative NGCC plant, using PCC to capture the bulk of the CO_2 emissions and DAC to capture any residual emissions. Mullen et al. [270] used 100-1000 £/tCO2 as the cost range for DAC, which was use d to offset the indirect emissions in hydrogen supply chains. This study showed the cost of hydrogen through steam methane reforming (SMR) with 100% PCC is 69£/MWh_{th} (2.7 £/kg), and with DAC compensating for supply chain emissions it is 71-86 £/MWh_{th}. This is comparable to H_2 via electrolysis which ranges between 3.8-5.8 £/kg (2025 commissioning) and uses dedicated renewable power.

Carbon neutral hydrogen is interesting because it can be used in gas turbines to provide dispatchable power [271, 272]. ETN [273] showed the potential of hydrogen and hydrogen blending in OCGT, CCGT, and CHP power generators. For a small OCGT (20 MWe) the LCOE increases the higher the H_2 blending percentage as shown in Figure 34. Fuel switching is possible and drives the carbon intensity down, but the cost increase is due to additional cost of H_2 fuel which is set at 1.5 €/kg. The break-even carbon price required for 100% H_2 to be economically favourable is 223 €/tCO2. These costs will be used in the techno-economic assessment to compare OCGT+CCS with 100% H_2 turbines.

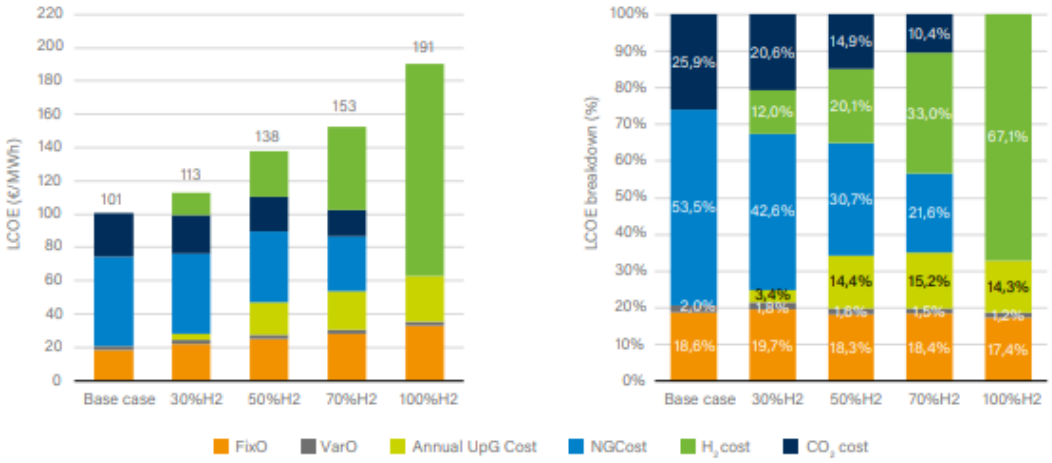

Figure 34: OCGT LCOE (left) and LCOE breakdown (right) with increasing H_2 blending [273].

Another alternate dispatchable technology is energy storage, which has the potential to store surplus renewable energy and re-introduce it to the grid during periods of peak demand [274]. CEC [275] compared gas turbines and batter energy storage systems (BESS) for peak power supply in Australia. The study showed the LCOE for a 250 MW gas fired OCGT is 234 AUD$/MWh, whereas a two-hour 250 MW BESS is 195 AUD$/MWh, and a four-hour 250 MW BESS is 156 AUD$/MWh. The study concluded that large-scale battery storage, in Australia, is now the more affordable choice for dispatchable power generation, and this is without the inclusion of CCS for the OCGT. For the UK, the levelized cost of storage (LCOS) is shown in Figure 35 from BEIS [276], where the LCOS ranges approximately between 30-300 £/MWh depending on the technology used and the cycling levels.

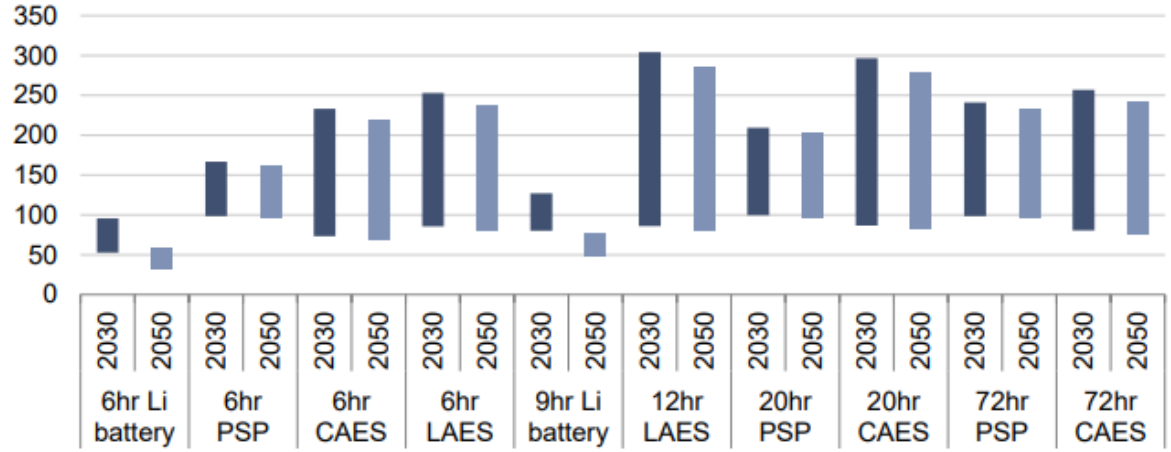

Figure 35: Levelised cost of medium and lond duration energy storage using batteries, pumped storage plants (PSP), compressed air energy storage (CAES), liquid-air energy storage (LAES) [276].

2.7.Conclusion

Energy systems globally need to become more sustainable, with fossil-based power generators incorporating CCS. This chapter reviews CCS technologies specifically for PCC, evaluating their potential for flexible operation attached to quick-response gas turbines. Within, the various CO_2 capture technologies are described in terms of their commercial availability and readiness. The benchmark PCC technology is amine-absorption using 20-30 wt.% MEA. Of the other technologies reviewed (adsorption, membrane separation, chemical looping combustion, calcium looping, and fuel cell integration) physical adsorption and membrane separation are the closest to commercialisation, with PSA/VSA moving to TRL9 with the latest developments at Air Product's Port Arthur SMR CCS project. Therefore, the two technologies further investigated in this study and amine-absorption and zeolite-adsorption.

Included in the review is CO_2 conditioning, as the capture sources need to be prepared for transportation to storage or utilisation sites. The two main conditioning routes are conventional multistage centrifugal compression, and compression with liquefaction (either sub- or super-critical). Both techniques will be analysed in this study.

A key factor in the potential deployment of these PCC systems is their cost-effectiveness. As the generators in question (OCGT's) have a low-capacity factor, i.e., they only operate during peak load, the capture systems need to be inexpensive to avoid drastically increasing the cost of electricity generation. The cost of electricity generation for other low-carbon power sources is shown to highlight the cost range required to keep OCGT+CCS competitive in future markets. Forming the benchmarks within the techno-economic evaluation.

The literature surrounding CCS technologies is vast due to importance of such systems to combat the effects of climate change. Hence, not all technologies are included in this literature review, but where applicable sources are given to provide the reader a greater understanding of the technical and economic challenges CCS faces.

Chapter 3 : Modelling and Methodology

To transition to a low-carbon future and maintain security of electricity supply, understanding the dynamic behaviour of PCC on flexible fossil power is of the utmost importance [277]. The necessity and role CCS can play in future energy system is explained by Domenichini et al. [278], Heuberger et al. [279] and Mac Dowell and Staffell [280]. It can even be economically beneficial by exploiting higher electricity prices during peak periods [281]. Several simulation based studies have investigated operational flexibility of coal- and gas-PCC, focussing on comparing operating strategies [282, 228], developing process control strategies [229, 283], and multi-period optimisation [284]. Montañés et al. [238] identifies the operational requirements of flexible CO_2 capture, concluding that future work should consist of validated dynamic process models evaluating various transient operating scenarios, to discover potential bottlenecks during flexible operation. However, almost all of the flexible PCC studies focus on amine-based CO_2 capture. Rui et al. [111] analysed CO_2 capture from flue gas using VPSA under unstable feed concentrations. The model-based study incorporated PID control strategies (closed-loop and open-loop feedback control) to adjust adsorption step duration for product quality control during variable feed concentration. To the authors knowledge, adsorption technologies for flexible-PCC have not previously been investigated.

Another gap within the literature is the scale of flexible PCC: the majority of work revolves around large-scale power sources >300MW and some work has been done on micro-gas turbines <1MW [285, 286]. To the authors knowledge, no studies have focused on the transient operation of absorption-based PCC on small-scale fossil power sources (>1MW to <50MW). This study aims to fill this gap in the literature and focuses on PCC for OCGT power plants, due to their expected growth in the UK energy market [17]. Since these power sources have no HRSG units, there is no possibility of re-routing reboiler steam for increased power output in a frequency response scenario [65].

Therefore, there is a gap in the literature for small-scale (between 1-300 MW) flexible-PCC. Based on the literature review in Chapter 2, the two capture technologies further investigated in this study capable of transient OCGT-PCC are:

- **MEA Absorption** – this is considered the benchmark capture technology, with extensive pilot scale research and flexible-response studies,
- **Zeolite 13X Adsorption** – adsorption-based technologies are improving and are one of the closest to commercialisation of the all the competing capture technologies. For this study vacuum-pressure swing adsorption (VPSA) is used as the majority of pilot-scale studies focus on this operating cycle.

3.1. Aims and objectives

With the role small-scale decentralised power can play in decarbonising the energy sector, this project analyses the transient behaviour of OCGTs in the UK electricity system. This data is translated into exhaust gas flowrates and used to simulate the flexible operation of small–scaled CO_2 capture plants using MEA absorption and VPSA with Zeolite 13X. Figure 36 highlights the different components analysed in this study. The transient nature of OCGT power plants is assessed using data from the BMRS and industrial suppliers. Within this study, the possible complexities of PCC for OCGTs are addressed through:

- Evaluating the transient operational behaviour of **OCGT** power generation.
- Development and validation of a dynamic model for an **MEA-PCC** process.
- Development and validation of a dynamic model for a **VPSA-PCC** process.
- Assessing the flexible response of PCC under different operating scenarios.
- Developing economics models for power generation and CO_2 capture.
- Techno-economic comparison of CO_2 absorption vs adsorption for **Flexible-PCC**.

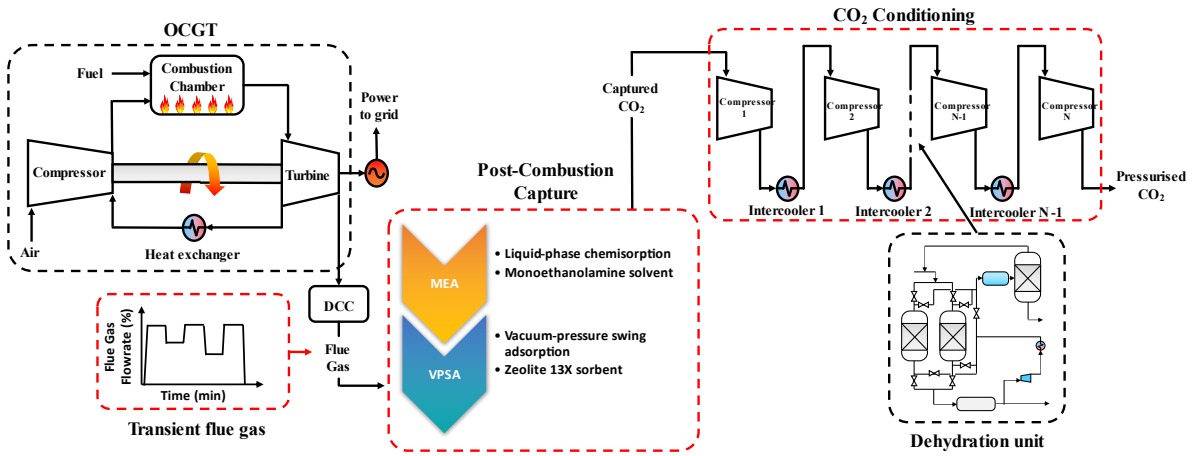

Figure 36: Study overview focussing on the main aspects investigated (red dotted boxes) in this project.

Another aspect investigated in this project is CO_2 compression and conditioning. One of the issues with designing the compression train is the end point specifications. Alongside the various transportation methods, there are also different composition guidelines depending on the end use of the CO_2 (geological storage or utilisation) [44]. Various sources mentioned in the literature review (Chapter 2) have examined the effects of impurities in the CO_2 feed, or the effects of reaching different end points in terms of composition, pressure, and temperature, however few sources look at both ends of the problem. Therefore, included in this project is the impact that different CO_2 sources and end point specifications have on the power demand for the conditioning (compression and moisture removal) train. For each technology, the compression system will elevate the CO_2 stream pressure to 111 bar and 70℃ as specified in IEAGHG [60]. The two processes for conditioning are multistage compression based of the IEAGHG base case B0, and multistage compression and liquefaction based on the IEAGHG case D2c. As moisture content is a limitation for transport, utilisation, and storage, three moisture levels are analysed within this study to compare different end-point composition guidelines:

- **Low** – 20 ppm specification for the food and beverages industry [208].
- **Medium** – 300 ppm cost-optimal level for pipeline transportation from Brunsvold et al. [222].
- **High** – 600 ppm specification for pipeline transportation from Kinder Morgan [209].

Large CCS clusters will have a range of flowrates attached with some having transient production; this is a key challenge highlighted in [239]. A sensitivity analysis focussed on inlet flowrate and pressure for both conditioning routes is included to identify the relationship between system size and power demand. A growing focus for power generation CO_2 capture is transient/flexible operation, due to a growing renewable capacity driving fossil fuel-based sources to act as balancing services [44]. Therefore, a dynamic study based on realistic load-following capture plant operation is also included, comparing both conditioning trains and highlighting the issues of transient operation.

3.2. Flexible gas turbine operation

To evaluate the transient operation of an OCGT plant, data is analysed from the BMRS, which provides operational data on the balancing and settlement arrangements in Great Britain, with a 30-minute time interval [287]. Figure 37 is a compilation of OCGT generation over the last four years in the GB. The data is grouped per generation type: individual loads for each power station are not reported. OCGT plants come on the system as a balancing service during periods of high demand, typically used in the colder months of January, February, and December. The maximum load on the system for that given year is dependent on the amount of generation contracted in the capacity auction market and therefore changes each year.

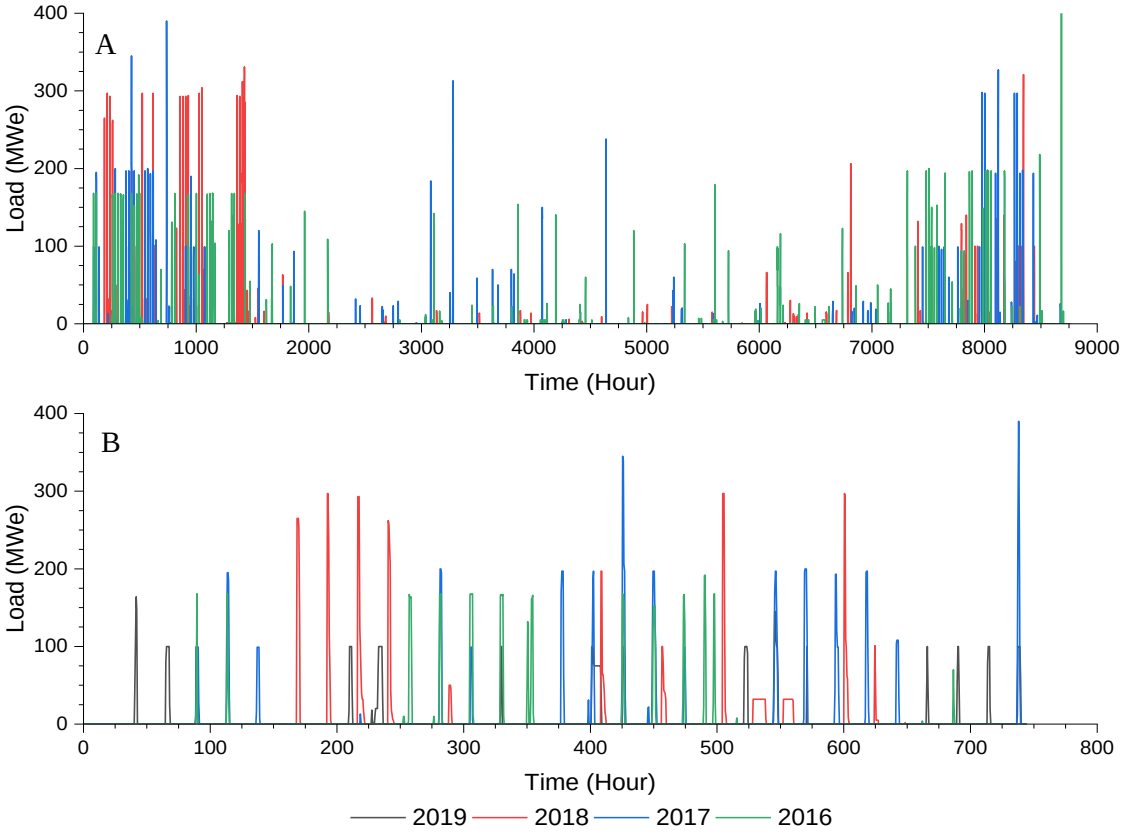

Figure 37: Half hourly OCGT generation over previous four years in GB, showing data for A) the entire year and B) January. Data sourced from ELEXON [287].

Figure 38 compares the time of the day OCGT generation has come on in the month of January over the last 4 years. Over this 744-hour period, OCGT generation comes on the system on average of 15 times but ranges between 12 to 17 times, typically active between 15:00-20:00, corresponding to the peak daily demand in GB. In 2018, OCGT generation was on the system mostly overnight instead of in the evenings, as a result of severe weather conditions. However, the plants still operated for a similar amount of time, averaging 5 hours per day. The maximum annual operation over the previous four years was in 2018 with 230 hours. The difficulty lies with predicting these ramping cycles, in order to develop suitable control strategies for efficient PCC performance. For instance, several days show two distinct peaks with several hour gaps in between. Also, OCGTs typically have one major power output peak per operating cycle (from start-up to shutdown), however, the magnitude and timescale of these peaks vary. Combining this with the information in Figure 37 shows multiple periods where the power output has changed, and the new power output is maintained for several hours.

The key observations from the BMRS data for OCGT generation are as follows:

- Sporadic operation largely deployed in the winter months.
- Used for peak demand typically in the evenings.
- Highly transient behaviour i.e., ramping to different power outputs during the same operating cycle, with multiple operating cycles within a 24-hour period.
- Average operating cycle is 5 hours.
- Total power generated from OCGTs varies annually.

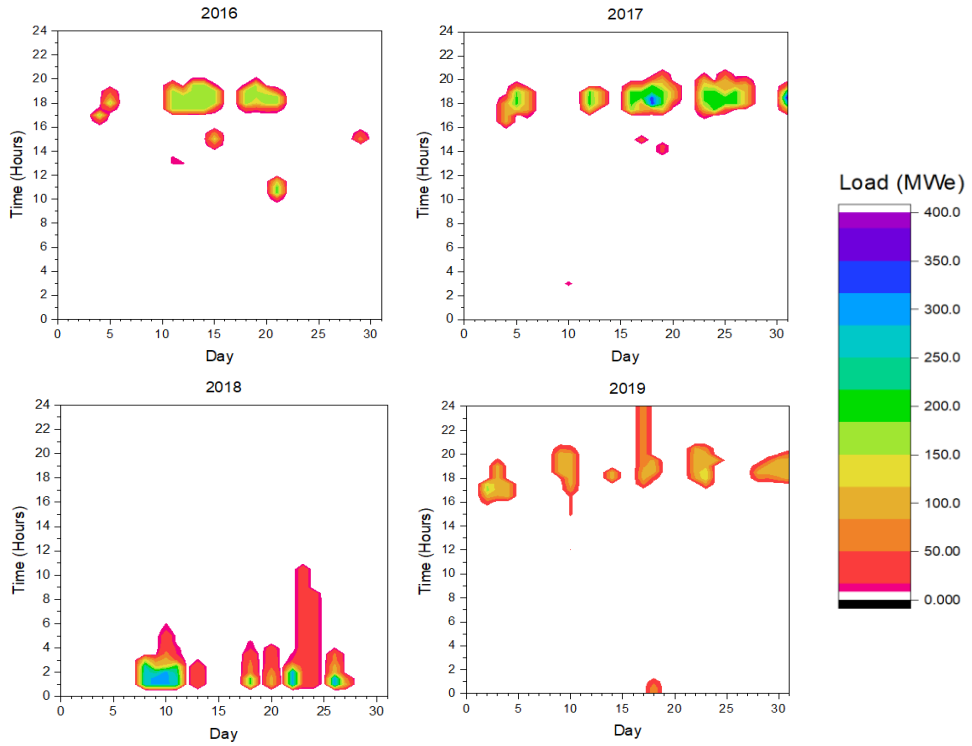

Figure 38: Contour plot of OCGT generation in January over the previous four years in the GB. Data sourced from ELEXON [287].

Table 20 shows the total power generated from OCGTs between 2016-2022, included in the table is the associated carbon emissions and the comparison to the overall UK emissions. OCGT's contribute a small portion of the overall emissions, however, this has recently increased due to the heavy reliance on this dispatchable thermal generator to countering intermittency issues. In 2021, over 50% of the electricity generated came from low-carbon energy sources such as nuclear and renewables [288]. In the same year, OCGT annual electricity generation increased to almost 50 GWh, and accounting for 28% of the total electricity system emissions.

Table 20: Annual OCGT power generation and emissions, compared to overall UK values.

Year	OCGT annual electricity generation (MWh) [287]	Total electricity system carbon emissions ($MtCO_2e$) [289]	OCGT annual carbon emissions ($MtCO_2e$) [a]	OCGT Carbon share (%)
2016	3,504	114.9	1.61	1.40
2017	5,759	104.6	2.65	2.53
2018	4,563	97.4	2.10	2.15
2019	3,580	89.3	1.65	1.84
2020	8,739	78.1	4.02	5.15
2021	48,618	80.8	22.36	27.69
2022	25,897	82.2	11.91	14.50

[a] OCGT carbon intensity set at 460 g/kWh based on [290]

The Electricity Market Reform (EMR) set the Emissions Performance Standard for CO_2 emissions at 450g/kWh for baseload operation, however, due to OCGTs operating as essential balancing services they are allowed higher emissions guidelines (averaged at 460 g/kWh) [290].

This study uses the Siemens SGT-400 as an example modern gas turbine; the 11 MW version produces 33.8 kg/s of exhaust mass flow with low NO_X (≤25 ppm) and 4.27 vol.% CO_2 (6.78 wt.% or 4.42 mol.%). The rated power output in open-cycle configuration is 10.4 MWe [42]. Assuming the exhaust temperature can be brought down to a suitable inlet absorber or adsorber temperature through a heat recovery unit, the dynamic models for MEA-PCC and VPSA-PCC are scaled to handle 33.8 kg/s of exhaust gas. Based on average data from Agora Energiewende [291], the start-up and shutdown rates are 12.5% baseload per minute and the ramping rates are 10% baseload per minute. Figure 39 shows the flowrate changes throughout each operating scenario as a percentage of the baseload operation. Each new power output is maintained for 1 hour, or two settlement periods based of the balancing and settlement period in GB. The scaled capture plants consist of non-optimised equipment sizes used for comparative analysis and not for process design.

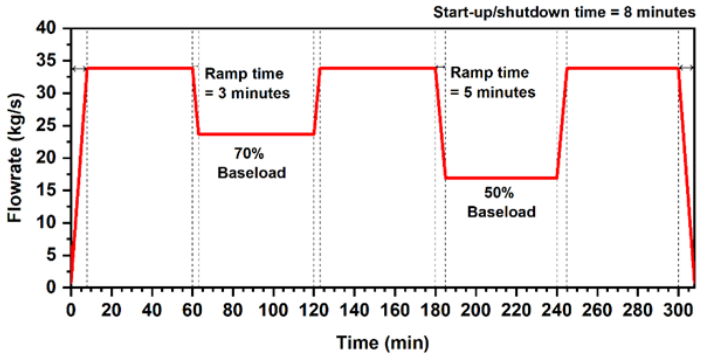

Figure 39: Flue gas flowrate changes throughout the operating scenarios

3.3. Process simulation

Included in this section is the method and models used to simulate CO_2 adsorption, CO_2 absorption, and CO_2 compression. Also included is the economic model, which requires equipment sizing from the scaled process models in order to calculate key performance indicators (KPIs) for the capture systems. Within this study, three main KPIs are analysed for each capture technology: CO_2 capture rate (η), CO_2 purity, and specific energy demand (E_T) , calculated using Equations 24, 25, and 26, respectively.

$$\eta\ [\%] = \frac{M_{CO_2}^{in} - M_{CO_2}^{out}}{M_{CO_2}^{in}} \times 100 \quad (24)$$

$$Purity\ [\%] = \frac{M_{CO_2}^{Product}}{M_{Total}^{Product}} \times 100 \quad (25)$$

$$E_T\ [kWh/tCO_2] = \frac{Total\ Energy\ Demand\ [kWh]}{M_{CO_2}^{in} - M_{CO_2}^{out}\ [ton]} \quad (26)$$

Where, $M_{CO_2}^{in}$ and $M_{CO_2}^{out}$ are the input and output mass flowrates of CO_2. $M_{CO_2}^{Product}$ and $M_{Total}^{Product}$ are the mass flowrates of CO_2 in the product stream and the total mass flowrate of the product stream, respectively, i.e., the concentration of CO_2 in the product stream.

3.3.1. Benchmark MEA absorption

The complex reaction chemistry and process design of amine-absorption can be captured through steady-state modelling. However, to capture the transient process behaviour, high-fidelity dynamic models must be used to account for any variation due to time. Chikukwa et al. [292], Bui et al. [293]

and Wu et al. [294] have reviewed dynamic modelling of amine-absorption, and showed throughout the literature simulations using a rate-based approach yield more accurate predictions of key process parameters. For rate-based simulations, the multi-component mass and heat transfer in a packed absorption/desorption column is described by two-film theory, where an infinitesimally thin interface separates the liquid and gas films. For this study, each column is represented by a cascade of non-equilibrium stages (j). Assuming negligible radial variation of properties and minimal solvent degradation, the material balances for component i in the liquid and gas phases are [295]:

$$\frac{\partial M_{i,j}^{L}}{\partial t} = \frac{\partial L_{i,j}}{\partial z} + \mathcal{N}_{\mathrm{i,j}}^{L} \quad i = 1, \dots, c, \;\; j = 1, \dots, \mathrm{n} \tag{27}$$

$$\frac{\partial M_{i,j}^{G}}{\partial t} = \frac{\partial G_{i,j}}{\partial z} - \mathcal{N}_{\mathrm{i,j}}^{G} \quad i = 1, \dots, c, \;\; j = 1, \dots, \mathrm{n} \tag{28}$$

Where M is the molar holdup or accumulation of components i to c in stages j to n, axially distributed across height z (m), L is the liquid molar flow (kmol/s) and G is the gas molar flow (kmol/s). The superscripts L and G denote the liquid and gas phases, respectively. At any position in the column there must be continuity between the molar fluxes ($\mathcal{N}$) across the interface, which are functions of the mass transfer coefficients for the gas and liquid flows [296]. Mores et al. [297] compared mass transfer correlations for MEA-CO_2 desorption from Bravo and Fair [298] and Onda et al. [299] using experimental data from Dugas [300]. The report concluded the correlation in Onda et al. [299] was more suitable due to the overall smaller deviation between predicted and experimental values. Onda et al. [299] developed the following mass transfer correlations for gas absorption and desorption systems:

$$k_{i,j}^{L} = 0.0051 \left(\frac{L}{a_w \mu_L}\right)^{\frac{2}{3}} \left(\frac{\mu_L}{\rho_L D_L}\right)^{-\frac{1}{2}} \left(a_t d_p\right)^{0.4} \left(\frac{\mu_L g}{\rho_L}\right)^{0.333} \tag{29}$$

$$k_{i,\mathrm{j}}^{G} = 5.23 \left(\frac{G}{a_t \mu_G}\right)^{0.7} \left(\frac{\mu_G}{\rho_G D_G}\right)^{\frac{1}{3}} \left(a_p d_p\right)^{-2} \left(\frac{\mathrm{RT}}{\mathrm{a_T d_p}}\right)^{-1} \tag{30}$$

Where k is the mass transfer co-efficient of component i in the liquid (m/s) and gas phases (kg.mol/m^2/s/atm), a_T is the total packing surface area (m^2/m^3), a_w is the wetted packing surface area (m^2/m^3), μ is the viscosity (kg/m/s), d_p is the packing nominal size (m), g is the acceleration due to gravity (m/s^2), ρ is density (kg/m^3), D is the diffusion coefficient (m^2/s), R is the gas constant (m^3.atm/kg/mol/K) and T is the temperature (K). Phase equilibrium is assumed at the vapour-liquid interface, and chemical equilibrium is assumed in the entire liquid phase. Reactions are treated implicitly and the thermophysical properties are described through the Statistical Associating Fluid Theory (SAFT) properties package gSAFT-VR [301]. The fluid phase behaviour of CO_2 in aqueous MEA described by gSAFT-VR is discussed at length in Mac Dowell et al. [302]. The pressure decrease over each spatial element is modelled using the approach in Billet and Schultes [303] for irrigated random or structured packing. The overall equation is:

$$\frac{\partial P}{\partial z} = \psi_L \frac{a_W}{(\varepsilon - h_l)^3} \frac{F_G^2}{2} \frac{1}{K} \tag{31}$$

Where P is pressure (Pa), ψ_L is the resistance coefficient, ε is the void fraction, h_l is the liquid holdup, F_G is the gas capacity factor ($Pa^{0.5}$), and K is the wall factor. A more detailed explanation of the equations and limits is shown in Billet and Schultes [303]. Under adiabatic conditions, the energy balances for the liquid and gas phases are [304]:

$$\frac{\partial U_j^L}{\partial t} = \frac{\partial H_j^L}{\partial z} + \varepsilon_{f,j}^L \qquad j = 1, \dots, n \tag{32}$$

$$\frac{\partial U_j^V}{\partial t} = \frac{\partial H_j^V}{\partial z} - \varepsilon_{f,j}^V \qquad j = 1, \dots, n \tag{33}$$

Where U is the energy holdup or accumulation of energy in that phase on stage j to n. H is the energy flow (kJ/s), and $\boldsymbol{\varepsilon_f}$ is the energy flux across the interface (kJ/s). Figure 40 shows the model topology of a conventional amine-absorption process, developed in gPROMS® gCCS 1.1.0. The model includes the dynamic operation of the condenser, reboiler, and heat-exchanger units. For non-equilibrium stage models for multicomponent distillation, the reboiler and condenser units can be considered equilibrium stages, modelled using the MESH equations described in Taylor and Krishna [296]. The heat exchangers are modelled using the number of transfer units (NTU) method, described in Shah and Sekulić [305]. The heat transfer area is calculated to give the desired rich-solvent temperature prior to entering the stripping column. This assumes the system is under adiabatic conditions, with a fixed heat transfer co-efficient and pressure drop [301]. The height of packing for the absorber and stripping columns are scaled using the transfer unit method described in Mores et al. [297].

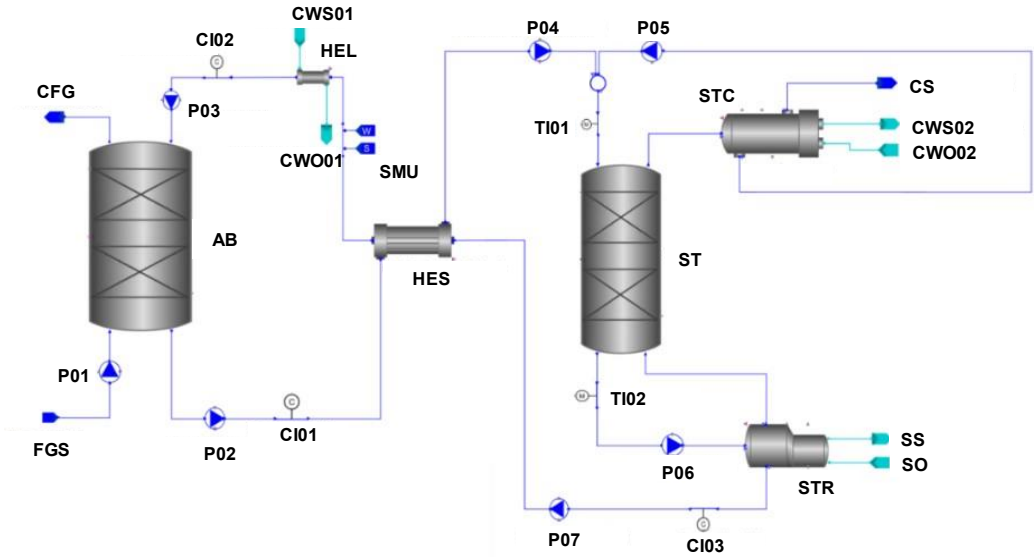

Legend

AB	Absorption column	**CSO**	Cooling water source	**P**	Pump	**ST**	Stripping column
CFG	Cleaned flue gas	**CWO**	Cooling water outlet	**SMU**	Solvent make-up	**STR**	Stripper reboiler
CI	Composition indicator	**HEL**	Lean heat-exchanger	**SO**	Steam outlet	**STC**	Stripper condenser
CS	CO_2 sink	**HES**	Solvent heat-exchanger	**SS**	Steam source	**TI**	Temperature indicator

Figure 40: Model topology for MEA CO_2 capture developed in gPROMS gCCS

Throughout the literature, CO_2 capture technologies are analysed and compared through capture efficiency and energy demand. In this study, the key operating parameter is the CO_2 capture rate. A key process indicator is the reboiler duty, representing the process energy demand. The CO_2 capture rate is the percentage of CO_2 removed from the flue gas. Bui et al. [68] highlights two potential ways to calculate the reboiler duty, where the energy supplied to the reboiler is divided by either the CO_2 product flow post-stripping or the difference between the flue gas inlet and clean gas outlet CO_2 flowrates. The energy supplied to the reboiler is the difference between the enthalpy of the inlet utility steam and saturation enthalpy of the outlet condensed steam [306]. The reboiler duty, in GJ per ton of CO_2 captured, is calculated using:

$$R_d = \mathrm{Q_R}\left(M_{CO_2}^{in} - M_{CO_2}^{out}\right) \quad 34$$

Where R_d is the reboiler duty (GJ/tCO₂), Q_R is the energy supplied to the reboiler (MJ/h), $M_{CO_2}^{in}$ is the mass flowrate of the CO_2 in the flue gas (kg/h) and $M_{CO_2}^{out}$ is the mass flowrate of CO_2 in the cleaned gas (kg/h). Over the duration of the simulation, the reboiler duty can be calculated for that instance as a continuous calculation. Alternatively, averages for the reboiler duty and the total quantity of CO_2 removed per the time frame can be used to determine the overall energy demand for a given operation.

3.3.1.1.Case study: MEA pilot plant

Although a large number of pilot plant data is openly available, the number of dynamic operating data limited. Dynamic model validation against steady-state data is beneficial [307, 308, 309, 310, 311], however, it doesn't automatically correspond to dynamic operation. Several studies have validated dynamic models against dynamic pilot scale plant data [312, 313, 314] and demonstration scale plant data [315, 316]. Tait et al. [65] presented pilot-scale results for flexible gas-PCC operation. Their investigation tested five different dynamic capture plant scenarios: start-up, shutdown, capture plant decoupling, reboiler decoupling, and frequency response. The baseload operating conditions are shown in Table 21. The capture plant uses 30.16 wt.% MEA, and the flue gas is representative of a GT with 4.27 vol.% CO_2.

Table 21: Key process parameters for the baseload operating scenario from Tait et al. [65]

Process Parameter		**Value**
Absorber	Packing material	Sulzer Mellapak 250.X
	Packing height (m)	6.92
	Packing diameter (mm)	158.00
Stripper	Packing material	Sulzer Mellapak 500.X
	Packing height (m)	5.00
	Packing diameter (mm)	350.00
Flue gas flowrate (Nm^3/h)		120.50
Flue gas temperature (°C)		46.14
Flue gas CO_2 concentration (vol.%)		4.27
Solvent flowrate (L/h)		344.40
Solvent temperature into absorber (°C)		40.05
Solvent temperature into stripper (°C)		104.07
L/G ratio (L/m^3)		2.86
Steam flowrate to reboiler (kg/h)		19.50
Steam pressure (bar)		4.00
Stripper pressure (bar)		1.80
Reboiler Duty (GJ/tCO₂)		3.96
CO_2 capture rate (%)		89.70
Lean loading (mol CO_2/mol MEA)		0.232
Rich Loading (mol CO_2/mol MEA)		0.345

The choice of packing material dictates the hydraulic parameters required to calculate the pressure drop, and the coefficients required in the mass transfer correlations. Table 22 shows the values used in this study, based off the values from Billet and Schultes [303] for Mellapak 250Y. For the stripping column the specific area is 500 m^2/m^3.

To accurately assess the model's capability under different transient operating scenarios, both the start-up and shutdown experiments are used for validation, these aspects of full-cycle operation will also be included in the full-scale study. In Tait et al. [65], during the shutdown procedure the flue gas and solvent flowrates are simultaneously decreased over 16 minutes to 40% baseload, then further decreased to 30% baseload over the next 4 minutes. The steam flowrate to the reboiler, is decreased to 0% load in the first 10 minutes. At 20 minutes the flue gas is flowrate is dropped to 0% baseload. The ramp rates in Tait et al. [65] were taken from a Siemens STG5-4000F. For the start-up procedure, the steam flowrate and gas flowrates start at 0% baseload, whilst the solvent flowrate remains at 30% baseload. Over 5.25 minutes the gas flowrate is increased to 30% baseload, and then both gas and solvent flowrates are increased simultaneously to maintain a constant L/G ratio. A more detailed explanation of the operating procedures can be found in Tait et al. [65].

Table 22: Packing specific parameters

Packing Specific Parameter	**Value**
Void Fraction	0.970
Specific Area (m^2/m^3)	250
Nominal Size (mm)	50
Loading Point Coefficient	3.157
Flooding Point Coefficient	2.464
Liquid Holdup Coefficient	0.554
Pressure drop Coefficient	0.292

3.3.2.Vacuum pressure swing adsorption

Physical adsorption is an inherently dynamic process, and as the more strongly adsorbed species (CO_2) never breaks through the bed, it can be classed as being in cyclic steady state. Capturing the systems complex behaviour requires a set of partial differential and algebraic equations (PDAEs) for the conservation of mass, energy, and momentum [317]. Li et al. [318] provides a literature review of mathematical models of carbon capture by adsorption (CCA). Throughout the literature, models are usually one-dimensional and axially dispersed, assuming plug flow regime and negligible temperature, pressure, and concentration variation in the radial domain. Figure 41 illustrates the composition of physical adsorption model. The material balance over the fixed bed includes two important sub-models: adsorption kinetics (rate of mass transfer between gas and solid) and adsorption equilibrium (isotherm model). Within the literature, the Linear Driving Force (LDF) model is the most commonly used diffusion mechanism to describe mass transfer between the fluid and adsorbent, as it considers internal diffusional and external convection [317].

Isotherm models calculate the equilibrium adsorption amount of each species. The equations contain multiple semiempirical parameters that are determined through adsorption experiments over a range of temperatures. For CO_2 separation, several isotherm models are commonly used in the literature, see Table 49 in Section 10.1 Appendix A, usually an extension of the Langmuir isotherm model (dual-site Langmuir, Freundlich, Langmuir-Freundlich, BET, Sips, Toth) which accounts for multicomponent mixtures. The Ideal Adsorption Solution (IAS) theory has also been used, utilising pure component adsorption isotherms, and enabling different isotherm models to be used for each component [319, 320, 321, 322].

The energy balance describes the heat transfer between the gas and solid particles, as well as the column wall. Mathematic models in the literature vary in complexity of the heat transfer. Non-isothermal and non-adiabatic models that take into consideration heat transfer between the gas and solid adsorbent are classified as non-equilibrium models. Those that consider the energy flux between the gas and solid adsorbent as negligible are in thermal equilibrium [318]. The momentum balance considers the pressure drop in the column due to resistances in gas flow, modelled using the Blake-Kozeny equation (linear-laminar flow), the Ergun equation (non-linear turbulent flow) or the Darcy equation [317].

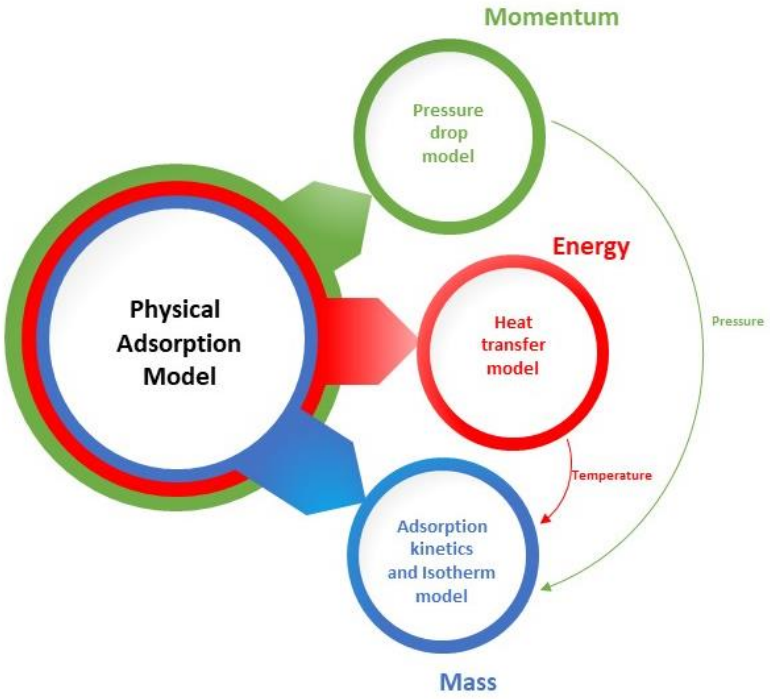

Figure 41: Physical adsorption model components

The process models (single column used for validation and multi-column used for large-scale dynamic analysis) are one dimensional and axially dispersed, with fluid flow described through the plug flow model, i.e., no radial variation in temperature, pressure, and concentration. The fluid phase material balance for component i through the packed bed is represented by the axial plug flow model [319]:

$$-D_L \frac{\partial^2 C_i}{\partial z^2} + \frac{\partial}{\partial z}(v_s C_i) + \frac{\partial C_i}{\partial t} + \left(\frac{1-\varepsilon}{\varepsilon}\right)\frac{\partial \overline{q}_i}{\partial t} = 0 \qquad 35$$

Where D_L is the axial dispersion coefficient [m^2/s], C_i is the fluid component concentration [kmol/m^3], and v_s is superficial fluid velocity [m/s]. The mass transfer rate is described through the LDF model [323]:

$$\frac{\partial \overline{q}_i}{\partial t} = k\left(q_{eq,i} - \overline{q}_i\right) \qquad 36$$

Where $\overline{q}_i$ is the averaged absorption quantity of species i [kmol/kg] and $q_{eq,i}$ is the equilibrium absorption quantity of species i [kmol/kg]. The dual-site Langmuir isotherm model was chosen [324, 325, 326, 327, 115, 328] and is non-competitive as N_2 adsorption is low and does not significantly affect

the adsorption amount of CO_2 [329]. Dual-site Langmuir Isotherm model determines the equilibrium adsorption amount [115] :

$$q_{eq,i} = \frac{q_{sb,i} b_i C_i}{1 + b_i C_i} + \frac{q_{sd,i} d_i \mathrm{C_i}}{1 + d_i C_i} \quad 37$$

$$b_i = b_0 e^{(-\Delta H_{b,i}/RT)} \quad 38$$

$$d_i = d_0 e^{(-\Delta H_{d,i}/RT)} \quad 39$$

Where $q_{sb,i}$ is the maximum equilibrium adsorption amount of species i on site 1 [mol/kg_{ads}], $q_{sd,i}$ is the maximum equilibrium adsorption amount of species i on site 2 [mol/kg_{ads}], b_i and d_i are equilibrium adsorption constants [m^3/kmol], b_o and d_0 are pre-exponential constants [K], and $\Delta H_{b,i}$ and $\Delta H_{d,i}$ are the heat of adsorptions at each site [j/mol]. The equilibrium parameters b_i and d_i, in equations 38 and 39 respectively, follow the Van't Hoff equilibrium temperature dependence equation [319]. The momentum balance/pressure drop along each column is expressed through the Ergun equation [330]:

$$-\frac{\partial P}{\partial z} = 150 \frac{\mu_g (1-\varepsilon)^2}{\varepsilon^3 d_{pp}^2} v_s + 1.75 \frac{(1-\varepsilon)}{\varepsilon^3 d_p} \rho_g {v_s}^2 \quad 40$$

Where P is the pressure [bar], μ_g is the dynamic viscosity [Pa.s], d_p is the pellet particle diameter [m] and ρ_g is the fluid phase mass density [kg/m^3]. The model is non-isothermal and non-adiabatic, accounting for heat transfer between the bed and column wall using thermal inertia properties of the column (i.e., thermal conductivity and specific heat capacity), excluding heat transfer between the solid adsorbent and gas flow, i.e., thermal equilibrium. The fluid phase energy balance [318]:

$$\frac{\partial T}{\partial t}\left(\varepsilon \rho_g C_g + (1-\varepsilon)\rho_p C_p\right) + \rho_g C_g \left(u \frac{\partial T_g}{\partial z}\right) = \varepsilon \lambda_e \frac{\partial^2 T}{\partial z^2} + (1-\varepsilon)\rho_p \sum_i (-\Delta H_i) \frac{\partial \overline{q_i}}{\partial t} - \frac{4 h_W}{d_b}(T_g - T_w) \quad 41$$

Where C_g is the gas phase specific heat capacity [kJ/kg/K], C_p is the solid phase specific heat capacity [kJ/kg/K], ρ_p is the solid phase density [kg/m^3], ρ_g is the gas phase density [kg/m^3], λ_e is the effective axial thermal conductivity [W/m^2/K], h_W heat transfer coefficient between the gas and column wall [W/m^2/K], d_b is the bed diameter [m], T_g is the gas phase temperature [K] and T_w is the bed wall temperature [K]. The bed wall energy balance is shown Equation 42 [331].

$$\rho_w C_{p,w} A_w \frac{\partial T_w}{\partial t} = A_w \lambda_w \frac{\partial^2 T_w}{\partial z^2} + h_w \frac{4}{d_b}\left(T_g - T_w\right) + h_{w,a} \frac{4(d_b + 2l_w)}{d_b^2}(T_w - T_a) \quad 42$$

Where ρ_w is the bed wall mass density [kg/m3], $C_{p,w}$ is the bed wall specific heat capacity [kJ/kg/K], A_w is the bed wall cross-sectional area [m^2], λ_w is the wall material thermal conductivity [W/m/K], $h_{w,a}$ heat transfer coefficient between the column wall and external environment [W/m^2/K] and l_w is the wall thickness [m].

Process simulation tools, such as Aspen Adsorption [332, 320, 321, 333] and gPROMS Process [334, 335], have been used to effectively simulate, analyse and optimise CO_2/N_2 adsorption. In this study, the model is developed in gPROMS Process utilising the physical properties package Multiflash™. Within gPROMS Process, you can directly specify an adsorption isotherm model and input the respective parameters. However, to use the format and units specified in [115] a custom sub-model for the dual-site Langmuir isotherm model was developed, and is shown in Appendix A (Chapter 10Section 10.1).

Adsorption processes are inherently dynamic; the process models must include valves to control the flow in and out of the adsorption bed. For this study each valve is considered adiabatic, where the mass flowrate (F) and pressure drop (Δp) are related through:

$$F\ [kg/s] = C_v x \Delta P \tag{43}$$

As the model is pressure driven, the flow coefficient (C_v in kg/s/kPa) for each valve is calculated to give the required pressure drop during each stage of the simulation. The timings of the valve stem position (x) are defined using a scheduling unit. This controls which valves are open at any given time, allowing for step management and cyclic behaviour. Figure 42 shows the model topology for single column, used to validate the fidelity of the isotherm model.

The energy demand comes from the compressors needed to elevate the bed pressure and the vacuum pumps needed to depressurise the bed to desorb the CO_2. For real gas compression and evacuation power (W) consumption Nikolaidis et al. [109] used:

$$Power_{comp} = F_{in} T_{in} R \frac{1}{n_c} \left(\frac{\gamma}{\gamma - 1}\right) \left[\left(\frac{P_{out}}{P_{atm}}\right)^{\frac{\gamma-1}{\gamma}} - 1\right] \tag{44}$$

$$Power_{evac} = F_{in} T_{in} R \frac{1}{n_v} \left(\frac{\gamma}{\gamma - 1}\right) \left[\left(\frac{P_{atm}}{P_{vac}}\right)^{\frac{\gamma-1}{\gamma}} - 1\right] \tag{45}$$

The ratio of specific heat capacities (γ), also known as the adiabatic constant, is assumed to be 1.4. Within the literature the isentropic efficiency (n_c and n_v) for N_2/CO_2 systems is 0.72 [336]. Alongside CO_2 capture rate, CO_2 purity, and specific energy demand (calculated using Equations 24, 25, and 26, respectively), adsorption systems are also evaluated using the Productivity (P_r):

$$P_r[mol/m^3 Adsorbent/s] = \frac{CO_2\ Captured\ [mol]}{Volume\ of\ Adsorbent\ [m^3] \times\ total\ cycle\ time\ [s]} \tag{46}$$

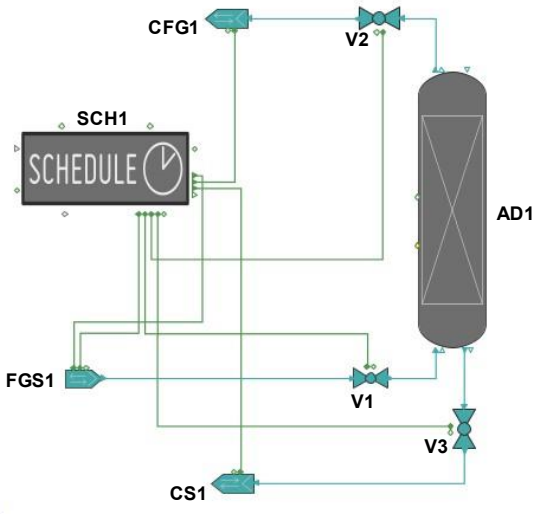

Legend	
Notation	**Description**
AD	Absorption bed
CFG	Cleaned flue gas
CS	CO_2 sink
FGS	Flue gas source
SCH	Scheduler
V	Valve

Figure 42: Single column VPSA model topology, developed in gPROMS PROCESS

3.3.2.1.Case study: VPSA pilot plant

In order to evaluate the fidelity of the process model, a single column is validated against pilot scale data from Krishnamurthy et al. [115]. The pilot study investigated CO_2/N_2 vacuum-pressure swing adsorption on the commercial sorbent Zeolite 13X. The feed contains 15 mol.% CO_2 and 85 mol.% N_2 at 1000 SLPM. The column specifications are shown in Table 23.

Table 23: Single column specifications [115]

Parameter	Value
Column internal diameter (m)	0.3
Column packing height (m)	0.867
Mass of adsorbent (kg)	41
Particle size (mm)	1.6-2.6
Bed Voidage	0.428

Run 1 in [115] is chosen for its high purity (94.7±1.05%) and high recovery (85.4±4.52%). The four-step Skarstrom cycle VPSA system includes: pressurisation to P_H using the feed gas, adsorption at high pressure with product valve open, forward blowdown to depressurise the column to P_i, and reverse evacuation to recover CO_2 at P_L. The step duration and pressure specifications are shown in Table 24.

Table 24: Step duration and pressure specifications [115]

Step	Time (s)	Pressure (level)	Pressure (bar)
Pressurisation	20	P_H	1.5
Adsorption	60	P_H	1.5
Blowdown	150	P_i	0.07
Evacuation	310	P_L	0.025

The model used in [115] was previously developed by [327] and uses the dual-site Langmuir isotherm model. The gravimetric equilibrium isotherm data is shown in Table 25. Zeolite 13 X is a Faujisite

type zeolite, and [337] determined the thermal conductivity to be 2.28 (W/m K). Mass transfer coefficients for N_2 and CO_2 on Zeolite 13X are taken as 2.733 s^{-1} and 0.065 s^{-1} respectively, and the axially dispersion co-efficient is 0.23 m^2/s [338].

Table 25: Dual-site Langmuir isotherm parameters [327]

Parameter	**N_2**	**CO_2**
$q_{sb,i}$ (mol kg^{-1})	5.84	3.09
$q_{sd,i}$ (mol kg^{-1})	0	2.54
b_0 (m^3mol^{-1})	2.50x10-6	8.65x10-7
d_0 (m^3mol^{-1})	0	2.63x10-8
$-\Delta H_{b,i}$ (kJ $mmol^{-1}$)	-1580000	-36641.21
$-\Delta H_{d,i}$ (kJ $mmol^{-1}$)	0	-35690.66

Table 26 highlights the other key process parameters necessary to calculate the mass and heat transfer along the adsorption column.

Table 26: Mass and heat transfer parameters [327]

Parameter	**Value**
Pellet bulk density (kg m^{-3})	1130
Pellet void fraction (m^3 m^{-3})	0.35
Specific heat capacity of fluid (J mol^{-1} K^{-1})	30.7
Specific heat capacity of adsorbent (J kg^{-1} K^{-1})	1070
Wall thickness (mm)	17.5
Wall density (kg m^{-3})	7800
Heat transfer coefficient between bed and wall (W m^{-2} K^{-1})	8.6
Heat transfer coefficient between wall and ambient (W m^{-2} K^{-1})	2.5
Specific heat capacity of the column wall (J kg^{-1} K^{-1})	502
Thermal conductivity of the column wall (W m^{-1} K^{-1})	16
Universal gas constant (m^3 Pa mol^{-1} K^{-1})	8.314

3.3.3. CO_2 Compression and Conditioning

There are several important characteristics that influence the design and operation of centrifugal compressors, explained in [339] and [340]. The flow coefficient (φ) determines the size of the volumetric flow through the compressor for a given impeller diameter, with constant inlet temperature and specific heat ratio [340]:

$$\varphi = \frac{V_{in}}{\frac{\pi}{4} d_i^2 u_i} \quad (47)$$

Where V_{in} is the inlet volumetric flowrate (m^3/s), d_i is the impeller diameter (m), and u_i is the impeller tip speed (m^2/s). Centrifugal compressors can be considered polytropic processes [190]. The polytropic head coefficient (ψ_p) relates the polytropic work and the impeller tip speed [339]:

$$\psi_p = \frac{\Delta h_p}{u_i^2} \quad (48)$$

Where Δh_p is the polytropic work/enthalpy change (J/kg). It can also be related to the polytropic efficiency (η_p) and work coefficient (w) [340]:

$$\psi_p = w\,\eta_p \tag{49}$$

The work co-efficient, is similar to the polytropic head coefficient, but instead of using the polytropic enthalpy change it uses the actual enthalpy change [339]:

$$w = \frac{\Delta h_t}{u_i^2} \tag{50}$$

Where (Δh_t) is the actual enthalpy change (J/kg). It is the difference between the inlet flow enthalpy ($h_{t,in}$) and the outlet flow enthalpy ($h_{t,out}$):

$$\Delta h_t = h_{t,in} - h_{t,out} \tag{51}$$

Whereas the polytropic enthalpy change includes leakage and frictional head losses [339]:

$$\Delta h_p = \Delta h_t - \frac{(\Delta \mathrm{s})(\Delta \mathrm{T})}{\ln(T_{out} - T_{in})} \tag{52}$$

Where Δs is the entropy change between the outlet and inlet compressor flows (J/K/kg), and ΔT is the temperature difference between the outlet and inlet compressor flows (K). Therefore, combining equations 48, 49 and 50 the polytropic efficiency (η_p) compares the polytropic work to the actual work, and is independent of the pressure ratio:

$$\eta_p = \frac{\Delta h_p}{\Delta h_t} \tag{53}$$

The impeller tip speed Mach number (M_i) explains the compressibility of the fluid, it is a ratio of the impeller tip speed and sonic inlet velocity [339]:

$$M_i = \frac{u_i}{a_0} \tag{54}$$

Where a_0 is the speed of sound in the inlet flow (m/s) [341]. High Mach numbers result in the choke and surge points being closer to the design point, reducing the operational flexibility. The pressure ratio $\left(\frac{P_2}{P_1}\right)$ defined by Lüdtke [340] as being dependent on the Mach number:

$$\frac{P_{out}}{P_{in}} = \left[w(k_n - 1)M_i^2 + 1\right]^{\frac{k_n \eta_p}{k_n - 1}} \tag{55}$$

Where P_{out} is the compressor outlet pressure, P_{in} is the compressor inlet pressure, and k is the isentropic exponent.

The process models for compression and liquefaction are developed in gPROMS gCCS, utilising the model library to construct a flowsheet of the conditioning systems, including the compressor sections, inter-stage cooling, knock-out drums, surge valves and dehydration unit. Figure 43a shows the model topology for conventional multistage compression, based on the base case B0 from IEAGHG [60]. Figure 43b shows the model topology for multistage compression and liquefaction, based on case D2c

from IEAGHG [60]. More information on the cases is given in Section 3.3.3.1. Each compressor section consists of multiple stages, modelled via polytropic efficiency with negligible hold-up and inertia of gas. The thermo-physical properties and phase equilibrium of the fluid is determined through gSAFT [301].

As specific outlet conditions for the individual water coolers are not given in IEAGHG [60], the two inter-stage water cooling steps are lumped into one and modelled via a heat exchanger unit. The heat exchanger units operate in counter-current flow, with a constant heat transfer area used to deliver a specific outlet CO_2 stream temperature. The heat exchanger models assume adiabatic operation with constant pressure drop. The knock-out drums remove condensed water, and the models are based on vapour-liquid phase equilibrium with no liquid entrainment. The dehydration unit removes H_2O from the CO_2 stream to a specified moisture content, and consists of three molecular sieve beds, two used for drying and one in regeneration mode operating simultaneously. The dehydrator unit assumes no degradation or loss in performance of the molecular sieve over time. The regeneration fraction and temperature are specified parameters, and the model calculates the heat requirement and power consumption. See PSE's gCCS documentation [301] for additional information on these unit operations.

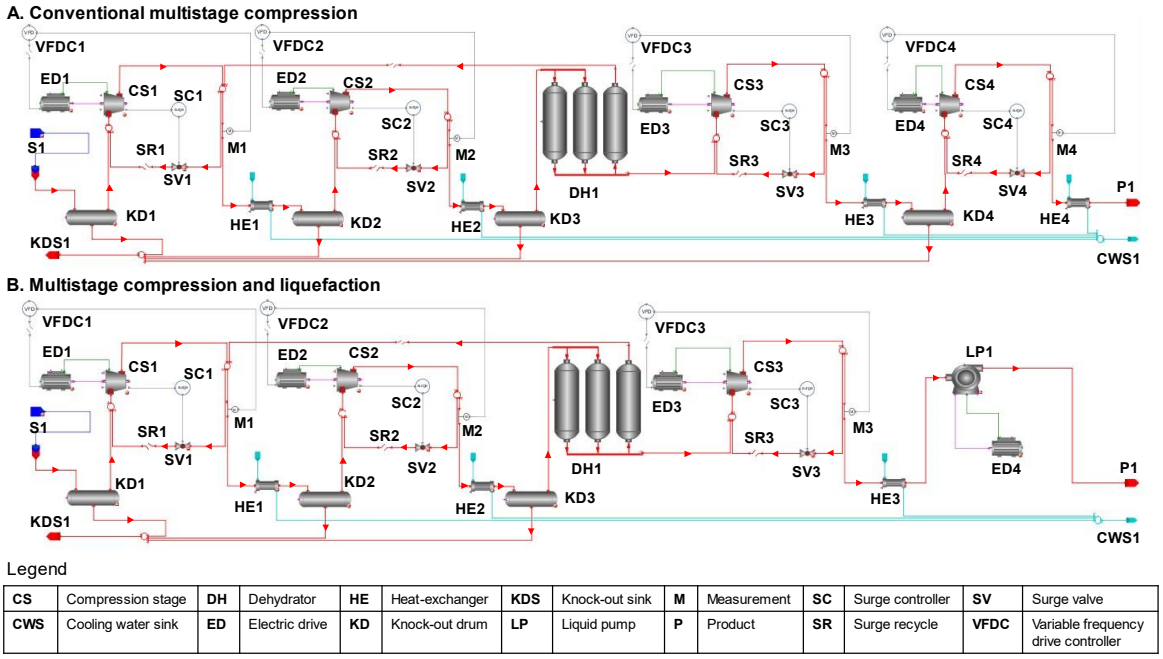

Legend

CS	Compression stage	**DH**	Dehydrator	**HE**	Heat-exchanger	**KDS**	Knock-out sink	**M**	Measurement	**SC**	Surge controller	**SV**	Surge valve
CWS	Cooling water sink	**ED**	Electric drive	**KD**	Knock-out drum	**LP**	Liquid pump	**P**	Product	**SR**	Surge recycle	**VFDC**	Variable frequency drive controller

Figure 43: a) model topology for conventional multistage CO_2 compression, b) model topology for multistage CO_2 compression and liquefaction

For dynamic compressor stability a surge control system is required to prevent flow reversal and extreme flow oscillation [342]. The surge control system includes a valve to recycle flow, a recycle-breaker that opens when a surge is encountered, and a Proportional-Integral (PI) controller that dictates the valve stem position based on the volumetric flow through the compressor. The Variable Frequency Drive (VFD) controller is a PID controller. It manipulates the speed of the electric drive attached to the compression stage, to deliver a desired output pressure determined by:

$$z_{out} = \max(\min(z_{calc}, z_{max}), z_{min}), \tag{56}$$

$$z_{min} = v_D \left(1 - \frac{\Delta v_-}{100}\right) \tag{57}$$

$$z_{max} = v_D \left(1 - \frac{\Delta v_+}{100}\right) \quad (58)$$

Where z_{out} is the controller output (Hz), z_{min} is the minimum controller output (Hz), z_{max} is the maximum controller output (Hz), z_{calc} is the calculated controller output based on PID control law (Hz), v_D is the design speed (Hz), Δv_- is the turndown speed (Hz), and Δv_+ is the overspeed (Hz) [301].

3.3.3.1. Case study: compression train

The IEAGHG compression base case (B0) for post-combustion capture (see Figure 44), assumes the CO_2 stream comes from an ultra-supercritical pulverised coal fired power plant, with NO_X, SO_X and CO_2 treatment. The vapour stream leaving the CO_2 solvent regeneration unit comprises of 95.88 vol.% CO_2, 4.11 vol.% H_2O, and 0.01 vol.% N_2, at 556451 kg/h, 38°C and 1.6 bar. A four-stage compression system, with intercooling and dehydration produces a product stream at 546855 kg/h, 73°C, 111 bar and 50 ppm moisture. The intercooling is performed in two stages, one stream produces water for condensate pre-heating, the other stream is cooling water. The dehydration unit consists of three beds, two in drying mode and one in regeneration mode, using molecular sieves as the solid desiccants. Regeneration is carried out using 10% of the dried gas stream, at 250°C [60].

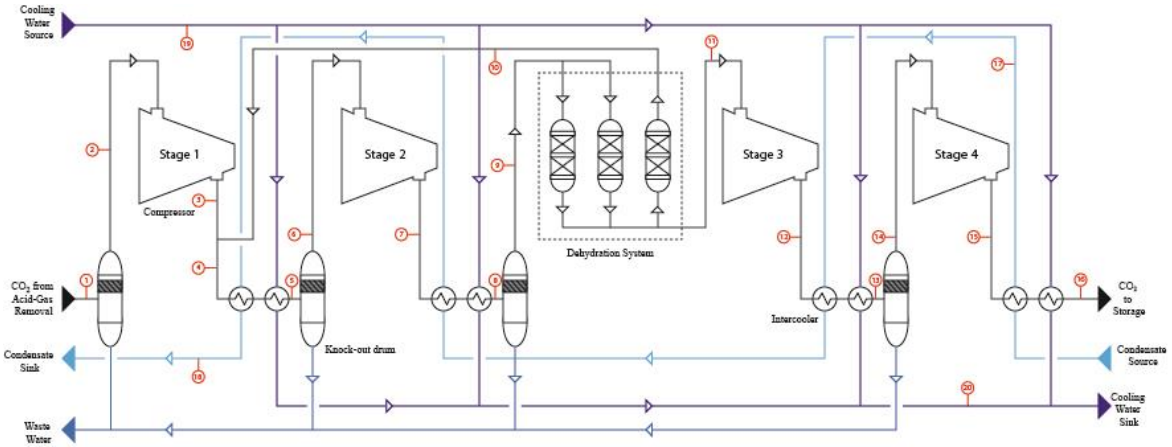

Figure 44: Post-combustion CO_2 compression system, base case B0 from IEAGHG [60]

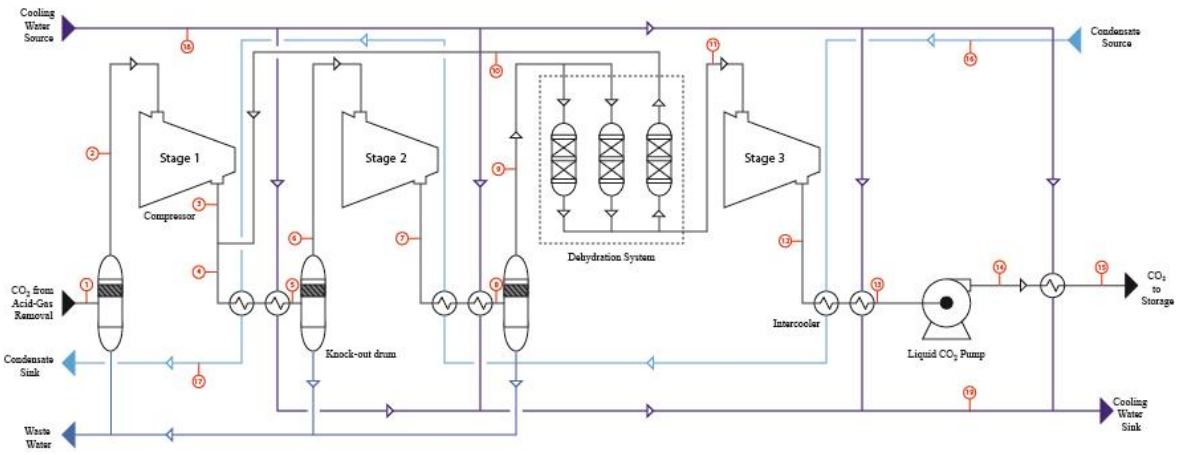

Figure 45: Post-combustion CO_2 compression and liquefaction system, case D2c from IEAGHG [60]

The IEAGHG compression and sub-critical liquefaction case D2c (Figure 45) for post-combustion capture assumes the same CO_2 source as the base case B0. Conditioning up to the 3rd compression stage is identical to base case B0. The 3rd compression stage pressurises the stream to 66 bar, after cooling to 20 ℃ it can be pumped to 111 bar. The lower pressure ratio for the 3rd compression stage and use of liquid pumps reduces the overall energy penalty by 3.7 MWe, compared to the base case. This is offset by the reduction in available waste heat for condensate preheating and the higher cooling water demand [60]. Table 27 shows the main consumptions from the B0 and D2c cases. It is worth noting, case D2c is subject to sufficiently low cooling water availability (12℃), with high ambient conditions full sub-critical liquefaction is unachievable.

Table 27: IEAGHG cases B0 and D2c unit consumption [60]

Parameter	B0	D2c
1st Compression Stage Outlet Pressure (bar)	7	7.0
2nd Compression Stage Outlet Pressure (bar)	34	34
3rd Compression Stage Outlet Pressure (bar)	70	66.0
4th Compression Stage/Liquid Pump Outlet Pressure (bar)	111	111
Cooling water demand (t/h)	5392	8932
Condensate Pre-heating (MWth)	34.0	31.4
1st Compression Stage Power (MWe)	21.7	21.7
2nd Compression Stage Power (MWe)	24.1	23.6
3rd Compression Stage Power (MWe)	8.0	7.3
4th Compression Stage/Liquid Pump Power (MWe)	3.7	1.2
Total power consumption (MWe)	57.5	53.8

3.3.4. Complete system design

For the scaled system design, each process model (for MEA, VPSA and conditioning) is scaled in order to obtain similar KPI's to the pilot-scale validation. For the conditioning model, the validation study is for a large-scale compression system. Therefore, the conditioning model scaled down to handle the output flowrates from the MEA and VPSA processes.

3.3.4.1. Scaled-MEA

The model is scaled to handle 33.8 kg/s of flue gas, whilst maintaining the same L/G ratio from Tait et al. [65], equating to 83.04 kg/s of solvent flow with 30.16 wt. % MEA. The model is designed in such a way that the absorber solvent MEA concentration is maintained at this concentration through the "SMU" unit shown in Figure 40. Using the method described in Section 3.3, the main calculated process parameters for the scaled model are shown in Table 28 alongside the steady-state model output. The scaled values for the absorber and stripping columns represent non-optimised values to attain similar capture rate and loadings as the baseload conditions presented in Tait et al. [65]. The solvent crossover heat-exchanger heat transfer area is the value required to ensure the rich solvent temperature entering the stripping column is 104.07°C. The calculated reboiler steam flowrate achieves the same temperature (at TI02 on Figure 40) as the validation simulation. The flue gas flowrate is 33.80 kg/s or 104,530 Sm^3/h, similar in scale to the TCM capture plant which can process 60,000 Sm^3/h of flue gas. The TCM plant absorber packing height is 24m with a column cross sectional area of 3.55x2m, the stripping column is smaller with a packing height of 8m and a diameter of 1.33m [68]. The demonstration facility also incorporates a solvent crossover heat-exchanger with an area of $308m^2$ [316].

Table 28: MEA-PCC scaled model parameters

Process Parameter	Value
Flue Gas Flowrate (kg/s)	33.80
Absorber Inlet Solvent Flowrate (kg/s)	83.04
Absorber Column Height (m)	18.5
Absorber Column Diameter (m)	8.2
Stripper Column Height (m)	15.5
Stripper Column Diameter (m)	4.5
Solvent Crossover Heat-exchanger Area (m^2)	448.45
Reboiler Volume (m^3)	5.00
Condenser Volume (m^3)	5.00
Reboiler Steam Flowrate (kg/s)	3.75

The scaled MEA-PCC system produces a CO_2 stream at 2.12 kg/s. This flows through the conditioning system to produce a CO_2 stream at 111 bar and 20ppm moisture. Table 29 shows the process parameters for the MEA-PCC compression model.

Table 29: MEA-PCC conditioning train process parameters

Process Parameter	Value
1^{st} Compression stage pressure increase (bar)	7.00
1^{st} Compression stage power demand (kWe)	403.84
2^{nd} Compression stage pressure increase (bar)	34.00
2^{nd} Compression stage power demand (kWe)	512.46
3^{rd} Compression stage pressure increase (bar)	70.00
3^{rd} Compression stage power demand (kWe)	215.45
4^{th} Compression stage pressure increase (bar)	111.00
4^{th} Compression stage power demand (kWe)	134.35
Dehydration power demand (kWe)	98.37
Knock-out drum height (m)	2.00
Knock-out drum height (m)	1.00
Heat-exchanger surface area (m^2)	280.00

Within the UK, PCC plants require efficient use of heat and electricity [343]. As the MEA plant requires steam for solvent regeneration, this is provided through heat recovery from the exhaust gas. There is sufficient heat in the exhaust of the 10 MWe gas turbine to provide the thermal energy required to regenerate the solvent [344]. In order to size the HRSG unit there are several assumptions:

- Shell and tube heat exchanger design
- Exhaust temperature = 565℃
- Outlet temperature = 100℃
- Water temperature = 20℃
- Reboiler stream flowrate = 3.75 kg/s
- Reboiler steam temperature = 120℃
- Heat exchanger area calculated using the log-mean temperature difference (LMTD)
- Overall heat transfer coefficient = 50 $W/m^2℃$ [345]

The incoming water stream requires 9.5 MJ of energy to heat it to 120℃, and based on the HRSG assumptions the heat exchanger area is 1,792 m^2. The cost of the single pressure HRSG is based on correlations from Chauvel et al. [346] which are shown in Appendix C Table 54. The inclusion of the HRSG removes the energy penalty for the MEA plant. A direct contact cooler (DCC) is required to reduce the temperature of the flue gas to 40-50℃ prior to absorption [230, 347], it is also useful to remove and acid gases such as SO2, HCL and HF [348]. The DCC size is based on the NTU method, assuming each transfer height is 1.2 m [230]. The sizing and costing values are shown in Appendix C Table 54.

3.3.4.2.Scaled-VPSA

Large-scale CCA systems require multiple beds and multiple stages for continuous separation of the desired component. A limitation for large-scale vacuum-adsorption systems is the ability of industrial machinery to deliver the vacuum pressure necessary for desorption [349], i.e., the vacuum pressures achieved in lab/pilot-scale systems may not be achievable at large-scale [110]. Therefore, the large-scale VPSA system used in this study is based on Luberti et al. [110], where the 1st stage is split into two identical two bed VPSA units to handle the large inlet flowrate. The process topology for this studies adsorption CO_2 capture system is shown in Figure 46. In Shen et al. [108], Wang et al. [84], and Luberti et al. [110] a secondary stage in series is used to ensure the end CO_2 purity is above 95%; however, in this study the purity is already >95% meaning the second stage is not required. In Figure 46, the scheduling unit dictates the valve stem position (x in Equation 43), i.e., how open the valve is. The valve flow coefficient (C_V in Equation 43) is specified to give an adequate pressure drop over each valve.

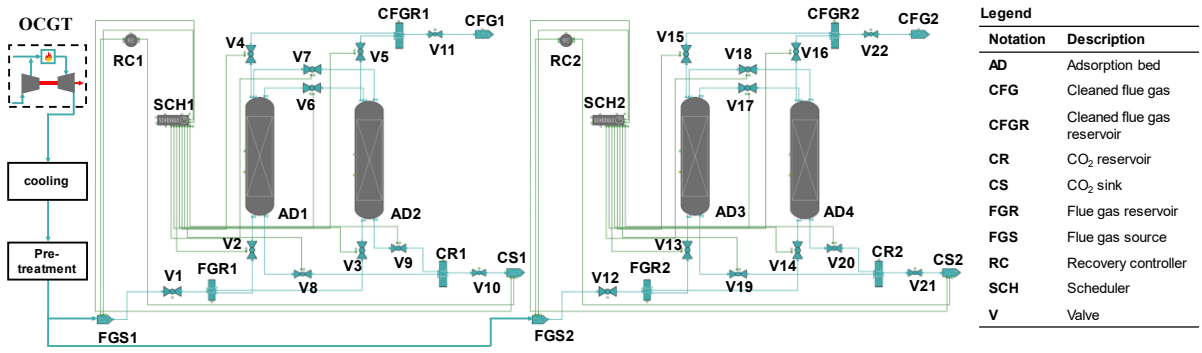

Legend

Notation	Description
AD	Adsorption bed
CFG	Cleaned flue gas
CFGR	Cleaned flue gas reservoir
CR	CO_2 reservoir
CS	CO_2 sink
FGR	Flue gas reservoir
FGS	Flue gas source
RC	Recovery controller
SCH	Scheduler
V	Valve

Schedule

Steps	V1	V2	V3	V4	V5	V6	V7	V8	V9	V10	V11	V12	V13	V14	V15	V16	V17	V18	V19	V20	V21	V22
Press – Bd	1	1	0	0	1	0	0	0	0	1	1	1	1	0	0	1	0	0	0	0	1	1
Ads – Ev	1	1	0	1	0	0.1	0	0	1	1	1	1	1	0	1	0	0.1	0	0	1	1	1
Bd – Press	1	0	1	1	0	0	0	0	0	1	1	1	0	1	1	0	0	0	0	0	1	1
Ev – Ads	1	0	1	0	1	0	0.1	1	0	1	1	1	0	1	0	1	0	0.1	1	0	1	1
C_V (kg/s/kPa)	20	88	88	84.4	84.4	0.15	0.15	8.2	8.2	0.34	8	20	88	88	84.4	84.4	0.15	0.15	8.2	8.2	0.34	8

Press = Pressurisation, Ads = Adsorption, Bd = Blowdown, and Ev = Evacuation

Figure 46: Large-scale VPSA model topology developed in gPROMS PROCESS, where the flue gas stream is split into two parallel streams, included in the figure is valve scheduling and each valve's flow co-efficient.

Assuming the power generation source is a 10 MWe open-cycle gas turbine (OCGT), 33.8 kg/s of flue gas is produced with 4.27 vol.% CO_2 (6.78 wt.% or 4.42 mol.%). Each parallel train processes 16.9 kg/s of flue gas (FGS1 and FGS2 on Figure 46). The input composition only includes N_2 and CO_2, for information on the affect impurities (NO_X, SO_X, and H_20) have on the operation of post-combustion VPSA CO_2 capture, see Zhang et al. [350], Li et al. [351], and Majchrzak-Kucęba et al. [352]. The

process simulation uses the same isotherm (Table 25) and mass and heat transfer parameters (Table 26) as the validation study. In order to deal with the large flue gas flowrate, the column properties are scaled such that each adsorption column has 11.15 m packing height, 4.80 m bed diameter, 2 mm particle size, and the bed voidage is 0.428 (see Table 30). These column properties ensured the scaled design has the same adsorbent surface area to volume ratio (3000 m^2/m^3) as the pilot study.

Table 30: VPSA-PCC scaled model parameters

Process Parameter	Value
Flue Gas Flowrate (kg/s)	33.80
Adsorber Column Height (m)	11.50
Adsorber Column Diameter (m)	4.80
Mass of Zeolite 13x (kg)	130998
Bed voidage (%)	0.428
Particle Size (mm)	2
Cycle steps	Pressurisation, Adsorption, Blowdown, and Evacuation
Cycle time (s)	600

The scheduling unit dictates the valve stem positions, within Figure 46 the scheduling table highlights each valves stem position during each of the two bed four step operations, i.e., Press – Bb denotes the first bed is in pressurisation mode and the second bed is in blowdown mode. Also included in scheduling table is each valve's flow co-efficient used in Equation 43 to calculate the pressure drop across each valve. Similar to the pilot study used for the validation simulation, the scaled-up system design has four process steps with three main target pressures. The step timings and corresponding pressure levels are shown in Table 31. These are different to the pilot study to meet cycle scheduling objectives: continuous operation, bed switching, and bed alignment [353].

Table 31: Step duration and pressure specification for the large-scale VPSA system

Step	Time (s)	Pressure (level)	Pressure (bar)
Pressurisation	80	P_H	1.5
Adsorption	220	P_H	1.5
Blowdown	80	P_i	0.07
Evacuation	220	P_L	0.025

The VPSA system produces a CO_2 stream at 2.22 kg/s. The compression train for the VPSA system (Table 32) is almost identical to the MEA scenario (Table 29). The slightly increased power demand for all the stages is due to the higher CO_2 flowrate and lower starting pressure (1 bar).

Table 32:VPSA-PCC conditioning train process parameters

Process Parameter	Value
1st Compression stage pressure increase (bar)	7.00
1st Compression stage power demand (kWe)	416.32
2nd Compression stage pressure increase (bar)	34.00
2nd Compression stage power demand (kWe)	519.09
3rd Compression stage pressure increase (bar)	70.00
3rd Compression stage power demand (kWe)	217.52
4th Compression stage pressure increase (bar)	111.00

4th Compression stage power demand (kWe)	134.95
Dehydration power demand (kWe)	99.98
Knock-out drum height (m)	2.00
Knock-out drum height (m)	1.00
Heat-exchanger surface area (m^2)	280.00

For the VPSA plant, a DCC unit is required to reduce the temperature to 40°C prior to adsorption similar to the MEA case. Adsorbents are susceptible to moisture content, whilst some moisture is removed in the DDC unit a dehydration unit is required for additional moisture removal. The dehydration unit is similar to conditioning plant, but it is larger due to the higher mass flowrate of the flue gas. The sizing and costing values are shown in Appendix C Table 55.

3.4.Economic modelling

The cost of plants rises non-linearly with scale, a simplistic method for costing CO_2 capture is looking at previous studies and scaling according to:

$$Cost\ of\ plant\ A = Cost\ of\ plant\ B\ \left(\frac{Capacity\ of\ plantA}{Capacituy\ of\ plant\ B}\right)^{n_e} \quad 59$$

Where n_e is the scaling factor (~0.6) [45]. However, for a more in-depth economic evaluation of CO_2 capture for power generation applications, the cost of CCS is defined as the difference between a plant without CCS and a plant with CCS. As highlighted in Chapter 2, the LCOE is used to calculate other metrics such as the cost of CO_2 captured, the cost of CO_2 abated, and the cost of CO_2 avoided (which incorporates compression, transportation, and storage). The LCOE is calculated using Equation 20 [354].

$$LCOE = \frac{\sum_n \left(\frac{\mathrm{TCC_t}}{(1+r)^t} + \frac{\mathrm{FOM_t}}{(1+r)^t} + \frac{VOM_t}{(1+r)^t}\right)}{\sum_n \frac{(\text{net electricty generated})_\mathrm{t}}{(1+r)^t}} \quad 60$$

Where TCC is the total capital costs, FOM is the fixed operating and maintenance costs, VOM is the variable operating and maintenance costs, r is the discount rate, and t is the time period. The main capture metric used is the cost of CO_2 avoided (CCA), as this study includes the compression and conditioning train into the cost model [248].

$$CCA = \frac{(LCOE)_{ccs} - (LCOE)_{ref}}{\left(\frac{tCO_2}{MWh}\right)_{ref} - \left(\frac{tCO_2}{MWh}\right)_{ccs}} \quad 61$$

Where tCO_2/MWh is the carbon intensity of the process, i.e., the amount of CO_2 released into the atmosphere per unit power generated. To enable a comparison with sources that do not include the cost of compression in their analysis, the cost of CO_2 capture (CCC) metric is used [248]:

$$CCC = \frac{(LCOE)_{cc} - (LCOE)_{ref}}{\left(\frac{tCO_2}{MWh}\right)_{cc}} \quad 62$$

Where the subscript 'CC' only include the capture technology in the LCOE calculations. Assumptions required to calculate the LCOE, CCA and CCC:

- Plant location – Yorkshire, England
- Plant lifetime – 25 years
- Construction time – 2 years
- Start of construction- 2019
- Discount rate – 7.8% for the proven conventional technologies and 8.9% for higher risk novel technologies [261]
- Capacity factor – 17.14 % (based on 1500 hours annual operating time [355])
- Carbon price - £21.70/tCO_2 (set price for 2021 from [261])

Within BEIS's report benchmarking state-of-the-art and next generation technologies for electricity supply [261], the carbon price increases from £21.6/tCO_2 in 2017 to £233.3/tCO_2 in 2050. For simplification of the NPV the carbon price is set at the 2021 price at £21.70/tCO_2, i.e., the first year of operation.

3.4.1. Total capital cost

The TCC is the cost of designing, constructing, and installing the plant. To estimate the major equipment cost the most accurate method is direct quotation from original equipment manufacturers (OEMs) [356], however, this is difficult to obtain and requires in-depth and accurate equipment sizing for all major components. From Towler & Sinnott [345] the capital investment consists of:

- Inside battery limits (ISBL) investment, the direct and indirect equipment costs
- Offsite battery limits (OSBL) investment, the modifications, and improvements to site infrastructure
- Engineering and construction costs
- Contingency costs

The most accurate way to estimate equipment costs is to directly contact suppliers. Alternatively, equipment sizes (based on the scaled process models) are used with cost correlations to work out purchased equipment cost (PEC) delivered but not installed:

$$PEC = \sum_{1}^{total} E_i \qquad \forall i = 1 \dots \dots total \tag{63}$$

Where the individual equipment cost (E_i) is based on the correlation from Towler & Sinnott [345]:

$$E_i = a + bS^n \tag{64}$$

Where S is the sizing factor specific to each piece of processing equipment, and a, b, and n are cost factors found in Towler & Sinnot [345]. The calculated prices ($) are for 2010, and to scale to the current day the following equation is used [357]:

$$E_{\mathrm{i}}^{2019} = E_{\mathrm{i}}^{2010}\left(\frac{F^{2019}}{F^{2010}}\right) \tag{65}$$

The Chemical Engineering Plant Cost Index (CEPCI) for 2010 is 551 (F^{2010}) and for 2019 is 607.5 (F^{2019}) [358]. The purchased equipment cost requires an installation cost from Couper et al. [359]. Chauvel et al. [346] proposed a method that uses observed relationships of process unit investments, summarised in Table 33. The method uses the Inside battery-limits investment (ISBL), which is the cost of the main process equipment and their installation. This was the method was used by Le Moullec and

Kanniche [360], Abu-Zahra et al. [361] and Alhajaj et al. [231] for the techno-economic analysis of absorption-based CO_2 capture.

Table 33: Capital cost relationships [346]

Capital cost factor	Code	Relationship
Purchased equipment cost (PEC)	C_1	See Equation 63
Instrument cost (I)	C_2	$C_2 = \sum_i^n I_i$ (66)
Direct equipment cost (DEC)	C_3	$C_3 = \sum_i^n E_i F_E + \sum_i^n I_i F_I$ (67)
Indirect equipment cost	C_4	$C_4 = C_3 \times 0.31$
Inside battery-limits investment (ISBL)	C_5	$C_5 = C_3 + C_4$
Off sites	C_6	$C_6 = C_3 \times 0.31$
Process unit investment (PUI)	C_7	$C_7 = C_5 + C_6$
Engineering	C_8	$C_8 = C_7 \times 0.12$
Paid-up royalties	C_9	$C_9 = C_5 \times 0.07$
Process book	C_{10}	$C_{10} = 265{,}000\ US\$\ in\ 2004$ [a]
Facility capital cost (FCC)	C_{11}	$C_{11} = C_7 + C_8 + C_9 + C_{10}$
Initial charge of feedstock's	C_{12}	$C_{12} = Feedstock\ required \times Cost$
Interest during construction	C_{13}	$C_{13} = C_{11} \times 0.07$
Start-up costs	C_{14}	$C_{14} = 1\ month\ of\ operating\ costs$ [a]
Working capital (WC)	C_{15}	$C_{15} = 1\ month\ of\ operating\ costs$ [a]
Total capital cost (TCC)	C_{16}	$C_{16} = C_{11} + C_{12} + C_{13} + C_{14}$

[a] [231]

The TCC calculations vary depending on the engineering book used and are directly linked to their respective FOM and VOM calculations. VOM is based off process requirements, and FOM uses factors to calculate depreciation, maintenance, taxes, insurance and overhead [362].

3.4.2. Fixed and variable operating and maintenance costs

Similar to the TCC, the FOM and VOM can be calculated using a factorial approach. Sinnott [362] explained the division into FOM and VOM is subjective to the particular organisations practice. The TCC calculations vary depending on the engineering book used and are directly linked to their respective FOM and VOM calculations.

The operating cost calculation used in Chauvel et al. [346] is shown in Table 34. VOM is based off process requirements, and FOM uses factors to calculate depreciation, maintenance, taxes, insurance and overhead. In the absence of actual data, the labour costs are based off the number of personnel required, assumed to be 4.5 people + 20% for supervision. The utilities cost is dependent on the process requirements, and the local cost of those utilities. Electricity costs incorporate the energy demand from primary process equipment (boilers, heat exchangers, pumps, blowers, compressors, etc.) and are based of energy balances and flow diagrams [362].

Table 34: Operating costs relationships [346]

Operating cost factor	Code	Relationship
Raw materials	O_1	Based on process flow diagram
Electricity	O_2	Based on process requirements
Fuel	O_3	Based on process requirements
Cooling water	O_4	Based on process requirements
Steam	O_5	Based on process requirements
Utilities	O_6	$O_6 = O_2 + O_3 + O_4 + O_5$
Variable operating and maintenance cost (VOM)	O_7	$O_7 = O_6 + O_1$
Labour	O_8	$O_{18} = Cost\ of\ 4.5\ \text{people/day} + 20\%$
Maintenance	O_9	$O_9 = C_7 \times 0.04$
Taxes and insurance	O_{10}	$O_{10} = C_7 \times 0.02$
Overhead	O_{11}	$O_{11} = C_7 \times 0.01$
Financing working capital	O_{12}	$O_{12} = C_{15} \times 0.09$
Fixed operating and maintenance cost (FOM)	O_{13}	$O_{13} = O_8 + O_9 + O_{10} + O_{11} + O_{12}$

For the calculation of VOM several utilities are required, the prices of these are shown in Table 35. The steam supplied to the MEA stripping column (solvent regeneration), is calculated as a water and electricity demand. The electricity demand is calculated from the specific energy demand (kWh/ tCO_2 or GJ/tCO_2) for each process (including conditioning), which is then multiplied by the quantity of CO_2 captured annually. The raw materials for the MEA and VPSA cases are replaced annually for ease of VOM cost calculation. The OCGT does not have a HRSG, therefore, there is no steam demand included in Table 35.

Table 35: Utility prices

Raw material/utility	Process	Price [a]	Source
Natural gas	OCGT	0.033 £/kWh	[363]
Electricity	MEA and VPSA	0.14 £/kWh	[364]
Cooling water	OCGT and MEA	1.3885 £/m3	[365]
MEA solvent	MEA	5.0 £/L	[366]
Zeolite 13X sorbent	VPSA	1.5 £/kg	[367]

[a] costs are for 2020/2021

This economic model can be classified as an EPRI Class II, similar to AACE Class 3. This work is not considered EPRI Class I (simplified) as it includes general site conditions, geographic location, plant design, material flow, and major equipment specification. The equipment sizes are based on validated process models with up-to-date utilities and purchasing costs. Therefore, the project contingency range is 15-30% [368].

3.5. Conclusion

Multiple studies have investigated Flexible-PCC, specifically for amine-based CO_2 capture. To the authors knowledge, no studies have investigated Flexible-VPSA, and no studies have focused on small-scale power production. Extensive research has been conducted on large-scale (>300 MW) operation due to regulations (Large Combustion Plant Directive) stating these generators must be CCS capable. In future energy system, small-scale plants will also require abatement in order to achieved Net Zero targets. Therefore, this chapter details the process and economic models used to investigate CO_2 capture and conditioning from OCGT flue gas.

Data from the BMRS is used to show the real-world operation of OCGTs operating in GB. The data showed the highly sporadic and transient nature of OCGTs, which are used for peak demand in the evenings. The average operating cycle is 5-hours, and in some cases the power output is ramped to one or more power outputs within the same operating cycle. This information, alongside data from industrial suppliers, is translated into flue gas flowrate profiles and used as inputs into the dynamic PCC process models. The MEA process model is developed in gPROMS gCCS, the VPSA process model is developed in gPROMS Process, and the compression model is developed in gPROMS gCCS. The capture models can be interlinked with the compression model for complete system analysis. Included in each section is a case study, whereby the operating parameters are used to validate each individual model. Once the fidelity of the models is quantified, the scaled system design could be completed. The scaled Flexible-MEA and Flexible-VPSA process models are explained, and key process parameters are shown.

From the literature review in Chapter 2, a key aspect of economic assessments is the choice of costing metric. This study uses the LCOE and CCA, as these are commonly used in the literature and will enable cross-comparison to alternative low-carbon power sources. The economic model is based on the method proposed in Chauvel et al. [346], where the TCC is a function of the PEC. The PEC for each technology (power, capture, and conditioning) is determined by cost correlations from Towler & Sinnot [345], scaled to 2019 values through the CEPCI.

Chapter 4 : CO_2 Capture Results

This chapter compiles the results for MEA and VPSA CO_2 capture. Each section within this chapter can be found within the peer reviewed publications outlined on Page V.

4.1.CO_2 Capture using MEA

This section presents the results for the PCC plant using MEA. The dynamic model described in Chapter 3 Section 3.3.1 is first validated against pilot-scale data, the process parameters are then scaled to handle flue gas flow from the small-scale OCGT. The technical evaluation looks at how affective the MEA-PCC plant is at processing highly transient flue gas flow.

4.1.1. Model validation

The model validation refers to the case study presented in Chapter 3, Section 3.3.1.1. Figure 47 and Figure 48 show a comparison of the flowrates during both operating scenarios (start-up and shutdown, respectively). Due to model constraints 0% baseload is un-obtainable, therefore, as close to 0% as possible is achieved (<1% for all flowrates). The flowrates from Tait et al. [65] are used as process inputs, and the figures show the accuracy of the models' flowrates.

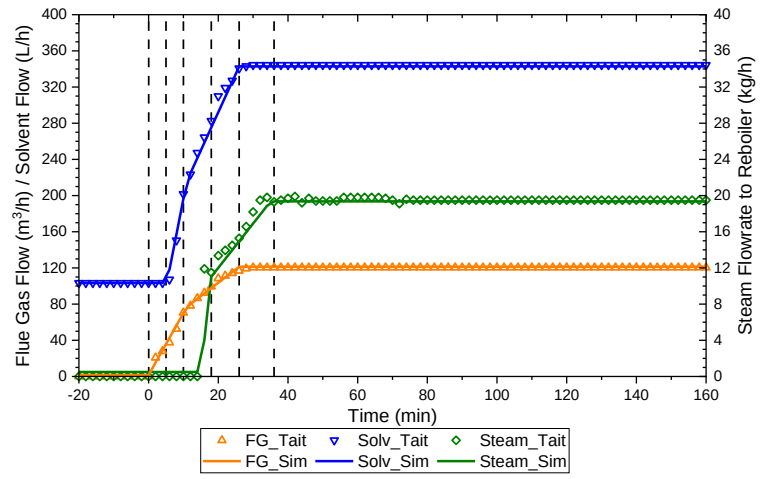

Figure 47: Comparison of flue gas, solvent, and steam flowrates during the start-up scenario

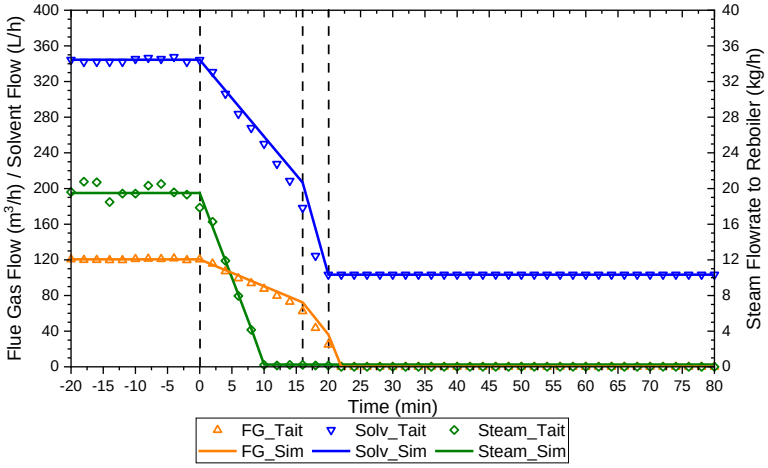

Figure 48: Comparison of flue gas, solvent, and steam flowrates during the shutdown scenario

Tontiwachwuthikul et al. [369] concluded that absorption column model validation should be performed using concentration and temperature profiles, instead of top and bottom conditions, as the mass/heat transfer has a complex relationship with the column temperature. The temperature profile is indicative of the reactions occurring in the column, and as a result it is directly linked to the capture rate. The steady-state capture rate is 92.48%, which is 3.09% higher than the baseline results (89.79%) shown in Table 21 (Chapter 3 Section 3.3.1.1). The absorber temperatures profiles at 0 and 20 minutes are shown in Figure 49, highlighting the steady state and dynamic capabilities respectively.

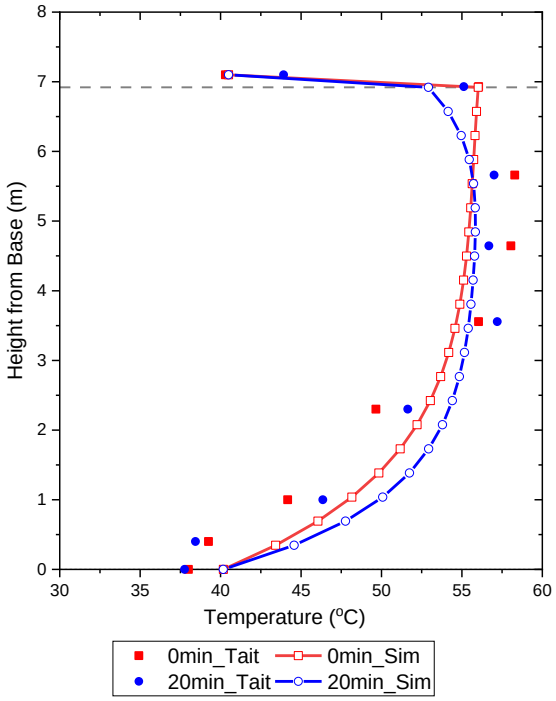

Figure 49: Absorber temperature profile comparison for the shutdown scenario

The top of the column is at 6.92 m, the reading at 7.1m is the inlet solvent stream. In the initial steady state region (0 min) the temperature is the same as the input parameter. However, this temperature decreases as the scenario advances in time. This difference is not accounted for within the current model, as the inlet absorber solvent temperature is a set model input. Kvamsdal and Rochelle [370] describes and analyses a phenomenon called the temperature bulge, which is dependent on column parameters such as: packing height, CO_2 concentration, choice of solvent and L/G ratio. The temperature bulge in each one of the simulations is in the correct location but the magnitude of the temperature bulges deviates by a maximum of 4.85 and 2.28°C at 0 minutes and 20 minutes respectively. The model overall under predicts the temperature profile. As mentioned previously, this is due to the solvent inlet temperature decreasing over time, causing the overall magnitude of the temperature profile to be higher in the model.

Figure 50 and Figure 51 show the dynamic comparison of the capture rate and CO_2 loadings during the dynamic start-up and shutdown scenarios, respectively. During the steady-state operation in the shutdown scenario, the predicted rich- and lean-loadings are 0.333 and 0.218 mol CO_2/mol MEA respectively, which are within the errors indicated by Tait et al. [65]. However, both values are lower than the baseload values shown in Table 21 (Chapter 3 Section 3.3.1.1). The specific reboiler duty is calculated by dividing the heat duty of the reboiler by the quantity of CO_2 captured, the predicted value is 4.33 GJ/tCO_2. Tait et al. [65] does not specify the size of the reboiler or condenser, therefore, equipment sizes had to be calculated based off the utility flowrates, resulting in the predicted value for

the reboiler duty being 8.54% higher. During the steady-state operation in the start-up procedure the rich- and lean loadings are 0.286 and 0.236 mol CO_2/mol MEA respectively, within the error bars stated by Tait et al. [65]. Therefore, the model accurately simulates steady-state operation.

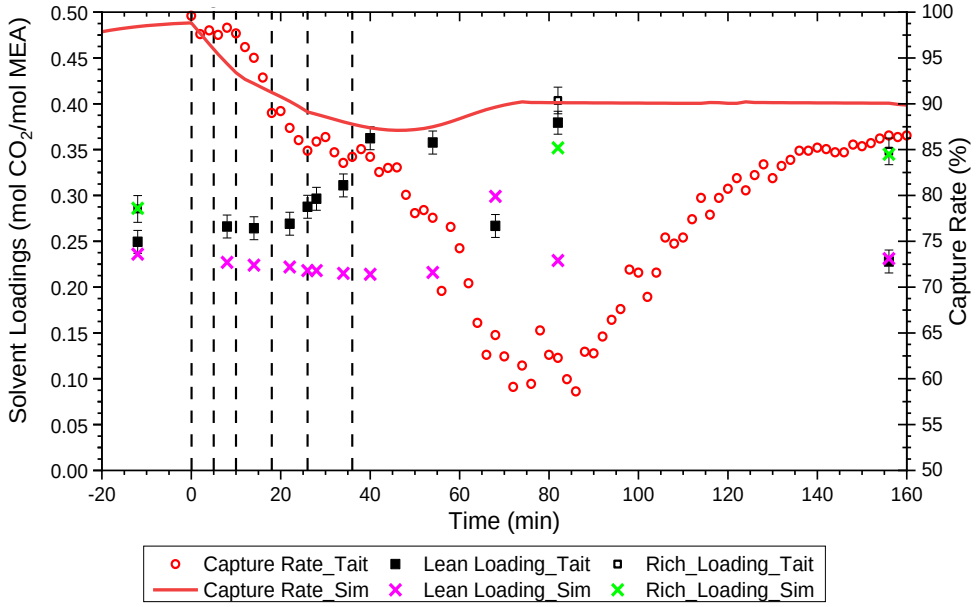

Figure 50: Dynamic comparison of the capture rate and solvent loadings during the start-up scenario

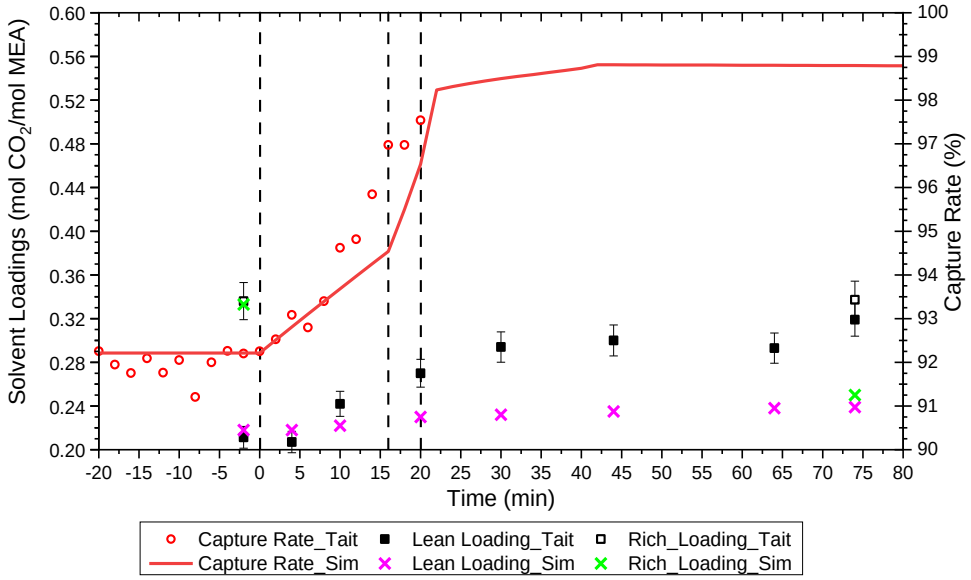

Figure 51: Dynamic comparison of the capture rate and solvent loadings during the shutdown scenario

During dynamic operation, the start-up scenario capture rate predicated by the model follows the same trajectory as the experiment, the major deviation occurs when the steam flowrate to the reboiler is 0 kg/h at t=10 minutes. At this point the gradient of the capture rate in the experiment increases, whereas the model remains on the same course, until the flue gas and solvent flowrate ramp rates are changed at t=16 minutes. At this time the model under predicts the capture rate by 2.44%, which is the largest

difference exhibited throughout this scenario. At the end of the dynamic operation, at t=20 minutes, the predicted capture rate is 1% lower than presented in Tait et al. [65]. Over the entire shutdown scenario, the rich- and lean-loadings predicted by the model are lower than the experiment, although they follow a similar profile. A similar problem occurs in the shutdown scenario indicating the working fluid contains a lower percentage of CO_2. Further research is required on the desorption unit to determine the reason for this lower loading. In the start-up scenario, the initial and end loadings predicted by the model are within the error bars presented in Tait et al. [65].

As mentioned previously, due to the time taken for real-world systems to return to steady state following a perturbation, the differences in the loadings during the middle of the operation are expected to be greater than at the start and end. Alongside the capture rate curve, this highlights that the model returns to steady state at a faster rate than the experiment. It is worth noting that the experiment did not incorporate rich-solvent heating (used to simulate the temperature increase caused by the solvent cross-over heat exchanger) until t=60 minutes. Consequently, the desorber solvent inlet temperature increases to 50-60°C higher than the baseload experiment, causing the lean loading (recorded after the desorption step) to increase gradually. This explains the larger lean loading deviation between t=0 to 60 minutes.

4.1.2. Scaled MEA-PCC

The scaled system analysis focusses on the effects transient operation have on the processes KPIs this study does not look at the optimisation of the scaled VPSA design. The scenarios investigated for MEA-PCC are as follows:

- **Baseload** – Flue gas flowrate is ramped to full-load to simulate start-up procedure, until the end of the 5-hour operation and then the flue gas is ramped down to simulate the shutdown procedure.
- **Scenario A** – The flue gas start-up and shutdown ramping are the same as the Baseload scenario. Included in this scenario is ramping the flue gas to different loads (70% and 50%) during the 5-hour operation.
- **Scenario B** – Similar to Scenario A but also include ramping the solvent flowrate to maintain a constant L/G ratio throughout entirety of the operation.
- **Scenario C** – Similar to Scenario B, but also include ramping the steam supply to the reboiler to minimise the energy penalty at low load operation.

4.1.2.1. Flexible response

The dynamic changes for the flue gas, solvent and reboiler steam flowrates are shown in Figure 52. In Scenario A, only the flue gas flow entering the absorber is ramped, see Figure 39 Chapter 3 Section 3.2 for ramp times and percentage changes in flowrate. Each subsequent scenario includes the manipulation of an additional flowrate, i.e., the solvent entering the absorber, or the steam used to heat the reboiler. In reality the ramping rates of the steam supply to the reboiler will be higher, however, for the purpose of determining the effects each variable has, it follows the same ramp rates as the flue gas and the solvent flows. It is worth noting that due to model constraints the streams cannot converge to 0 kg/s, therefore, all flowrates are decreased to a minimum of 1% baseload.

Figure 52 also highlights the capture rate for each scenario during the five-hour dynamic operation. Over the course of each operating Scenario A, B, C and Baseload the capture rate is 1.08, 0.73, 1.2% and 0.81% points lower, respectively, compared to the steady-state value of 92.48% in Table 5. This is a result of including the start-up, ramping and shutdown procedures; over the entire simulation this drop is insignificant and the time-averaged capture rates are around 90% for all scenarios. The largest capture rate drops are during the periods directly after 70% or 50% load. This is a result of the transition time, showing the new set of parameters have not reached steady-state. The decrease in capture rate during each new load is less than 2%, similar to the rate changes published in Bui et al. [68] when the L/G ratio is kept constant (Scenario B and C). It is worth mentioning that in Bui et al. [68] during the dynamic

operation each new set of process conditions are maintained for several hours, re-reaching steady-state or near steady-state conditions. The decrease in capture rate is a result of the lean-loading increasing by 3.28% between t=8 to 300 minutes in the Baseload scenario. As more CO_2 is entrained in the solvent, less CO_2 can be absorbed. Interestingly, when returning to full load the capture rates continue their original trajectory, and the start-up/shutdown procedures balance each other out.

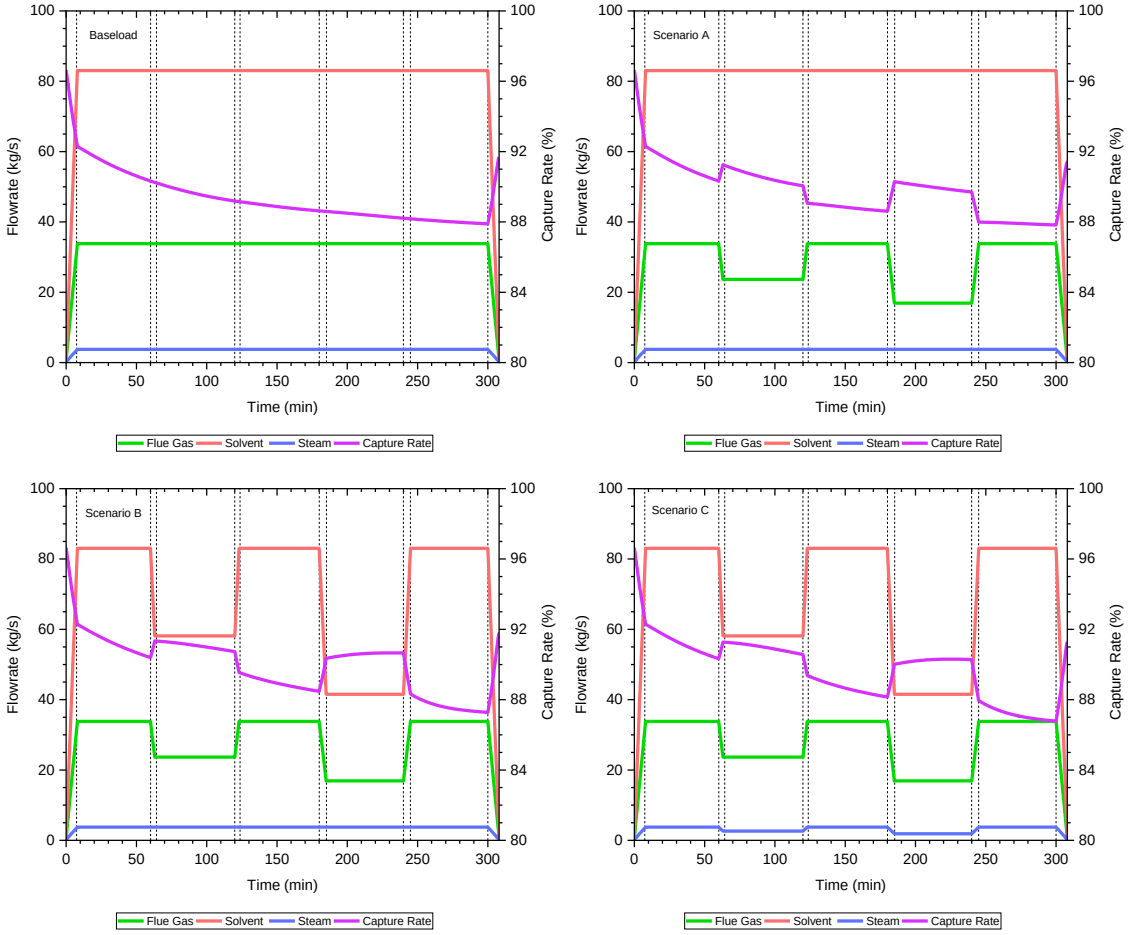

Figure 52: Flowrate changes and capture rate profile for each operating scenario

Figure 52 shows the one-hour operating cycle is not long enough for the capture rate to stabilise. The time-averaged capture rate is 89.81, 90.01, 89.75 and 89.35% in Scenario A, B, C and the Baseload, respectively. In Scenario A the increase in capture rate is a result of a higher L/G ratio, as more solvent is available to absorb CO_2. Interestingly, this increase is also shown in Scenario B and C, indicating the lower flowrates through the column also increase the capture efficiency. Although the capture rate changes seem small and within normal plant operation guidelines, the simulations show the highly transient operation, i.e., alternating between partial and full loads every hour, is beneficial in delivering a time-averaged capture rate around 90%.

During the transition from 50% to 100% between t=240 to t=245 minutes, Scenario B and C exhibit the largest capture rate drop: 1.89% in both cases. This is also highlighted in Figure 54, which illustrates the bulk vapour temperature profiles for each scenario. With Scenario B and C exhibiting more prolific temperature drops at t=240 minutes. The 3-D temperature profiles show Scenario A and the Baseload scenario remain reasonably constant throughout the simulation. However, the top section of the column, between 12 to 18.5m, the temperature increases by 4K over the course of the simulating. This results in

more water evaporation and less CO_2 absorption. The temperature drops following the temperature spikes in Scenario B and C at t = 60, 180, and 300 minutes, indicates a change in solvent flowrate and leads to an increase in capture rate.

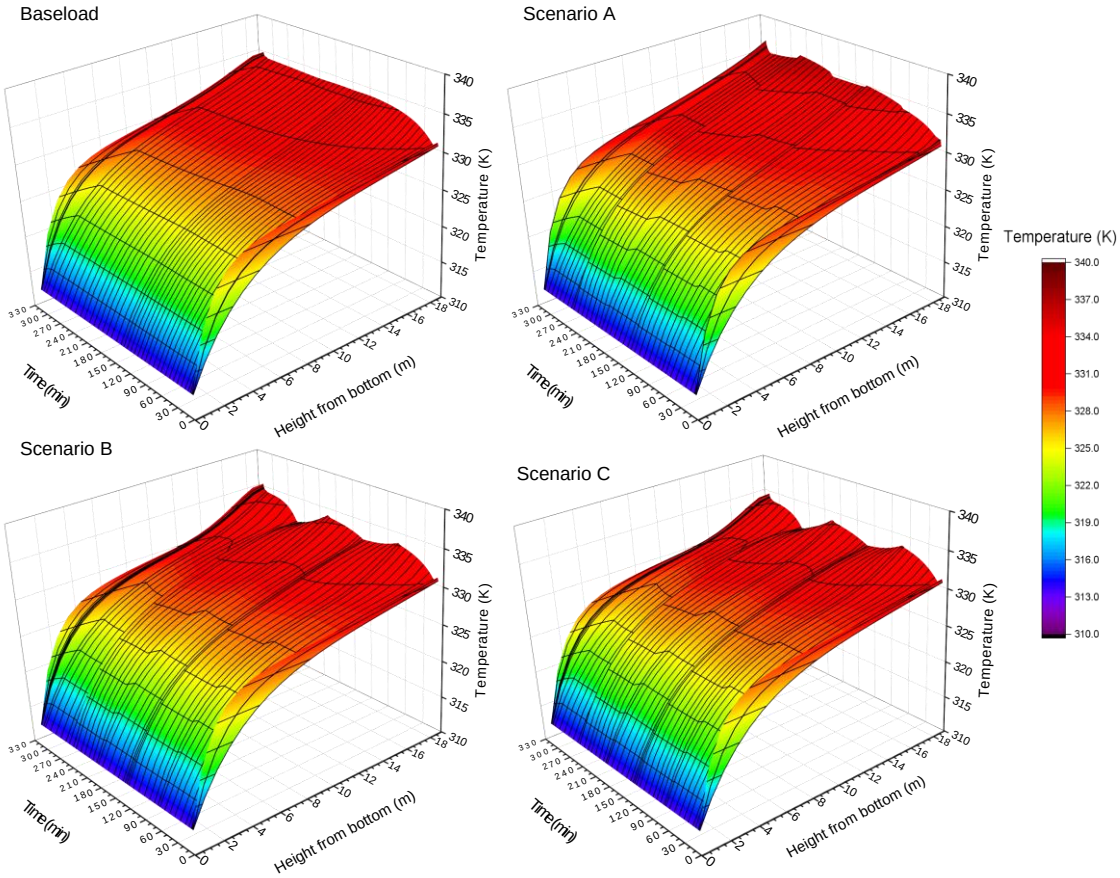

Figure 53: Stripping column inlet and outlet temperatures during each scenario

One of the key challenges with using amine solvents for CO_2 capture is oxidative and thermal degradation. Oxidative degradation is a result of the O_2 content in flue gas, this is not analysed in the study. Thermal degradation is a result of the high temperatures and pressures in the stripping column, hence the limitation of 120°C [371]. As shown in Figure 53 this value is not exceeded at any point in the simulation, and Moser et al. [372] showed minimal thermal degradation at 120°C during the 18-month test campaign at RWE's pilot-scaled capture plant in Niederaussem, Germany.

Interestingly, the inlet stripper temperature directly correlates to the flowrate changes, shown more so in Scenario B and C as the magnitude of change is greater. Nevertheless, the rapid temperature and pressure transitioning influences the lean-loading. Figure 55 shows the lean and rich loading throughout each dynamic scenario. The steady-state baseload lean-loading is 0.237 mol CO_2/mol MEA, the rich-loading is 0.329 mol CO_2/mol MEA and the calculated reboiler duty is 3.93 GJ/tCO_2, within the 3.6-4 GJ/tCO_2 range specified in Bui et al. [44]. The steady-state values are not presented in Figure 55 as the results shown begin with the start-up operation. For the Baseload and Scenario A simulations the lean-loading remains reasonably constant post start-up and pre shutdown. This results from a constant solvent to steam (S/S) ratio. In Scenario B, the smaller solvent flowrate at low load and lower S/S value, means more energy is supplied per unit of rich-solvent. Enabling more CO_2 to be stripped, causing the lean loading to decrease between t=60 to 120 minutes, and t=180 to 240 minutes. Whereas in Scenario

C the lean-loading increases due to the drop in steam supplied to the reboiler, increasing the S/S ratio and reducing the energy available to strip the CO_2. Due to the rapid transitioning, the lean-loading levels do not stabilise in Scenario B and C. Jin et al. [373] explains the effects the lean-loading has on the reboiler duty for the conventional amine-absorption process, and showed a minimum reboiler duty of 3.472 GJ/tCO_2 at 0.2 mol CO_2/mol MEA lean-loading, similar to the results shown in this Chapter.

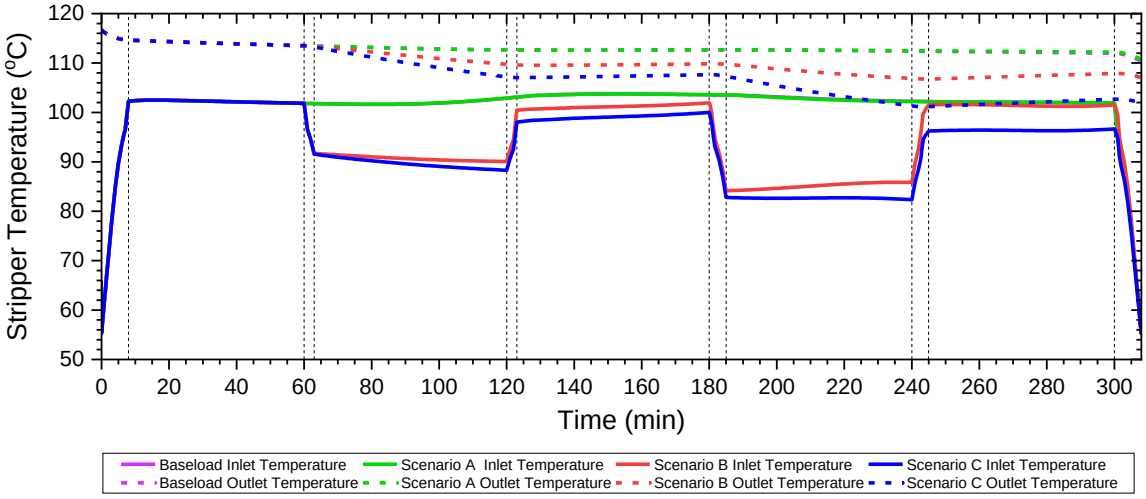

Figure 54: Absorber bulk vapour temperature profile in each scenario

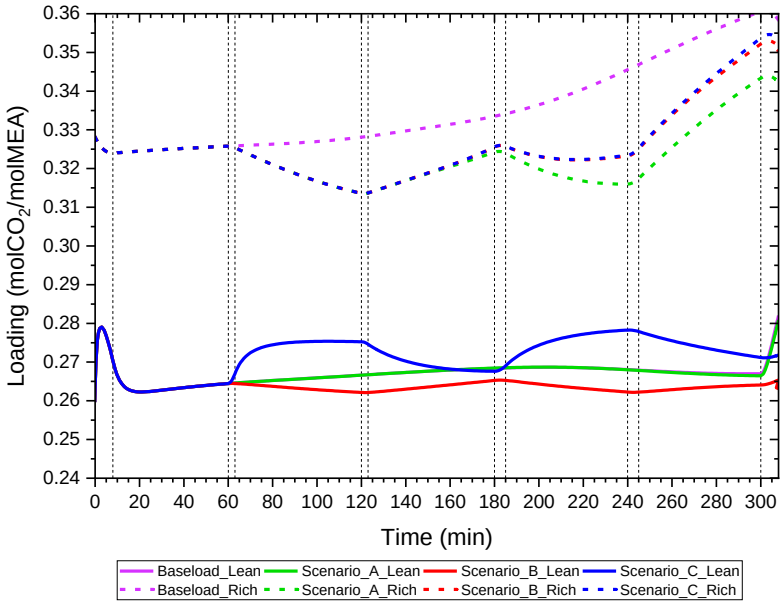

Figure 55: Lean and rich loading throughout each dynamic scenario

Table 36 highlights the percentage differences between the loadings from t=0 to t=308 minutes. The flexible operating scenarios provide a greater control of process parameters compared to the Baseload, which exhibits the greatest overall changes in both rich- and lean-loading, hence the lowest time-averaged capture rate. As the capture rate decreases, theoretically the rich-loading should decrease as well as less CO_2 is absorbed. However, the CO_2 mass fraction in the rich-solvent stream increases due a greater quantity of water evaporating in the column. The rich-loading is not necessarily a good indicator of the effectiveness of the process.

The transient operation aids in counteracting the long transition periods, which, as Bui et al. [68] explains, takes up to 114 minutes to re-reach steady state in a large-scale PCC system. In this study the Baseload operation does not reach steady-state until the end of the five hour operation, longer than that reported in Montañés et al. [66] and Bui et al. [68]. This is due to the larger flowrates and equipment sizes, increasing solvent circulation time. As well as non-optimised equipment geometries, which have been scaled to produce the same key operating parameters as the pilot facility, in reality the larger systems will not have identical performance.

Table 36: Loading changes over the entire simulation for each scenario

Scenario	Lean-loading (mol CO_2/mol MEA)			Rich-loading (mol CO_2/mol MEA)		
	t=0 min	t=308 min	%Difference	t=0 min	t=308 min	%Difference
Baseload	0.263	0.282	7.22	0.328	0.358	9.15
A	0.263	0.281	6.84	0.328	0.341	3.96
B	0.263	0.263	0	0.328	0.350	6.71
C	0.263	0.272	3.42	0.328	0.353	7.62

Figure 56 shows the reboiler duties for each scenario, based on the energy supplied to the reboiler via the pressurised steam, and the quantity of CO_2 captured over the five-hour operation. Scenario B captures the most CO_2 out of the flexible operating scenarios. During the operation it captures 26kg more than Scenario C and 67kg more than Scenario A. The KPIs for each operating scenario, and the steady-state baseline results from Tait et al. [65], are shown in Table 37. The aim of the scale-up was to achieve similar KPIs to the pilot results, this is evident for all of the KPIs. Interestingly, there is a potential energy saving when manipulating the reboiler steam flowrate in accordance with the GT load. Scenario C shows an 18.22% energy saving compared to Scenario A, with a reboiler duty of 1097 kWh/tCO_2 (3.95 GJ/tCO_2). This is 0.01 GJ/tCO_2 lower than the Baseload scenario, where the capture plant is operated at full load for the entirety of the five-hour operation. This is within the accuracy of model, highlighting there are no negative energy related effects of transient operation. Further research is required to determine the potential savings associated with manipulating the reboiler steam flowrate, and to develop an optimal operating strategy to minimise energy losses.

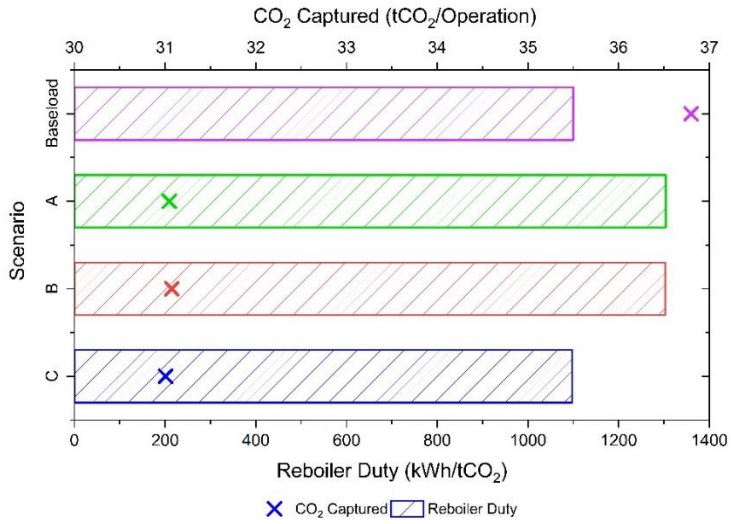

Figure 56: Reboiler duty and quantity of CO_2 captured during each operating scenario

Table 37: Key performance indicators for the different operating scenarios, including pilot-scale data from Tait et a. [65]

KPI	Pilot	Baseload	Scenario A	Scenario B	Scenario C
Capture Rate (%)	89.70	89.35	89.81	90.01	89.75
Reboiler duty (kWh/tCO_2)	1100.00	1099.93	1303.70	1302.59	1096.95
Purity (%)	-	97.78	97.79	97.47	96.69
Lean loading (molCO_2/mol MEA)	0.232	0.268	0.268	0.265	0.271
Rich loading (molCO_2/mol MEA)	0.345	0.336	0.326	0.329	0.328

Figure 57 shows the pressure drop in the reboiler for each scenario, and as expected Scenario C shows the greatest decline in reboiler pressure, similar to the outlet stripper temperatures shown in Figure 53. Compared to the initial reboiler pressure of 1.8 bar, the overall pressure drop is 15.49, 26.70, 41.24, and 19.37% for Scenario A, B, C and the Baseload respectively. The pressure drop and the consequent loss in purity has an effect on the compression system required to pressurise the CO_2 for pipeline transportation and storage [193, 185]. More information on the effects of transient CO_2 production on a compression system can be found in Chapter 5.

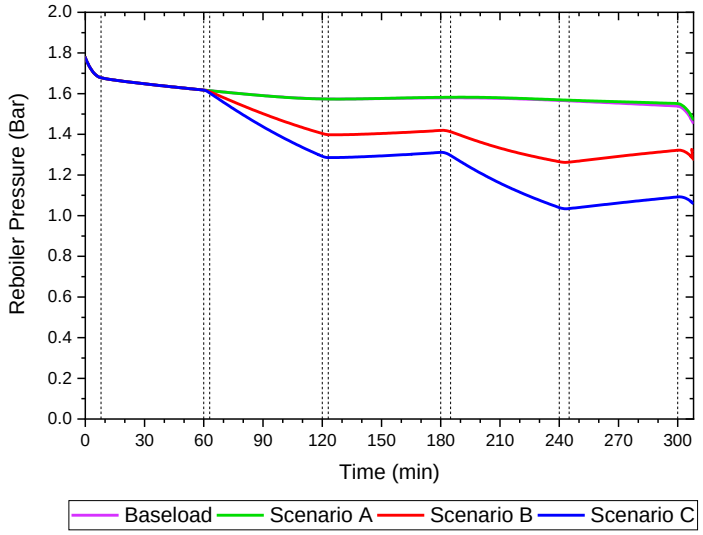

Figure 57: Reboiler pressure drop over each dynamic scenario

The scale process parameters are non-optimised solutions based on existing pilot studies, due to lack of operational CCS data on OCGT power plants. The capture rate is comparable to results in the literature [44]. Li et al. [374] showed the lean loading is optimal between 0.25-0.275 molCO_2/mol MEA. The scaled results in this study range between 0.265-0.271 molCO_2/mol MEA. The rich loading in the literature ranges between 0.45-0.5 molCO_2/mol MEA [ref] which is higher than the range (0.326-0.336 molCO_2/mol MEA) exhibited in this study and Tait et al. [65]. This results in a higher energy requirement. However, the reported energy demand for 30 wt.% MEA ranges between 3.2 to 5.5 GJ/tCO_2 or 889-1,528 kWh/tCO_2 [375], and the scaled results in this study range between 1,097-1,304 kWh/tCO_2. Therefore, as the energy demand results are within the range specified in the literature, the scaled results are based on the pilot results presented in Tait et al. [65].

4.2. CO_2 capture using Vacuum Pressure Swing Adsorption

This section presents the results for the PCC plant using VPSA. The dynamic model described in Chapter 3 Section 3.3.2 is first validated against pilot-scale data, the process parameters are then scaled to handle flue gas flow from the small-scale OCGT. The technical evaluation looks how affective the VPSA-PCC plant is at processing highly transient flue gas flow.

4.2.1. Model validation

Figure 58 compares the simulations adsorption bed pressure and temperature against the pilot results (Run 1) from Krishnamurthy et al. [115]. The simulation exhibits an almost identical pressure increase during the pressurisation step (t=0-20s), using 1000 SLPM flowrate containing 85 mol.% N_2 and 15 mol.% CO_2. During the adsorption (t=20-60s) and blowdown (t=80-230s) steps, similar pressure profiles are seen between the simulation and pilot results, the pressure drop rate is slightly greater in the pilot test, however, both results produce a bed pressure of 0.07 bar once the blowdown step is complete. Small variations between the results could be due to data extraction errors, and the pilot experiments performance indicators are for the 300th cycle, however, individual error bars are not available for the dynamic pilot results. Included in Figure 58 is the feed and product header temperatures, within [115] the temperature profile is not given for a single cycle, however, they have been included to compare with the full-scale VPSA simulations.

Two important key performance indicators for CO_2 capture technologies are the recovery rate and CO_2 purity. The recovery rate is defined as the percentage difference between the CO_2 flow entering and exiting the system [314]; in this case, the flowrates (Figure 59) and compositions (Figure 60) are used to calculate the amount of CO_2 captured (84.30%), which lies within the bounds (85.4 ± 4.52%) specified in Krishnamurthy et al. [115]. The purity of the end product during the evacuation step in the simulation is 89.56% (mol/mol), 5.14% points lower than the pilot facility (94.7 ± 1.05%). The simulation's predicted purity is not only a function of bed dynamics, in particular the adsorption rate calculated through the isotherm model, it is also affected by the valve stem position and the flowrate through the evacuation valve.

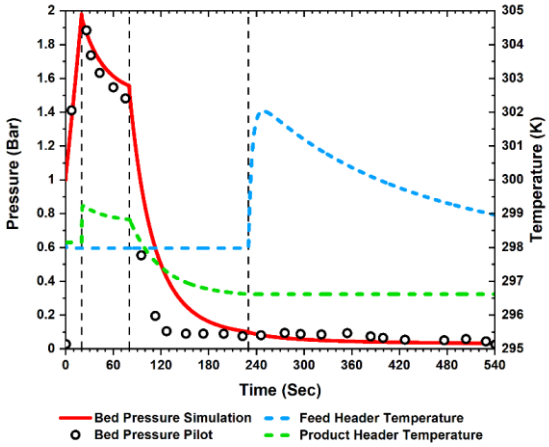

Figure 58: Adsorption bed pressure and temperature profiles

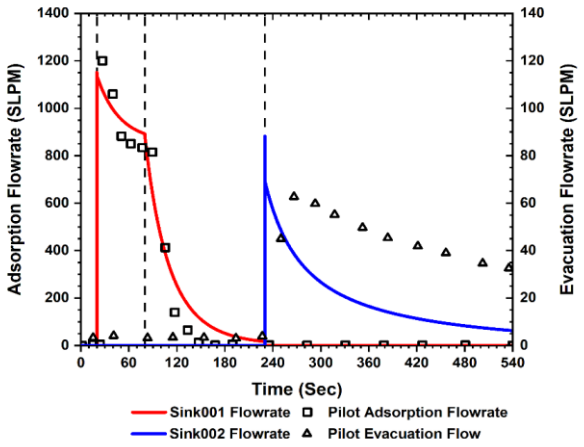

Figure 59: Flowrate profiles for the adsorption/blowdown and evacuation steps

Figure 59 compares the flowrates exiting the adsorption column, and the composition profiles during the adsorption, blowdown and evacuation steps are shown in Figure 60. The adsorption flowrate exiting the top of the column (mainly composed of N_2) exhibits the similar profile as the bed pressure, this is also shown in the evacuation profile, however, the pilot evacuation profile shows a smaller decease in

flowrate compared to the simulation, as a result of a more rapid pressure drop from the intermediate pressure (0.07 bar) to the low pressure (0.025 bar) used to desorb the captured CO_2.

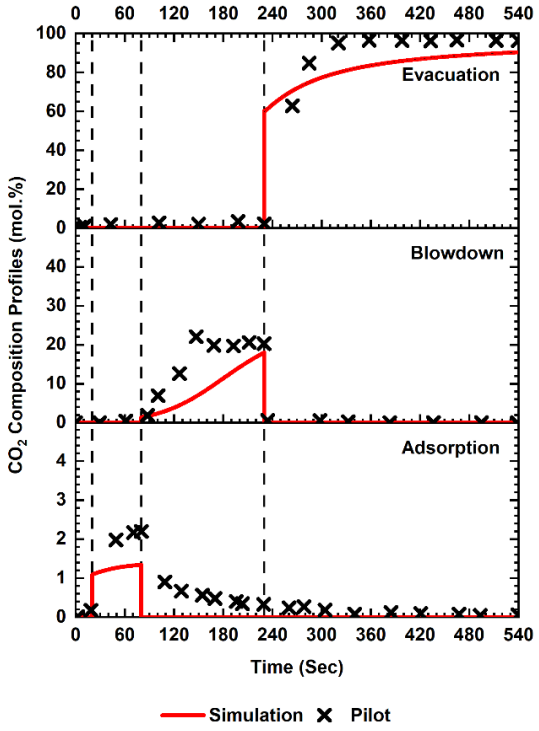

Figure 60: Comparison of CO_2 composition profiles during the Adsorption, Blowdown and Evacuation steps

The feed velocity ranges between 0.128-0.249 m/s, the adsorption ranges between 0.143-0.144 m/s, the blowdown between 0.028-0.142 m/s, and the evacuation velocity ranges between 0.062-0.151 m/s.

The pilot results productivity was 1.4 $tCO_2/m^3/day$, the simulation result is 15% lower at 1.18 $tCO_2/m^3/day$. The overall power demand (for the flue gas blower and vacuum pumps) is 934.05 kWh/tCO_2, 74.26% higher than the pilot run power demand (510.5 ± 25.5 kWh/tCO_2). If the efficiency of the pumps is set at 100% the overall power demand is 672.52 kWh/tCO_2 and 25.47% higher than the pilot test. The accuracy is further improved if the ratio of specific heat capacities is closer to that of CO_2 (1.28 [376]), specifically during the evacuation step due to the higher CO_2 concentration, the power demand is 611.79 kWh/tCO_2 and 14.14% higher than the upper bound of the pilot test. Highlighting the need for variable specific heat capacity ratios when determining overall pump power requirement.

During the adsorption step the average adsorption amount for CO_2 and N_2 is 3.569 mmol/g and 0.464 mmol/g, respectively, comparable to sources in the literature looking specifically at Zeolite 13x [377, 378]. Even though the CO_2 concentration leaving the column is lower than expected, the accuracy of the capture rate and the adsorption capacity shows the fidelity of the overall process model.

4.2.2. Scaled VPSA-PCC

The scaled system analysis focusses on the effects transient operation have on the processes key performance indicators (KPI), this study does not look at the optimisation of the scaled VPSA design. This results section shows the large-scale VPSA operation for two different scenarios:

- **Baseload** - No transient behaviour or start-up/shutdown procedures, to investigate how this inherently dynamic process handles constant flow.
- **Flexible** - Transient flue gas, including start-up, ramping, and shutdown procedures.

4.2.2.1. Flexible response

Figure 61 shows the flowrates through flue gas source (FGS), cleaned flue gas (CFG) and CO_2 sink (CS) streams, these are highlighted in Figure 46 Chapter 3 Section 3.3.2.1, for both the Baseload and Flexible operating scenario. Each parallel train handles 16.9 kg/s exhaust flow. The flowrate profiles for the CFG and CS flows are similar to the pilot study, where there is a sharp initial spike in flow that levels out during each operating step. When one bed is adsorbing the other bed is evacuating, allowing for continuous CO_2 capture. In the Baseload scenario, the system is fed with a constant flue gas flowrate for the entire 5-hour operating period. In the Flexible scenario, the system is fed with a transient flue gas supply. Included in this scenario is the start-up procedure, ramping to 70% and 50% loads, and the shutdown procedure. Due to computational limitations the simulation cannot operate at 0 kg/s feed, therefore, the system starts at 0.9 kg/s and ramps to 16.9 kg/s during start-up in 8 minutes. Similarly, for the shutdown operation, the feed is at 16.9 kg/s and ramps to 0.9 kg/s in 8 minutes.

The simulations also produced similar adsorption bed pressure profiles compared to the pilot study, see Figure 62. As the models are pressure driven it is important the pressure profiles are accurate. There is a sharp initial increase in pressure (pressurisation step), which then equalises during the adsorption step when the product valves are opened. At t=300 seconds in each adsorption cycle the blowdown valve (V4, V5, V15, and V16 in Figure 46 Chapter 3 Section 3.3.2.1) is opened and the bed pressure drops to 0.07 bar, at t=500 seconds in each cycle the blowdown valve is closed, and the evacuation valve is opened (V8, V9, V19, and V20 in Figure 46 Chapter 3 Section 3.3.2.1), further reducing the bed pressure to 0.025 bar and the CO_2 is desorbed from the bed. In the Flexible scenario the valve coefficient for V6, V7, V17, and V18 is changed from 0.15 to 0.01 kg/s/kPa to ensure an adequate exchange between the adsorption columns during the low load (50%) operation, without this alteration the full operation could not be completed.

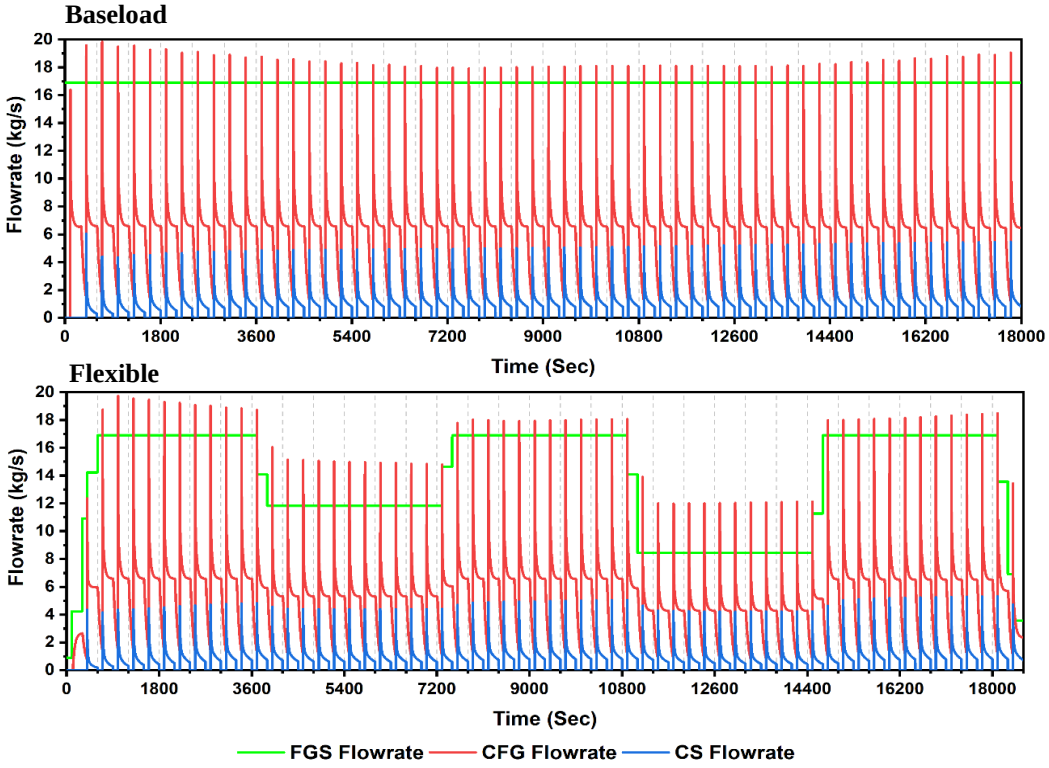

Figure 61: Flowrate profiles for the flue gas source (FGS), cleaned flue gas (CFG) and CO_2 sink (CS) flowrates in each of the parallel VPSA units, during the Baseload and Flexible scenarios.

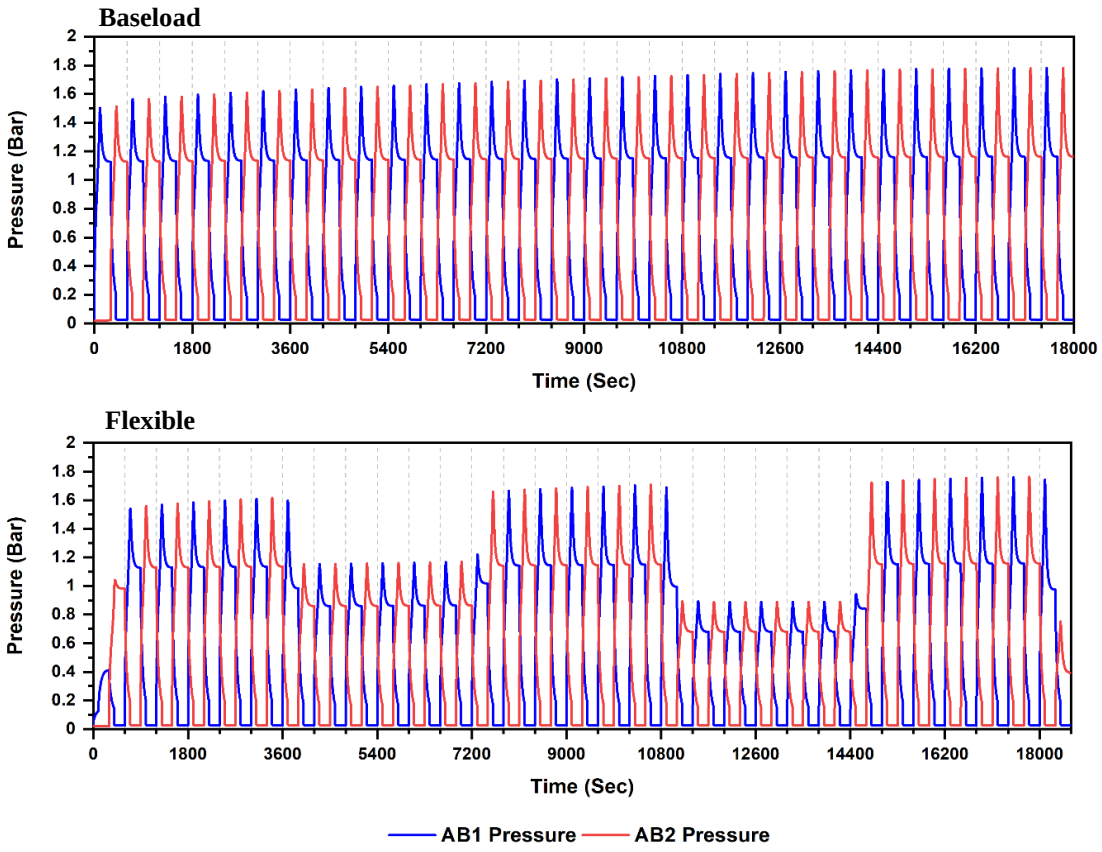

Figure 62: Pressure profiles for adsorption bed 1 (AB1) and adsorption bed 2 (AB2) in each of the parallel VPSA units, during the Baseload and Flexible scenarios.

Over the course of operation there is a gradual increase in the initial pressure spike during the pressurisation step. During the pressurisation step in the first cycle (baseload operation), the bed pressure (AB1) is elevated to 1.47 bar. Whereas, in the final cycle the bed pressure is elevated to 1.76 bar. The increase in step pressure is also shown in the pilot scale results in Krishnamurthy et al. [115]. At the end of each adsorption cycle the columns equalise to 0.025 bar ready for the next adsorption cycle. During the Flexible scenario, less flow is going through the system during the start-up, ramping and shutdown periods, therefore the adsorption columns cannot pressurise to 1.5 bar. Hence, the bed pressure follows the same profile as the input (FGS) flowrate.

The temperature profile in the adsorption column changes throughout each of the 5-hour operations, Figure 63 and Figure 64 highlight this transient behaviour for the Baseload and Flexible scenarios, respectively. As the adsorption process releases the heat of adsorption when CO_2 is adsorbed, the temperature increases in the column. In the beginning of the operation, the temperature bulge is located at the bottom of the column; indicating most of the adsorption is taking place within the first 2 m of packing. The temperature bulge transitions towards the centre of the column (between 4 and 8 m) as the operation progresses.

There is a small difference in the rate at which the temperature increases in the first operating cycle, between the Baseload and Flexible operating scenarios. This is due to the start-up procedure lasting 480 seconds; therefore, it is at full load by the end of the first operating cycle. As less CO_2 is entering the system, less CO_2 is adsorbed onto the zeolite surface and less heat is emitted into the column. There is a sudden drop in temperature in the Flexible scenario in the bottom of the column between t=10000 to

t=14000 seconds. Overall, there is a small difference in the temperature increase (<1.5K) at the temperature bulge, highlighting that less CO_2 is being adsorbed in the column.

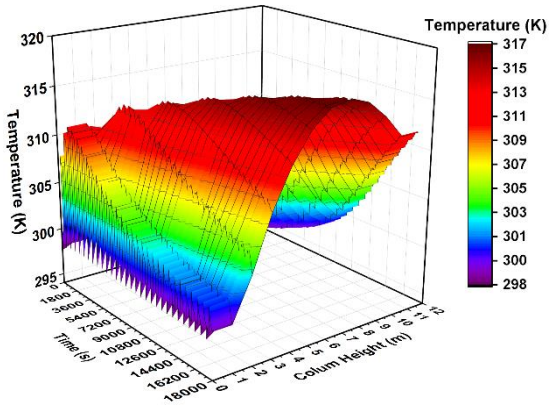

Figure 63: Adsorption bed (AB1) 3-D temperature profile for the Baseload scenario

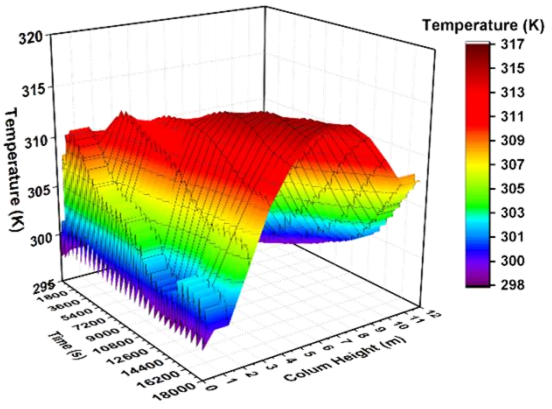

Figure 64: Adsorption bed (AB1) 3-D temperature profile for the Flexible scenario

The dissimilarities between scaled Baseload and pilot KPI results (see Table 38) are related to the scaled system design. The adsorption cycle steps and timings needed to be modified for continuous operation. The timings used in this study enabled the large adsorption columns to pressurise and minimise the inlet FGS velocity, preventing issues such as flow reversal, increased pressure drop, and loss in separation efficiency. Krishnamurthy et al. [115] showed the effect of altering the step duration and blowdown pressure on the recovery rate and purity. Longer adsorption step times increases the purity and decreases the recovery rate, due to the CO_2 front moving further into the column. This is observed in the 3-D temperature profile, see Figure 63. Highlighting, the adsorption timing within this study needs to be longer, however, this is limited by the pressure increase in the bed. Parameter scaling is another important issue, without demonstration scale results it is difficult to ascertain the fidelity of the scaled models.

The continuous operation and modified step timings also explain the increase in energy demand. The scaled Baseload results are more than double the pilot scale results, due to constant flue gas processing (increased flow through the FGS blower, CFG vacuum pump and CS vacuum pump), thus requiring more energy. From the literature review in Chapter 2 Section 2.2 and to the authors knowledge, no studies have investigated Flexible-VPSA. Despite the issues with the scaled design, it is important to see the ramifications transient operation has on the performance of VPSA CO_2 capture.

An issue observed in industrial adsorption processes is complex valve operation [379, 380]. Within this study the valves are operated based on flow coefficients dictating the pressure drop. Each valve operates simultaneously with the active status constantly changing. The complex partnership between the valves within the system make scaling up the VPSA processes difficult and affects the KPI's. When scaling the VPSA design it is important to consider the adsorption steps and timings, column geometry, process design and valve operation.

The differences between the Baseload and Flexible operating scenarios KPI's can be explained by the non-identical temperature profiles in Figure 63 and Figure 64. In this study, for VPSA there is a small decrease in recovery rate (0.03% points). This is lower than all of the MEA CO_2 capture flexible response scenarios (0.73 -1.20% points lower than the steady-state results at 92.48%) shown in Chapter 4 Section 4.1.2. There is also a small drop in purity for flexible VPSA system (1.20 % points). This will affect downstream compression equipment, so too will the transient operation, this is highlighted in Chapter 5.

Table 38: Key performance indicators (KPI) for the Baseload and Flexible VPSA simulations

KPI	**Pilot** [115]	**Scaled-Baseload**	**Deviation (%)**	**Scaled-Flexible**	**Deviation (%)**
Recovery rate (%)	85.40 ± 4.52	97.07	+13.66	97.03	-0.04
Purity (%)	94.7 ± 1.05	80.74	-14.74	79.54	-1.49
Energy demand (kWh/tCO_2)	510.5 ± 25.5	1191.72	+133.67	1274.04	+6.91
Productivity (tCO_2/m^3 ads/day)	1.40 ± 0.07	1.28	-9.02	1.07	-15.85

Figure 65 highlights the FGS blower, CFG vacuum pump and CS vacuum pump power requirements for the Baseload and Flexible scenarios. The majority of the energy demand comes from the CFG vacuum pump used in the adsorption and reverse blowdown steps. This has the largest energy demand because it handles a large amount of flow compared to the CS vacuum pump, and the energy drop is the greatest (approximately 1.5 to 0.07 bar). Despite the Flexible scenario consuming less energy, it has a higher specific energy demand (see Table 38) due to the smaller quantity of CO_2 captured (see Figure 65). The quantity of CO_2 captured during the Baseload (39.99 tCO_2/operation) and Flexible (33.65 tCO_2/operation) operations are comparable to the results in Section 4.1.2 (31-37 tCO_2/operation), the slightly higher amount is due to the higher capture rate (92.48 % MEA steady-state results).

In Section 4.1.2 the energy demand for the flexible response varies between each of the flexible operating scenarios. When the steam supply to the reboiler (for solvent regeneration) is constant, the energy demand for the process is 4.69 GJ/tCO_2 (1302.78 kWh/tCO_2). When the steam supply is altered in accordance with flue gas changes, the energy demand decreases to 3.95 GJ/tCO_2 (1097.22 kWh/tCO_2). For Flexible-VPSA the energy demand (for the pumps) is 4.59 GJ/tCO_2 and 16.11% higher than the best flexible-MEA case. This is due to the fact that no specific energy minimisation scenario was considered in this study. Therefore, future work should focus on developing dedicated operating scenarios for VPSA system, in order to minimise the negative energy effects of transient operation and scale-up. A possible solution is manipulating the scheduling (step time and pressure level) to deliver lower specific energy demands for the pumps during low load operation.

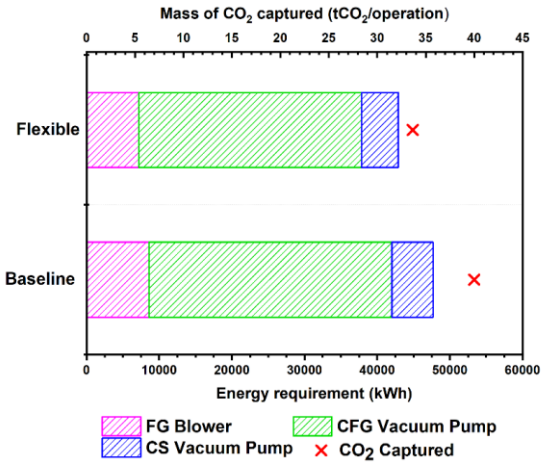

Figure 65: Pump energy requirement and mass of CO_2 captured during the 5-hour operation for the Baseload and Flexible scenarios.

4.3.Conclusion

Herein, the process and economic models described in Chapter 3 are validated to illuminate their fidelity. The MEA and VPSA model validations showed the flowrate, capture rate, and column temperature profiles were accurate compared against the pilot plant results. The energy demands calculated by the model were slightly higher than those reported in the respective pilot studies, but they only deviated <15%. Therefore, the models are in good agreement with pilot-scale data.

The scale-up process ensured the systems could handle 33.8 kg/s of flue gas from a 10.4 MWe OCGT with 4.27 vol.% CO_2 (6.78 wt.% or 4.42 mol.%), whilst maintaining similar KPIs to the respective pilot studies. During the Baseload scenario for the scaled MEA design, the capture rate and specific energy demand is 89.35% and 1099.93 kWh/CO_2, respectively. These are only slightly lower than the 89.70% capture rate and 1100 kWh/tCO_2 specific energy demand from the pilot study [65]. During the Baseload scenario for the scaled VPSA design, the capture rate and specific energy demand is 97.07% and 1191.72 kWh/CO_2, respectively. These are higher than the 85.40% capture rate and 510.50 kWh/tCO_2 specific energy demand from the pilot study [115]. Highlighting the issues with scaling adsorption system and proves the need for larger demonstration scale studies for VPSA.

Both technologies can adequately handle transient flue gas production. The Flexible VPSA scenario showed a better performance in terms of recovery rate and purity (only deviating <2% compared to the Baseload results). Whereas, the Flexible MEA scenarios showed a better performance in terms of energy demand, but only when incorporating a scenario that specifically aims at reducing the energy demand during low load operation.

Chapter 5 : CO_2 Conditioning Results

This section presents the results for CO_2 compression and conditioning. The dynamic models described in Chapter 3 Section 3.3.3 are first validated against data from the IEAGHG. Three studies were conducted using the validated process models for conventional multistage compression and multistage compression with sub-critical liquefaction. The first study investigated the effects different CO_2 sources (various inlet composition, pressures, and temperatures) have on the two conditioning routes. The second study is a sensitivity analysis looking at varying the inlet flowrate and starting pressure, seeing the effect these input parameters have on the energy demand for the process. The final study investigates the dynamic response of the conditioning system, to analyse the effects of transient capture plant output.

5.1. Model validation

Using input parameters specified in Table 27 in Chapter 3 Section 3.3.3.1 and IEAGHG [60] the process simulator calculates several important design characteristics shown in Table 39. The polytropic efficiency (η_p) typically used for compressor evaluation, ranges between 79-87%. Aspelund [381] states centrifugal compressors have a polytropic efficiency between 80-85%, and compression stages have a pressure ratio between 1-5. The simulations show the 1st and 2nd compression stages lie outside these specified bounds, therefore, may not be the most energy-efficient systems. Nevertheless, for the purposes of this study they provide a baseline for source to transport evaluation. More design characteristics for the validation models are shown in Appendix B Chapter 10 Section 10.2.

Table 39: Design characteristics for the individual compression and pumping stages.

Compressor Stage	**Flow Coefficient (φ)**		**Polytropic Coefficient (ψ_p)**		**Polytropic Efficiency (η_p)**		**Pressure Ratio (P_{out}/P_{in})**	
	B0	**D2c**	**B0**	**D2c**	**B0**	**D2c**	**B0**	**D2c**
1st	0.1751	0.1751	1.24	1.24	79.38	79.38	4.38	4.38
2nd	0.0685	0.0685	1.72	1.72	86.66	86.66	5.15	5.15
3rd	0.0693	0.0679	2.09	1.94	82.92	82.94	2.13	2.02
4th/Pump	0.0692	-	1.97	-	80.82	90.00	1.60	1.69

Figure 66 compares the process simulation for the multistage compression system against the IEAGHG base case B0, for which the key performance indicators are shown in Table 39. The inlet and outlet pressures are extremely accurate, less than 0.04% for all streams. The flowrates into the 2nd, 3rd and 4th compression stages are slightly smaller (<2.33%) than presented in IEAGHG [60] as less flow is recycled from the dehydrator. The inlet temperature into the 1st compression stage is higher than expected due to the surge control system, resulting in a higher outlet temperature. These small differences result in the 1st, 2nd, 3rd and 4th compression stage power demand deviating -4.68, 15.41, 12.95, and 8.94%, respectively. Overall, the total power demand (53.42 MW) is 7.10% lower than expected (57.51 MW).

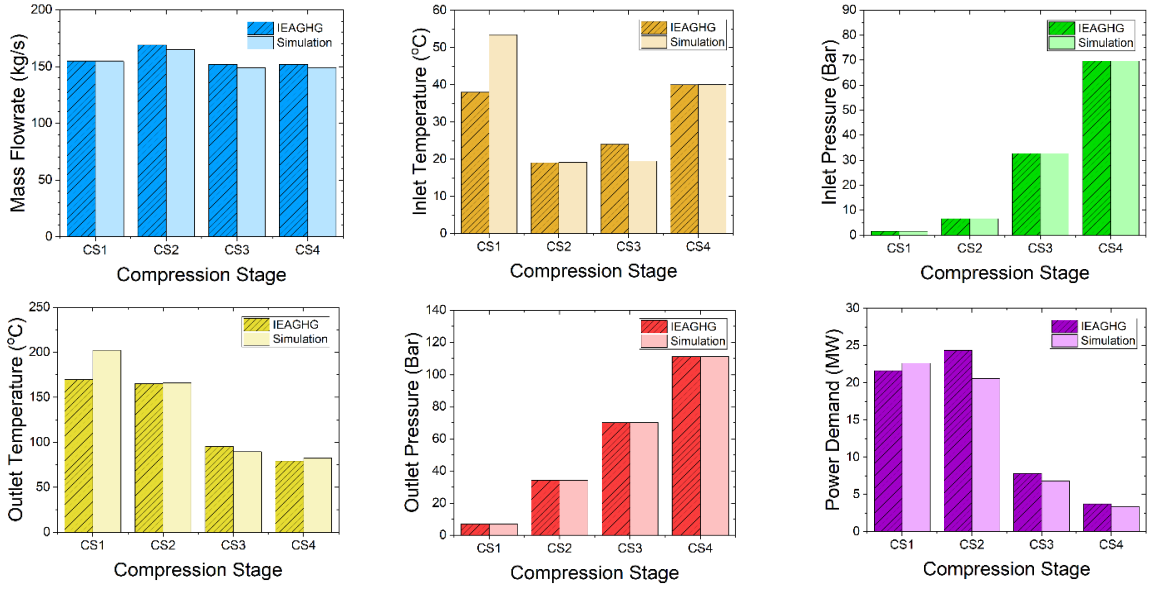

Figure 66: IEAGHG base case B0 process simulation validation. CS = compression stage.

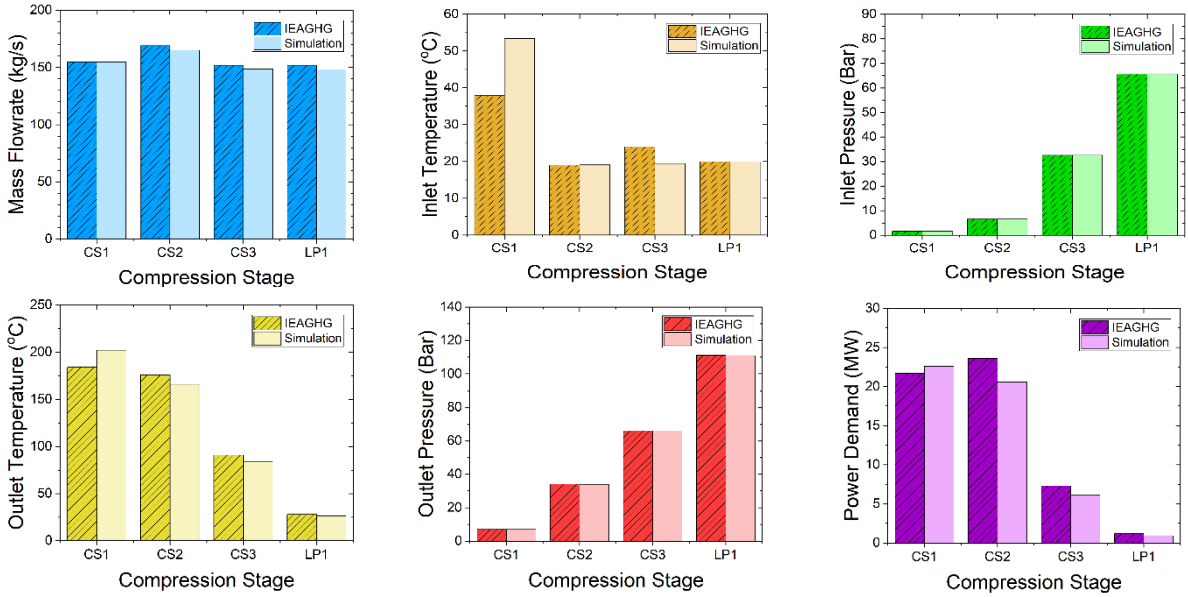

Figure 67: IEAGHG case D2c process simulation validation. CS = compression stage. LP = liquid pump

Figure 67 compares the process simulation for the multistage compression and liquefaction system against the IEAGHG case D2c, for which the key performance indicators are shown in Table 39. Similar to the previous case the flowrates into compression sections 2, 3, and 4 are slightly smaller than presented in IEAGHG [60] as less flow is recycled from the dehydration unit. The inlet temperature into the 1st compression stage is higher than expected due to the surge control system, resulting in a higher outlet temperature. Again, the inlet and outlet pressures are extremely accurate, less than 0.2%

for all streams. The only differences between the two cases is the 3rd compression stage outlet pressure and the use of a liquid pump instead of a 4th compression stage. Overall, the total power demand for the liquefaction simulation (50.41 MW) is 6.30% lower than in IEAGHG [60] (53.80 MW). The liquefaction route power demand is 5.64% lower than the conventional case simulation.

5.2. Different CO_2 sources

The process model for the conventional and liquefaction conditioning routes is scaled down to handle 1 kg/s of CO_2 flow. Each capture technology presented in Table 15 Chapter 2 Section 2.4.3.1 is used as an input in the process model, the compression stage rotational speed is corrected in each simulation to produce the desired output pressures shown in Table 27 Chapter 3 Section 3.3.3.1. The correct values are shown in Table 52 and Table 53 in Appendix B Chapter 10 Section 10.2.

Figure 68 shows the power demand for individual units for the conventional CO_2 compression system, where CS and DH refer to the compression stage and dehydrator unit, respectively. The various captured CO_2 sources range from power generation to industrial sources such as hydrogen and steel production. Figure 68 also includes the specific energy demand in kWh/tCO_2 for each captured CO_2 source. The initial moisture content in all scenarios is low enough that all 600 ppm cases do not require a dehydration unit, reducing overall energy demand, especially in the 2nd compression stage (due to the decreased flowrate). For example, the low moisture MEA case is 179.18 kWh/tCO_2, whereas the high moisture MEA case is 9.35% lower at 162.43 kWh/tCO_2. For Selexol, the low moisture case is 161.15kWh/tCO_2, whereas the high moisture scenario is 10.44% lower at 144.32 kWh/tCO_2. As the Selexol process produces two CO_2 streams, a pre-compressor is required to combine and equalise the streams, offsetting the potential savings of a higher starting pressure.

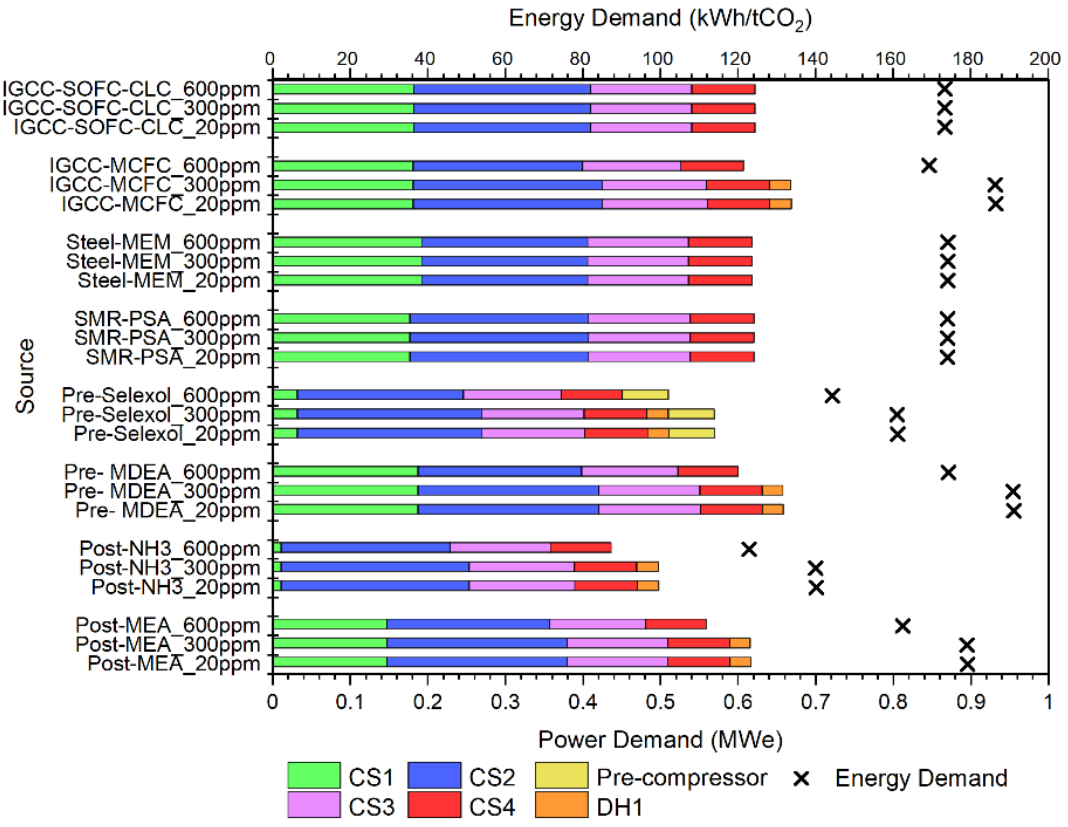

Figure 68: Unit power consumption for conventional CO_2 compression

For all the scenarios shown in Figure 68, the difference between 20 and 300 ppm is below 1%. As long as there is a need for the dehydration unit, the specified moisture removal has very little influence on the overall power demand. Interestingly, as the knock-out drums are sufficient enough to remove the moisture low enough for the 600 ppm cases, the high moisture MEA case is lower than the steel membrane case at 174.14 kWh/tCO_2. The membrane system requires no moisture removal, hence no dehydrator power consumption. Potential energy savings are offset by a higher initial temperature (40℃) and low initial pressure (1 bar), increasing the power demand and energy required for the 1st compression stage, similar to the SCF-CLC case with 100% pure CO_2 it requires 173.34 kWh/tCO_2. Pre-combustion capture using MDEA requires the highest conditioning energy requirement, consuming 0.66MWe with a specific energy demand of 191.06 kWh/tCO_2, similar to the low moisture MCFC case with 186.46 kWh/tCO_2. Both scenarios start at 30℃, however, the MCFC case has a higher purity CO_2 (99.95 %) and starts at a slightly elevated pressure (1.1 bar), hence the slightly lower energy demand. Higher starting pressure is beneficial, see Selexol and NH_3 absorption scenarios, it reduces the overall pressure ratio and thus the power demand, similar to the results in [192]. In the low moisture NH_3 case the starting pressure is 6 bar, 3.75 times higher than the MEA case, resulting in 19.23% less energy requirement. Hence the inlet pressure of the CO_2 stream is more impactful than the initial level of moisture.

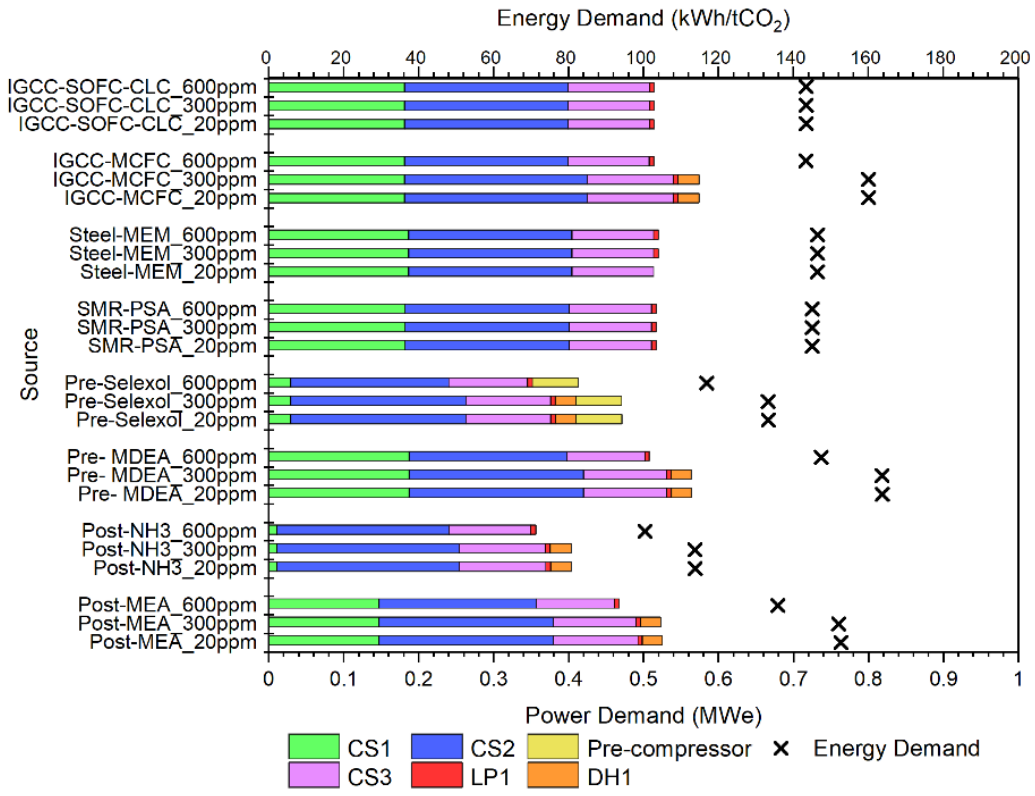

Figure 69: Unit power consumption for CO_2 compression and liquefaction

Figure 69 shows the power demand for individual units of the CO_2 compression and liquefaction route, similar to Figure 68 it includes the overall energy demand for each capture CO_2 source. Identical patterns are exhibited as in the conventional case, with a lower power demand for every scenario due to the much smaller power consumption of liquid pumps. In the low moisture conventional MEA case the 4th compression stage power demand is 80020 W, whereas in the liquefaction case the liquid pump is 6036 W, 92.46% lower despite the higher pressure ratio, see Table 39.

Table 40 highlights the percentage difference between the conventional and liquefaction routes for each scenario, ranging between 14 to 19%. Similarly to Martynov et al. [185], who showed CO_2 streams >95% v/v purity can use liquefaction around 62 bar to improve the compression efficiency by 15%, this route proved less feasible for low purity sources. The overall specific energy demands range from 100-191 kWh/tCO_2.

Table 40: Comparison between conventional compression and liquefaction routes

Source	Moisture	Overall energy demand (kWh/tCO_2)		
		Conventional	Liquefaction	Difference (%)
Post-MEA	Low	179.18	152.72	14.77
Post-MEA	Medium	179.04	152.05	15.07
Post-MEA	High	162.43	135.87	16.35
Post-NH3	Low	140.15	113.79	18.81
Post-NH3	Medium	140.01	113.72	18.77
Post-NH3	High	122.87	100.35	18.32
Pre- MDEA	Low	191.07	163.75	14.30
Pre- MDEA	Medium	190.93	163.68	14.27
Pre- MDEA	High	174.27	147.45	15.39
Pre-Selexol	Low	161.16	133.29	17.29
Pre-Selexol	Medium	161.01	133.23	17.26
Pre-Selexol	High	144.32	116.84	19.04
SMR-PSA	Low	174.03	145.01	16.67
SMR-PSA	Medium	174.03	145.01	16.67
SMR-PSA	High	174.03	145.01	16.67
Steel-MEM	Low	174.13	146.42	15.91
Steel-MEM	Medium	174.13	146.42	15.91
Steel-MEM	High	174.13	146.42	15.91
IGCC-MCFC	Low	186.46	160.08	14.15
IGCC-MCFC	Medium	186.28	160.09	14.06
IGCC-MCFC	High	169.28	143.36	15.31
IGCC-SOFC-CLC	Low	173.34	143.42	17.26
IGCC-SOFC-CLC	Medium	173.34	143.42	17.26
IGCC-SOFC-CLC	High	173.34	143.42	17.26

Table 41 compares the capture and conditioning energy demand for each of the capture technologies. Although it is not an accurate comparison as the conditioning energy demands are for 1kg/s systems, it does highlight the difference between the capture and conditioning requirements. In relation to CCS clusters, this poses a unique challenge of balancing quantity and efficiency. Certain systems may capture CO_2 with a lower specific energy requirement (for both capture and conditioning), however, the quantity captured may be small. Both industrial CO_2 capture technologies (SMR-PSA and Steel-MEM) have lower capture energy demands compared to the conditioning energy demand, highlighting these systems may benefit from sharing the conditioning duty with neighbouring facilities, or utilising intermediate storage prior to compression at a centralised hub [225].

Table 41: Capture and conventional conditioning energy demand

Source	Capture Energy Demand (kWh/tCO_2)	Conditioning Energy Demand (kWh/tCO_2)	Combined Energy demand (kWh/tCO_2)
Post- MEA	1055.56 [44]	179.17	1234.72
Post- NH3	694.45 [44]	140.00	834.45
Pre- MDEA	323.61 [218]	190.83	514.44
Pre- Selexol	-	161.11	325.56 [382]
SMR-PSA	111.11 [383]	174.17	285.28
Steel-MEM	161.94 [220]	174.17	336.11
MCFC	391.67 [166]	186.39	577.78
SOFC-CLC	172.22 [384]	173.33	345.56

5.3. Sensitivity Analysis

The specific energy demands for the conventional cases range between 123-191 kWh/tCO_2, and for the liquefaction cases range between 100-164 kWh/tCO_2, which are higher than the range specified (90-120 kWh/tCO_2) in Aspelund and Jordal [192]. The higher than expected energy demand is related to the small size of the inlet flowrate. Furthermore, as highlighted in Figure 68 and Figure 69, technologies such as Selexol and NH_3 absorption have a lower power consumption because of elevated inlet pressures. Therefore, included in this study is a sensitivity analysis looking at various inlet pressures and flowrates.

5.3.1. Effect of changing the inlet stream pressure

Figure 70 shows the energy demand for different inlet stream pressures ranging from 1 bar to 10 bar, for the MEA conventional and liquefaction scenarios. The mass flowrate is kept at 1kg/s, and the pressure range was chosen to investigate the effects of removing the 1st compression stage. A greater increase is shown during the initial pressure increase, this rate slows down as we approach 7 bar (the outlet pressure of the first compression stage). At 7 bar and higher the first compression stage is no longer needed; however, the knock-out drum and cooling stage is still required. Otherwise, there is an increased power demand for the second compression stage due to a higher inlet flowrate.

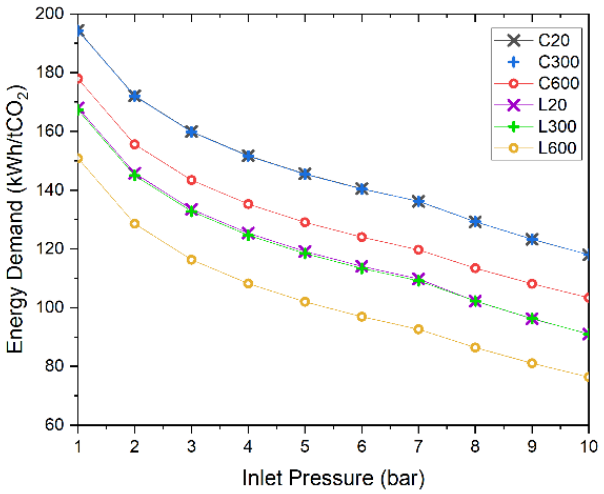

Figure 70: Energy demand as a function of inlet stream pressure

As can be seen for both conventional and liquefaction routes, there is no difference between 20 and 300 ppm, so moisture content is not an issue as long as the initial purity is >95%, the knock-out drums do most of the moisture removal. Between 7 to 10 bar there is a greater decrease in the rate of energy drop, this is due to the 2nd compression stage inlet pressure decreasing, the initial drop in pressure has a greater effect than the final drops in pressure (per stage). Overall, the specific energy demand decreases as the starting pressure increases, a similar trend is presented in Aspelund and Jordal [192]

5.3.2. Effect of changing the inlet flowrate

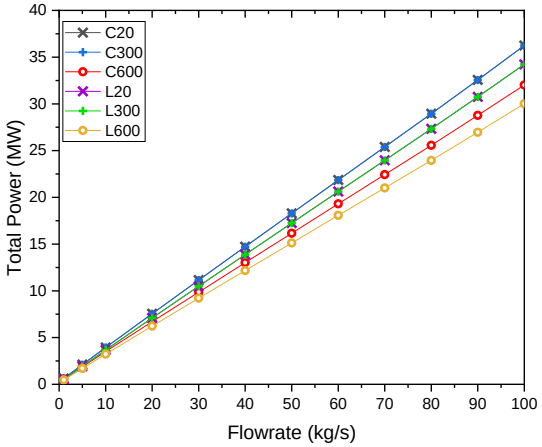

Figure 71: Total power demand for various inlet

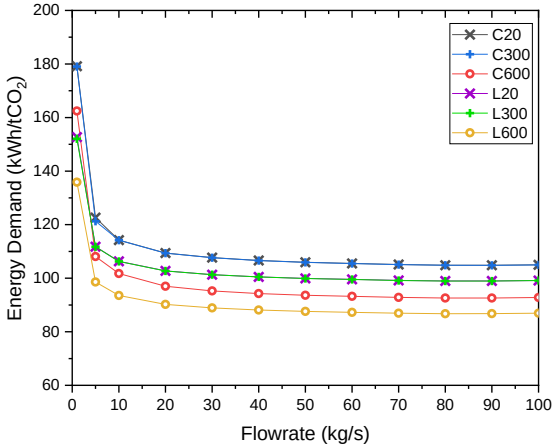

Figure 72: Specific energy demand for various inlet flowrates

Figure 71 and Figure 72 show the total power demand and specific energy demand, respectively, for different model input flowrates ranging from 1 to 100 kg/s, for both the MEA conventional and liquefaction conditioning scenarios. The flowrate range was chosen to encompass all possible inputs into large CCS clusters. This highlights the rate at which the energy demand changes as a function of inlet flowrate or plant size. Total power demand increases almost linearly with increasing inlet flowrate, a greater flow requires a greater amount of power to compress it. At 100 kg/s for the low

moisture conventional and liquefaction routes the power demand is 36.24 and 34.23 MW, respectively. Interestingly, a point is reached around 10 kg/s where the specific energy demand increases rapidly. A large difference is exhibited between 1kg/s and 10 kg/s, for the 20 ppm MEA conventional case the 1 kg/s simulation showed a 179.18 kWh/tCO_2 specific energy demand, at 10 kg/s this is reduced by 36.24% to 114.24 kWh/tCO_2. A smaller difference is shown between 10 kg/s and 100 kg/s, only reducing 8.09% to 105.00 kWh/tCO_2. Overall, for the 20 ppm conventional case there is a 41.4% reduction in power demand when increasing from 1kg/s to 100 kg/s flow.

In relation to the power generation technology for the source of CO_2, Section 3.2 shows a Siemens SGT-400 gas turbine operating in open-cycle configuration produces 10.4 MWe of power and 38 kg/s of exhaust flow, assuming 4.27 vol.% CO_2 concentration and 90% CO_2 capture this equates to 2.06 kg/s of CO_2 flow into the conditioning system. For a MHPS M701J series producing 478 MWe of power in open-cycle and 896 kg/s of exhaust flow [385], the CO_2 output flow is 54.59 kg/s. Based on Figure 72, assuming the CO_2 is captured through an MEA based absorption system, a small-scale 10 MWe plant will require approximately 167 kWh/tCO_2 to conventionally condition the capture CO_2 at a 300 ppm moisture control level, whereas a large-scale 478 MWe plant will require approximately 105 kWh/tCO_2. Therefore, conditioning a CO_2 stream from a small-scale power source is 59.05% more energy intensive than the large-scale source.

5.4.Dynamic study

Another challenge highlighted in Moe et al. [239] is the effect of transient CO_2 production on the downstream compression and transportation network. Therefore, to assess each systems capability under real-world transient conditions, assuming that load following capture plant operation directly relates to fluctuations in the captured CO_2 product, the input flowrate in the dynamic models is ramped based on real-world gas turbine operation. Using a 1 kg/s flowrate basis, this correlates to a 5 MW gas turbine operating in open-cycle configuration. The ramp rate for modern gas turbines is between 8-12% max load per minute [291], assuming 10% ramp rate the gas turbine would take 3 minutes to decrease to 70% load. Furthermore, assuming constant capture plant performance, the ramp rate is used to simulate a scenario where the gas turbine after 2 hours of operation is forced to reduce to 70% full load for 1 hour, then ramps to full load and continues for another 2 hours, simulating a typical 5-hour operation. The reporting interval for the dynamic simulations is 10s.

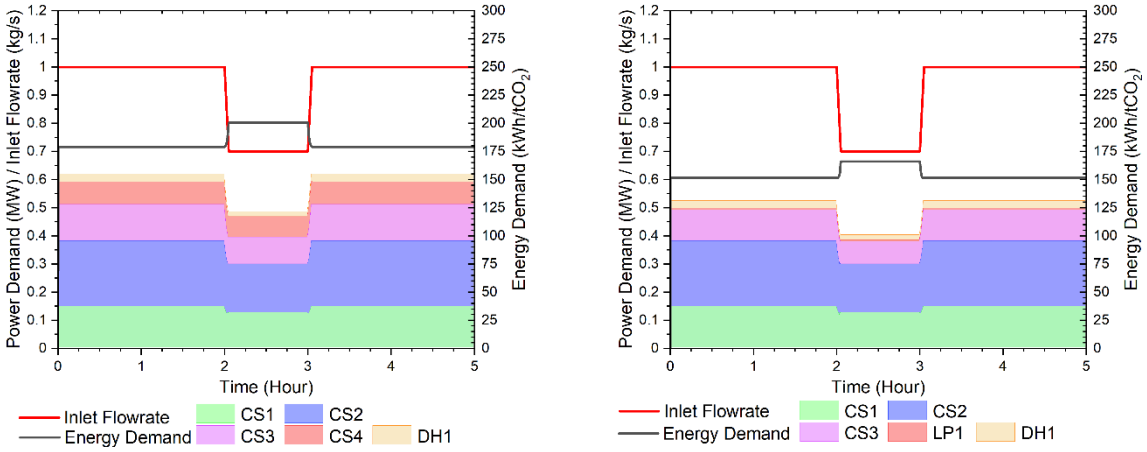

Figure 73: Dynamic power consumption and energy demand for the 20 ppm MEA conventional (left) and liquefaction (right) compression cases

Figure 73 shows the power consumption and energy demand for the MEA 20 ppm moisture conventional and liquefaction cases. Considering the total mass of CO_2 processed and the total energy supplied to the compression stages and dehydration unit, the overall specific energy demand for the 5-hour transient operation for the conventional and liquefaction processes is 182.08 kWh/tCO_2 and 153.66 kWh/tCO_2, respectively. Even though in both scenarios the power demand decreased during the partial load stage (t=2 to 3 hours), the lower CO_2 flowrate means the overall specific energy demand increased. At 2.5 hours, the conventional case required 0.4844 MW to process 0.7 kg/s of CO_2, equating to an instantaneous specific energy demand of 192.25 kWh/tCO_2, this is 7.29% higher than the steady-state simulation, highlighting transient CO_2 conditioning has a negative effect on specific energy demand.

Figure 74 shows that throughout the simulation the individual outlet pressures for each compression stages are kept constant, through the use of the surge and variable frequency drive control systems. Implementing these control system enables a realistic response to transient CO_2 production [341]. The increased outlet compression stage temperature at lower loads should lead to an increased water demand for interstage cooling, however, there is a 23.38% (conventional) and 25.84% (liquefaction) decrease in overall water demand due to the lower flowrate through the entire system. There is an increased inlet stream temperature to all the compression stages, however, this is not related to the cooling system but rather the activation of the surge system recycling hot gases. The temperature and enthalpy change across the compression stages is related to the polytropic efficiency (see Equation 53 in Chapter 3 Section 3.3.3) The ratio between the inlet and outlet temperatures, also known as polytropic ratio [386], increases for the first compression stage resulting in the polytropic efficiency decreasing by 1.34%.

Whereas the polytropic ratio in the 2nd and 3rd stages is smaller at lower loads, resulting in the polytropic efficiency increasing by 4.62% and 12.72%, respectively. During the 4th stage the ratio remains constant, hence no change in efficiency, highlighting the importance of controlling the inlet temperature during load changes.

It is possible to incorporate a cooling step within the surge recycle, however, Budinis and Thornhill [387] showed this increases the power consumption due to a greater volume of flow and cooling requirement of the recycle stream. The study focused on the compression stage configuration, a possible alternative configuration for CO_2 systems could be recycling the surge system prior to the heat exchanger unit, ensuring a constant inlet compression stage temperature. Another possible solution is model predictive control (MPC), capable of preventing surge and reducing the volume of recycled flow [388]. Future work should focus on utilising MPC during load changes originating from upstream capture units, to optimise the conditioning train during transient operation.

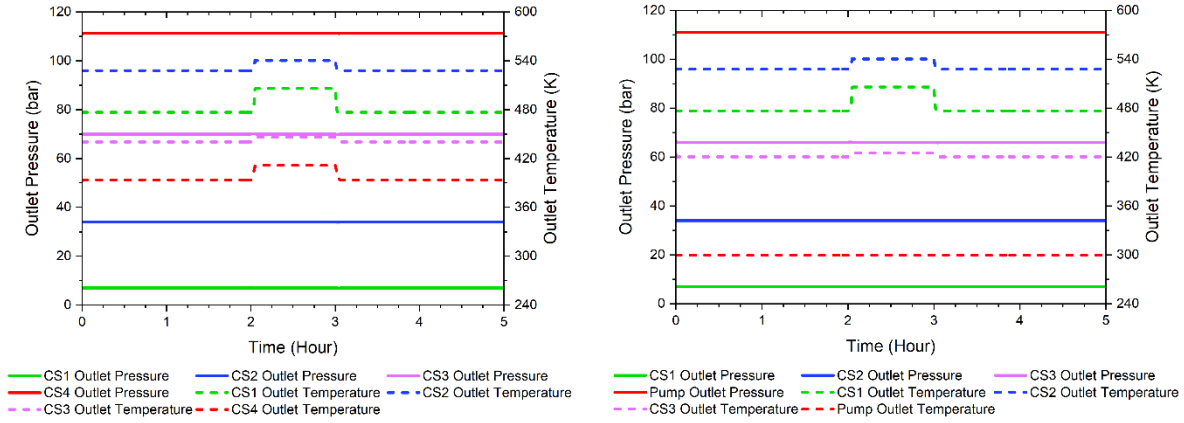

Figure 74: Outlet pressure and temperature profiles for the 20ppm MEA conventional (left) and liquefaction (right) compression cases

5.5. Conclusion

Herein, the process and economic models described in Chapter 3 Section 3.3.3 are validated to illuminate their fidelity. The compression train model validation showed good agreement with data from IEAGHG [60], for both conditioning routes. The power demand for the sub-critical liquefaction route is 5.64% lower than the conventional case simulation. Within the case study evaluation, using various sources of CO_2 from power and industry, the liquefaction route is unanimously more energy efficient than conventional multistage compression. This is due to the use of liquid pumps, which require less power than centrifugal compressors.

The CO_2 conditioning study provides valuable insight into the link between CO_2 source and transportation, which can be used as design guidelines for CCS clusters. For power generation sources, the scale of operation is extremely import. The sensitivity analysis showed as you decrease from 100 kg/s to 1 kg/s of CO_2 flowrate, the specific power demand increases by over 40%. Highlighting, smaller capture facilities could benefit from sharing the conditioning load with other neighbouring CO_2 emitters.

Chapter 6 : Economic Results

This section evaluates the economics of applying MEA and VPSA CO_2 capture for small-scale OCGT's. Included in the economic comparison is the cost of generating electricity from an OCGT, capturing CO_2, and conditioning CO_2 ready from pipeline transportation. Both capture systems have the same flue gas input and end-point characteristics, creating a black-box in which the economic evaluation occurs. It is worth noting, the specific energy demand for the MEA plant, shown in Table 42, is completely met by HRSG unit and the plant suffers no power losses due to the capture facility. The VPSA plant has a lower power output as some of the electricity generates is used to power the large vacuum pumps and blowers used for adsorption.

Table 42: System characteristics for OCGT power generation with MEA or VPSA CO_2 capture.

	MEA	**VPSA**
Power generation	OCGT	OCGT
Power output (MWe)	10.24	9.06
Fuel source	Natural gas	Natural gas
Gross heat rate (kJ/kWh)	10173	10173
Thermal Efficiency (%)	35.4	35.4
CO_2 capture technology	Amine-based absorption	Vacuum-pressure swing adsorption
Solvent/Sorbent	30 wt.% Monoethanolamine	Zeolite 13x
Capture rate (~%)	92	97
Flue gas flowrate (kg/s)	33.8	33.8
Flue gas CO_2 concentration (vol.%)	4.27	4.27
Specific energy demand (kWh/tCO_2)	1481.94	1461.39

6.1. Equipment cost breakdown

A major aspect of the TCC is the PEC, shown in Figure 75 for the MEA plant and Figure 76 for the VPSA plant, both include the cost for the conditioning train. The breakdown of OCGT+CCS PEC is shown in Figure 77. The total PEC for the MEA and VPSA plants (excluding conditioning) is 1.51 M£ and 1.24 M£, respectively. The total PEC for the MEA and VPSA plants (including conditioning) is 4.24M£ and 3.92 M£, respectively. CO_2 conditioning accounts for 64% (MEA) and 68% (VPSA) of the total PEC. In Section 5.3.2, the energy demand for the conditioning train significantly increases at low flowrates. Similarly, the cost of the equipment per mass of fluid process is significantly higher at low flowrates. The equipment cost breakdown and specific factors used in the calculation for each PEC is shown in Table 54 and Table 55 in Appendix C Chapter 10 Section 10.3. For the compressors, the cost is a function of the power requirement (kW) which is calculated in the conventional multistage compression model and depends on the flowrate of the CO_2 stream coming from the capture plant. All pieces of equipment are assumed to be made from stainless steel with a density of 7,500 kg/m, and all column walls are 2.5cm thick.

Despite the MEA plant consisting of more processing equipment, the overall capture plant cost is cheaper than the VPSA plant. The contributing factor for the VPSA case is the vacuum pumps. As such a large quantity of gas needs to be processed, the size and cost of the pumps increases. In total, there are 2 blowers (for the flue gas) and 4 vacuum pumps (for the blowdown and evacuation steps) assumed for the large-scale system.

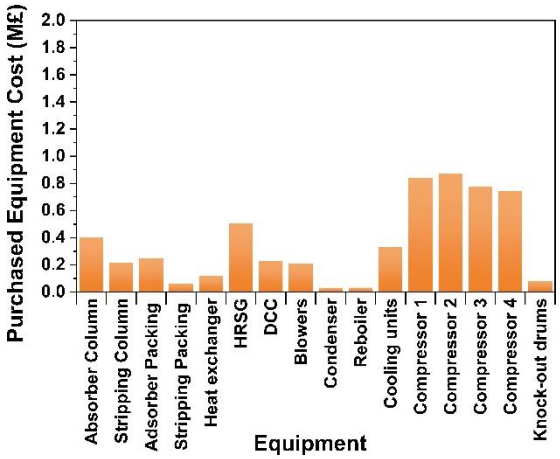

Figure 75: Purchased equipment cost for the MEA capture plant and conditioning train.

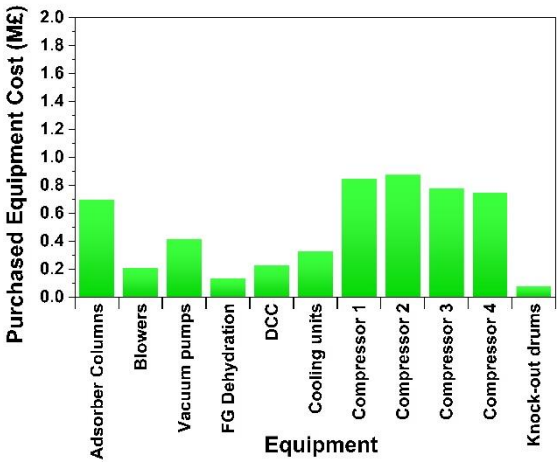

Figure 76: Purchased equipment cost for the VPSA capture plant and conditioning train.

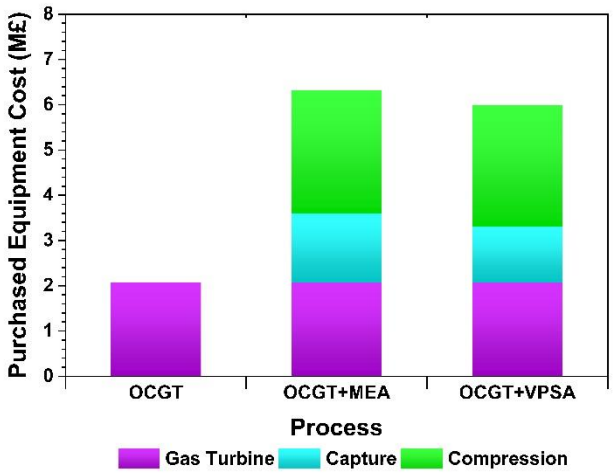

Figure 77: Purchased equipment cost breakdown for the OCGT, OCGT+MEA, and OCGT+VPSA plants.

6.2.Capital and operating costs

The calculation of the TCC requires the PEC for the main pieces of equipment. The CAPEX breakdown for the OCGT, MEA, and VPSA systems is shown in Table 43. Included in the MEA and VPSA plant costs are the costs associated with compressing and conditioning the CO_2 stream ready for pipeline transportation. The TCC for the OCGT is 6.53 M£, equating to 628.26 £/kW. This is within the range specified in the literature, see Chapter 2 Section 2.6, the TCC for OCGT's ranges between 532.5-719 £/kW for a 100 MWe plant [260]. Figure 78 shows the comparison between the OCGT, OCGT+MEA, and OCGT+VPSA plant costs, with and without CO_2 conditioning. Including CO_2 capture for small-scale OCGT's almost triples the initial capital investment. Although, half of the additional costs are associated with the conditioning train, therefore, these systems would benefit from sharing the conditioning load. Similarly, the technical evaluation in Chapter 5 Section 5.3 also showed these small-scale systems would benefit from sharing a conditioning and transportation network.

Table 43: CAPEX breakdown for the OCGT, MEA, and VPSA systems

CODE	CAPEX	Units	OCGT	MEA	VPSA
C1	Purchased Equipment Cost	M£	2.08	4.24	3.92
C2	Instrument cost	M£	1.04	2.49	2.21
C3	Direct equipment Cost	M£	3.12	6.72	6.13
C4	Indirect equipment Cost	M£	0.97	2.08	1.90
C5	Inside battery limit Investment	M£	4.09	8.81	8.03
C6	Offsite battery limit investment	M£	0.97	2.08	1.90
C7	Process Unit Investment	M£	5.05	10.89	9.93
C8	Engineering	M£	0.61	1.31	1.19
C9	Royalties	M£	0.29	0.62	0.56
C10	Process data book	M£	0.006	0.01	0.01
C11	Fixed Capital Cost	M£	5.95	12.82	11.68
C12	Initial feed stock	M£	0.002	0.00	0.00
C13	interest during construction	M£	0.42	0.90	0.82
C14	Start-up cost	M£	0.17	0.12	0.30
C15	Total Capital Cost	M£	6.53	13.84	12.80
C16	Working capital	M£	0.17	0.12	0.30
	TCC	**M£**	**6.53**	**13.84**	**12.80**

The OPEX for the OCGT, MEA, and VPSA plants is shown in Table 44. The calculation of VOM requires input data from the scaled process models. The fuel (natural gas) cost is the quantity of energy required per annum (kWh/yr) multiplied by the price of natural gas for UK businesses (0.033 £/kWh in March 2021 [363], also bearing in mind the thermal efficiency of the gas turbine. The electricity cost for the capture technologies is:

- **MEA** – The primary energy demand comes from the solvent regeneration. The baseload results highlighted in Chapter 4 Section 4.1.2 shows the specific energy demand is 1302.78 kWh_{th}/tCO_2. All of the solvent regeneration thermal energy is supplied through the HRSG unit. The only power demand for the MEA plant is the compression energy requirement which is 179.16 kWh/tCO_2.
- **VPSA** – The energy demand comes from the flue gas blower and vacuum pumps. The baseload results highlighted in Chapter 4 Section 4.2.2 shows the specific energy demand is 1275.00 kWh_e/tCO_2. The compression energy requirement is 186.39 kWh/tCO_2.

These values are used to calculate the annual electricity demand for each process, which is multiplied by the electricity price to give the cost. The water demand for the OCGT is set at 3 L/MWh [389] and for MEA it comes from the process model set at 300 L/h. The utilities prices are shown in Table 35 Chapter 3 Section 3.4.2.

Even though the MEA plant is supplied with thermal energy from the HRSG unit, it does not cover all of the plants power needs. The power requirement for the conditioning unit is much smaller in comparison to the capture plant, but this still reduces the overall power output of the plant from 10.4 MWe to 10.24 MWe.

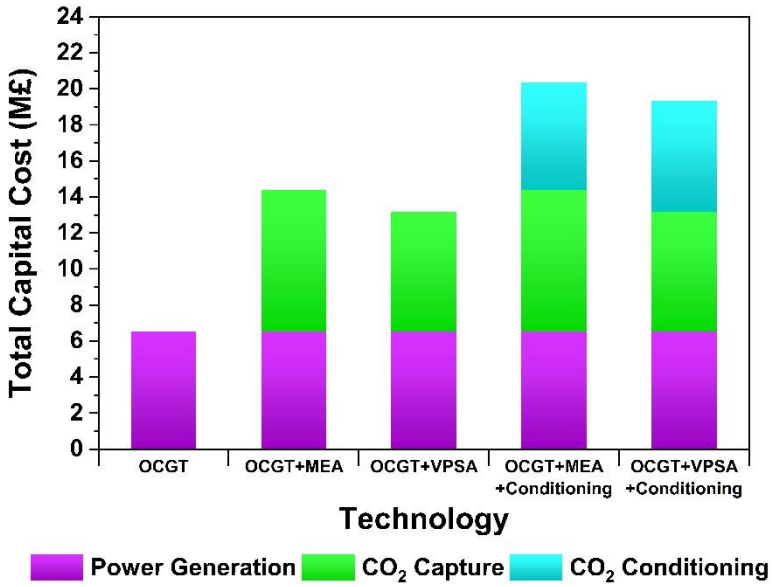

Figure 78: Total capital cost comparison for the OCGT, OCGT+MEA, and OCGT+VPSA plants, with and without CO_2 conditioning.

For the scaled MEA process the quantity of solvent required is 44841.6 kg/yr, which costs £4.5/L at 1.02 kg/L [366]. For the scale VPSA process the quantity of Zeolite 13X is 130998 kg/yr, which costs 1.5 £/kg [367]. It is assumed both capture materials requirement replacement each year, for simplification of the economic cash flows.

Table 44: OPEX breakdown for the OCGT, OCGT+MEA, and OCGT+VPSA systems

CODE	OPEX	Units	OCGT	MEA	VPSA
O1	Natural gas price	M£/yr	1.45	0.00	0.00
O2	Electricity price	M£/yr	0.00	0.29	2.46
O3	Steam cost	£/yr	0.00	0.00	0.00
O4	Water cost	£/yr	64.98	624.83	0.00
O5	Utilities	M£/yr	1.45	0.29	2.46
O6	Solvent/adsorbent	M£/yr	0.00	0.21	0.20
O7	Variable operations and maintenance	M£/yr	1.45	0.49	2.65
O8	Labour	M£/yr	0.20	0.20	0.20
O9	Maintenance	M£/yr	0.20	0.44	0.40
O10	Insurance	M£/yr	0.10	0.22	0.20
O11	Overhead	M£/yr	0.05	0.11	0.10
O12	Financing working capital	M£/yr	0.02	0.01	0.03
O13	Fixed operations and maintenance	M£/yr	0.57	0.97	0.92
	VOM	**M£/yr**	**1.45**	**0.49**	**2.65**
	FOM	**M£/yr**	**0.57**	**0.97**	**0.92**

6.3. Levelised cost of electricity

The LCOE for the OCGT, OCGT+MEA, and OCGT+VPSA plants, is shown in Figure 79. Included in the graph is the cost without CO_2 conditioning, to highlight the effect the compression train has on the cost of power. The LCOE for the OCGT plant (189 £/MWh) is comparable to sources in the literature, LeighFisher [262] showed the LCOE ranges between 155-371 £/MWh for a 100 MWe plant, and BEIS [255] showed the LCOE ranges between 161-383 £/MWh for a 100 MWe plant. Including PCC for OCGT's drastically increases the LCOE. For an OCGT with MEA CO_2 capture (including conditioning, transport, and storage) the LCOE is 394 £/MWh. For an OCGT with VPSA CO_2 capture (including conditioning, transport, and storage) the LCOE is 588 £/MWh. Excluding the cost associated with CO_2 conditioning reduces the LCOE for the MEA and VPSA cases to 289 and 420 £/MWh. These scenarios do not include a carbon price, the effect of carbon price is shown in Table 45.

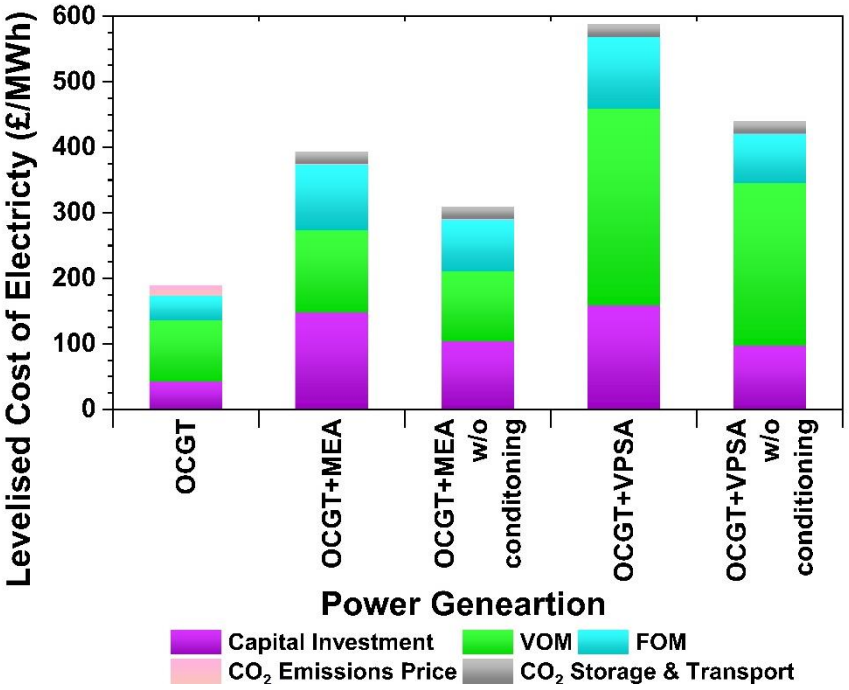

Figure 79: Levelised cost of electricity for the OCGT, OCGT+MEA, and OCGT+VPSA plants. Also included is the cost without CO_2 conditioning.

Table 45 highlights the KPI's for OCGT with and without CO_2 capture, and without the costs associated with transportation and storage. Using VPSA to capture CO_2 results in slightly lower CAPEX and higher OPEX compared to the MEA case. Overall, the CCA (including carbon price) for OCGT+MEA is 300 £/tCO_2 and for OCGT+VPSA it is 553£/tCO_2. Excluding conditioning from the calculations (CCC rather than CCA), the OCGT+MEA case costs 150 £/tCO_2 and the OCGT+VPSA case cost 321 £/tCO_2. The energy penalty for including carbon capture is 1.5% for the MEA case and 12.85% for the VPSA. Utilising waste heat from the exhaust to supply steam for solvent regeneration significantly improves the performance and cost effectiveness of the MEA capture plant. Without utilising the waste heat the capture costs are similar to VPSA, but this study shows the CCC is almost halved through incorporating thermal integration. Also, as there is no loss in power output of the OCGT, the specific (per MWh) costs are decreased, making MEA capture the more cost-effective option for small-scale

OCGT operation. Chapter 7 Section 7.2 compares the performance of the systems investigated in this study to other power generation sources and CCS technologies.

Table 45: Key performance indicators for open-cycle gas turbines with and without CO_2 capture

KPI	OCGT	OCGT+MEA	OCGT +VPSA	Difference (%)
Net power output (MWe)	10.40	10.24	9.06	-11.52
CO_2 capture rate (%)	-	92.48	97.07	4.96
CO_2 emitted (tCO_2/yr)	12374.86	981.33	362.58	-63.05
CO_2 captured (tCO_2/yr)	-	11444.27	12012.27	4.96
CAPEX (M£)	6.53	20.38	19.33	-5.13
OPEX (M£/yr)	2.00	3.47	5.58	60.80
LCOE (£/MWh)	173.04	392.31	521.98	33.05
LCOE including CP (£/MWh)	189.21	393.70	522.49	32.71
CCA (£/tCO_2)	-	322.02	483.83	50.25
CCA Including CP (£/tCO_2)	-	300.32	462.13	53.88
CCC (£/tCO_2)	-	171.24	336.52	96.53
CCC Including CP (£/tCO_2)	-	149.54	314.82	110.54
CO_2 energy penalty (%)	-	1.50	12.85	756.17

6.4. Conclusion

Herein, the process and economic models described in Chapter 3 Section 0 are used to highlight the cost of incorporating PCC onto OCGT power plants. In order to calculate the LCOE, the scaled process design parameters (shown in Chapter 3 Section 3.3.4) are used to calculate the cost of the major pieces of equipment. The PEC breakdown showed the cost for the MEA capture plant is 1.51 M£ and for the VPSA capture plant it is 1.24 M£, which in both cases is significantly lower than the cost for the conditioning plants. This provides additional reasoning behind the conclusion made in Chapter 5 Section 5.5, which highlighted the importance of sharing the conditioning load with neighbouring emitters.

The LCOE for only the OCGT plant (173-189 £/MWh) is comparable to sources in the literature (155-383 £/MWh), showing the accuracy of the economic model. When including CO_2 capture into OCGT plants, the LCOE drastically increases but depends on the level of detail included in the cost model. The results show the LCOE for all the scenarios with and without the cost associated with conditioning, transportation, storage, and carbon price. The LCOE for the MEA case ranges between 290-394 £/MWh, which is lower than the VPSA case which ranges between 420-588 £/MWh. The MEA case utilises waste heat from the gas turbine exhaust to provide the thermal energy for solvent regeneration, whereas this thermal integration is not applicable to the VPSA case which has an electrical energy demand.

Chapter 7 : Techno-economic comparison

This chapter combines the information from Chapter 4, Chapter 5, and Chapter 6; to techno-economically analyse Flexible-PCC for OCGT's. Included in this chapter the technical and economic assessment of the two PCC technologies to capture CO_2 from a small-scale OCGT. The challenges of combing OCGT's and PCC is discussed, and recommendations for future work is given.

7.1. Technical Assessment

The technical comparison focuses on the ability of each of the technologies to handle the highly transient flue gas production. The scaled process parameters are based on validated process models; these are non-optimised parameters but represent real operational data from pilot-studies. Both capture technologies can have higher CO_2 recovery rates; as mentioned in Section 2.5, there is often an artificial constraint attached to capture plants (typically 90-95%) when in reality they can potentially achieve 100% capture. The figures presented are guidelines on the techno-economics of OCGT+CCS, based on our current level of understanding of these types of generators with CCS. The KPI's for the OCGT, OCGT+MEA, and OCGT+VPSA plants is shown in Table 46. The results use a constant carbon price of 21.7 £/tCO_2, and both capture plants incorporate CO_2 conditioning. The capture rate, energy demand, and quantity of CO_2 capture per operation is shown Figure 80. The difference in carbon footprint is due to higher CO_2 capture rate in the scaled VPSA process model. If the capture rate is constant the carbon footprint for the MEA case will be lower than the VPSA case due to the higher net power output. Despite the lower specific energy demands shown in the literature, scaled VPSA systems required more beds for continuous operation and to handle the large flue gas size. Therefore, more blowers and vacuum pumps are required to ensure the necessary pressure profiles in the adsorption columns. It is worth noting, as the VPSA unit has a flue gas dehydration unit and the purity of the end product is on a dry basis, whereas the MEA unit contains moisture and is on a dry basis.

Table 46: KPI's for OCGT+CCS

Case	Net Power Output (MWe)	CO_2 Captured (kg/h)	Capture Rate (%)	Carbon Footprint (kg CO_2/MWh)	Cost of Avoidance (£/tCO_2)	LCOE (£/MWh)
OCGT	10.40	0	0	733.61	0	187.79
OCGT+MEA	10.24	7.36	92.34	62.91	324.00	405.09
OCGT+VPSA	9.06	8.00	97.07	26.67	485.09	516.96

The dynamic models enabled the analysis of different flexible operating scenarios. Both capture technologies processed the same transient flue gas and were capable of removing CO_2 with no major loss in efficiency or effectiveness. For both capture technologies there is a small drop in purity during transient operation. Similarly, the specific energy demand increases in most of the flexible response scenarios, expect for the MEA Scenario C case. This scenario included the manipulation of the reboiler steam flowrate to minimise the energy demand during low load operation. No specific energy related operating scenarios were included for the VPSA case, as they have not been proven to work in practice. There is a large literature base surrounding Flexible-PCC using MEA (hence flexible operating scenarios could be included), but to the authors knowledge there are no studies in the literature for Flexible-PCC using VPSA. Therefore, future work should investigate VPSA for Flexible-PCC at pilot-scale, implementing specific low load energy minimisation scenarios. A potential option is changing the adsorption step durations, to hold more CO_2 in the column during low load periods, and then alter the step duration once back at full load operation. Determining these alterations and implementing them into the process models only at low loads is time-consuming, and beyond the scope of this techno-economic analysis.

The CO_2 conditioning study investigated the effects of varying the input CO_2 source, starting pressure, and throughput flowrate. The study highlighted the energy saving potential of utilising sub-critical liquefaction instead of a final compression stage. A major influence on the conditioning system is the throughput flowrate, it is almost 60% more energy intensive to condition CO_2 from small-scale 10.4 MWe OCGT plant than it is for a 478 MWe OCGT plant. The dynamic models for the conditioning systems included specific control strategies (surge and variable frequency drive control systems), which showed the effectiveness of the systems to handle transient CO_2 production. At low load operation, the specific energy demand increases <10%. However, the energy demand for the conditioning system is significantly lower than the energy demand for the capture plants, see Table 41 Chapter 5 Section 5.2. Therefore, potential energy savings from implementing optimised conditioning strategies is over-shadowed by the large parasitic energy consumption of capturing CO_2 from the low CO_2 concentration flue gas.

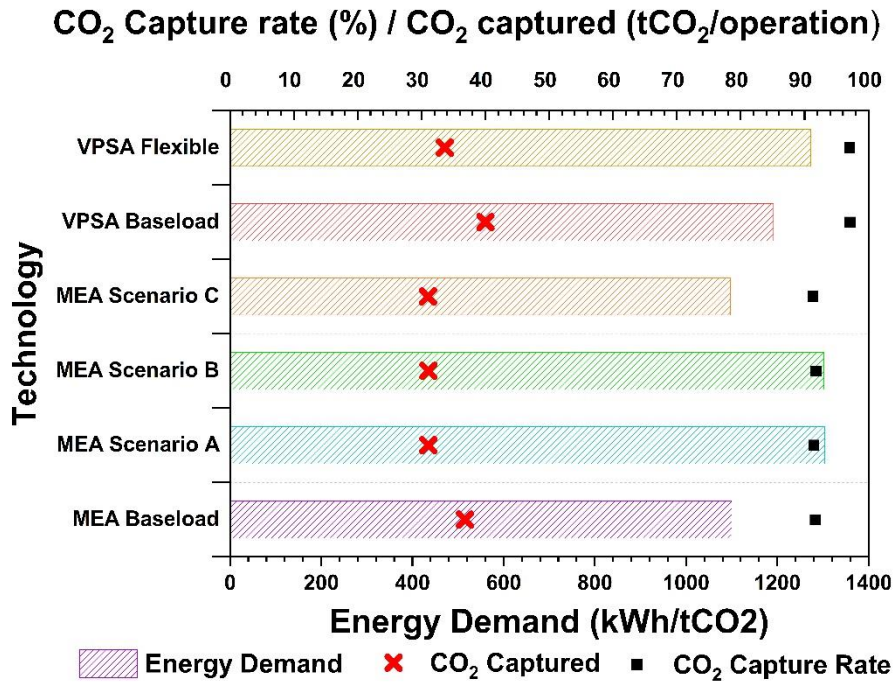

Figure 80: Technical comparison of MEA and VPSA CO_2 capture

7.2. Economic Assessment

The economic model shown in Chapter 3 Section 3.4 is used to calculate the cost of including PCC for OCGT power generation. The CAPEX for either capture technology is similar, 13.84 M£ for MEA and 12.80 M£ for VPSA, but MEA is more capital intensive due to the HRSG unit used to generate the steam necessary for solvent regeneration. However, the HRSG unit reduces the operating cost for the MEA plant, 2.58 M£ (VOM) and 0.86 M£ (FOM) for MEA and 2.65 M£ (VOM) and 0.91 M£ (FOM) for VPSA. Overall, the MEA capture plant is the economic option in terms of LCOE and CCA, see Table 46. Figure 81 shows the comparison between the LCOE and net power export for the systems evaluated in this study (OCGT, OCGT+MEA, and OCGT+VPSA), compared to other power generation sources that include CCS. The LCOE (including CP) for OCGT+CCS (394-588 £/MWh) is much higher compared to the other power sources (70.7-204.3 £/MWh). However, the net power output in this study (10 MWe) is almost 36 times smaller than smallest plant analysed in BEIS [261] (356 MWe). Per MWh the TCC, FOM, and VOM are all higher in the OCGT cases compared to the other power generators.

However, Figure 82 highlights the comparison between the CCA for the systems evaluated in this study (OCGT, OCGT+MEA, and OCGT+VPSA), compared to other power generation sources that include CCS from BEIS [261]. In the BEIS study, the plant availability or capacity factor was set at 100% (8760 hours), in this study the capacity factor is 17.12% (1500 hours). The CCA is much higher for the OCGT+CCS cases compared to the other power sources, except BECCS. Without the carbon price included BECCS costs 617.20-660.70 £/tCO_2, whereas OCGT+CCS costs 322-575 £/tCO_2 When including the carbon price, BECCS costs 524.10-571.70 £/tCO_2, whereas OCGT+CCS costs 300-553 £/tCO_2. The larger drop in CCA when including a carbon price for BECCS is due to the quantity of CO_2 captured and the variable carbon price used (21.6-223.3 £/tonne CO_2). The CCA for OCGT+CCS is comparable to BECCS sources, and both will be crucial in achieving net-zero emissions targets. Highlighting, these small gas-fuelled dispatchable generators may need government assistance to stay competitive in a future low/zero-carbon energy system.

Danaci et al. [390] highlights the economies of scale for PCC and showed at smaller flue gas flowrates and low CO_2 feed concentrations, the cost of capture drastically increases. Hence, the LCOE, CCA, and CCC values for the systems investigated in this study are so high. This poses a real problem for future energy systems. As we move towards a net-zero power grid, these small dispatchable generators that provide security of supply and system inertia will also require CO_2 capture; however, the cost to do so is much higher than other power sources due to:

- **Economies of scale** – the power generation plant, capture plant and conditioning train suffer from their relatively small size.
- **Low-capacity factor** – as less CO_2 is captured due to less active annual operating hours, the overall cost per ton of CO_2 captured is much higher.

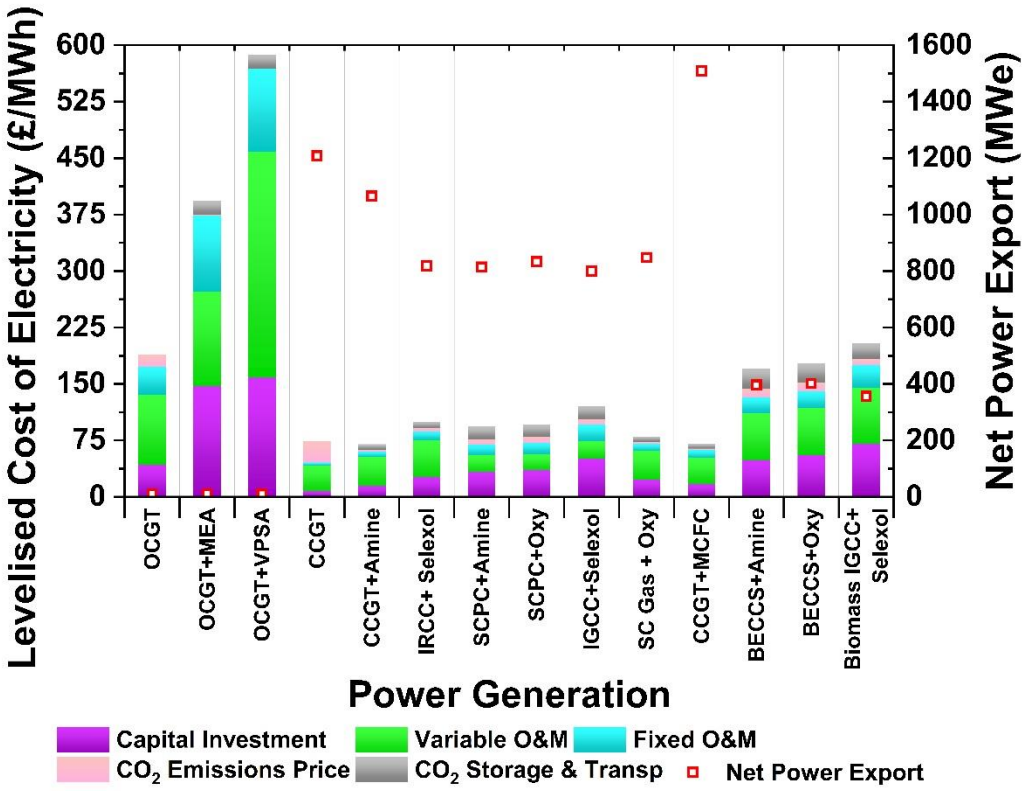

Figure 81: LCOE and net power export comparison between OCGT+CCS (this studies work) and other power generation sources that include CO_2 capture from BEIS [261].

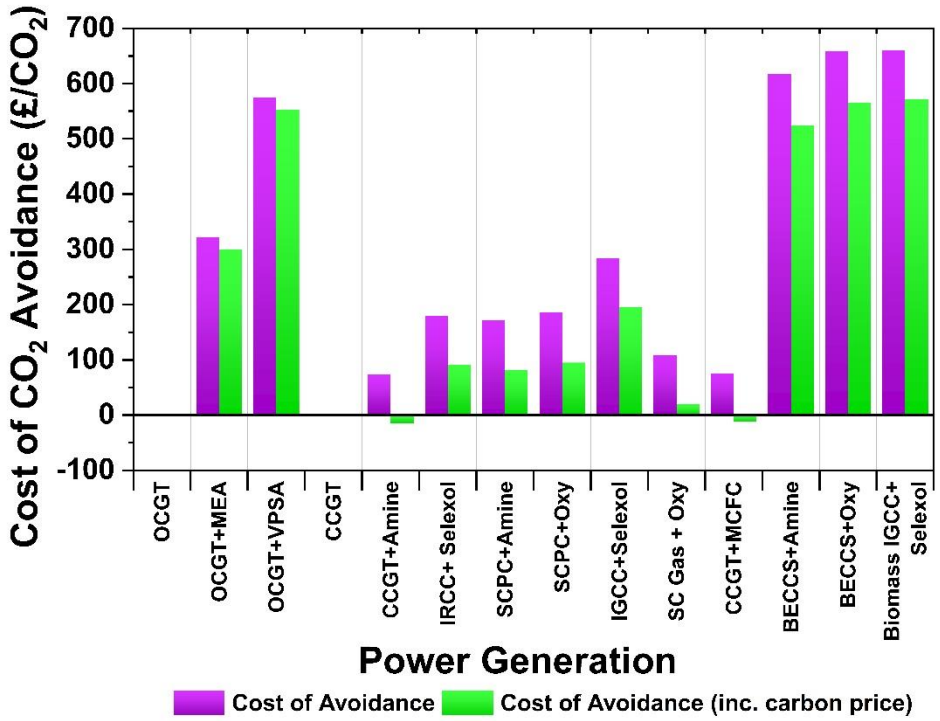

Figure 82: Cost of avoidance comparison between OCGT+CCS (this studies work) and other power generation sources that include CO_2 capture from BEIS [261].

In the literature review, alternate dispatchable technologies include H_2 gas turbines and energy storage. Figure 83 compares the LCOE of OCGTs with varying degrees of H_2 firing and four different types of energy storage, against the OCGT+CCS case studies investigated in this study. The OCGT with H_2 is from ETN [273], where the power output is 20 MWe, double the size of the OCGT in this study. Also, as there is no capture plant, the low-firing scenarios will have high CO2 emissions. The OCGT with 100% H_2 firing (and no plant based emissions) will cost 165.8 £/MWh (converted from 191 €/MWh), which is significantly lower than the range (394-588 £/MWh) for natural gas fired OCGT+CCS. Therefore, in a future energy system where carbon neutral H_2 is cheap and readily available, H_2 turbines could be used for dispatchable thermal power generation if the carbon price is high enough. The energy storage technologies shown in Figure 83, from BEIS [276], range between 93-251 £/MWh. Again, this is lower than OCGT+CCS. Hence, with the expected increase in low-carbon H_2 and cheap renewable power, OCGT+CCS will not be cost-effective solutions for dispatchable power generation.

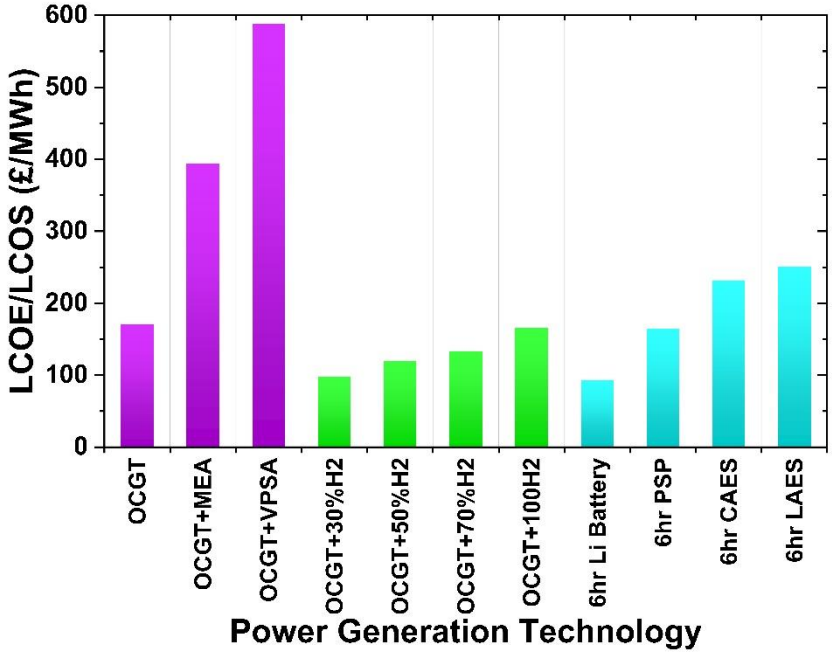

Figure 83: Levelised cost of energy and storage comparison between OCGT with CCS, OCGT with H_2 firing, and energy storage using Li batteries, pumped storage plant (PSP), compressed air energy storage (CAES), and liquid-air energy storage (LAES).

As part of the economic assessment, a sensitivity analysis on capacity factor was performed. Figure 84 shows the LCOE for the OCGT, OCGT+MEA, and OCGT+VPSA systems at 250-8,000 total annual operating hours, i.e., at different capacity factors. There is a drastic increase in cost at <2000 hours. From the BMRS data analysed in Chapter 3 Section 3.2, OCGT's between 2016-2019 had an average annual operating time of 250 hours. This pushes the LCOE up to almost £1955/MWh, which is not competitive in any electricity market.

At 2000 annual operating hours, considered a peak capacity factor value [262, 255], the LCOE for an unabated OCGT is 153 £/MWh (170 £/MWh with CP). Including MEA or VPSA CO_2 capture increases the LCOE to 327 £/MWh (329 £/MWh with CP) and 518 £/MWh (519 £MWh), respectively. At 8760 hours (100% capacity factor) the LCOE for an unabated OCGT is 108 £/MWh (124 £/MWh with CP). Including MEA or VPSA CO_2 capture increases the LCOE to 177 £/MWh (179 £/MWh with CP) and 357 £/MWh (358 £MWh with CP), respectively. At higher capacity factors the cost of including CO_2 capture decreases. Interestingly, as the capacity factor increases more CO_2 is produced annually, therefore, it should become more costly due to the carbon price. However, the curves never cross, i.e., the carbon price is not high enough to counteract the cost of capture. Figure 85 shows the effect annual operating hours has on the CCA, it follows an identical profile as the LCOE and shows the rate at which the costs increase as the plant operates less. At full capacity these generators are comparable to other low carbon (Figure 81) or dispatchable (Figure 83) power sources. Highlighting the significant issues with low-capacity factor, even large scale systems would be economically unfeasible due to this specific mode of operation.

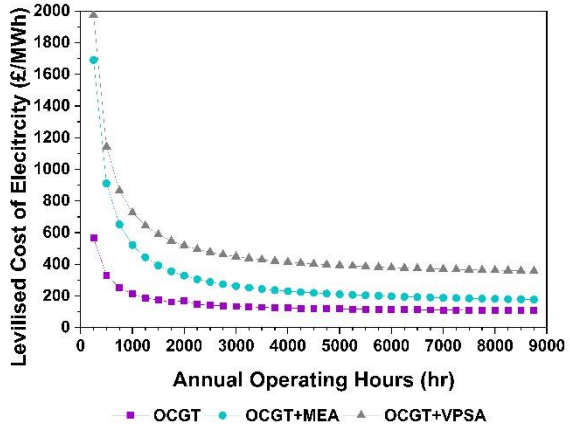

Figure 84: Levelised cost of electricity for OCGT, OCGT+MEA, OCGT+VPSA plants, at different total annual operating hours

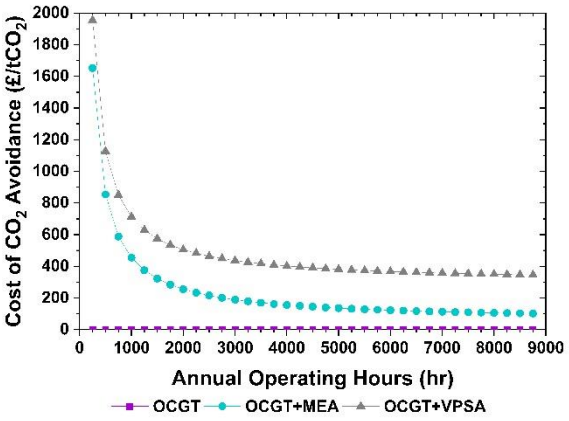

Figure 85: Cost of avoidance for OCGT, OCGT+MEA, OCGT+VPSA plants, at different total annual operating hours

Contour plots showing the relationship between the LCOE, CP and CF are shown in Figure 86, for the OCGT (A), OCGT+MEA (B), and OCGT+VPSA (C) plants. The LCOE range for the OCGT scenario is much lower than the OCGT+CCS scenarios; however, the OCGT plant is much more susceptible to carbon price. The OCGT+CCS technologies are mainly influenced by the total annual operating hours, hence the stacked colour flow. For each system, the highest LCOE range is <1000 annual operating hours. This is an issue for OCGTs as they usually operate within this region. The results show the OCGT+MEA becomes the economically favourable option, compared to an unabated OCGT, when the carbon price is >125 £/tCO_2 and when the annual operating time is >6000 hours.

Figure 87 and Figure 88 shows the influence carbon price has on the LCOE for all three processes. For CO_2 capture to be worthwhile economically for small-scale OCGT's, the carbon price would need to be >323 £/tCO_2 at 1500 annual operating hours, and >102 £/tCO_2 at 8760 annual operating hours. This break-even price is also known as the cost of CO_2 avoidance or CCA. Figure 87 shows at 1500 annual operating hours, the VPSA case is not feasible. At 100% capacity factor, VPSA becomes feasible if the carbon price is >346 £/tCO_2.

The cost of capturing and compressing CO_2 from small-scale power sources is extremely high, even if those sized plants operated continuously (100% CF) they're still more costly in terms of LCOE and CCA compared to other low-carbon sources. Therefore, the compression demand needs to be shared with other neighbouring CO_2 emitters in cluster systems, or the CO_2 needs to be directly utilised on site. Investigating CO_2 utilisation for OCGT+CCS is beyond the scope of this project; however, the ready might find these sources helpful in understand the Carbon Dioxide Utilisation (CDU) [391, 392].

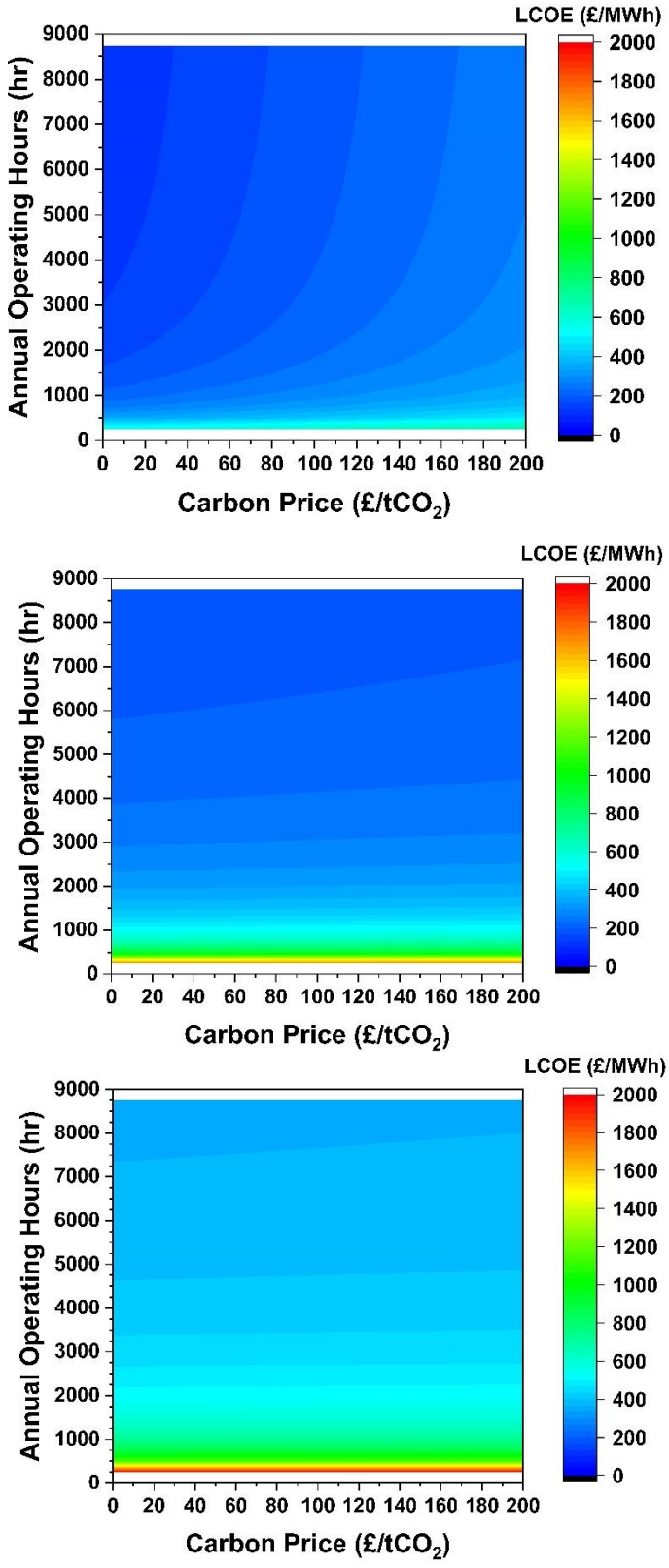

Figure 86: Contour plot showing the levelised cost of electricity at different carbon prices and annual operating hours for the OCGT (A), OCGT+MEA (B), and OCGT+VPSA (C) scenarios.

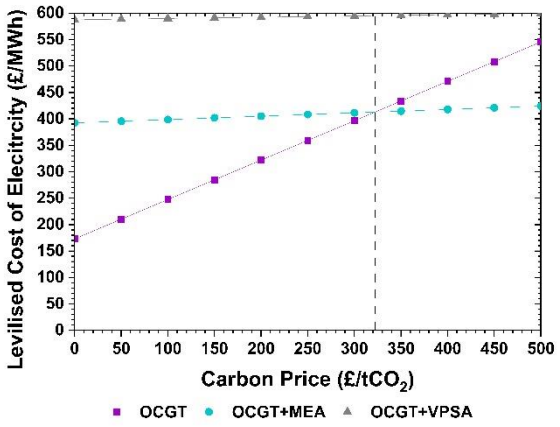

Figure 87: Levelised cost of electricity at different carbon prices for OCGT, OCGT+MEA, OCGT+VPSA plants. All scenarios are based on 1,500 annual operating hours.

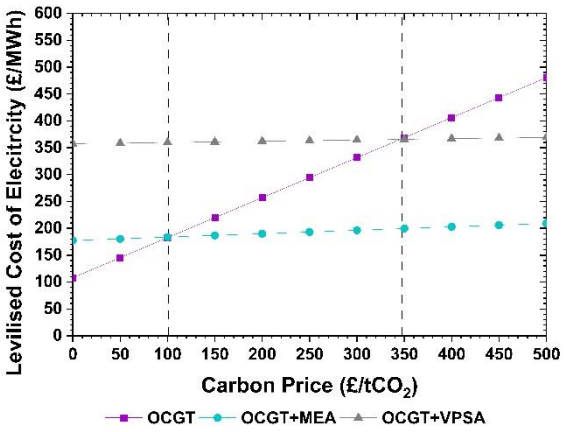

Figure 88: Levelised cost of electricity at different carbon prices for OCGT, OCGT+MEA, OCGT+VPSA plants. All scenarios are based on 8,760 annual operating hours.

7.3. Conclusion

Incorporating amine-absorption using MEA or vacuum-pressure swing adsorption using Zeolite 13X for CO_2 capture on OCGT's is feasible. These capture systems can withstand the transient operation and have shown minimal fluctuations in key performance indicators during flexible operation. Both capture systems can capture >90% of the CO_2 in the flue gas. Reducing the carbon footprint from 744 $kgCO_2$/MWh to 63.86 $kgCO_2$/MWh and 26.67 $kgCO_2$/MWh, for the MEA and VPSA options respectively. However, this reduces the net power output from 10.4 MWe, to 10.24 MWe and 9.06 MWe, for the MEA and VPSA options respectively.

The economics of including MEA and VPSA CO_2 capture onto an OCGT power plant is shown in Chapter 6. This chapter compares the performance of these systems, to other low-carbon power generation sources. The LCOE for OCGT+CCS (394-588 £/MWh) is much higher than the sources investigated in BEIS [261] (70.7-204.3 £/MWh). This is due to low capacity factor for OCGT plants. A sensitivity analysis on CF showed the extreme increase in cost between 250-2000 annual operating hours. This is problematic as OCGTs typically operate in this window. A similar trend is observed for the CCA, reaching 1,955 £/tCO_2 at 250 annual operating hours (CF=2.85%). Another factor influencing the LCOE is the CP, which has more of an effect on the unabated power plant than it does the MEA and VPSA cases. At 1,500 annual operating hours (typical of OCGTs) the carbon price would need to be >323 £/tCO_2 to break-even. Overall, the two main factors effecting OCGT+CCS is the economies of scale (small plant size) and the low-capacity factor (only used for peak demand). The results show the CCA is comparable to BECCS. Therefore, much like the subsidies provided to BECCS for negative emissions, government aid might also be required for these dispatchable generators in order to provide system security whilst also being low carbon. Other technologies such as 100% H_2 fired gas turbines and energy storage are cheaper options for low-carbon dispatchable power, however, in future energy markets a diverse portfolio of options is a necessity for security of supply. Therefore, future work should focus on alternative capture technologies that can help reduce the capture cost for these small-scale system.

Chapter 8 : Conclusion

Since the industrial revolution, global cumulative GHG emissions have adversely impacted our climate. Countries across the world have set up plans to limit emissions through the use of climate agreements, and much more work is required to ensure the global temperature rise is limited to 1.5℃. In the UK, Carbon Budgets are used to highlight the work required to meet the targets set out in the Climate Change Act 2008. Initially, the target was to achieve 80% reduction in GHG's by 2050 compared to 1990 levels. The last update (Sixth Carbon Budget) set guidelines to meet Net Zero by 2050 at the latest. Although there are a range of GHG's, CO_2 is considered the baseline. Impressive improvements have been made to the energy sector, and research is being carried out on possible routes to decarbonise industry, business, transport, and household emissions. As we move towards a sustainable low-carbon future, energy systems are expected to become more reliant on renewable power generation as this is the most effective way to limit CO_2 emissions. However, to counteract the intermittency issues of renewables, there needs to be an increase in responsive and dispatchable energy sources.

Currently, balancing capacity is achieved through 'peaking plants', which become active during periods of imbalance between supply and demand. A range of options are available for quick and responsive balancing capacity: gas turbines, diesel generators, interconnectors, energy storage and demand side response technologies. In the UK, OCGTs are used due to their short start-up times, ramping capabilities, reliability, low emissions (compared to other fossil sources), frequency response capabilities, and operational flexibility. However, as they usually combust natural gas, they produce CO_2 (1-5 vol.%). Therefore, in future low-carbon energy systems these generators will require CCS in order to meet Net Zero emissions targets.

This project investigates CO_2 capture for highly transient OCGTs. To not impede the normal operation of the gas turbine, and for retrofitting capabilities, post-combustion capture is the chosen capture technology. Within the literature, the focus for flexible-PCC has been on large-scale systems (>300MW). This project techno-economically compares different CO_2 capture technologies for small-scale OCGT (1-50 MWe) power generation. The literature review in Chapter 2 highlights applicable and commercially available capture methods (absorption, adsorption, membranes separation, chemical looping combustion, calcium looping, and fuel cell integration). The capture technologies chosen for further investigation in this study are:

- **Amine-absorption:** Liquid phase chemisorption using 30 wt.% Monoethanolamine (MEA) as this is considered the benchmark PCC technology.
- **Zeolite-adsorption:** Vacuum-pressure swing adsorption using Zeolite 13X is close to commercialisation for PCC, and has already been proven for natural gas sweetening and steam methane reforming.

To ensure a fair comparison between the capture models, a black box analysis is created that includes CO_2 conditioning ready for pipeline transportation. Therefore, the capture models used the same flue gas source, and produce a CO_2 stream at the same pressure, temperature, and concentration. An overview of the study is illustrated in Figure 36.

As OCGT capacity is expected to increase and given the role these quick-response generators will play in small-scale decentralised power production, this project analysed real-world OCGT operation. Data from the BMRS and industrial suppliers showed OCGTs typically come on during the evenings and in the colder winter months, i.e., corresponding to peak demand on the system. On average, OCGTs operate for 5-hours and can ramp to different power outputs within the same operating cycle. This data is translated into flue gas flowrate profiles and used as model inputs into the scaled dynamic CO_2 capture process models. The flexible scenario is used for both capture cases. The power output (directly

proportional to flue gas flowrate) is ramped to 70% load and 50% load. Each new power output is maintained for 1 hour or 2 operating periods (30 minutes each).

The study is split into two main sections: technical comparison of capture and conditioning technologies, and an economic evaluation including a comparison to other low-carbon power sources. The mathematical models, assumptions, pilot-scale case studies (for validation) and scaled system designs are shown in Chapter 3 Sections 3.3.1.1 (MEA), 3.3.2.1 (VPSA), and 3.3.3.1 (CO_2 conditioning). The process models for MEA-PCC, CO_2 conditioning are developed in gPROMS gCCS. Whereas the process model for VPSA-PCC is developed in gPROMS Process. For CO_2 compression, conventional multistage compression is compared against compression and sub-critical liquefaction. All technologies are validated (to prove model fidelity) prior to process scale-up.

The MEA process model was validated against pilot-scale data from Tait et al. [65]. The pilot study investigated flexible gas-PCC and included data for the start-up and shutdown procedures. The system used 30.16 wt.% MEA to capture CO_2 from 120.50 NM^3/h flue gas representative of a gas turbine (4.27 vol.%). Both the start-up and shutdown simulations showed good agreement with pilot-scale data. The VPSA process model was validated against pilot-scale data from Krishnamurthy et al. [115]. The pilot study processed 1000 SLPM of flue gas containing 15 mol.% CO_2. As adsorption systems are inherently dynamic, the system flowrates, compositions, pressures, and temperatures are all compared to highlight the accuracy of the process and isotherm models. All of which showed good agreement with the pilot results.

The compression models were validated against results from IEAGHG [60] for case B0 (conventional multistage centrifugal compression) and case D2c (multistage compression and sub-critical liquefaction). The study investigated the effects of different CO_2 sources, flowrates, and initial pressures, providing an insight into the link between CO_2 capture and transportation. Interestingly, the results showed the increased power demand when processing smaller flowrates. For example, when conditioning a CO_2 stream from an MEA capture plant there is a 40% decrease in specific power demand when going from 100 kg/s to 1 kg/s. Therefore, in future cluster networks, small-scale CO_2 capture plants will benefit from sharing the conditioning load with neighbouring CO_2 emitters. The conditioning models also include surge and variable frequency drive controllers, enabling the simulation of realistic dynamic operation. Assuming any fluctuation in power demand proportionally effects the flue gas flowrate, which in turn proportionally effects the output CO_2 flowrate, the dynamic simulations showed the conditioning systems are capable of processing transient input flow. However, the specific energy demand increases at low load periods. Overall, the energy demand for the conditioning system is much lower than the capture system, therefore, it is important to analyse the flexible operation of the capture system.

Both capture processes are scaled to handle 33.8 kg/s of flue gas from a 10.4 MWe OCGT with 4.27 vol.% CO_2 (6.78 wt.% or 4.42 mol.%), whilst maintaining similar KPIs to the respective pilot studies. The comparison between the scaled (Baseload) and pilot results are shown in Table 47. The MEA scale up is very accurate, due to the simplified process design and availability of in depth flexible operation data. The scaled VPSA model overestimates the capture rate and specific energy demand, highlighting the issues with scaling adsorption systems and proves the need for larger demonstration scale studies for VPSA. Both capture systems adequately handled transient flue gas through-put. Flexible-VPSA showed the best performance in terms of capture rate and purity, only deviating <2% compared to the Baseload flexible results. Flexible-MEA showed the better performance in terms of energy demand, although this is only the case during the flexible operating scenarios specifically designed the minimise the energy demand at low-load. No specific flexible operating scenario for energy minimisation was included for VPSA, due to the lack of pilot-scale data available to verify the accuracy of such operating procedures.

Table 47: Comparison between pilot-scale data and scaled process model results for the MEA and VPSA capture systems.

	MEA Pilot [65]	**MEA Scaled**	**Deviation (%)**	**VPSA Pilot** [115]	**VPSA Scaled**	**Deviation (%)**
CO_2 Capture Rate (%)	87.70	89.35	1.85	85.40	97.07	12.02
Specific Energy Demand (kWh/tCO_2)	1100.00	1099.93	-0.01	510.50	1191.72	57.16

The second aspect of this study uses the economic model described in Chapter 3 Section 3.4 to calculate the cost of OCGT+CCS. The results (shown in Chapter 6), show the LCOE for an OCGT plant is 173 £/MWh (189 £/MWh with the carbon price set at 21.7 £/tCO_2), comparable to other sources in the literature (155-383 £/MWh). Including MEA or VPSA (with conditioning and a carbon price included) increases the LCOE to 394 £/MWh and 588 £/MWh, respectively. The much higher cost of electricity is a result of the low capacity factor. A sensitivity analysis showed the drastic increase in cost below 2000 annual operating hours, which goes as high as 1950 £/MWh at 250 annual operating hours. The higher capital cost of the capture equipment and high operating cost for the capture plant energy demands, are exacerbated by the small annual operating hours. The cost of CO_2 capture is 322 £/tCO_2 and 575 £/tCO_2, for the MEA and VPSA scenarios, respectively. This is much higher than other low-carbon power generation sources but is comparable to BECCS (524.10-660.70£/tCO_2). Therefore, as OCGT's will be a vital role in balancing future energy systems and providing system security and flexibility, these small-scale dispatchable generators will require similar carbon subsidies as BECCS. The results also showed small-scale OCGT with PCC has a more comparable CCA at maximum operating time (102 £/tCO_2). Therefore, future work should investigate economies of scale specifically for 1-100 MWe OCGT's, to identify the size at which these generators become comparable to other power generation sources.

8.1. Key findings

This project has produced several peer-reviewed articles listed on Page V. The key highlights from each of the papers is summarised in Table 48.

Table 48: Peer-reviewed paper highlights

Title	**Key highlights**
"Evaluating the Transient Operation of PCC for Fast Response Gas Turbines in a Future Low-Carbon Energy System" Status: published [393]	• Transient MEA capture from and OCGT power plant. • Rapid load transitioning is beneficial in maintaining a high time-average capture rate. • Energy penalty during low load operation needs to be minimised.
"Transient CO_2 capture for open-cycle gas turbines in future energy systems" Status: published [394]	• Dynamic MEA-based PCC model validated against dynamic experimental data. • Realistic OCGT load changes based off operational data from BMRS. • Rapid load change is beneficial in delivering time-averaged capture rate >90%. • No negative energy related issues to highly transient PCC operation.

"Evaluating the flexible operation of vacuum-pressure swing adsorption for CO_2 capture from modern gas turbines" Status: published [395]	• Flexible-VPSA process model is developed in gPROMS Process. • Model fidelity is high with the capture rate within the errors bounds of the pilot results. • Flexible-VPSA is technically feasible, with minimal deviation in KPI's.
"Flexible CO_2 capture for open-cycle gas turbines via vacuum-pressure swing adsorption: A model-based assessment" Status: published [396]	• Flexible-VPSA model developed and validated against pilot scale data. • Concerns with process scaling VPSA systems are shown and explained. • Minimal deviation in CO_2 recovery rate or product purity during transient operation • Increased specific energy demand is attributed to the lower mass of CO_2 captured. • Flexible-VPSA is comparable to Flexible-MEA CO_2 capture.
"Compression system power requirements for various CO_2 sources and transportation options" Status: published [397]	• Different CO_2 sources are compression to pipeline transportation. • Three end-point moisture specifications were chosen: 20 ppm, 300 ppm, and 600 ppm. • Initial stream pressure has a greater effect than moisture control level. • The specific energy demand is high due to the low flowrate of CO_2 processed.
"Linking CO_2 capture and pipeline transportation: sensitivity analysis and dynamic study of the compression train" Status: published [398]	• A range of CO_2 sources are conditioned to different end-point specifications. • Subcritical liquefaction is 14-19% more effective than conventional compression. • Small scale capture streams (<10kg/s) suffer from higher specific energy demands. • Transient operation increases specific energy demand for both conditioning routes.
"Cost of CO_2 capture for small-scale dispatchable power generation." Status: published [399]	• An economic model is used to calculate the LCOE for a dispatchable OCGT with and without MEA CO_2 capture. • The LCOE for a 10 MWe OCGT increases when using MEA based CCS.
"Cost of small-scale CO_2 capture: technology comparison and case study evaluation." Status: out for review	• An economic model is used to calculate the LCOE for a dispatchable OCGT with and without CCS. • Dispatchable OCGTs required alternative CO_2 capture technologies, such as a MCFC, SOFC, or CLC.

8.2.Project limitations

Although the analysis uses real world OCGT data, detailed process modelling, and EPRI Class II economic modelling, there are several limitations that need to be discussed. Firstly, the lack of demonstration scale data means the scaled process models' fidelities are difficult to ascertain. Especially for the VPSA system as the size of the pilot study is much smaller than the MEA case. Also, there are no flexibility studies for VPSA, whereas there are several for MEA based CO_2 capture from flue gas. The scale-up operation highlighted issues with adsorption systems, as you increase the flue gas flowrate more processing units are required. Adding to the complexity of the process model, and as the models solve the PDAE's simultaneously not sequentially, this increases the processing time and frequency of failure. For Flexible-MEA several pilot-scale studies have investigated different operating strategies to optimise flexible operation. For both capture systems, demonstration scale studies are required to highlight the fidelity of scaled models and analyse various operating scenarios.

The scaled designs produce adequate KPIs similar to the pilot studies. To improve the design, the processes can be optimised specifically for OCGTs, i.e., the inclusion of heat integration using Pinch analysis; as the exhaust from an OCGT does not pass through a HRSG, there is a large amount of waste heat available to be used in a district heating network or CO_2 capture plant. Due to time-constraints this could not be included in the study.

The economic model developed in this study can be improved by attaining purchased equipment costs directly from the OEM's/supplier. To further improve the models, a more in-depth pre-FEED design of the power generation, CO_2 capture, and CO_2 conditioning plants is required. However, due to time-constraints, software limitations, and lack of available information, they could not be implemented in this economic evaluation.

When comparing the various low-carbon power generation sources it is important to consider the size of the plant, capacity factor, and type of operation. It is difficult to compare larger PCC systems to OCGT+CCS as they operate in different markets with different costs of electricity. Currently, the size of the OCGT investigated in this study does not require CO_2 abatement or even to be CCS capable. However, future projections indicate a growth in OCGT plants and with the new targets of Net Zero further research is required in the feasibility of OCGT+CCS. Therefore, alternative capture technologies need to be investigated. Within the literature review (Chapter 2) two technologies are particularly interesting: molten carbonate fuel cells and chemical looping. Both technologies have the potential to generate heat or power alongside capturing CO_2 from flue gas, although both technologies are in the early stages of development. Unfortunately, due to time constraints only MEA absorption and Zeolite 13X adsorption could be investigated within this study. Future work should focus on utilising alternative technologies that have the potential to offset the high operating costs for small-scale dispatchable OCGTs.

This study focuses on gas turbines that combust natural gas. However, there are various other fuels that could be used, all of which produce a flue gas with varying CO_2 concentrations. There is also the potential for using Hydrogen, with several gas turbine manufacturers currently developing turbines that can be powered with H_2. As no nation wants to be dependent on natural gas, future system could be dominated by H_2 and biofuels. Therefore, alternative fuel sources need to be investigated for OCGTs, looking at the affect the fuel source has on both the power generation and the capture plant.

8.3. Future research

The techno-economic evaluation of OCGT+CCS presented in this thesis has shown the high cost for decarbonising dispatchable power. Within this study, two CO_2 capture technologies have been compared against one another: chemical absorption using 30 wt.% MEA and vacuum-pressure swing adsorption using Zeolite 13X. The research and results have shown that several important aspects of OCGT+CCS still need to be answered/investigated.

Secondly, both capture plants were evaluated using the same flexible operating scenario. The analysis of the BMRS data showed the rapid increase in OCGT generation over the past few years; hence, we could see more dramatic shifts in power output. Therefore, future work should analyse the effect of different flue gas profiles (directly related to the OCGT power output). Also, there should be scenarios specifically designed to minimise the parasitic energy demand during low-load operation. For the MEA case study, specific operating scenarios have been investigated to reduce the reboiler energy demand. For the VPSA case study, no operating scenarios exist within the literature to minimise the specific energy demand during low-load operation; potential options include modifying the scheduling unit at low load to reduce the time it takes adsorb and desorb CO_2. Thus, reducing the pumping power required. This can be achieved through implementing mathematical code within the scheduling unit and by incorporating model predictive control. In order to optimise the entire process, future work should look at developing and combing power generation, CO_2 capture, and CO_2 conditioning models. Enabling global optimisation to find the best operating case to minimise the energy demand and the subsequent operating cost.

One of the limitations of the project is that only two CO_2 capture technologies were investigated. Future work should compare MEA and VPSA CO_2 capture to other technologies that offer additional power/heat generation alongside CO_2 capture, for example: chemical looping, calcium looping, molten-carbonate fuel cells and solid-oxide fuel cells. The revenue from providing additional power/heat can offset the high operating costs for the capture and conditioning plants. Furthermore, a comparison between other fuels, i.e., using H_2 instead of CH_4, will help highlight the best location to put CCS in the power generation train. As the majority of H_2 is produce through fossil fuels, it is important to investigate whether blue hydrogen (H_2+CCS) or OCGT+CCS is more cost effective. This will highlight the best available technologies for small-scale gas turbines to remain competitive in the capacity market.

Finally, this project investigated CCS for a 10 MWe OCGT power plant, but power demand curves at different flowrates in the conditioning train (highlighted in Chapter 5 Section 5.3) showed the drastic increase in power at low flowrates. Therefore, future work should investigate economies of scale for 1-100 MWe OCGT's, to identify the minimum size of plant required for these generators to become comparable with other dispatchable power sources. This information can be used alongside the LCOE and CCA sensitivity analysis shown in Figure 87 and Figure 88; thus, highlighting the minimum size and operating hours for a low-carbon small-scale gas turbine to remain competitive in future energy markets.

Chapter 9 : References

[1] CCC, “UK climate action following the Paris Agreement,” Committee on Climate Change, London, 2016.

[2] IPCC, “Climate Change 2014: Mitigation of Climate Change. Contribution of Working Group III to the Fifth Assessment Report of the Intergovernmental Panel on Climate Change,” Cambridge University Press, Cambridge, United Kingdom and New York, USA, 2014.

[3] IEA, “Net Zero by 2050 - A Roadmap for the Global Energy Sector,” IEA Publications, 2021.

[4] CCC, “Meeting Carbon Budgets: Closing the Policy Gap,” Committee on Climate Change, London, 2017.

[5] CCC, “The Sixth Carbon Budget - The UK's path to Net Zero,” Committee on Climate Changed, 2020.

[6] Global CCS Institute, “Global Status of CCS: 2020,” Global CCS Institute, Australia, 2020.

[7] Global CCS Institute, “The Carbon Capture and Storage Readiness Index 2018: Is the world ready for carbon capture and storage?,” Global CCS Institute, 2018.

[8] HM Government, “The Ten Point Plan for a Green Industrial Revolution,” Crown copyright, 2020.

[9] BEIS, “The Carbon Capture and Storage Infrastructure Fund,” Crown copyright, 2021.

[10] BEIS, “2020 UK greenhouse gas emissions, provisional figures,” Crown copyright, London, 2021.

[11] BEIS, “Provisional UK greenhouse gas emissions national statistics 2020,” 25 March 2021. [Online]. Available: https://www.gov.uk/government/statistics/provisional-uk-greenhouse-gas-emissions-national-statistics-2020. [Accessed 20 October 2021].

[12] Global CCS Institute, “The Value of Carbon Capture and Storage (CCS),” Global CCS Institute, 2020.

[13] Parsons Brinckerhoff, “Technical Assessment of the Operation of Coal & Gas Fired Plants,” Department of Energy and Climate Change, London, 2014.

[14] J. Stern, “The Future of Gas in Decarbonising European Energy Markets: the need for a new approach,” Oxford Institute for Energy Studies, Oxford, 2017.

[15] G. Wynn and D. Schlissel, “Electricity-Grid Transition in the U.K.: As Coal-Fired Generation Recedes, Renewables and Reliable Generation Can Fill the Gap,” The Institute for Energy Economics and Financial Analysis, Cleveland, 2017.

[16] Energy UK, “Pathways for the GB Electricity Sector to 2030,” Energy UK, London, 2016.

[17] C. F. Heuberger and N. Mac Dowell, “Real-World Challenges with a Rapid Transition to 100% Renewable Power System,” *Joule,* vol. 2, no. 3, pp. 367-370, 2018.

[18] DECC, “Overarching National Policy Statement for Energy (EN-1),” Crown copyright, 2011.

[19] BEIS, “Decarbonisation Readiness: Joint call for evidence on the expansion of the 2009 Carbon Capture Readiness requirements,” Crown copyright , 2021.

[20] BEIS, “Carbon Capture, Usage and Storage: An Update on the Dispatchable Power Agreement Business Model,” Crown copyright, 2021.

[21] I. Staffell and S. Pfenninger, “The increasing impact of weather on electricity supply and demand,” *Energy,* vol. 145, pp. 65-78, 2018.

[22] M. A. Gonzalez-Salazar, T. Kirsten and L. Prchlik, “Review of the operational flexibility and emissions of gas- and coal-fired power plants in a future with growing renewables,” *Renewable and Sustainable Energy Reviews,* vol. 82, no. 1, pp. 1497-1513, 2018.

[23] IEA, Energy Technology Perspectives 2014: Harnessing Electricity's Potential, Paris: International Energy Agency, 2014.

[24] A. G. Memon, R. A. Memon, K. Harijan and M. A. Uqaili, “Thermo-environmental analysis of an open cycle gas turbine power plant with regression modeling and optimization,” *Journal of the Energy Institute,* vol. 87, pp. 81-88, 2014.

[25] Pöyry, “COST OF NEW ENTRANT PEAKING PLANT AND COMBINED CYCLE PLANT IN I-SEM,” Pöyry Management Consulting (UK) Ltd, 2018.

[26] R. Lee, S. Homan, N. M. Dowell and S. Brown, “A closed-loop analysis of grid scale battery systems providing frequency response and reserve services in a variable inertia grid,” *Applied Energy,* vol. 236, pp. 961-972, 2019.

[27] M. Dreidy, H. Mokhlis and S. Mekhilef, “Inertia response and frequency control techniques for renewable energy sources: A review,” *Renewable and Sustainable Energy Reviews,* vol. 69, pp. 144-155, 2017.

[28] S. Homan, N. Mac Dowell and S. Brown, “Grid frequency volatility in future low inertia scenarios: Challenges and mitigation options,” *Applied Energy,* vol. 290, p. 116723, 2021.

[29] T. C. Lieuwen and V. Yang, Gas Turbine Emissions, Cambridge: Cambridge University Press, 2013.

[30] A. Yamasaki, “An Overview of CO2 Mitigation Options for Global Warming - Emphasizing CO2 Sequestration Options,” *Journal of Chemical Engineering of Japan,* vol. 36, no. 4, pp. 361-375, 2003.

[31] W. P. Jones and R. P. Lindstedt, “Global reaction schemes for hydrocarbon combustion,” *Combustion and Flame*, vol. 73, no. 3, pp. 233-249, 1988.

[32] A. Razak, Industrial Gas Turbines: Performance and Operability, Cambridge: Woodhead Publishing Limited, 2007.

[33] M. M. Schorr and J. Chalfin, “Gas Turbine NOx Emissions Approaching Zero - Is it Worth the Price?,” GE Power Generation, Schenectady, New York, 1999.

[34] R. Pavri and G. D. Moore, “Gas Turbine Emissions and Control GER-4211,” GE Power Systems, 2001.

[35] T. Lecomte, J. F. F. d. l. Fuente, F. Neuwahl, M. Canova, A. Pinasseau, I. Jankov, T. B. S. Roudier and L. D. Sancho, “Best Available Techniques (BAT) Reference Document for Large Combustion Plants,” European Commission, 2017.

[36] Environment Agency, “Pollution inventory reporting – combustion activities guidance note,” Environment Agency, Bristol, England, 2013.

[37] U. Desideri, “Fundamentals of gas turbine cycles: thermodynamics, efficiency and specific power,” in *Modern Gas Turbine Systems*, P. Jansohn, Ed., Cambridge, Woodhead Publishing Limited, 2013, pp. 44-85.

[38] K. Abudu, U. Igie, I. Roumeliotis and R. Hamilton, “Impact of gas turbine flexibility improvements on combined cycle gas turbine performance,” *Applied Thermal Engineering*, vol. 189, p. 116703, 2021.

[39] P. Jansohn, Modern gas turbine systems, Philadelphia, USA: Woodhead Publishing Limited, 2013.

[40] MHPS, “Gas Turbines H-25 Series,” 2019. [Online]. Available: https://www.mhps.com/products/gasturbines/lineup/h25/index.html. [Accessed 20 April 2019].

[41] GE, “TM2500 POWER PLANTS,” General Electric Power , 2019.

[42] Siemens, “Gas Turbine Portfolio Brochure,” Siemens, Munich, 2019.

[43] Solar Turbines, “Product Handbook for Power Generation,” Solar Turbines, 2019.

[44] M. Bui, C. S. Adjiman, A. Bardow, E. J. Anthony, A. Boston, S. Brown, P. S. Fennell, S. Fuss, A. Galindo, L. A. Hackett, J. P. Hallett, H. J. Harzog, G. Jackson, J. Kemper, S. Krevor, G. C. Maitland, M. Matuszewski, I. S. Metcalfe, C. Petit, G. Puxty, J. Reimer, D. Reiner, E. Rubin, S. Scott, N. Shah, B. Smit, J. P. Trusler, P. Webley, J. Wilcox and N. Mac Dowell, “Carbon capture and storage (CCS): the way forward,” *Energy & Environmental Science*, vol. 11, no. 5, pp. 1062-1176, 2018.

[45] D. Kearns, H. Liu and C. Consoli, “Technology Readiness and Costs of CCS,” Global CCS Institute, 2021.

[46] N. Mirza and D. Kearns, “State of the Art: CCS Technologies,” Global CCS Institute , 2022.

[47] IEA, “Energy Technology Perspectives 2020: Special Report on Carbon Capture Utilisation and Storage,” IEA Publications, France, 2020.

[48] P. Brandl, M. Bui, J. P. Hallett and N. M. Dowell, “Beyond 90% capture: Possible, but at what cost?,” *International Journal of Greenhouse Gas Control,* vol. 105, p. 103239, 2021.

[49] Y. Wang, L. Zhaoa, A. Otto, M. Robinius and D. Stolten, “A Review of Post-combustion CO2 Capture Technologies from Coal-fired Power Plants,” *Energy Procedia,* vol. 114, pp. 650-665, 2017.

[50] A. Adamu, F. Russo-Abegão and K. Boodhoo, “Process intensification technologies for CO2 capture and conversion – a review,” *BMC Chemical Engineering,* vol. 2, no. 2, 2020.

[51] C. Chao, Y. Deng, R. Dewil, J. Baeyens and X. Fan, “Post-combustion carbon capture,” *Renewable and Sustainable Energy Reviews,* vol. 138, p. 110490, 2021.

[52] M. K. Mondal, H. K. Balsora and P. iVarshney, “Progress and trends in CO2 capture/separation technologies: A review,” *Energy,* vol. 46, no. 1, pp. 431-441, 2012.

[53] J. Singh and D. W. Dhar, “Overview of Carbon Capture Technology: Microalgal Biorefinery Concept and State-of-the-Art,” *Frontiers in Marine Science,* vol. 6, no. 29, 2019.

[54] C. Font-Palma, D. Cann and C. Udemu, “Review of Cryogenic Carbon Capture Innovations and Their Potential Applications,” *Journal of Carbon Research,* vol. 7, no. 3, p. 58, 2021.

[55] N. Mac Dowell, N. Florin, A. Buchard, J. Hallett, A. Galindo, G. Jackson, C. S. Adjiman, C. K. Williams, N. Shahb and P. Fennell, “An overview of CO2 capture technologies,” *Energy & Environmental Science,* vol. 3, no. 11, pp. 1645-1669, 2010.

[56] B. Lv, B. Guo, Z. Zhou and G. Jing, “Mechanisms of CO2 Capture into Monoethanolamine Solution with Different CO2 Loading during the Absorption/Desorption Processes,” *Environmental Science & Technology,* vol. 49, no. 17, pp. 10728-10735, 2015.

[57] T. A. Adams II, Y. K. Salkuyeh and J. Nease, “Processes and simulations for solvent-based CO2 capture and syngas cleanup,” in *Reactor and Process Design in Sustainable Energy Technology*, F. Shi, Ed., Oxford, Elsevier, 2014, pp. 164-229.

[58] S. A. Freeman, R. Dugas, D. H. V. Wagener, T. Nguyen and G. T. Rochelle, “Carbon dioxide capture with concentrated, aqueous piperazine,” *International Journal of Greenhouse Gas Control,* vol. 4, no. 2, pp. 119-124, 2010.

[59] G. Rochelle, E. Chen, S. Freeman, D. V. Wagener, Q. Xu and A. Voice, “Aqueous piperazine as the new standard for CO2 capture technology,” *Chemical Engineering Journal,* vol. 171, no. 3, pp. 725-733, 2011.

[60] IEAGHG, “Rotating equipment for carbon dioxide capture and storage,” 2011.

[61] X. Liu, Y. Huang, Y. Zhao, R. Gani, X. Zhang and S. Zhang, "Ionic Liquid Design and Process Simulation for Decarbonization of Shale Gas," *Industrial & Engineering Chemistry Research,* vol. 55, no. 20, pp. 5931-5944, 2016.

[62] S. Zeng, X. Zhang, L. Bai, X. Zhang, H. Wang, J. Wang, D. Bao, M. Li, X. Liu and S. Zhang, "Ionic-Liquid-Based CO2 Capture Systems: Structure, Interaction and Process," *Chemical Reviews,* vol. 117, pp. 9625-9673, 2017.

[63] M. E. Boot-Handford, C. Abanades, E. J. Anthony, M. J. Blunt, S. Brandani, N. M. Dowell, J. R. Fernandez, M. Ferrari, R. Gross, J. P. Hallet, R. S. Haszeldine, P. Heptonstall, A. Lyngfelt, Z. Makuch, E. Mangano, R. Porter, M. Pourkashanian, G. Rochelle, N. Shah, J. Yao and P. S. Fennel, "Carbon capture and storage update," *Energy & Environmental Science,* vol. 7, pp. 130-189, 2014.

[64] P. Tait, B. Buschle, K. Milkowski, M. Akram, M. Pourkashanian and M. Lucquiaud, "Flexible operation of post-combustion CO2 capture at pilot scale with demonstration of capture-efficiency control using online solvent measurements," *International Journal of Greenhouse Gas Control,* vol. 71, pp. 253-277, 2018.

[65] P. Tait, B. Buschle, I. Ausner, P. Valluri, M. Wehrli and M. Lucquiaud, "A pilot-scale study of dynamic response scenarios for the flexible operation of post-combustion CO2 capture," *International Journal of Greenhouse Gas Control,* vol. 48, no. 2, pp. 216-233, 2016.

[66] R. M. Montañés, N. E. Flø and L. O. Nord, "Experimental results of transient testing at the amine plant at Technology Centre Mongstad: Open-loop responses and performance of decentralized control structures for load changes," *International Journal of Greenhouse Gas Control,* vol. 73, pp. 42-59, 2018.

[67] N. Mac Dowell and N. Shah, "Optimisation of Post-combustion CO2 Capture for Flexible Operation," *Energy Procedia,* vol. 63, pp. 1525-1535, 2014.

[68] M. Bui, N. E. Flø, T. Cazenove and N. Mac Dowell, "Demonstrating flexible operation of the Technology Centre Mongstad (TCM) CO2 capture plant," *International Journal of Greenhouse Gas Control,* vol. 93, p. 102879, 2020.

[69] A. Mangiaracina, L. Zangrilli, L. Robinson, H. M. Kvamsdal and P. V. Os, "OCTAVIUS: Evaluation of Flexibility and operability of Amine Based Post Combustion CO2 Capture at the Brindisi Pilot Plant," *Energy Procedia,* vol. 63, pp. 1617-1636, 2014.

[70] M. Bui, I. Gunawan, V. Verheyen, P. Feron and E. Meuleman, "Flexible operation of CSIRO's post-combustion CO2 capture pilot plant at the AGL Loy Yang power station," *International Journal of Greenhouse Gas Control,* vol. 48, no. 2, pp. 188-203, 2016.

[71] A. Kohl and R. Nielsen, Gas Purification, 5th ed., Houston, Texas: Gulf Publishing Company, 1997.

[72] M. Gatti, E. Martelli, F. Marechal and S. Consonni, “Review, modeling, Heat Integration, and improved schemes of Rectisol®-based processes for CO2 capture,” *Applied Thermal Engineering,* vol. 70, no. 2, pp. 1123-1140, 2014.

[73] Z. Kapetaki, P. Brandani, S. Brandani and H. Ahn, “Process simulation of a dual-stage Selexol process for 95% carbon capture efficiency at an integrated gasification combined cycle power plant,” *International Journal of Greenhouse Gas Control,* vol. 39, pp. 17-26, 2015.

[74] H. C., “5 - Gasification process technology,” in *Advances in Clean Hydrocarbon Fuel Processing*, Woodhead Publishing Series in Energy, 2011, pp. 155-185.

[75] S. A. Rackley, “Chapter 6 - Absorption Capture Systems,” in *Carbon Capture and Storage*, Elsevier, 2010, pp. 103-131.

[76] J.-R. Li, Y. Ma, M. C. McCarthy, J. Sculley, J. Yu, H.-K. Jeong, P. B. Balbuena and H.-C. Zhou, “Carbon dioxide capture-related gas adsorption and separation in metal-organic frameworks,” *Coordination Chemistry Reviews,* vol. 225, no. 16, pp. 1791-1823, 2011.

[77] A. Samanta, A. Zhao, G. K. H. Shimizu, P. Sarkar and R. Gupta, “Post-Combustion CO2 Capture Using Solid Sorbents: A Review,” *Industrial & Engineering Chemistry Research,* vol. 51, pp. 1438-1463, 2012.

[78] R. Ben-Mansour, M. A. Habib, O. E. Bamidele, M. Basha, N. A. A. Qasem, A. Peedikakkal, T. Laoui and M. Ali, “Carbon capture by physical adsorption: Materials, experimental investigations and numerical modeling and simulations – A review,” *Applied Energy,* vol. 161, pp. 225-255, 2016.

[79] C. Song, Q. Liu, N. Ji, S. Deng, J. Zhao, Y. Li, Y. Song and H. Li, “Alternative pathways for efficient CO2 capture by hybrid processes—A review,” *Renewable and Sustainable Energy Reviews,* vol. 82, no. 1, pp. 215-231, 2018.

[80] A. Ntiamoah, J. Ling, P. Xiao, P. A. Webley and Y. Zhai, “CO2 Capture by Temperature Swing Adsorption: Use of Hot CO2-Rich Gas for Regeneration,” *Industrial & Engineering Chemistry Research,* vol. 55, no. 3, pp. 703-713, 2016.

[81] R. Zhao, L. Zhao, S. Deng, C. Song, J. He, Y. Shao and S. Li, “A comparative study on CO2 capture performance of vacuum-pressure swing adsorption and pressure-temperature swing adsorption based on carbon pump cycle,” *Energy,* vol. 137, pp. 495-509, 2017.

[82] S. E. Zanco, L. Joss, M. Hefti, M. Gazzani and M. Mazzotti, “Addressing the criticalities for the deployment of adsorption-based CO2 capture processes,” *Energy Procedia,* vol. 114, pp. 2497-2505, 2017.

[83] M. Clausse, J. Merel and F. Meunier, “Numerical parametric study on CO2 capture by indirect thermal swing adsorption,” *International Journal of Greenhouse Gas Control,* vol. 5, no. 5, pp. 1206-1213, 2011.

[84] L. Wang, Z. Liu, P. Li, J. Yu and A. E. Rodrigues, "Experimental and modelling investigation on post-combustion carbon dioxide capture using zeolite 13X-APG by hybrid VTSA process," *Chemical Engineering Journal,* vol. 197, pp. 151-161, 2012.

[85] L. Wang, Y. Yang, W. Shen, X. Kong, P. Li, J. Yu and A. E. Rodrigues, "CO2 Capture from Flue Gas in an Existing Coal-Fired Power Plant by Two Successive Pilot-Scale VPSA Units," *Industrial & Engineering Chemistry Research,* vol. 52, no. 23, pp. 7947-7955, 2013.

[86] P. G. Ghougassian, J. A. P. Lopez, V. I. Manousiouthakis and P. Smirniotis, "CO2capturing from power plant flue gases: Energetic comparison ofamine absorption with MgO based, heat integrated,pressure–temperature-swing adsorption," *International Journal of Greenhouse Gas Control,* vol. 22, pp. 256-271, 2014.

[87] J. Y. Lai, L. H. Ngu and S. S. Hashim, "A review of CO2 adsorbents performance for different carbon capture technology processes conditions," *Greenhouse Gases: Science and Technology,* vol. 11, no. 5, pp. 1076-1117, 2021.

[88] S. Choi, J. Drese and C. Jones, "Adsorbent Materials for Carbon Dioxide Capture from Large Anthropogenic Point Sources," *ChemSusChem,* vol. 2, no. 9, pp. 796-854, 2009.

[89] P. J. E. Harlick and A. Sayari, "Applications of Pore-Expanded Mesoporous Silicas. 3. Triamine Silane Grafting for Enhanced CO2 Adsorption," *Peter J. E. Harlick, and Abdelhamid Sayari*,* vol. 45, no. 9, pp. 3248-3255, 2006.

[90] F. Rezaei, A. A. Rownaghi, S. Monjezi, R. P. Lively and C. W. Jones, "SOx/NOx Removal from Flue Gas Streams by Solid Adsorbents: A Review of Current Challenges and Future Directions," *Energy Fuels,* vol. 29, no. 9, pp. 5467-5486, 2015.

[91] W. Zhao, Z. Zhang, Z. Li and N. Cai, "Continuous CO2 Capture in Dual Fluidized Beds Using Silica Supported Amine," *Energy Procedia,* vol. 37, pp. 89-98, 2013.

[92] T. Pröll, G. Schöny, G. Sprachmann and H. Hofbauer, "Introduction and evaluation of a double loop staged fluidized bed system for post-combustion CO2 capture using solid sorbents in a continuous temperature swing adsorption process," *Chemical Engineering Science,* vol. 141, pp. 166-174, 2016.

[93] G. Schöny, F. Dietrich, J. Fuchs, T. Pröll and H. Hofbauer, "A multi-stage fluidized bed system for continuous CO2 capture by means of temperature swing adsorption – First results from bench scale experiments," *Powder Technology,* vol. 316, pp. 519-527, 2017.

[94] K. Kim, Y.-K. Park, J. Park, E. Jung, H. Seo, H. Kim and K. S. Lee, "Performance Comparison of Moving and Fluidized bed Sorption Systems for an Energy-efficient Solid Sorbent-Based Carbon Capture Process," *Energy Procedia,* vol. 63, pp. 1151-1161, 2014.

[95] C. A. Grande, H. Kvamsdal, G. Mondino and R. Blom, "Development of Moving Bed Temperature Swing Adsorption (MBTSA) Process for Post-combustion CO2 Capture: Initial Benchmarking in a NGCC Context," *Energy Procedia,* vol. 114, pp. 2203-2210, 2017.

[96] G. Mondino, C. A. Grande, R. Blom and L. O. Nord, "Moving bed temperature swing adsorption for CO2 capture from a natural gas combined cycle power plant," *International Journal of Greenhouse Gas Control,* vol. 85, pp. 58-70, 2019.

[97] M. G. Plaza, S. García, F. Rubiera, J. J. Pis and C. Pevida, "Post-combustion CO2 capture with a commercial activated carbon: Comparison of different regeneration strategies," *Chemical Engineering Journal,* vol. 163, no. 1-2, pp. 41-47, 2010.

[98] R. Thiruvenkatachari, S. Su, X. X. Yu and J.-S. Bae, "Application of carbon fibre composites to CO2 capture from flue gas," *International Journal of Greenhouse Gas Control,* vol. 13, no. 1, pp. 191-200, 2013.

[99] S. Hosseini, I. Bayesti, E. Marahel, F. E. Babadi, L. C. Abdullah and T. S. Y. Choong, "Adsorption of carbon dioxide using activated carbon impregnated with Cu promoted by zinc," *Journal of the Taiwan Institute of Chemical Engineers,* vol. 52, pp. 109-117, 2015.

[100] T. L. Dantas, F. M. T. Luna, I. J. S. Jr., A. E. B. Torres, D. C. S. d. Azevedo, A. E. Rodrigues and R. F. P. M. Moreira, "Carbon dioxide–nitrogen separation through pressure swing adsorption," *Chemical Engineering Journal,* vol. 3, no. 172, pp. 698-704, 2011.

[101] M. Hefti, D. Marx, L. Joss and M. Mazzotti, "Adsorption equilibrium of binary mixtures of carbon dioxide and nitrogen on zeolites ZSM-5 and 13X," *Microporous and Mesoporous Materials,* vol. 215, pp. 215-228, 2015.

[102] J. A. Mason, K. Sumida, Z. R. Herm, R. Krishna and J. R. Long, "Evaluating metal–organic frameworks for post-combustion carbon dioxide capture via temperature swing adsorption," *Energy & Environemental Science,* vol. 4, no. 8, pp. 3030-3040, 2011.

[103] A. Nalaparaju, M. Khurana, S. Farooq, I. A. Karimi and J. W. Jiang, "CO2 capture in cation-exchanged metal–organic frameworks: Holistic modeling from molecular simulation to process optimization," *Chemical Engineering Science,* vol. 124, pp. 70-78, 2015.

[104] S. Xian, J. Peng, Z. Zhang, Q. Xi, H. Wang and Z. Li, "Highly enhanced and weakened adsorption properties of two MOFs by water vapor for separation of CO2/CH4 and CO2/N2 binary mixtures," *Chemical Engineering Journal,* vol. 270, pp. 385-392, 2015.

[105] N. Jiang, Y. Shen, B. Liu, D. Zhang, Z. Tang, G. Li and B. Fu, "CO2 capture from dry flue gas by means of VPSA, TSA and TVSA," *Journal of CO2Utilization,* vol. 35, pp. 153-168, 2020.

[106] H. Yang, S. Fan, X. Lang, Y. Wang and J. Nie, "Economic Comparison of Three Gas Separation Technologies for CO2 Capture from Power Plant Flue Gas," *Chinese Journal of Chemical Engineering,* vol. 19, no. 4, pp. 615-620, 2011.

[107] Z. Liu, L. Wang, X. Kong, P. Li, J. Yu and A. E. Rodrigues, "Onsite CO2 Capture from Flue Gas by an Adsorption Process in a Coal-Fired Power Plant," *Industrial and Engineering Chemistry Research,* vol. 51, pp. 7355-7363, 2012.

[108] C. Shen, Z. Liu, P. Li and J. Yu, "Two-Stage VPSA Process for CO2 Capture from Flue Gas Using Activated Carbon Beads," *Industrial & Engineering Chemistry Research,* vol. 51, no. 13, pp. 5011-5021, 2012.

[109] G. N. Nikolaidis, E. S. Kikkinides and M. C. Georgiadis, "Modelling and Optimization of Pressure Swing Adsorption (PSA) Processes for Post-combustion CO2 Capture from Flue Gas," in *Process Systems and Materials for CO2 Capture,* A. I. Papadopoulos and P. Seferlis, Eds., John Wiley & Sons Ltd, 2017, pp. 343-369.

[110] M. Luberti, G. D. Oreggioni and H. Ahn, "Design of a rapid vacuum pressure swing adsorption (RVPSA) process for post-combustion CO2 capture from a biomass-fuelled CHP plant," *Journal of Environmental Chemical Engineering,* vol. 5, no. 4, pp. 3973-3982, 2017.

[111] R. Xing, W. Shi, Y. Shen, B. Liu and D. Zhang, "Vacuum pressure swing adsorption system for N2/CO2 separation in consideration of unstable feed concentration," *Adsorption,* vol. 25, pp. 1147-1158, 2019.

[112] M. Ishibashi, H. Ota, N. Akutsu, S. Umeda, M. Tajika, J. Izumi, A. Yasutake, T. Kabata and Y. Kageyama, "Technology for removing carbon dioxide from power plant flue gas by the physical adsorption method," *Energy Conversion and Management,* vol. 37, no. 6-8, pp. 929-933, 1996.

[113] J. Merel, M. Clausse and F. Meunier, "Experimental Investigation on CO2 Post−Combustion Capture by Indirect Thermal Swing Adsorption Using 13X and 5A Zeolites," *Industrial & Engineering Chemistry Research,* vol. 47, no. 1, pp. 209-215, 2008.

[114] J. Zhang, P. A. Webley and P. Xiao, "Effect of process parameters on power requirements of vacuum swing adsorption technology for CO2 capture from flue gas," *Energy Conversion and Management,* vol. 49, no. 2, pp. 346-356, 2008.

[115] S. Krishnamurthy, V. R. Rao, S. Guntuka, P. Sharratt, R. Haghpanah, A. Rajendran, M. Amanullah, I. A. Karimi and S. Farooq, "CO2 Capture from Dry Flue Gas by Vacuum Swing Adsorption: A Pilot Plant Study," *AIChE Journal,* vol. 60, no. 5, pp. 1830-1842, 2014.

[116] D. Wawrzyńczak, I. Majchrzak-Kucęba, K. Srokosz, M. Kozak, W. Nowak, J. Zdeb, W. Smółka and A. Zajchowski, "The pilot dual-reflux vacuum pressure swing adsorption unit for CO2 capture from flue gas," *Separation and Purification Technology,* vol. 31, pp. 560-570, 2019.

[117] R. W. Baker and K. Lokhandwala, "Natural Gas Processing with Membranes: An Overview," *Industrial & Engineering Chemistry Research,* vol. 47, no. 7, pp. 2109-2121, 2008.

[118] A. Brunetti, F. Scura, G. Barbieri and E. Drioli, "Membrane technologies for CO2 separation," *Journal of Membrane Science,* vol. 359, pp. 115-125, 2010.

[119] R. Khalilpour, K. Mumford, H. Zhai, A. Abbas and G. Stevens, "Membrane-based carbon capture from flue gas: a review," *Journal of Cleaner Production,* vol. 103, pp. 286-300, 2015.

[120] J. Mustafa, M. Farhan and M. Hussain, "CO2 Separation from Flue Gases Using Different Types of Membranes," *Journal of Memberane Science & Technology,* vol. 6, no. 2, 2016.

[121] I. Sreedhar, R. Vaidhiswaran, B. M. Kamani and A. Venugopal, “Process and engineering trends in membrane based carbon capture,” *Renewable and Sustainable Energy Reviews,* Vols. 659-684, p. 68, 2017.

[122] D. Yang, Z. Wang,). Wang and). S. Wang, “Potential of Two-Stage Membrane System with Recycle Stream for CO2 Capture from Postcombustion Gas,” *Energy Fuels,* vol. 23, pp. 4755-4762, 2009.

[123] H. Lin and B. D. Freeman, “Gas solubility, diffusivity and permeability in poly(ethylene oxide),” *Journal of Membrane Science,* vol. 239, no. 1, pp. 105-117, 2004.

[124] W. Yave, A. Car, S. S. Funari, S. P. Nunes and K.-V. Peinemann, “CO2-Philic Polymer Membrane with Extremely High Separation,” *Macromolecules,* vol. 43, pp. 326-333, 2010.

[125] A. Car, Chrtomir, Stropnik, W. Yave and K.-V. Peinemann, “PEG modified poly(amide-b-ethylene oxide) membranes for CO2 separation,” *Journal of Membrane Science,* vol. 307, no. 1, pp. 88-95, 2008.

[126] H. Matsuyama, A. Terada, T. Nakagawara, Y. Kitamura and M. Teramoto, “Facilitated transport of CO2 through polyethylenimine/poly(vinyl alcohol) blend membrane,” *Journal of Membrane Science,* vol. 163, no. 2, pp. 221-227, 1999.

[127] L. Deng and M.-B. Hägg, “Swelling behavior and gas permeation performance of PVAm/PVA blend FSC membrane,” *Journal of Membrane Science,* vol. 363, no. 1-2, pp. 295-301, 2010.

[128] S. Yuan, Z. Wang, Z. Qiao, M. Wang, J. Wang and S. Wang, “Improvement of CO2/N2 separation characteristics of polyvinylamine by modifying with ethylenediamine,” *Journal of Membrane Science,* vol. 378, no. 1-2, pp. 425-437, 2011.

[129] R. Yegani, H. Hirozawa, M. Teramoto, H. Himei, O. Okada, T. Takigawa, N. Ohmura, N. Matsumiya and H. Matsuyama, “Selective separation of CO2 by using novel facilitated transport membrane at elevated temperatures and pressures,” *Journal of Membrane Science,* vol. 291, no. 1-2, pp. 157-164, 2007.

[130] H. Z. Chen, P. Li and T.-S. Chung, “PVDF/ionic liquid polymer blends with superior separation performance for removing CO2 from hydrogen and flue gas,” *International Journal of Hydrogen Energy,* vol. 37, no. 16, pp. 11796-11804, 2012.

[131] W. Yave, A. Car and K.-V. Peinemann, “Nanostructured membrane material designed for carbon dioxide separation,” *Journal of Membrane Science,* vol. 350, no. 1-2, pp. 124-129, 2010.

[132] Z. Aghaei, L. Naji, V. H. Asl, G. Khanbabaei and F. Dezhagah, “The influence of fumed silica content and particle size in poly (amide 6-b-ethylene oxide) mixed matrix membranes for gas separation,” *Separation and Purification Technology,* vol. 199, no. 1, pp. 47-56, 2018.

[133] S. Zhao, X. Cao, Z. Ma, Z. Wang, Z. Qiao, J. Wan and S. Wang, “Mixed-Matrix Membranes for CO2/N2 Separation Comprising a Poly(vinylamine) Matrix and Metal−Organic Frameworks,” *Industrial & Engineering Chemistry Research,* vol. 54, pp. 5139-5148, 2015.

[134] X. Li, Y. Cheng, H. Zhang, S. Wang, Z. Jiang, R. Guo and H. Wu, "Efficient CO2 Capture by Functionalized Graphene Oxide Nanosheets as Fillers To Fabricate Multi-Permselective Mixed Matrix Membranes," *Applied Materials & Interfaces,* vol. 7, no. 9, pp. 5528-5537, 2015.

[135] J. Shen, G. Liu, K. Huang, Q. Li, K. Guan, Y. Li and W. Jin, "UiO-66-polyether block amide mixed matrix membranes for CO2 separation," *Journal of Membrane Science,* vol. 513, no. 1, pp. 155-165, 2016.

[136] N. Matsumiya, M. Teramoto, S. Kitada and H. Matsuyama, "Evaluation of energy consumption for separation of CO2 in flue gas by hollow fiber facilitated transport membrane module with permeation of amine solution," *Separation and Purification Technology,* vol. 46, no. 1-2, pp. 26-32, 2005.

[137] R. Bounaceur, N. Lape, D. Roizard, C. Vallieres and E. Favre, "Membrane processes for post-combustion carbon dioxide capture: A parametric study," *Energy,* vol. 31, no. 14, pp. 2556-2570, 2006.

[138] M. T. Ho, G. W. Allinson and D. E. Wiley, "Reducing the Cost of CO2 Capture from Flue Gases Using Membrane Technology," *Industrial & Engineering Chemistry Research,* vol. 47, no. 5, pp. 1562-1568, 2008.

[139] H. Zhai and E. S. Rubin, "Techno-Economic Assessment of Polymer Membrane Systems for Postcombustion Carbon Capture at Coal-Fired Power Plants," *Environmental Science & Technology,* vol. 47, no. 6, pp. 3006-3014, 2013.

[140] D. M. Turi, M. Ho, M. C. Ferrari, P. Chiesa, D. E. Wiley and M. C. Romano, "CO2 capture from natural gas combined cycles by CO2 selective membranes," *International Journal of Greenhouse Gas Control,* vol. 61, pp. 168-183, 2017.

[141] M. Yuan, H. Teichgraeber, J. Wilcox and A. R. Brandt, "Design and operations optimization of membrane-based flexible carbon capture," *International Journal of Greenhouse Gas Control,* vol. 84, pp. 154-163, 2019.

[142] J. Asadi and P. Kazempoor, "Techno-economic analysis of membrane-based processes for flexible CO2 capturing from power plants," *Energy Conversion and Management,* vol. 246, p. 114633, 2021.

[143] R. Baker and B. Freeman, "Large Pilot Testing of the MTR Membrane Post-Combustion CO2 Capture Process," U.S. DEPARTMENT OF ENERGY NATIONAL ENERGY TECHNOLOGY LABORATORY, 2018.

[144] Office of Fossil Energy and Carbon Management, "DOE Awards Approximately $99 Million for Demonstration of Large-Scale Pilot Carbon Capture Technologies," U. S. Department of Energy, 30 April 2021. [Online]. Available: https://www.energy.gov/fecm/articles/doe-awards-approximately-99-million-demonstration-large-scale-pilot-carbon-capture. [Accessed 22 June 2021].

[145] M. Sandru, T.-J. Kim, W. Capala, M. Huijbers and M.-B. Hägg, "Pilot scale testing of polymeric membranes for CO2 capture from coal fired power plants," *Energy Procedia,* vol. 37, pp. 6473-6480, 2013.

[146] L. S. White, X. Wei, S. Pande, T. Wu and T. C. Merkel, "Extended flue gas trials with a membrane-based pilot plant at a one-ton-per-day carbon capture rate," *Journal of Membrane Science,* vol. 496, pp. 48-57, 2015.

[147] J. Pohlmann, M. Bram, K. Wilkner and T. Brinkmann, "Pilot scale separation of CO2 from power plant flue gases by membrane technology," *International Journal of Greenhouse Gas Control,* vol. 53, pp. 56-64, 2016.

[148] H. Wu, Q. Li, M. Sheng, Z. Wang, S. Zhao, J. Wang, S. Mao, D. Wang, B. Guo, N. Ye, G. Kang, M. Li and Y. Cao, "Membrane technology for CO2 capture: From pilot-scale investigation of two-stage plant to actual system design," *Journal of Membrane Science,* vol. 624, p. 119137, 2021.

[149] L.-S. Fan, L. Zeng, W. Wang and S. Luo, "Chemical looping processes for CO2 capture and carbonaceous fuel conversion – prospect and opportunity," *Energy & Environmental Science,* vol. 5, pp. 7254-7280, 2012.

[150] M. N. Khan, P. Chiesa, S. Cloete and S. Amini, "Integration of chemical looping combustion for cost-effective CO2capturefrom state-of-the-art natural gas combined cycles," *Energy Conversion and Management: X,* vol. 7, p. 100044, 2020.

[151] H. C. Mantripragad and E. S. Rubin, "Chemical Looping for Pre-combustion and Post-combustion CO2 Capture," *Energy Procedia,* vol. 114, pp. 6403-6410, 2017.

[152] G. Diglio, P. Bareschino, E. Mancusi and F. Pepe, "Techno-Economic Evaluation of a Small-Scale Power Generation," *Industrial & Engineering Chemistry Research,* vol. 57, pp. 11299-11311, 2018.

[153] J. H. Cloete, M. N. Khan, S. Cloete and S. Amini, "Simulation-Based Design and Economic Evaluation of a Novel Internally Circulating Fluidized Bed Reactor for Power Production with Integrated CO2 Capture," *Processes,* vol. 7, no. 10, p. 723, 2019.

[154] C. A. d. Pozo, J. H. Cloete, S. Cloete, Á. J. Álvaro and S. Amini, "Integration of gas switching combustion in a humid airturbine cycle for flexible power production from solid fuelswith near-zero emissions of CO2and other pollutants," *International Journal of Energy Research,* vol. 44, pp. 7299-7322, 2020.

[155] T. Shimizu, T. Hirama, H. Hosoda, K. Kitano, M. Inagaki and K. Tejima, "A twin fluid-bed reactor for removal of CO2 from combustion processes," *Chemical Engineering Research and Design,* vol. 77, pp. 62-68, 1999.

[156] M. Osman, M. N. Khana, A. Zaabout, S. Cloete and S. Amini, "Review of pressurized chemical looping processes for power generation and chemical production with integrated CO2 capture," *Fuel Processing Technology,* vol. 214, p. 106684, 2021.

[157] M. Erans, V. Manovic and E. J. Anthony, “Calcium looping sorbents for CO2 capture,” *Applied energy,* vol. 180, pp. 722-742, 2016.

[158] J. Blamey, E. J. Anthony, J. Wang and P. Fennell, “The calcium looping cycle for large-scale CO2 capture,” *Progress in Energy and Combustion Science,* vol. 6, no. 2, pp. 260-279, 2010.

[159] A.-M. Cormos and A. Simon, “Assessment of CO2 capture by calcium looping (CaL) process in a flexible power plant operation scenario,” *Applied Thermal Engineering,* vol. 80, pp. 319-327, 2015.

[160] M. Astolfi, E. D. Lena, F. Casella and M. C. Romano, “Calcium looping for power generation with CO2 capture: The potential of sorbent storage for improved economic performance and flexibility,” *Applied Thermal Engineering,* vol. 194, p. 117048, 2021.

[161] O. Z. Sharaf and M. F. Orhan, “An overview of fuel cell technology: Fundamentals and applications,” *Renewable and Sustainable Energy Reviews,* vol. 32, pp. 810-853, 2014.

[162] L. Duan, S. Sun, L. Yue, W. Qu and Y. Yang, “Study on a new IGCC (Integrated Gasification Combined Cycle) system with CO2 capture by integrating MCFC (Molten Carbonate Fuel Cell),” *Energy,* vol. 87, pp. 490-503, 2015.

[163] S. Campanari, P. Chiesa and G. Manzolini, “CO2 capture from combined cycles integrated with Molten Carbonate Fuel Cells,” *International Journal of Greenhouse Gas Control,* vol. 4, pp. 441-451, 2010.

[164] J. Rosen, T. Geary, A. Hilmi, R. Blanco-Gutierrez, C.-Y. Yuh, C. S. P. L. Han, R. A. Johnson, C. A. Willman and H. Ghezel-Ayagh, “Molten Carbonate Fuel Cell Performance for CO2 Capture from Natural Gas Combined Cycle Flue Gas,” *Journal of The Electrochemical Society,* vol. 167, no. 6, p. 064505, 2020.

[165] M. Spinelli, D. Bona, M. Gattia, E. Martelli, F. Viganò and S. Consonni, “Assessing the potential of molten carbonate fuel cell-based schemes for carbon capture in natural gas-fired combined cycle power plants,” *Journal of Power Sources,* vol. 448, p. 227223, 2020.

[166] R. Cooper, D. Bove, E. Audasso, M. C. Ferrari and B. Bosio, “A feasibility assessment of a retrofit Molten Carbonate Fuel Cell coal-fired plant for flue gas CO2 segregation,” *International Journal of Hydrogen Energy,* p. in proof, 2020.

[167] S. Ferguson and A. Tarrant, “Molten Carbonate Fuel Cells for 90% Post Combustion CO2 Capture From a New Build CCGT,” *Frontiers in Energy Research,* vol. 9, p. 668431, 2021.

[168] IEAGHG, “CO2RE Facilities Database,” IEAGHG, 2 June 2020. [Online]. Available: https://co2re.co/FacilityData. [Accessed 3 October 2021].

[169] C. K. Preston, “The Carbon Capture Project at Air Products’ Port Arthur Hydrogen Production Facility,” IEAGHG, Cheltenham, England, 2017.

[170] K. Kadono, A. Suzuki, M. Iijima, T. Ohishi, H. Tanaka, T. Hirata and M. Kondo, "New Energy Efficient Processes and Newly Developed Absorbents for Flue Gas CO2 Capture," *Energy Procedia,* vol. 37, pp. 1785-1792, 2013.

[171] O. Miyamoto, C. Maas, T. Tsujiuchi, M. iInui, T. Hirata, H. Tanaka, T. Yonekawa and T. Kamijo, "KM CDR ProcessTM Project Update and the New Novel Solvent Development," *Energy Procedia,* vol. 114, pp. 5616-5623, 2017.

[172] A. K. Morken, S. Pedersen, S. O. Nesse, N. E. Flø, K. Johnsen, J. K. Feste, T. d. Cazenove, L. Faramarzi and K. Vernstad, "CO2 capture with monoethanolamine: Solvent management and environmental impacts during long term operation at the Technology Centre Mongstad (TCM)," *International Journal of Greenhouse Gas Control,* vol. 82, pp. 175-183, 2019.

[173] J. H. Lee, N. Kwak, H. Niu, J. Wang, S. Wang, H. Shang and S. Gao, "KEPCO-China Huaneng Post-combustion CO2 Capture Pilot Test and Cost Evaluation," *Korean Chemical Engineering Research,* vol. 58, no. 1, pp. 150-162, 2020.

[174] B. Baburao, S. Bedell, P. Restrepo, D. Schmidt, C. Schubert, B. DeBolt, I. Haji and F. Chopin, "Advanced Amine Process Technology Operations and Results from Demonstration Facility at EDF Le Havre," *Energy Procedia,* vol. 63, pp. 6173-6187, 2014.

[175] J. N. Knudsen and J. N. Jensen, "Experience with the CASTOR/CESAR Pilot Plant," in *Workshop on Operating Flexibility of Power Plants with CCS*, Imperial College, London, 2009.

[176] Drax, "Negative emissions pioneer Drax and leading global carbon capture company – Mitsubishi Heavy Industries Group – announce new BECCS pilot," Drax Group Plc, 24 June 2020. [Online]. Available: https://www.drax.com/press_release/negative-emissions-pioneer-drax-and-leading-global-carbon-capture-company-mitsubishi-heavy-industries-group-announce-new-beccs-pilot/. [Accessed 5 November 2020].

[177] M. Akram, K. Milkowski, J. Gibbins and M. Pourkashanian, "Comparative energy and environmental performance of 40 % and 30 % monoethanolamine at PACT pilot plant," *International Journal of Greenhouse Gas Control,* vol. 95, p. 102946, 2020.

[178] F. D. Fitzgerald, S. A. Hume, G. McGough and K. Damen, "Ferrybridge CCPilot100+ Operating Experience and Final Test Results," *Energy Procedia,* vol. 63, pp. 6239-6251, 2014.

[179] S. Saito, M. Udatsu, H. Kitamuraa and S. Murai, "Mikawa CO2 Capture Pilot Plant Test of New Amine Solvent," 10 September 2015. [Online]. Available: https://www.ieaghg.org/docs/General_Docs/PCCC3_PDF/4_PCCC3_7_Saito.pdf. [Accessed 5 November 2020].

[180] Y. C. Park, Sung-HoJo, D.-H. Lee, C.-K. Yi, C. K. Ryu, K.-S. Kim, C. H. You and K. S. Park, "The Status of the Development Project for the 10 MWe-Scale Dry-sorbent Carbon Dioxide Capture System to the real Coal-Fired Power Plant in Korea," *Energy Procedia*, vol. 37, pp. 122-126, 2013.

[181] C.-K. Yi, "Dry Solid Sorbent 2 Capture Project of 10MWe Scale," in *6th Carbon Sequestration Leadership Forum*, Riyadh, Saudi Arabia, 2015.

[182] R. Lihua, L. Xi, L. Haizhong, W. Li and L. Jia, "Preliminary Design of CRP Carbon Capture Test Platform Research on Compatibility Design of Carbon Capture Units," in *14th International Conference on Greenhouse Gas Control Technologies, GHGT-14*, Melbourne, Australia, 2018.

[183] B. Arias, M. E. Diego, A. Méndez, J. C. Abanades, L. Díaz, M. Lorenzo and A. Sanchez-Biezma, "Operating Experience in la Pereda 1.7 MWth Calcium Looping Pilot," *Energy Procedia,* vol. 114, pp. 149-157, 2017.

[184] HSE, "Assessment of the major hazard potential of carbon dioxide (CO2)," Health and Safety Executive, 2011.

[185] S. B. Martynov, N. K. Daud, H. Mahgerefteh, S. Brown and R. T. J. Porter, "Impact of stream impurities on compressor power requirements for CO2 pipeline transportation," *International Journal of Greenhouse Gas Control,* vol. 54, pp. 652-661, 2016.

[186] Tebodin , "KNOWLEDGE SHARING REPORT – CO2 Liquid Logistics Shipping Concept (LLSC) Overall Supply Chain Optimization," Global Carbon Capture and Storage Institute, Canberra, 2011.

[187] B. Wetenhall, "Impact of CO2 impurity on CO2 compression, liquefaction and transportation," *Energy Procedia,* vol. 63, pp. 2764-2778, 2014.

[188] A. L. Ling and V. Mulyandasari, "Compressor Selection and Sizing (Engineering Design Guideline)," KLM Technology Group, Johor, Malaysia, 2008.

[189] PIP, "Compressor Selection Guidelines," Process Industry Practices, Texas, 2013.

[190] M. Stewart, Surface Production Operations: Volume IV - Pump and Compressor Systems: Mechanical Design and Specification, Gulf Professional Publishing, 2018.

[191] D. L. McCollum and J. M. Ogden, "Techno-Economic Models for Carbon Dioxide Compression, Transport, and Storage & Correlations for Estimating Carbon Dioxide Density and Viscosity," Institute of Transportation Studies, University of California, California, 2006.

[192] A. Aspelund and K. Jordal, "Gas conditioning—The interface between CO2 capture and transport," *International Journal of Greenhouse Gas Control,* vol. 1, no. 3, pp. 343-354, 2007.

[193] A. S. Witkowski and M. Majkut, "The impact of CO2 compression systems on the compressor power required for a pulverized coal-fired power plant in post-combustion carbon dioxide sequestration," *The Journal of Committee on Machine Building of Polish Academy of Sciences,* vol. 59, no. 3, pp. 343-360, 2012.

[194] A. Alabdulkarem, Y. Hwang and R. Radermacher, "Development of CO2 liquefaction cycles for CO2 sequestration," *Applied Thermal Engineering,* Vols. 33-34, pp. 144-156, 2012.

[195] S. G. Lee, G. B. Choi and J. M. Lee, "Optimal Design and Operating Conditions of the CO2 Liquefaction Process, Considering Variations in Cooling Water Temperature," *Industrial & Engineering Chemistry Research,* vol. 54, pp. 12855-12866, 2015.

[196] H. Deng, S. Roussanaly and G. Skaugen, "Techno-economic analyses of CO2 liquefaction: Impact of product pressure and impurities," *International Journal of Refrigeration,* vol. 103, pp. 301-315, 2019.

[197] S. Jackson and E. Brodal, "Optimization of the CO2 Liquefaction Process-Performance Study with Varying Ambient Temperature," *Applied Science,* vol. 9, p. 4467, 2019.

[198] H. A. Muhammad, C. Roh, J. Cho, Z. Rehman, H. Sultan, Y.-J. Baik and B. Lee, "A comprehensive thermodynamic performance assessment of CO2 liquefaction and pressurization system using a heat pump for carbon capture and storage (CCS) process," *Energy Conversion and Management,* vol. 206, p. 112489, 2020.

[199] G. Hegerland, T. Jørgensen and J. O. Pande, "- Liquefaction and handling of large amounts of CO2 for EOR," *Greenhouse Gas Control Technologies 7,* vol. 2, no. 2, pp. 2541-2544, 2005.

[200] L. E. Øi, N. Eldrup, U. Adhikari, M. H. Bentsen, J. L. Badalge and S. Yang, "Simulation and Cost Comparison of CO2 Liquefaction," *Energy Procedia,* vol. 86, pp. 500-510, 2016.

[201] L. M. Romeo, I. Bolea, Y. Lara and J. M. Escosa, "Optimization of intercooling compression in CO2 capture systems," *Applied Thermal Engineering,* vol. 29, no. 8, pp. 1744-1751, 2009.

[202] S. Giannaris, B. Jacobs, W. Srisang, C. Bruce and D. Janowczyk, "Heat integration analysis and optimization for a post combustion CO2 capture retrofit study of SaskPower's Shand Power Station," *International Journal of Greenhouse Gas Control,* vol. 84, pp. 62-71, 2019.

[203] P. J. Oexmann and A. Kather, "Optimised integration of post-combustion CO2 capture process in greenfield power plants," *Energy,* vol. 35, no. 10, pp. 4030-4041, 2010.

[204] D. Hasler, D. Stopek, R. Smith and J. Klumpyan, "A CO2 Compression and Dehydration System Utilizing Absorption Chillers and Heat Recovery Concepts," Anaheim, California, 2012.

[205] J. Kemper, L. Sutherland, J. Watt and S. Santos, "Evaluation and analysis of the performance of dehydration units for CO2 capture," *Energy Procedia,* vol. 63, pp. 7568-7584, 2014.

[206] E.ON, "Kingsnorth Carbon Dioxide Capture and Storage Demonstration Project - Key Knowledge Reference Book," E.ON, 2011.

[207] EIGA, "Refrigerated CO2 storage at users' premises," European Industrial Gases Association AISBl, Brussels, 2008.

[208] EIGA, "Carbon Dioxide Food and Beverages Grade, Source Qualification, Quality Strandards and Verification," European Industrial Gases Association AISBL, Brussels, 2016.

[209] M. D. Jensen, J. A. S. Steven M. Schlasner and J. A. Hamling, “Operational flexibility of CO2 transport and storage,” *Energy Procedia,* vol. 63, pp. 2715-2722, 2014.

[210] Element Energy , “Shipping CO2 - UK Cost Estimation Study,” Department for Business, Energy and Industrial Strategy, Cambridge, 2018.

[211] MEP, “Feasibility study for full-scale CCS in Norway,” Ministry of Petroleum and Energy, 2016.

[212] IPCC, “Carbon Dioxide Capture and Storage,” Cambridge University Press, Cambridge, 2005.

[213] G. Pipitone and O. Bolland, “Power generation with CO2 capture: Technology for CO2 purification,” *International Journal of Greenhouse Gas Control,* vol. 3, no. 5, pp. 528-534, 2009.

[214] E. d. Visser, C. Hendriks, M. Barrio, M. J. Mølnvik, G. d. Koeijer, S. Liljemark and Y. L. Gallo, “Dynamis CO2 quality recommendations,” *International Journal of Greenhouse Gas Control,* vol. 2, no. 4, pp. 478-484, 2008.

[215] T. Harkin, I. Filby, H. Sick, D. Manderson and R. Ashton, “Development of a CO2 specification for a CCS hub network,” *Energy Procedia,* vol. 114, pp. 6708-6720, 2017.

[216] J. Yan and Z. Zhang, “Carbon Capture, Utilization and Storage (CCUS),” *Applied Energy,* vol. 235, pp. 1289-1299, 2019.

[217] H. Yu, S. Morgan, A. Allport, A. Cottrell, T. Do, J. McGregor, L. Wardhaugh and P. Feron, “Results from trialling aqueous NH3 based post-combustion capture in a pilot plant at Munmorah power station: Absorption,” *Chemical Engineering Research and Design,* vol. 89, no. 8, pp. 1204-1215, 2011.

[218] M. C. Romano, P. Chiesa and G. Lozza, “Pre-combustion CO2 capture from natural gas power plants, with ATR and MDEA processes,” *International Journal of Greenhouse Gas Control,* vol. 4, no. 5, pp. 785-797, 2010.

[219] S. Sircar and T. C. Golden, “Purification of Hydrogen by Pressure Swing,” *Seperation Science and Technology,* vol. 35, no. 5, pp. 667-687, 2000.

[220] W. Chung, K. Roh and J. H. Lee, “Design and evaluation of CO2 capture plants for the steelmaking industry by means of amine scrubbing and membrane separation,” *International Journal of Greenhouse Gas Control,* vol. 74, pp. 259-270, 2018.

[221] S. Chen, N. Lior and W. Xiang, “Coal gasification integration with solid oxide fuel cell and chemical looping combustion for high-efficiency power generation with inherent CO2 capture,” *Applied Energy,* vol. 146, pp. 298-312, 2015.

[222] A. Brunsvold, J. P. Jakobsen, M. J. Mazzetti, G. Skaugen, M. Hammer, C. Eickhoff and F. Neele, “Key findings and recommendations from the IMPACTS project,” *International Journal of Greenhouse Gas Control,* vol. 54, no. 2, pp. 588-598, 2016.

[223] S. P. Peletiri, I. M. Mujtaba and N. Rahmanian, "Process simulation of impurity impacts on CO2 fluids flowing in pipelines," *Journal of Cleaner Production,* vol. 240, p. 118145, 2019.

[224] G. Skaugen, S. Roussanaly, J. Jakobsen and A. Brunsvold, "Techno-economic evaluation of the effects of impurities on conditioning and transport of CO2 by pipeline," *International Journal of Greenhouse Gas Control,* vol. 54, no. 2, pp. 627-639, 2016.

[225] S.-L. Kahlke, M. Pumpa, S. Schütz, A. Kather and H. Rütters, "Potential Dynamics of CO2 Stream Composition and Mass Flow Rates in CCS Clusters," *Processes,* vol. 8, p. 1188, 2020.

[226] S. Roussanaly, G. Bureau-Cauchois and J. Husebye, "Costs benchmark of CO2 transport technologies for a group of various size industries," *International Journal of Greenhouse Gas Control,* vol. 12, pp. 341-350, 2013.

[227] U. Ali, C. Font-Palma, M. Akram, E. O. Agbonghae, D. B. Ingham and M. Pourkashanian, "Comparative potential of natural gas, coal and biomass fired power plant with post - combustion CO2 capture and compression," *International Journal of Greenhouse Gas Control,* vol. 63, pp. 184-193, 2017.

[228] T. Spitz, A. G. Díaz, H. Chalmers and M. Lucquiaud, "Operating flexibility of natural gas combined cycle power plant integrated with post-combustion capture," *International Journal of Greenhouse Gas Control,* vol. 88, pp. 92-108, 2019.

[229] E. Mechleri, A. Lawal, A. Ramos, J. Davison and N. Mac Dowell, "Process control strategies for flexible operation of post-combustion CO2 capture plants," *International Journal of Greenhouse Gas Control,* vol. 57, pp. 14-25, 2017.

[230] A. Alhajaj, N. Mac Dowell and N. Shah, "A techno-economic analysis of post-combustion CO2 capture and compression applied to a combined cycle gas turbine: Part I. A parametric study of the key technical performance indicator," *International Journal of Greenhouse Gas Control,* vol. 44, pp. 26-41, 2016.

[231] A. Alhajaj, N. Mac Dowell and N. Shah, "A techno-economic analysis of post-combustion CO2 capture and compression applied to a combined cycle gas turbine: Part II. Identifying the cost-optimal control and design variables," *International Journal of Greenhouse Gas Control,* vol. 52, pp. 331-343, 2016.

[232] T. Adams and N. M. Dowell, "Off-design point modelling of a 420 MW CCGT power plant integratedwith an amine-based post-combustion CO2 capture and compressionprocess," *Applied Energy,* vol. 178, pp. 681-702, 2016.

[233] M. Nienoord, M. Ogink, P. Khakharia, E. L. V. Goetheer and R. d. Kler, "Dynamic behaviour CO2 capture and compression: an assessment," *Energy Procedia,* vol. 63, pp. 2727-2737, 2014.

[234] IEA, "20 Years of Carbon Capture and Storage: Accelerating Future Deployment," International Energy Agency, Paris, France, 2016.

[235] J. Gibbins and M. Lucquiaud, "BAT Review for New-Build and Retrofit Post-Combustion Carbon Dioxide Capture Using Amine-Based Technologies for Power and CHP Plants Fuelled by Gas and Biomass as an Emerging Technology under the IED for the UK," UKCCSRC Report, Sheffield, England, 2021.

[236] Global CCS Institute, "CO2 Capture Technologies: Post Combustion Capture (PCC)," Global CCS Institute, Canberra, Australia, 2012.

[237] B. Smit, A.-H. A. Park and G. Gadikota, "The grand challenges in carbon capture, utilization, and storage," *Frontiers in Energy Research,* vol. 2, p. 55, 2014.

[238] R. M. Montañés, M. Korpås, L. O. Nord and S. Jaehnertb, "Identifying operational requirements for flexible CCS power plant," *Energy Procedia,* vol. 86, pp. 22-31, 2016.

[239] A. M. Moe, A. Dugstad, D. Benrath, E. Jukes, E. Anderson, E. Catalanotti, E. Durusut, F. Neele, F. Grunert, H. Mahgerefteh, J. Gazendam, J. Barnett, M. Hammer, R. Span, S. Brown, S. T. Munkejod and V. Weber, "A Trans-European CO2 Transportation Infrastructure for CCUS: Opportunities & Challenges," Zero Emissions Platform, Brussels, 2020.

[240] G. Magneschi, T. Zhang and R. Munson, "The Impact of CO2 Capture on Water Requirements of Power Plants," *Energy Procedia,* vol. 114, pp. 6337-6347, 2017.

[241] BEIS, "Digest of UK Energy Statistics (DUKES): electricity," 28 July 2022. [Online]. Available: https://www.gov.uk/government/statistics/electricity-chapter-5-digest-of-united-kingdom-energy-statistics-dukes. [Accessed 2023].

[242] BEIS, "CCS deployment at dispersed industrial sites," Crown Copyright, London, 2020.

[243] Environment Agency, "233_08_SD50 Decision document new bespoke," 2019.

[244] R. L. Siegelman, P. J. Milner, E. J. Kim, S. C. Weston and J. R. Long, "Challenges and opportunities for adsorption-based CO2 capture from natural gas combined cycle emissions," *Energy & Environmental Science,* vol. 12, no. 7, pp. 2161-2173, 2019.

[245] P. Brandl, S. M. Soltani, P. S. Fennell and N. Mac Dowell, "Evaluation of cooling requirements of post-combustion CO2 capture applied to coal-fired power plants," *Chemical Engineering Research and Design,* vol. 122, pp. 1-10, 2017.

[246] CCUS Cost Challenge Taskforce, "Delivering Clean Growth: CCUS Cost Challenge Taskforce Report," Department for Business, Energy & Industrial Strategy, 2018.

[247] Summit Power Caledonia UK Ltd , "Caledonia Clean Energy Project: Feasibility Study Phase 2 Final Report," Summit Power Caledonia UK Ltd , 2018.

[248] E. S. Rubin, "Understanding the pitfalls of CCS cost estimates," *International Journal of Greenhouse Gas Control,* vol. 10, pp. 181-190, 2012.

[249] A. B. Rao and E. S. Rubin, "A Technical, Economic, and Environmental Assessment of Amine-Based CO2 Capture Technology for Power Plant Greenhouse Gas Control," *Environmental Science & Technology,* vol. 36, no. 20, pp. 4467-4475, 2002.

[250] M.-O. Schach, R. Schneider, H. Schramm and J.-U. Repke, "Techno-Economic Analysis of Postcombustion Processes for the Capture of Carbon Dioxide from Power Plant Flue Gas," *Industrial & Engineering Chemistry Research,* vol. 49, pp. 2363-2370, 2010.

[251] E. S. Rubin, J. E. Davison and H. J. Herzog, "The cost of CO2 capture and storage," *International Journal of Greenhouse Gas Control,* vol. 40, pp. 378-400, 2015.

[252] M. R. M. Abu-Zahra, J. P. M. Niederer, P. H. M. Feron and G. F.Versteeg, "CO2 capture from power plants: Part II. A parametric study of the economical performance based on mono-ethanolamine," *International Journal of Greenhouse Gas Control,* vol. 1, no. 2, pp. 135-142, 2007.

[253] K. Riahi, E. S. Rubin, M. R. Taylor, L. Schrattenholzer and D. Hounshell, "Technological learning for carbon capture and sequestration technologies," *Energy Economics,* vol. 26, no. 4, pp. 539-564, 2004.

[254] L. Clarke, P. Kyle, M. Wise, K. Calvin, J. Edmonds, S. Kim, M. Placet and S. Smith, "CO2 Emissions Mitigation and Technological Advance: An Updated Analysis of Advanced Technology Scenarios (Scenarios Updated January 2009)," U.S. Department of Energy, Washington , 2008.

[255] BEIS, "Electricty Generation Costs 2020," Department for Business, Energy & Industrial Strategy, London, 2020.

[256] Mott MacDonald, "UK Electricity Generation Costs Update," Mott MacDonald, Brighton, Unitd Kingdom, 2010.

[257] C. Zhang, "Absorption principle and techno-economic analysis of CO2 absorption technologies: A review," *IOP Conference Series: Earth and Environmental Science,* vol. 657, p. 012045, 2021.

[258] S. E. Zanco, J.-F. Pérez-Calvo, A. Gasós, B. Cordiano, V. Becattini and M. Mazzotti, "Postcombustion CO2 Capture: A Comparative Techno-Economic Assessment of Three Technologies Using a Solvent, an Adsorbent, and a Membrane," *ACS Engineering Au,* vol. 1, no. 1, pp. 50-72, 2021.

[259] D. Pauschert, "ESMAP Technical Paper 122/09: Study of Equipment Prices in the Power Sector," THE WORLD BANK GROUP, Washington, U.S.A, 2009.

[260] Parsons Brinckerhoff, "Electricity Generation Cost Model - 2011 Update Revision 1," Department of Energy and Climate Change, 2011.

[261] BEIS, “Assessing the Cost Reduction Potential and Competitiveness of Novel (Next Generation) UK Carbon Capture Technology,” UK Department for Business, Energy & Industrial Strategy, 2018.

[262] LeighFisher, “Electricity Generation Costs and Hurdle Rates,” LeighFisher Ltd, 2016.

[263] Parsons Brinckerhoff, “Electricity Generation Cost Model - 2013 Update of Non-Renewable Technologies,” Department of Energy and Climate Change, Manchester, United Kingdom, 2013.

[264] EIA, “Levelized Costs of New Generation Resources in the Annual Energy Outlook 2021,” U.S Energy Information Administration, 2021.

[265] CCC, “The Sixth Carbon Budget: The UK's path to Net Zero,” Committee on Climate Change, 2020.

[266] Global CCS Institute, “The Economics of Direct Air Carbon Capture and Storage,” Global CCS Institute, 2022.

[267] A. Kiani, K. Jiang and P. Feron, “Techno-Economic Assessment for CO2 Capture From Air Using a Conventional Liquid-Based Absorption Process,” *Frontiers in Energy Research,* vol. 8, p. 92, 2020.

[268] N. McQueen, K. V. Gomes, C. McCormick, K. Blumanthal, M. Pisciotta and J. Wilcox, “A review of direct air capture (DAC): scaling up commercial technologies and innovating for the future,” *Progress in Energy,* vol. 3, no. 3, p. 032001, 2021.

[269] P. Cheng, D. M. Thierry, H. Hendrix, K. D. Dombrowski, D. J. Sachde, M. J. Realff and J. K. Scott, “Modeling and optimization of carbon-negative NGCC plant enabled by modular direct air capture,” *Applied Energy,* vol. 341, p. 121076, 2023.

[270] D. Mullen, L. Herraiz, J. Gibbins and M. Lucquiaud, “On the cost of zero carbon hydrogen: A techno-economic analysis of steam methane reforming with carbon capture and storage,” *International Journal of Greenhouse Gas Control,* vol. 126, p. 103904, 2023.

[271] J. Goldmeer, “Power to Gas: Hydrogen for Power Generation,” General Electric Company, 2019.

[272] “Role of Hydrogen in a Low-Carbon Electric Power System: A Case Study,” *Frontiers in Energy Research,* vol. 8, p. 585461, 2021.

[273] ETN, “Hydrogen Deployment in Centralised Power Generation: A techno-economic case study,” ETN a.i.s.b.l, Brussels, Belgium, 2022.

[274] McKinsey & Company, “Net-zero power: Long duration energy storage for a renewable grid,” LDES Council, 2021.

[275] CEC, “Battery Storage: The new, clean peaker,” Clean Energy Council, 2021.

[276] BEIS, “Benefits of Long Duration Electrcity Storage,” Crown Copyright, 2022.

[277] IEAGHG, “Valuing Flexibility in CCS Power Plants,” IEA Greenhoouse Gas R&D Programme, Cheltenham, 2017.

[278] R. Domenichini, L. Mancuso, N. Ferrari and J. Davison, “Operating Flexibility of Power Plants with Carbon Capture and Storage (CCS),” *Energy Procedia,* vol. 37, pp. 2727-2737, 2013.

[279] C. F. Heuberger, I. S. N. Shahbc and N. M. Dowell, “Quantifying the value of CCS for the future,” *Energy & Environmental Science,* vol. 9, pp. 2497-2510, 2016.

[280] N. Mac Dowell and Staffell, “The role of flexible CCS in the UK's future energy system,” *International Journal of Greenhouse Gas Control,* vol. 48, no. 2, pp. 327-344, 2016.

[281] D. L. Oates, P. Versteeg, E. Hittinger and P. Jaramillo, “Profitability of CCS with flue gas bypass and solvent storage,” *International Journal of Greenhouse Gas Control,* vol. 27, pp. 279-288, 2014.

[282] E. Sanchez-Fernandez, M. Sanchez del Rio, H. Chalmers, P. Khakharia, E. L. V. Goetheer, J. Gibbins and M. Lucquiaud, “Operational flexibility options in power plants with integrated post-combustion capture,” *International Journal of Greenhouse Gas Control,* vol. 48, pp. 275-289, 2016.

[283] X. Wu, M. Wang and K. Y. Lee, “Flexible operation of supercritical coal-fired power plant integrated with solvent-based CO2 capture through collaborative predictive control,” *Energy,* vol. 206, p. 118105, 2020.

[284] E. Mechleri, P. S. Fennell and N. Mac Dowell, “Optimisation and evaluation of flexible operation strategies for coal-and gas-CCS power stations with a multi-period design approach,” *International Journal of Greenhouse Gas Control,* vol. 59, pp. 24-39, 2017.

[285] M. M. Majoumerd, H. N. Somehsaraei, M. Assadi and P. Breuhaus, “Micro gas turbine configurations with carbon capture – Performance assessment using a validated thermodynamic model,” *Applied Thermal Engineering,* vol. 73, no. 1, pp. 172-184, 2014.

[286] S. Giorgetti, A. Parente, L. Bricteux, F. Contino and W. D. Paepe, “Optimal design and operating strategy of a carbon-clean micro gas turbine for combined heat and power applications,” *International Journal of Greenhouse Gas Control,* vol. 88, pp. 469-481, 2019.

[287] ELEXON, “Balancing Mechanism Reporting Service (BMRS),” 2023. [Online]. Available: https://www.bmreports.com. [Accessed 1 November 2022].

[288] BEIS, “2021 UK greenhouse gas emissions, provisional figures,” Crown Copyright, 2022.

[289] DESNZ & BEIS, “Provisional UK greenhouse gas emissions national statistics 2022,” 30 March 2023. [Online]. Available: https://www.gov.uk/government/statistics/provisional-uk-greenhouse-gas-emissions-national-statistics-2022. [Accessed 2023].

[290] DECC, “Electricity market reform: policy overview,” 22 May 2012. [Online]. Available: https://www.gov.uk/government/publications/electricity-market-reform-policy-overview. [Accessed 2023].

[291] Agora Energiewende, “Flexibility in thermal power plants,” Agora Energiewende, Berlin, 2017.

[292] A. Chikukwa, N. Enaasen, H. M. Kvamsdal and M. Hillestad, “Dynamic Modeling of Post-combustion CO2 Capture Using Amines–A Review,” *Energy Procedia,* vol. 23, pp. 82-91, 2012.

[293] M. Bui, I. Gunawan, V. Verheyen, P. Feron, E. Meuleman and S. Adeloju, “Dynamic modelling and optimisation of flexible operation in post-combustion CO2 capture plants—A review,” *Computers & Chemical Engineering,* vol. 61, pp. 245-265, 2014.

[294] X. Wu, M. Wang, P. Liao, J. Shen and Y. Li, “Solvent-based post-combustion CO2 capture for power plants: A critical review and perspective on dynamic modelling, system identification, process control and flexible operation,” *Applied Energy,* vol. 257, p. 113941, 2020.

[295] N. Mac Dowell and N. Shah, “The multi-period optimisation of an amine-based CO2 capture process integrated with a super-critical coal-fired power station for flexible operation,” *Computers & Chemical Engineering,* vol. 74, pp. 169-183, 2015.

[296] R. Taylor and R. Krishna, Multicomponent Mass Transfer, New York: John Wiley & Sons, Inc, 1993.

[297] P. Mores, N. Scenna and S. Mussati, “CO2 capture using monoethanolamine (MEA) aqueous solution: Modeling and optimization of the solvent regeneration and CO2 desorption process,” *Energy,* vol. 45, no. 1, pp. 1042-1058, 2012.

[298] J. L. Bravo and J. R. Fair, “Generalized correlation for mass transfer in packed distillation columns,” *Industrial & Engineering Chemistry Process Design and Development,* vol. 21, no. 1, pp. 162-170, 1982.

[299] K. Onda, H. Takeuchi and Y. Okumoto, “Mass Transfer Coefficients Between Gas and Liquid Phases in Packed Columns,” *Journal of Chemical Engineering Japan,* vol. 1, pp. 56-62, 1968.

[300] E. R. Dugas, “Pilot plant study of carbon dioxide capture by aqueous monoethanolamine, M.S.E. Thesis,” University of Texas at Austin, 2006.

[301] PSE, “gCCS Documentation,” Process Systems Enterprise Limited, London, 2016.

[302] N. Mac Dowell, F. Llovell, C. S. Adjiman, G. Jackson and A. Galindo, “Modeling the Fluid Phase Behavior of Carbon Dioxide in Aqueous Solutions of Monoethanolamine Using Transferable Parameters with the SAFT-VR Approach,” *Industrial & Engineering Chemistry Research,* vol. 49, no. 4, pp. 1883-1899, 2010.

[303] R. Billet and M. Schultes, “Prediction of Mass Transfer Columns with Dumped and Arranged Packings: Updated Summary of the Calculation Method of Billet and Schultes,” *Chemical Engineering Research and Design,* vol. 77, no. 6, pp. 498-504, 1999.

[304] N. Mac Dowell, N. J. Samsatli and N. Shah, "Dynamic modelling and analysis of an amine-based post-combustion CO2 capture absorption column," *International Journal of Greenhouse Gas Control,* vol. 12, pp. 247-258, 2013.

[305] R. K. Shah and D. P. Sekulić, Fundamentals of Heat Exchanger Design, New Jersey: John Wiley & Sons, 2003.

[306] L. Faramarzi, D. Thimsen, S. Hume, A. Maxon, G. Watson, S. Pedersen, E. Gjernes, B. F. Fostås, G. Lombardo, T. Cents, A. K. Morken, M. I. Shah, T. d. C. Espen and S. Hamborg, "Results from MEA testing at the CO2 Technology Centre Mongstad: Verification of baseline results in 2015," *Energy Procedia,* vol. 114, pp. 1128-1145, 2017.

[307] H. M. Kvamsdal, J. P. Jakobsen and K. Hoff, "Dynamic modeling and simulation of a CO2 absorber column for post-combustion CO2 capture," *Chemical Engineering and Processing: Process Intensification,* vol. 48, pp. 135-144, 2009.

[308] A. Lawal, M. Wang, P. Stephenson, G. Koumpouras and H. Yeung, "Dynamic modelling and analysis of post-combustion CO2 chemical," *Fuel,* vol. 89, pp. 2791-2801, 2010.

[309] M. T. Luu, N. A. Manaf and A. Abbas, "Dynamic modelling and control strategies for flexible operation of amine-based post-combustion CO2 capture systems," *International Journal of Greenhouse Gas Control,* vol. 39, pp. 377-389, 2015.

[310] F. Rezazadeh, W. F. Gale, M. Akram, K. J. Hughes and M. Pourkashanian, "Performance evaluation and optimisation of post combustion CO2 capture processes for natural gas applications at pilot scale via verified rate-based models," *International Journal of Greenhouse Gas Control,* vol. 53, pp. 243-253, 2016.

[311] L. Prentza, I. P. Koronaki, E. G. Papoutsis and V. D. Papaefthimiou, "Dynamic simulation and parametric sensitivity study in reactive CO2 capture systems – A solvent comparison study," *Thermal Science and Engineering Progress,* vol. 5, pp. 555-567, 2018.

[312] C. Biliyok, A. Lawal, M. Wang and F. Seibert, "Dynamic modelling, validation and analysis of post-combustion chemical absorption CO2 capture plant," *International Journal of Greenhouse Gas Control,* vol. 9, pp. 428-445, 2012.

[313] N. A. Manaf, A. Cousins, P. Feron and A. Abbas, "Dynamic modelling, identification and preliminary control analysis of an amine-based post-combustion CO2 capture pilot plant," *Journal of Cleaner Production,* vol. 113, pp. 635-653, 2016.

[314] M. Bui, P. Tait, M. Lucquiaud and N. Mac Dowell, "Dynamic operation and modelling of amine-based CO2 capture at pilot scale," *International Journal of Greenhouse Gas Control,* vol. 79, pp. 134-153, 2018.

[315] N. Enaasen, L. Zangrilli, A. Mangiaracina, T. Mejdell, H. M. Kvamsdal and M. Hillestad, "Validation of a Dynamic Model of the Brindisi Pilot Plant," *Energy Procedia ,* vol. 63, pp. 1040-1054, 2014.

[316] R. M. Montañés, N. E. Flø and L. O. Nord, "Dynamic Process Model Validation and Control of the Amine Plant at CO2 Technology Centre Mongstad," *Energies,* vol. 10, p. 1527, 2017.

[317] E. S. Kikkinides, D. Nikolic and M. C. Georgiadis, "Modeling of Pressure Swing Adsorption Processes," in *Dynamic Process Modelling,* M. C. Georgiadis, J. R. Banga and E. N. Pistikopoulos, Eds., Weinheim, Germany, Wiley-VCH Verlag GmbH & Co. KGaA, 2010, pp. 137-172.

[318] S. Li, S. Deng, L. Zhao, R. Zhao, M. Lin, Y. Du and Y. Lian, "Mathematical modeling and numerical investigation of carbon capture by adsorption: Literature review and case study," *Applied Energy,* vol. 221, pp. 437-449, 2018.

[319] D. M. Ruthven, Principles of Adsorption and Adsorption Processes, John Wiley & Sons, 1984, pp. 206-219.

[320] M. G. Plaza, I. Durán, N. Querejeta, F. Rubiera and C. Pevida, "Experimental and Simulation Study of Adsorption in Postcombustion Conditions Using a Microporous Biochar. 1. CO2 and N2 Adsorption," *Industrial & Engineering Chemistry Research,* vol. 55, no. 11, pp. 3097-3112, 2016.

[321] M. G. Plaza, I. Durán, N. Querejeta, F. Rubiera and C. Pevida, "Experimental and Simulation Study of Adsorption in Postcombustion Conditions Using a Microporous Biochar. 2. H2O, CO2, and N2 Adsorption," *Industrial & Engineering Chemistry Research,* vol. 55, no. 24, pp. 6854-6865, 2016.

[322] M. G. Plaza and F. Rubiera, "Evaluation of a novel multibed heat-integrated vacuum and temperature swing adsorption post-combustion CO2 capture process," *Applied Energy,* vol. 250, pp. 916-925, 2019.

[323] E. Glueckauf and J. I. Coates, "241. Theory of chromatography. Part IV. The influence of incomplete equilibrium on the front boundary of chromatograms and on the effectiveness of separation," *Journal of the Chemical Society (resumed),* pp. 1315-1321, 1947.

[324] H. Ahn, S.-H. Hong, Y. Zhang and C.-H. Lee, "Experimental and Simulation Study on CO2 Adsorption Dynamics of a Zeolite 13X Column during Blowdown and Pressurization: Implications of Scaleup on CO2 Capture Vacuum Swing Adsorption Cycle," *Industrial & Engineering Chemistry Research,* 2020.

[325] G. N. Nikolaidis, E. S. Kikkinides and M. C. Georgiadis, "An Integrated Two-Stage P/VSA Process for Postcombustion CO2 Capture Using Combinations of Adsorbents Zeolite 13X and MgMOF-74," *Industrial & Engineering Chemistry Research,* vol. 56, no. 4, p. 974=988, 2017.

[326] P. Xiao, J. Zhang, P. Webley, G. Li, R. Singh and R. Todd, "Capture of CO2 from flue gas streams with zeolite 13X by vacuum-pressure swing adsorption," *Adsorption,* vol. 14, pp. 575-582, 2008.

[327] R. Haghpanah, A. Majumder, R. Nilam, A. Rajendran, S. Farooq, I. A. Karimi and M. Amanullah, "Multiobjective Optimization of a Four-Step Adsorption Process for

Postcombustion CO2 Capture Via Finite Volume Simulation," *Industrial & Engineering Chemistry Research,* vol. 52, no. 11, p. 4249–4265, 2013.

[328] D. Ko, R. Siriwardane and L. T. Biegler, "Optimization of Pressure Swing Adsorption and Fractionated Vacuum Pressure Swing Adsorption Processes for CO2 Capture," *Industrial & Engineering Chemistry Research,* vol. 44, pp. 8084-8094, 2005.

[329] K. T. Chue, J. N. Kim, Y. J. Yoo, S. H. Cho and R. T. Yang, "Comparison of Activated Carbon and Zeolite 13X for CO2 Recovery from Flue Gas by Pressure Swing Adsorption," *Industrial & Engineering Chemistry Research,* vol. 34, pp. 591-598, 1995.

[330] S. Ergun, "Determination of Geometric Surface Area of Crushed Porous Solids," *Analytical Chemistry,* vol. 24, pp. 388-393, 1952.

[331] PSE, "gPROMS ProcessBuilder Documentation," Process Systems Enterprise Limited, London, 2019.

[332] D. Li, Y. Zhou, Y. Shen, W. Sun, Q. Fu, H. Yan and D. Zhang, "Experiment and simulation for separating CO2/N2 by dual-reflux pressure swing adsorption process," *Chemical Engineering Journal,* vol. 297, pp. 315-324, 2016.

[333] S. Lillia, D. Bonalumi, C. Grande and G. Manzolini, "A comprehensive modeling of the hybrid temperature electric swingadsorption process for CO2 capture," *Contents lists available atScienceDirectInternational Journal of Greenhouse Gas Control,* vol. 74, pp. 155-173, 2018.

[334] D.-K. Moon, Y. Park, H.-T. Oh, S.-H. Kim, M. Oh and C.-H. Lee, "Performance analysis of an eight-layered bed PSA process for H2 recovery from IGCC with pre-combustion carbon capture," *Energy Conversion and Management,* vol. 156, pp. 202-214, 2018.

[335] R. A. A. Solares, D. S. d. Santos, A. Ingram and J. Wood, "Modelling and parameter estimation of breakthrough curves for amine-modified activated carbons under pre-combustion carbon capture conditions," *Fuel,* vol. 253, pp. 1130-1139, 2019.

[336] R. Haghpanah, R. Nilam, A. Rajendran, S. Farooq and I. A. Karimi, "Cycle synthesis and optimization of a VSA process for postcombustion CO2 capture," *AIChE Journal,* vol. 59, no. 12, pp. 4735-4748, 2013.

[337] A. J. H. McGaughey and M. Kaviany, "Thermal conductivity decomposition and analysis using molecular dynamics simulations: Part II. Complex silica structures," *International Journal of Heat and Mass Transfer,* vol. 47, no. 8-9, pp. 1799-1816, 2004.

[338] T. L. P. Dantas, F. M. T. Luna, I. J. S. Jr., A. E. B. Torres, D. C. S. d. Azevedo, C. A. Grande, A. E. Rodrigues and R. F. P. M. Moreira, "Modeling of the fixed-bed adsorption of carbon dioxide and a carbon dioxide- nitrogen mixture on zeolite 13X," *Brazilian Journal of Chemical Engineering,* vol. 28, no. 3, pp. 533-544, 2011.

[339] R. H. Aungier, Centrifugal Compressors: A Strategy for Aerodynamic Design and Analysis, American Society of Mechanical Engineers, 2000.

[340] K. H. Lüdtke, Process Centrifugal Compressors: Basics, Function, Operation, Design, Application, Springer-Verlag Berlin Heidelberg New York, 2004.

[341] S. Modekurti, J. Eslick, B. Omell, D. Bhattacharyya, D. C. Miller and S. E. Zitney, "Design, dynamic modeling, and control of a multistage CO2 compression system," *International Journal of Greenhouse Gas Control,* vol. 62, pp. 31-45, 2017.

[342] G. K. McMillan, Centrifugal and Axial Compressor Control, 10th ed., New York: Momentum Press, 2010.

[343] Environment Agency, "Post-combustion carbon dioxide capture: best available techniques (BAT)," Environment Agency, 3 November 2022. [Online]. Available: https://www.gov.uk/guidance/post-combustion-carbon-dioxide-capture-best-available-techniques-bat. [Accessed 2023].

[344] S. A. Rackley, "Power generation fundamentals," in *Carbon Capture and Storage (Second Edition),* Elsevier, 2017, pp. 37-71.

[345] G. Towler and R. Sinnott, Chemical Engineering Design: Principles, Practice and Economics of Plant and Process Design, 2nd ed., Oxford: Elsevier, 2012.

[346] A. Chauvel, P. Leprince, Y. Barthel, C. Raimbault and J.-P. Arlie, Manual of Economic Analysis of Chemical Processes: Feasibility Studies in Refinery and Petrochemical Processes., McGraw-Hill, 1981.

[347] I. Ustadi, T. Mezher and M. R. M. Abu-Zahra, "Potential for Hybrid-Cooling System for the CO2 Post-Combustion Capture Technology," *Energy Procedia,* vol. 114, pp. 6348-6357, 2017.

[348] Global CCS Institute, "STATE OF THE ART: CCS TECHNOLOGIES 2022," Global CCS Institute, 2022.

[349] P. A. Webley, "Adsorption technology for CO2 separation and capture: a perspective," *Adsorption,* vol. 20, pp. 225-231, 2014.

[350] J. Zhang, P. Xiao, G. Li and P. A.Webley, "Effect of flue gas impurities on CO2 capture performance from flue gas at coal-fired power stations by vacuum swing adsorption," *Energy Procedia,* vol. 1, no. 1, pp. 1115-1122, 2009.

[351] G. Li, P. Xiao, J. Zhang, P. A. Webley and D. Xu, "The role of water on postcombustion CO2 capture by vacuum swing adsorption: Bed layering and purge to feed ratio," *AIChE Journal,* vol. 60, no. 2, pp. 673-689, 2014.

[352] I. Majchrzak-Kucęba, D. Wawrzyńczak, J. Zdeb, W. Smółka and A. Zajchowski, "Treatment of Flue Gas in a CO2 Capture Pilot Plant for a Commercial CFB Boiler," *Energies,* vol. 14, p. 2459, 2021.

[353] D. Danaci, P. A. Webley and C. Petit, "Guidelines for Techno-Economic Analysis of Adsorption Processes," *Frontiers in Chemical Engineering,* vol. 2, p. 602430, 2021.

[354] BEIS, “Electricty Generation Costs 2016,” Department for Business, Energy & Industrial Strategy, London, 2016.

[355] Millbrook Power Ltd., “The Millbrook Power (Gas Fired Power Station) Order,” Parsons Brinckerhoff, 2017.

[356] C. Nwaoha, M. Beaulieu, P. Tontiwachwuthikul and M. D. Gibson, “Techno-economic analysis of CO2 capture from a 1.2 million MTPA cement plant using AMP-PZ-MEA blend,” *International Journal of Greenhouse Gas Control,* vol. 78, pp. 400-412, 2018.

[357] R. Turton, J. A. Shaeiwitz, D. Bhattacharyya and W. B. Whiting, Analysis, Synthesis, and Design of Chemical Processes, 5th ed., Pearson Eduction Inc., 2018.

[358] S. Jenkins, “2019 CHEMICAL ENGINEERING PLANT COST INDEX ANNUAL AVERAGE,” Chemical Engineering, 20 March 2020. [Online]. Available: https://www.chemengonline.com/2019-chemical-engineering-plant-cost-index-annual-average/. [Accessed 25 October 2021].

[359] J. R. Couper, W. R. Penney, J. R. Fair and S. M. Walas, Chemical Process Equipment: selection and design, 3rd ed., Oxford: Butterworth-Heinemann, 2012.

[360] Y. Le Moullec and M. Kanniche, “Optimization of MEA based post combustion CO2 capture process: Flowsheeting and energetic integration,” *Energy Procedia,* vol. 4, pp. 103-1309, 2011.

[361] M. Abu-Zahra, A. E. Nasr, A. A. Hajaj and E. Goetheer, “Techno-economics of liquid absorbent-based post-combustion CO2 processes,” in *Absorption-Based Post-Combustion Capture of Carbon Dioxide*, Elselvier Science, 2016, pp. 685-710.

[362] R. K. Sinnott, Coulson and Richardson's Chemical Engineering: Chemical Engineering Design Volume 6, 4th ed., Oxford: Elsevier, 2005.

[363] Global Petrol Prices, “United Kingdom natural gas prices,” Global Petrol Prices, March 2021. [Online]. Available: https://www.globalpetrolprices.com/United-Kingdom/natural_gas_prices/. [Accessed May 2021].

[364] BEIS, “Quarterly Energy Prices: UK January to March 2021,” The Department for Business, Energy and Industrial Strategy, 2021.

[365] Yorkshire Water, “Charges for customers with a meter,” Yorkshire Water, September 2021. [Online]. Available: https://www.yorkshirewater.com/bill-account/how-we-work-out-your-bill/customers-with-a-meter/. [Accessed October 2021].

[366] Mistral Industrial Chemicals, “MONOETHANOLAMINE MEA 2-AMINOETHANOL,” Mistral Industrial Chemicals, June 2013. [Online]. Available: https://mistralni.co.uk/products/mea-monoethanolamine. [Accessed October 2021].

[367] D. Danaci, M. Bui, N. M. Dowell and C. Petit, “Exploring the limits of adsorption-based CO2 capture using MOFs with PVSA – from molecular design to process economics,” *Molecular Systems Design & Engineering,* vol. 5, pp. 212-231, 2020.

[368] e. Rubin, G. Booras, J. Davison, C. Ekstrom, M. Matuszewski, S. McCoy and C. Short, “Toward a Common MEthod of Cost Estimation for CO2 Capture and Storage at Fossil Fuel Power Plants,” Carnegie Mellon University, 2013.

[369] P. Tontiwachwuthikul, A. Meisen and C. J. Lim, “CO2 absorption by NaOH, monoethanolamine and 2-amino-2-methyl-1-propanol solutions in a packed column,” *Chemical Engineering Science,* vol. 47, no. 2, pp. 381-390, 1992.

[370] H. M. Kvamsdal and G. T. Rochelle, “Effects of the Temperature Bulge in CO2 Absorption from Flue Gas by Aqueous,” *Industrial & Engineering Chemistry Research,* vol. 47, no. 3, pp. 867-875, 2008.

[371] K.-S. Zoannou, D. J. Sapsford and A. J. Griffiths, “Thermal degradation of monoethanolamine and its effect on CO2 capture capacity,” *International Journal of Greenhouse Gas Control,* vol. 17, pp. 423-430, 2013.

[372] P. Moser, G. Wiechers, S. Schmidt, J. G. M.-S. Monteiro, C. Charalambous, S. Garcia and E. S. Fernandez, “Results of the 18-month test with MEA at the post-combustion capture pilot plant at Niederaussem – new impetus to solvent management, emissions and dynamic behaviour,” *International Journal of Greenhouse Gas Control,* vol. 95, p. 102945, 2020.

[373] H. Jin, P. Liu and Z. Li, “Energy-efficient process intensification for post-combustion CO2 capture: A modeling approach,” *Energy,* vol. 158, pp. 471-483, 2018.

[374] K. Li, A. Cousins, H. Yu, P. Feron, M. Tade, W. Luo and J. Chen, “Systematic study of aqueous monoethanolamine-based CO2 capture process: model development and process improvement,” *Energy Science & Engineering,* vol. 4, no. 1, pp. 22-39, 2015.

[375] P. Luis, “Use of monoethanolamine (MEA) for CO2 capture in a global scenario: Consequences and alternatives,” *Desalination,* vol. 380, pp. 93-99, 2016.

[376] Engineering ToolBox, “Ratios of Specific Heat of Gase,” 2003. [Online]. Available: https://www.engineeringtoolbox.com/specific-heat-ratio-d_608.html. [Accessed 25 October 2021].

[377] E. Khoramzadeh, M. Mofarahi and C.-H. Lee, “Equilibrium Adsorption Study of CO2 and N2 on Synthesized Zeolites 13X, 4A, 5A, and Beta,” *Journal of Chemical & Engineering Data,* vol. 64, no. 12, pp. 5648-5664, 2019.

[378] N. S. Wilkins and A. Rajendran, “Measurement of competitive CO2 and N2 adsorption on Zeolite 13X for post-combustion CO2 capture,” *Adsorption,* vol. 25, pp. 115-133, 2019.

[379] I. PRAXAIR TECHNOLOGY, “VPSA PROCESS AND ENHANCED OXYGEN RECOVERY”. Patent WO 2008/005492 A1, 10 January 2009.

[380] M. Stinn and J. Vance, “Selecting valves for pressure swing adsorption,” Emerson, 2018.

[381] A. Aspelund, “12 - Gas purification, compression and liquefaction processes and technology for carbon dioxide (CO2) transport,” in *Developments and Innovation in Carbon Dioxide (CO2) Capture and Storage Technology*, Woodhead Publishing , 2010, pp. 383-407.

[382] C.-C. Cormos, “Evaluation of power generation schemes based on hydrogen-fuelled combined cycle with carbon capture and storage (CCS),” *International Journal of Hydrogen Energy,* vol. 36, no. 5, pp. 3726-3738, 2011.

[383] A. Streb and M. Mazzotti, “Novel Adsorption Process for Co-Production of Hydrogen and CO2 from a Multicomponent Stream—Part 2: Application to Steam Methane Reforming and Autothermal Reforming Gases,” *Industrial & Engineering Chemistry Research,* vol. 59, no. 21, pp. 10093-10109, 2020.

[384] V. Spallina, P. Nocerino, M. C. Romano, M. v. S. Annaland, S. Campanari and F. Gallucci, “Integration of solid oxide fuel cell (SOFC) and chemical looping combustion (CLC) for ultra-high efficiency power generation and CO2 production,” *International Journal of Greenhouse Gas Control*, vol. 71, pp. 9-19, 2018.

[385] Mitsubishi Power, “M701J Series,” 2020. [Online]. Available: https://power.mhi.com/products/gasturbines/lineup/m701j. [Accessed 09 December 2020].

[386] A. l. o. o. p. C. Guo, W. C. Lyons and A. Ghalambor, “11 - Transportation Systems,” in *Petroleum Production Engineering - A Computer-Assisted Approach,* Gulf Professional Publishing, 2007, pp. 133-158.

[387] S. Budinis and N. F. Thornhill, “Supercritical fluid recycle for surge control of CO2 centrifugal compressor,” *Computers & Chemical Engineering,* vol. 91, pp. 329-342, 2016.

[388] S. Budinis and N. F. Thornhill, “Control of centrifugal compressors via model predictive control for enhanced oil recovery applications,” *IFAC-PapersOnLine,* vol. 48, no. 6, pp. 9-14, 2015.

[389] Wärtsilä, “Combustion Engine vs Gas Turbine: Water consumption,” Wärtsilä, September 2019. [Online]. Available: https://www.wartsila.com/energy/learn-more/technical-comparisons/combustion-engine-vs-gas-turbine-water-consumption. [Accessed April 2021].

[390] D. Danaci, M. Bui, C. Petit and N. Mac Dowell, “En Route to Zero Emissions for Power and Industry with Amine-Based Post-combustion Capture,” *Environmental Sceince & Technology,* vol. 55, no. 15, pp. 10619-10632, 2021.

[391] P. Styring, E. A. Quadrelli and K. Armstrong, Carbon Dioxide Utilisation: Closing the Carbon Cycle, Elsevier, 2015.

[392] C. Hepburn, E. Adlen, J. Beddington, E. A. Carter, S. Fuss, N. M. Dowell, J. C. Minx, P. Smith and C. K. Williams, “The technological and economic prospects for CO2 utilization and removal,” *Nature,* vol. 575, pp. 87-97, 2019.

[393] M. D. Wilkes and S. Brown, “Evaluating the Transient Operation of PCC for Fast Response Gas Turbines in a Future Low-Carbon Energy System,” *Computer Aided Chemical Engineering,* vol. 48, pp. 157-162, 2020.

[394] M. D. Wilkes, S. Mukherjee and S. Brown, “Transient CO2 capture for open-cycle gas turbines in future energy systems,” *Energy,* p. 119258, 2021.

[395] M. D. Wilkes and S. Brown, “Evaluating the flexible operation of vacuum-pressure swing adsorption for CO2 capture from modern gas turbines,” *Computer Aided Chemical Engineering,* vol. 51, pp. 427-432, 2022.

[396] M. D. Wilkes and S. Brown, “Flexible CO2 capture for open-cycle gas turbines via vacuum-pressure swing adsorption: A model-based assessment,” *Energy,* vol. 250, p. 123805, 2022.

[397] M. D. Wilkes, S. Mukherjee and S. Brown, “Compression system power requirements for various CO2 sources and transportation options,” *Computer Aided Chemical Engineering,* vol. 50, pp. 1439-14444, 2021.

[398] M. D. Wilkes, S. Mukherjee and S. Brown, “Linking CO2 capture and pipeline transportation: sensitivity analysis and dynamic study of the compression train,” *International Journal of Greenhouse Gas Control,* vol. 111, p. 103449, 2021.

[399] M. D. Wilkes, J. O. Ejeh, D. Roberts and S. Brown, “Cost of CO2 capture for small-scale dispatchable power generation,” in *Proceedings of the 16th Greenhouse Gas Control Technologies Conference (GHGT-16) 23-24 Oct 2022*, Lyon, France, 2022.

[400] D. Diagne, M. Goto and T. Hirose, “Numerical Analysis of a Dual Refluxed PSA Process During Simultaneous Removal and Concentration of Carbon Dioxide Dilute Gas from Air,” *Journal of Chemical Technology and Biotechnology,* vol. 65, no. 1, pp. 29-38, 1996.

[401] Y. Ding and E. Alpay, “Equilibria and kinetics of CO2 adsorption on hydrotalcite adsorbent,” *Chemical Engineering Science,* vol. 55, no. 17, pp. 3461-3473, 2000.

[402] W.-K. Choi, T.-I. Kwon, Y.-K. Yeo, H. Lee, H. K. Song and B.-K. Na, “Optimal Operation of the Pressure Swing Adsorption (PSA) Process for CO2 Recovery,” *Korean Journal of Chemical Engineering,* vol. 20, no. 4, pp. 617-623, 2003.

[403] C.-T. Chou and C.-Y. Chen, “Carbon dioxide recovery by vacuum swing adsorption,” *Separation and Purification Technology,* vol. 39, no. 1-2, pp. 51-65, 2004.

[404] A. Agarwal, “'Advanced Strategies for Optimal Design and Operation of Pressure Swing Adsorption Processes',PhD Thesis,” Carnegie Mellon University, Pittsburgh, 2010.

[405] R. Krishna and J. R. Long, “Screening Metal-Organic Frameworks by Analysis of Transient Breakthrough of Gas Mixtures in a Fixed Bed Adsorber,” *The Journal of Physical Chemistry C,* vol. 115, no. 26, pp. 12941-12950, 2011.

[406] R. Krishna and J. M. v. Baten, “A comparison of the CO2 capture characteristics of zeolites and metal–organic frameworks,” *Separation and Purification Technology,* vol. 87, pp. 120-126, 2012.

[407] V. P. Mulgundmath, R. Jones, F. H. Tezel and J.Thibault, “Fixed bed adsorption for the removal of carbon dioxide from nitrogen: Breakthrough behaviour and modelling for heat and mass transfer,” *Separation and Purification Technology,* vol. 85, pp. 17-27, 2012.

[408] R. P. P. L. Ribeiro, C. A. Grande and A. E. Rodrigues, “Activated carbon honeycomb monolith – Zeolite 13X hybrid system to capture CO2 from flue gases employing Electric Swing Adsorption,” *Chemical Engineering Science,* vol. 104, pp. 304-318, 2013.

[409] L. Riboldi and O. Bolland, “Evaluating Pressure Swing Adsorption as a CO2 separation technique in coal-fired power plants,” *International Journal of Greenhouse Gas Control,* vol. 39, pp. 1-16, 2015.

[410] J. F. Horstmeier, A. Lopez and D. Agar, “Performance improvement of vacuum swing adsorption processes for CO2 removal with integrated phase change material,” *International Journal of Greenhouse Gas Control,* vol. 47, pp. 364-375, 2016.

[411] M. G. Plaza, F. Rubiera and C. Pevida, “Evaluating the Feasibility of a TSA Process Based on Steam Stripping in Combination with Structured Carbon Adsorbents To Capture CO2 from a Coal Power Plant,” *Energy & Fuels,* vol. 31, no. 9, pp. 9760-9775, 2017.

[412] M. H. Zarghampoor, M. Mozaffarian, M. Soleimani and M. T. Ravanchi, “Modeling of CO2 Adsorption on Activated Carbon and 13X Zeolite via Vacuum Swing Adsorption,” *IOP Conference Series: Materials Science and Engineering,* vol. 206, 2017.

[413] R. Ben-Mansour, N. A. A. Qasem and M. A. Antar, “Carbon dioxide adsorption separation from dry and humid CO2/N2 mixture,” *Carbon dioxide adsorption separation from dry and humid CO2/N2 mixture,* vol. 117, pp. 221-235, 2018.

[414] N. A. A. Qasem and R. Ben-Mansour, “Adsorption breakthrough and cycling stability of carbon dioxide separation from CO2/N2/H2O mixture under ambient conditions using 13X and Mg-MOF-74,” *Applied Energy,* vol. 230, pp. 1093-1107, 2018.

[415] P. Goyal, M. J. Purdue and S. Farooq, “Adsorption and Diffusion of N2 and CO2 and Their Mixture on Silica Gel,” *Industrial & Engineering Chemistry Research,* vol. 58, no. 42, pp. 19611-19622, 2019.

[416] M. Xu, S. Chen, D. Seo and S. Deng, “Evaluation and optimization of VPSA processes with nanostructured zeolite NaX for post-combustion CO2 capture,” *Chemical Engineering Journal,* vol. 371, pp. 693-705, 2019.

[417] J. Tian, Y. Shen, D. Zhang and Z. Tang, “CO2 capture by vacuum pressure swing adsorption from dry flue gas with a structured composite adsorption medium,” *Journal of Environmental Chemical Engineering,* vol. 9, p. 106037, 2021.

[418] M. Boscherinia, F. Miccio, E. Papa, V. Medri, E. Landi, F. Doghieri and M. Minelli, “The relevance of thermal effects during CO2 adsorption and regeneration in a geopolymer-zeolite composite: Experimental and modelling insights,” *Chemical Engineering Journal,* vol. 408, p. 127315, 2021.

Chapter 10 : Appendix

10.1. Appendix A

Table 49: Compilation of studies presenting mathematical models of various adsorption-based PCC systems.

Source	Model					Adsorbent(s) Investigated	System
	Mass Transfer	Flow	Isotherm	Heat Transfer	Pressure Drop		
[329]	LDF	Axially dispersed plug flow regime	Langmuir	Thermal equilibrium	Negligible Pressure Drop	Activated Carbon and Zeolite 13X	PSA
[400]	LDF	Ideal plug flow	Langmuir	Isothermal conditions	Negligible Pressure Drop	Zeolite 13X, 5A, 4A	DAC PSA
[401]	LDF	Axially dispersed plug flow regime	Langmuir	Non-equilibrium	Ergun	Potassium promoted hydrotalcite	PSA
[402]	LDF	Ideal plug flow	Extended Langmuir	Non-isothermal Adiabatic conditions	Negligible Pressure Drop	Zeolite 13X	PSA
[403]	LEM	Axially dispersed plug flow regime	Langmuir	Non-isothermal	Negligible Pressure Drop	Zeolite 13X	VSA
[328]	LDF	Axially dispersed plug flow regime	Dual-site Langmuir	Non-isothermal	Ergun	Zeolite 13X	Fractionated VPSA
[404]	LDF	Axially dispersed plug flow regime	Dual-site Langmuir	Thermal equilibrium	Ergun	Zeolite 13X	PSA
[83]	LDF	Axially dispersed	Toth	Local thermal equilibrium	Darcy	Zeolite 5A	TSA
[100]	LDF	Axially dispersed plug flow regime	Toth	Non-equilibrium	Ergun	Activated Carbon	PSA
[338]	LDF	Axially dispersed plug flow regime	Toth	Non-equilibrium	Ergun	Zeolite 13X	PSA
[100]	LDF	Axially dispersed plug flow regime	Toth	Thermal equilibrium	Ergun	Zeolite 13X	PSA
[405]	LEM	Axially dispersed plug flow regime	IAS theory using dual-site Langmuir-Freundlich isotherm	Isothermal conditions	Negligible Pressure Drop	Zeolite 13X,Mg-MOF-74, MOF-177, CubTTri, BeBtB and Co(BDP)	Breakthrough analysis
[406]	LEM	Axially dispersed plug flow regime	IAS theory using dual-site Langmuir-Freundlich isotherm	Isothermal conditions	Negligible Pressure Drop	Zeolites (MFI, JBW, AFX, NaX) and Metal Organic	PSA

[407]	LDF	Axially dispersed plug flow regime	Langmuir	Thermal equilibrium	-	Frameworks (MgMOF-74, MOF-177, CuBTTri-mmen) Ceca 13X, Alcan AA320-AP and Alcan 650 PCA	TPSA
[108]	LDF	Axially dispersed	Virial	Non-equilibrium	Ergun	Activated Carbon Beads	VPSA
[84]	Bi-LDF	Axially dispersed plug flow regime	Modified multisite Langmuir	Thermal equilibrium	Ergun	Zeolite 13X-APG	VSA, TSA, VTSA
[408]	LDF	Axially dispersed plug flow regime	Multi-site Langmuir	Isothermal conditions	Ergun	activated carbon honeycomb monolith with zeolite 13X particle	ESA
[336]	LDF	Axially dispersed	Langmuir	Thermal equilibrium	Darcy	Zeolite 13X	VSA
[115]	LDF	Axially dispersed	Langmuir	Thermal equilibrium	Darcy	Zeolite 13X	VSA
[409]	LDF	Axially dispersed plug flow regime	Multi-site Langmuir	Thermal equilibrium	Ergun	Zeolite 5A and activated carbon	PSA
[410]	LDF	Axially dispersed	Toth	Non-equilibrium	Ergun	Zeolite 13X, Amine-functionalised Activated Carbon, Lewatit VP OC 1065	VSA
[320]	LDF	Axially dispersed	IAS theory using the Toth isotherm model	Thermal equilibrium	Ergun	Microporous Biochar	Ternary breakthrough analysis
[321]	LDF	Axially dispersed	IAS theory using Toth for CO_2 and N_2, CMMS theory for H_2O	Thermal equilibrium	Ergun	Microporous Biochar	Ternary breakthrough analysis
[110]	LDF	Axially dispersed plug flow regime	Langmuir	Thermal equilibrium	Ergun	Zeolite 13X	Rapid VPSA
[325]	LDF	Axially dispersed	Dual-site Langmuir	Thermal equilibrium	Ergun	Zeolite 13X and Mg-MOF-74	VPSA
[411]	LDF	Axially dispersed	IAS theory using Toth for CO_2 and N_2, CMMS theory for H2O	Non-equilibrium	Darcy	Activated Carbon Honeycomb	TSA
[412]	quasi-second order mass transfer	Axially dispersed plug flow regime	Toth	Isothermal conditions	Ergun	Activated Carbon and Zeolite 13X	VSA

[318]	LDF	Axially dispersed plug flow regime	Toth	Non-equilibrium	Ergun	Activated Carbon	PSA
[413]	LDF	2-D Mesh of structured quadrilateral elements	Dual-site Langmuir for CO_2 & N_2, Toth for H_2O	Thermal equilibrium	Ergun	Zeolite 13X and Mg-MOF-74	2D and 3D breakthrough analysis
[333]		Axially dispersed	Extended Langmuir	Non-isothermal and adiabatic	Karman-Kozeny	Zeolite MS13X and activated carbon honeycomb	T/ESA
[414]	LDF	2-D Mesh of structured quadrilateral elements	Toth model for Zeolite 13X and the dual-site Langmuir model for Mg-MOF-74	Thermal equilibrium	Ergun	Zeolite 13X and Mg-MOF-74	Breakthrough analysis
[415]	LDF	Axially dispersed plug flow regime	Langmuir	Thermal equilibrium	Darcy	Silica Gel	VSA
[96]	LDF	Axially dispersed	Extended Virial Isotherm	Non-equilibrium	Ergun	Zeolite 13X	MBTSA
[416]	LDF	Axially dispersed plug flow regime	Langmuir-Freundlich	Thermal equilibrium	Ergun	Nanostructured Zeolite pellets	VPSA
[324]	LDF	Axially dispersed	dual-site Langmuir isotherm	Thermal equilibrium	Ergun	Zeolite 13X	VSA
[105]	LDF	Axially dispersed	Extended Langmuir	Non-equilibrium	Ergun	Zeolite 13X	VPSA, TSA, TVSA
[417]	LDF	Axially dispersed	Extended Langmuir	Non-equilibrium	Ergun	Composite adsorption material	VPSA
[418]	LDF	Axially dispersed	Sips	Thermal-equilibrium	Ergun	Zeolite-geopolymer sorbent	TSA-PSA

Note: CMMS is cooperative multimolecular sorption, DAC is direct air capture, IAS is ideal adsorption solution, LDF is linear driving force, and LEM is the local equilibrium model.

Within gPROMS Process, you can directly specify an adsorption isotherm model and input the respective parameters. However, to use the format and units specified in [115] a custom sub-model for the dual-site Langmuir isotherm model was developed. Using gPROMS advanced process modelling platform, the following script was developed to calculate the equilibrium adsorption quantity of CO_2 and N_2 onto Zeolite 13X:

MODEL Isotherm_section_custom_gML

```
PARAMETER
T_ref                   AS REAL
R                       AS REAL
Components              AS ORDERED_SET
no_ads                  AS INTEGER
no_layers               AS INTEGER
layer_boundaries        AS ARRAY(no_layers+1) OF REAL

DISTRIBUTION_DOMAIN
axial           AS [ 0 : 1 ]


VARIABLE
# Inputs
  T   AS DISTRIBUTION (axial)                 OF temperature_gML                    # [K]
  p   AS DISTRIBUTION (Components, axial)     OF pressure_partial_bar_gML           # [bar]
  q   AS DISTRIBUTION (Components, axial)     OF no_type_gML  # solid_phase_concentration [mol/kg]
  C  AS DISTRIBUTION (components, axial)      OF molar_concentration_kmol_per_m3  # [kmol/m3]

# Specified
  k   AS ARRAY (4,no_layers,Components)       OF no_type_gML

# Calculated
  b1  AS DISTRIBUTION (Components,axial)      OF no_type_gezero # [m3/mol]
  b2  AS DISTRIBUTION (Components,axial)      OF no_type_gezero # [m3/mol]
  q1  AS DISTRIBUTION (Components,axial)      OF molar_concentration_per_mass_unit #[mol/kg]
  q2  AS DISTRIBUTION (Components,axial)      OF molar_concentration_per_mass_unit #[mol/kg]

# Outputs
  heat_of_adsorption      AS DISTRIBUTION (Components, axial) OF
molar_specific_enthalpy_kJ_per_mol_gML # Heat of adsorption [kJ/mol]
  qeq                     AS DISTRIBUTION (Components, axial) OF
molar_concentration_per_mass_unit_gML  # Equilibrium surface coverage [mol/kg]


SET
  T_ref  := 298.15; # [K]
   R       := 8.314e-3; # [kJ/mol.K]


EQUATION
# Dual-site Langmuir adsorption isotherm
FOR j:=1 TO 1 DO
```

```
    FOR z := layer_boundaries(j) TO layer_boundaries(j+1) DO

        FOR i IN Components DO
            qeq(i,z)  = ((q1(i,z)*(b1(i,z)*(C(i,z)))) / (1 + ((b1(i,z))*(C(i,z))))) + ((q2(i,z)*(b2(i,z)*(c(i,z)))) /
            (1    + ((b2(i,z))*(c(i,z)))));

          q1(i,z) = k(1,j,i); [mol/kg]
          q2(i,z) = k(2,j,i); [mol/kg]

          b1(i,z) = k(3,j,i)*EXP((heat_of_adsorption(i,z))/(R*T(z))); # [m3/kmol]
          b2(i,z) = k(4,j,i)*EXP((heat_of_adsorption(i,z))/(R*T(z))); # [m3/kmol]

        END

        heat_of_adsorption('CO2',z) = 36.64121 ; #kJ/mol
        heat_of_adsorption('N2',z) = 15.82000 ; #kJ/mol
    END
END

ASSIGN


k(1,1,'CO2') := 3.09; #[mol/kg] q_sb
k(1,1,'N2') := 5.84; #[mol/kg] q_sb


k(2,1,'CO2') := 2.54; #[mol/kg] q_sd
k(2,1,'N2') := 0; #[mol/kg] q_sd


k(3,1,'CO2') := 8.65e-4; #[m3/kmol] b0 in terms of kmol-1 to cancel out kmol used in C
k(3,1,'N2') := 2.5e-3; #[m3/kmol] b0


k(4,1,'CO2') := 2.63e-5; #[m3/kmol] d0
k(4,1,'N2') := 0; #[m3/mol] d0
```

10.2. Appendix B

For the process model validation against IEAGHG [60], shown in 3.3.3, the model calculates several important design characteristics shown in Table 27 and Table 50 for the conventional compression route and Table 51 for the multistage compression and liquefaction route.

Table 50: Process model outputs for the conventional multistage compression route based on the IEAGHG base case B0 [60]

Parameter	CS1	CS2	DH1	CS3	CS4
Inlet Mass Flowrate (kg/h)	556484	594440	592956	535447	536761
Inlet Temperature (°C)	53.47	19.21	24.00	19.48	40.07
Inlet Pressure (bar)	1.60	6.60	33.60	32.69	69.63
Rotational Speed (RPM)	4400.00	4800.00	-	4900.00	4800.00
Compressor Tip Speed (m/s)	306.00	251.00	-	136.00	97.10
Average Impeller Diameter (m)	1.22	1.00	-	0.53	0.38
Section Surge Margin (%)	28.20	25.40	-	26.30	36.20
Surge Volume Flow (m^3/s)	44.90	10.00	-	1.56	0.74
Electric Drive Speed (Hz)	79.90	80.10	-	81.30	80.60
Outlet Temperature (°C)	202.03	165.93	24.87	89.47	82.20
Outlet Pressure (bar)	7.00	33.99	32.70	70.03	111.23
Power Requirement (MW)	22.63	20.60	4.04	6.81	3.39
Percentage of Total Power (%)	39.38	35.84	7.03	11.85	5.89

Please refer to Figure 43 for unit descriptions and abbreviations.

Table 51: Process model outputs for the multistage compression and liquefaction route based on the IEAGHG case D2c [60]

Parameter	CS1	CS2	DH1	CS3	LP1
Inlet Mass Flowrate (kg/h)	556484	594440	592956	535323	533400
Inlet Temperature (°C)	53.47	19.21	24.00	19.46	20.00
Inlet Pressure (bar)	1.60	6.60	33.60	32.70	65.64
Rotational Speed (RPM)	4395.00	4800.00	-	4850	-
Tip Speed (m/s)	306.00	251.00	-	134	-
Average Impeller Diameter (m)	1.22	1.00	-	0.54	-
Section Surge Margin (%)	28.20	25.40	-	24.70	-
Surge Volume Flow (m^3/s)	45.00	10.00	-	1.54	-
Electric Drive Speed (Hz)	79.90	80.10	-	79.60	80.00
Outlet Temperature (°C)	202.12	165.91	24.87	83.69	26.37
Outlet Pressure (bar)	7.00	34.00	32.70	66.04	111.00
Power Requirement (MW)	22.65	20.59	4.04	6.23	0.95
Percentage of Total Power (%)	41.59	37.81	7.42	11.44	1.74

Please refer to Figure 43 for unit descriptions and abbreviations.

For each case study investigated in Chapter 5 Section 5.2, shown in Table 15 Chapter 2 Section 2.4.3.1, the individual models calculated design characteristics shown in Table 52 and Table 53.

Table 52: Process model outputs during each case study for the conventional compression route

Source	Rotational Speed (RPM)				Tip Speed (m/s)				Average Impeller Diameter (m)				Section Surge Margin (%)				Surge Volume Flow (m^3/s)			
	CS1	CS2	CS3	CS4	CS1	CS2	CS3	CS4	CS1	CS2	CS3	CS4	CS1	CS2	CS3	CS4	CS1	CS2	CS3	CS4
Post-MEA-20	4385	4150	3450	3050	77.20	64.50	63.90	64.90	0.31	0.25	0.25	0.25	28.60	37.00	45.00	50.80	0.2920	0.0759	0.0137	0.0057
Post-MEA-300	4385	4150	3450	3050	77.20	64.50	63.80	64.80	0.31	0.25	0.25	0.25	28.60	37.00	45.00	50.80	0.2920	0.0759	0.0136	0.0057
Post-MEA-600	4385	4150	3450	3050	77.20	62.80	61.90	63.60	0.31	0.25	0.25	0.25	28.70	33.90	44.70	50.70	0.2920	0.0740	0.0132	0.0056
Post-NH3-20	4700	4150	3400	3050	63.90	64.90	63.90	65.00	0.25	0.25	0.25	0.25	28.20	38.20	45.50	51.20	0.0669	0.0765	0.0138	0.0057
Post-NH3-300	4700	4150	3400	3050	63.90	64.90	63.70	64.90	0.25	0.25	0.25	0.25	28.20	38.20	45.50	51.20	0.0669	0.0765	0.0138	0.0057
Post-NH3-600	4700	4150	3400	3050	63.80	63.00	61.80	63.70	0.25	0.25	0.25	0.25	28.20	35.20	45.20	51.00	0.0669	0.0744	0.0134	0.0056
Pre- MDEA-20	4385	4150	3450	3050	87.00	64.60	64.00	65.10	0.35	0.25	0.25	0.25	28.30	37.10	45.10	50.90	0.4160	0.0760	0.0137	0.0057
Pre- MDEA-300	4385	4150	3450	3050	87.00	64.60	63.80	64.90	0.35	0.25	0.25	0.25	28.30	37.10	45.00	50.90	0.4160	0.0760	0.0136	0.0057
Pre- MDEA-600	4385	4150	3450	3050	87.00	62.90	62.00	63.80	0.35	0.25	0.25	0.25	28.30	34.00	44.70	50.70	0.4160	0.0741	0.0132	0.0056
SMR-PSA-20	4875	4000	3315	3000	86.70	63.80	63.80	64.70	0.35	0.25	0.25	0.25	26.70	38.80	45.90	51.30	0.4130	0.0708	0.0133	0.0058
SMR-PSA-300	4875	4000	3315	3000	86.70	63.80	63.80	64.70	0.35	0.25	0.25	0.25	26.70	38.80	45.90	51.30	0.4130	0.0708	0.0133	0.0058
SMR-PSA-600	4875	4000	3315	3000	86.70	63.80	63.80	64.70	0.35	0.25	0.25	0.25	26.70	38.80	45.90	51.30	0.4130	0.0708	0.0133	0.0058
Steel-MEM-20	4385	4150	3450	3050	84.10	61.80	62.20	63.60	0.36	0.25	0.25	0.25	27.20	34.50	45.10	50.80	0.4410	0.0736	0.0136	0.0059
Steel-MEM-300	4385	4150	3450	3050	84.10	61.80	62.20	63.60	0.36	0.25	0.25	0.25	27.20	34.50	45.10	50.80	0.4410	0.0736	0.0136	0.0059
Steel-MEM-600	4385	4150	3450	3050	84.10	61.80	62.20	63.60	0.36	0.25	0.25	0.25	27.20	34.50	45.10	50.80	0.4410	0.0736	0.0136	0.0059
IGCC-Selexol-20	4385	4150	3450	3050	61.30	64.10	64.20	65.30	0.25	0.25	0.25	0.25	30.50	37.20	45.30	51.10	0.0870	0.0755	0.0137	0.0057
IGCC-Selexol-300	4385	4150	3450	3030	63.70	64.80	64.20	64.90	0.25	0.25	0.25	0.25	30.60	37.50	45.30	51.10	0.0904	0.0763	0.0137	0.0058
IGCC-Selexol-600	4385	4150	3450	3030	63.70	63.10	62.30	63.70	0.25	0.25	0.25	0.25	30.60	34.50	45.00	50.90	0.0904	0.0742	0.0133	0.0056
IGCC-MCFC-20	4775	4050	3415	3050	87.10	63.50	63.90	65.10	0.35	0.25	0.25	0.25	27.70	38.30	45.50	51.30	0.4190	0.0766	0.0138	0.0057
IGCC-MCFC-300	4775	4050	3415	3050	87.10	63.40	63.70	65.00	0.35	0.25	0.25	0.25	27.70	38.30	45.50	51.20	0.4190	0.0766	0.0138	0.0057
IGCC-MCFC-600	4775	4175	3540	3050	87.10	63.40	63.80	65.00	0.35	0.25	0.25	0.25	27.70	35.40	45.30	51.20	0.4190	0.0743	0.0133	0.0057
IGCC-SOFC-CLC-20	4760	4000	3335	3000	86.80	63.50	63.80	64.30	0.35	0.25	0.25	0.25	27.50	38.70	45.80	51.20	0.4200	0.0705	0.0132	0.0058
IGCC-SOFC-CLC-300	4760	4000	3335	3000	86.80	63.50	63.80	64.30	0.35	0.25	0.25	0.25	27.50	38.70	45.80	51.20	0.4200	0.0705	0.0132	0.0058
IGCC-SOFC-CLC-600	4760	4000	3335	3000	86.80	63.50	63.80	64.30	0.35	0.25	0.25	0.25	27.50	38.70	45.80	51.20	0.4200	0.0705	0.0132	0.0058

Please refer to Figure 43 for unit descriptions and abbreviations.

Table 53: Process model outputs during each case study for the multistage compression and liquefaction route

Source	Rotational Speed (RPM)				Tip Speed (m/s)				Average Impeller Diameter (m)				Section Surge Margin (%)				Surge Volume Flow (m^3/s)			
	CS1	CS2	CS3	LP1	CS1	CS2	CS3	LP1	CS1	CS2	CS3	LP1	CS1	CS2	CS3	LP1	CS1	CS2	CS3	LP1
Post-MEA-20	4385	4150	3450	-	76.70	64.50	61.60	-	0.31	0.25	0.25	1.00	28.10	37.00	44.40	-	0.2900	0.0759	0.0132	-
Post-MEA-300	4385	4150	3575	-	77.20	64.50	63.80	-	0.31	0.25	0.25	1.00	28.60	37.00	44.40	-	0.2920	0.0759	0.0131	-
Post-MEA-600	4385	4200	3600	-	77.20	63.50	63.80	-	0.31	0.25	0.25	1.00	28.70	33.90	44.30	-	0.2920	0.0739	0.0126	-
Post-NH3-20	4700	4050	3525	-	63.90	63.80	63.90	-	0.25	0.25	0.25	1.00	28.20	38.00	44.90	-	0.0671	0.0770	0.0134	-
Post-NH3-300	4700	4050	3525	-	63.90	63.80	63.80	-	0.25	0.25	0.25	1.00	28.20	38.00	44.90	-	0.0671	0.0770	0.0133	-
Post-NH3-600	4700	4000	3535	-	63.80	64.00	63.80	-	0.25	0.25	0.25	1.00	28.20	38.50	44.90	-	0.0671	0.0710	0.0129	-
Pre- MDEA-20	4375	4150	3575	-	86.90	64.50	63.90	-	0.35	0.25	0.25	1.00	28.30	37.00	44.40	-	0.4160	0.0759	0.0132	-
Pre- MDEA-300	4375	4150	3575	-	86.90	64.50	63.80	-	0.35	0.25	0.25	1.00	28.30	37.00	44.40	-	0.4160	0.0759	0.0131	-
Pre- MDEA-600	4375	4175	3600	-	86.90	63.20	63.80	-	0.35	0.25	0.25	1.00	28.30	34.00	44.30	-	0.4160	0.0740	0.0126	-
SMR-PSA-20	4775	4175	3535	-	87.20	63.60	63.60	-	0.35	0.25	0.25	1.00	27.70	35.40	44.90	-	0.4200	0.0744	0.0129	-
SMR-PSA-300	4775	4175	3535	-	87.20	63.60	63.60	-	0.35	0.25	0.25	1.00	27.70	35.40	44.90	-	0.4200	0.0744	0.0129	-
SMR-PSA-600	4775	4175	3535	-	87.20	63.60	63.60	-	0.35	0.25	0.25	1.00	27.70	35.40	44.90	-	0.4200	0.0744	0.0129	-
Steel-MEM-20	4775	4175	3550	-	88.00	63.40	63.80	-	0.35	0.25	0.25	1.00	27.70	35.40	44.90	-	0.4330	0.0742	0.0128	-
Steel-MEM-300	4775	4175	3550	-	88.00	63.40	63.80	-	0.35	0.25	0.25	1.00	27.70	35.40	44.90	-	0.4330	0.0742	0.0128	-
Steel-MEM-600	4775	4175	3550	-	88.00	63.40	63.80	-	0.35	0.25	0.25	1.00	27.70	35.40	44.90	-	0.4330	0.0742	0.0128	-
IGCC-Selexol-20	4385	4150	3450	-	61.30	64.10	64.90	-	0.25	0.25	0.25	1.00	30.50	37.20	44.40	-	0.0870	0.0755	0.0139	-
IGCC-Selexol-300	4385	4150	3450	-	61.30	64.10	64.70	-	0.25	0.25	0.25	1.00	30.50	37.20	44.30	-	0.0870	0.0755	0.0138	-
IGCC-Selexol-600	4385	4250	3885	-	61.30	62.40	67.00	-	0.25	0.25	0.25	1.00	30.50	34.10	44.40	-	0.0870	0.0735	0.0127	-
IGCC-MCFC-20	4775	4050	3715	-	87.10	63.50	67.00	-	0.35	0.25	0.25	1.00	27.70	38.30	44.90	-	0.4190	0.0766	0.0133	-
IGCC-MCFC-300	4775	4050	3720	-	87.10	63.40	67.00	-	0.35	0.25	0.25	1.00	27.70	38.30	44.90	-	0.4190	0.0766	0.0133	-
IGCC-MCFC-600	4775	4200	3850	-	87.10	63.80	67.00	-	0.35	0.25	0.25	1.00	27.70	35.40	44.70	-	0.4190	0.0743	0.0128	-
IGCC-SOFC-CLC-20	4775	4175	3550	-	87.10	63.40	63.80	-	0.35	0.25	0.25	1.00	27.70	35.40	44.90	-	0.4190	0.0742	0.0128	-
IGCC-SOFC-CLC-300	4775	4175	3550	-	87.10	63.40	63.80	-	0.35	0.25	0.25	1.00	27.70	35.40	44.90	-	0.4190	0.0742	0.0128	-
IGCC-SOFC-CLC-600	4775	4175	3550	-	87.10	63.40	63.80	-	0.35	0.25	0.25	1.00	27.70	35.40	44.90	-	0.4190	0.0742	0.0128	-

Please refer to Figure 43 for unit descriptions and abbreviations.

10.3. Appendix C

Table 54: Purchased and installed equipment cost for the MEA CO_2 capture plant

Equipment	Unit	a	b	S	n	E	#	Cost Factor	2019 Cost ($)	Installation Multiplier [359]	Installation Cost ($)
Absorber Column	kg	11600	34	53533.48	0.85	367076.21	1	1.1	404716.51	2.1	445188.16
Stripping Column	kg	11600	34	24424.61	0.85	194045.16	1	1.1	213942.72	2.1	235336.99
Adsorber Packing	m^3	0	7600	29.31	1.00	222753.31	1	1.1	245594.62	1.0	0.00
Stripping Packing	m^3	0	7600	7.35	1.00	55843.22	1	1.1	61569.43	1.0	0.00
Rich/lean heat exchanger	m^2	28000	54	448.45	1.20	110120.31	1	1.1	121412.14	2.2	145694.57
HRSG	m^2	28000	54	1792.00	1.20	460911.74	1	1.1	507002.92	2.2	608403.50
DCC	kg	11600	34	26440.92	0.85	206770.42	1	1.1	227972.83	1.2	45594.57
Blowers	m^3/h	4450	57	10000.00	0.80	94788.91	2	1.1	209017.29	2.0	209017.29
Condenser	m^2	28000	54	2.12	1.20	28133.04	1	1.1	31017.83	2.2	37221.40
Reboiler	m^2	29000	400	2.12	0.90	29786.62	1	1.1	32840.96	2.2	39409.15
Cooling units	m^2	28000	54	280.00	1.20	74664.15	4	1.1	329281.12	2.5	493921.67
Compressor 1	kW	580000	20000	40.38	0.60	763973.05	1	1.1	842311.48	1.3	252693.45
Compressor 2	kW	580000	20000	51.25	0.60	792238.53	1	1.1	873475.33	1.3	262042.60
Compressor 3	kW	580000	20000	21.54	0.60	706193.32	1	1.1	778606.97	1.3	233582.09
Compressor 4	kW	580000	20000	13.43	0.60	675052.90	1	1.1	744273.39	1.3	223282.02
Knock-out drums	kg	10200	31	698.02	0.85	18303.09	4	1.1	80719.62	2.0	80719.62
Dehydration unit	kg	11600	34	698.02	0.85	20487.26	3	1.1	67764.13	2.1	74540.54
								Total M$	**5.77**		**3.39**
								Total M£	**4.24**		**2.49**

Table 55: Purchased and installed equipment cost for the VPSA CO_2 capture plant

Equipment	**Unit**	**a**	**b**	**S**	**n**	**E**	**#**	**Cost Factor**	**2019 Cost ($)**	**Installation Multiplier** [359]	**Installation Cost ($)**
Columns	kg	11600	34	18866.27	0.85	158091.38	4	1.1	697208.79	2.1	766929.67
column packing	m3	0	0	0	0.00	0.00	0	1.1	0.00	1.0	0.00
blowers	m^3/h	4450	57	10000	0.80	94788.91	2	1.1	209017.29	1.4	83606.92
vacuum pumps	m^3/h	4450	57	10000	0.80	94788.91	4	1.1	418034.58	2.0	418034.58
FG Dehydrator	kg	11600	34	2733.8	0.85	39961.37	3	1.1	131872.52	2.1	145059.78
DCC	kg	11600	34	26440.92	0.85	206770.42	1	1.1	227972.83	1.2	45594.57
cooling units	m^2	28000	54	280	1.20	74664.15	4	1.1	329281.12	2.5	493921.67
Compressor 1	kW	580000	20000	41.632	0.60	767364.09	1	1.1	846050.25	1.3	253815.07
Compressor 2	kW	580000	20000	51.909	0.60	793882.67	1	1.1	875288.06	1.3	262586.42
Compressor 3	kW	580000	20000	21.752	0.60	706919.84	1	1.1	779407.99	1.3	233822.40
Compressor 4	kW	580000	20000	13.4392	0.60	675072.31	1	1.1	744294.79	1.3	223288.44
knock-out drums	kg	10200	31	698.0226	0.85	18303.09	4	1.1	80719.62	2.0	80719.62
								Total M$	**5.34**		**3.01**
								Total M£	**3.92**		**2.21**